A STUDY OF HUMAN GENOMIC VARIANTS OF A MICROTUBULE AND KINETOCHORE ASSOCIATED PROTEIN ASTRIN.

Dr Asifa Islam

MARCH 2021

QUEEN MARY UNIVERSITY OF LONDON

Submitted in partial fulfilment of the requirements of the Degree of Doctor of Philosophy

STATEMENT OF ORIGINALITY

I, Dr Asifa Islam, confirm that the research included within this thesis is my own work and that where it has been carried out in collaboration with, or supported by others, that this is duly acknowledged below and my contribution indicated. Previously published material is also acknowledged below.

I attest that I have exercised reasonable care to ensure that the work is original, and does not to the best of my knowledge break any UK law, infringe any third party's copyright or other Intellectual Property Right, or contain any confidential material.

I accept that the College has the right to use plagiarism detection software to check the electronic version of the thesis.

I confirm that this thesis has not been previously submitted for the award of a degree by this or any other university.

Signature:

Date: 08.03.2021

Details of collaboration and publications:

Where indicated experiments were carried out in collaboration with Dr Duccio Conti or Parveen Gul from the Draviam group.

Some of the results from "CHAPTER 6: RESULTS-IV-C-TERMINUS OF ASTRIN IS IMPORTANT FOR SPINDLE CHECKPOINT SIGNALLING." are published in:

- Conti, D., Gul, P[1]., Islam A[1]., Martín-Durán, J., Pickersgill, R.W. and Draviam, V.M., Kinetochores attached to microtubule-ends are stabilized by Astrin bound PP1 to ensure proper chromosome segregation, DOI: 10.7554/eLife.49325.

[1] Equal contribution

ABSTRACT

During cell division, chromosomes are captured by microtubules via a multiprotein complex called the kinetochore. Genomic variations in kinetochore proteins can cause pregnancy loss and developmental defects such as primary microcephaly and cancer-susceptible disorder mosaic variegated aneuploidy. The kinetochore protein Astrin is specifically recruited to kinetochores following their attachment to microtubule-ends, and its arrival stabilizes chromosome-microtubule attachments. Human genomic variations in Astrin are known, but their impact on chromosome segregation has not been studied. I have used a combination of cell biology techniques to study the impact of Astrin variants- p.Q1012* and p.L7Qfs*21 - identified in a screen of healthy individuals and Astrin p.E755K found in cancer cells. I have shown that the Astrin p.Q1012* variant normally localizes at spindle microtubules but not kinetochores. Moreover, p.Q1012* expression prolongs mitosis and induces chromosome congression and segregation defects. Consistent with the defects observed, Astrin p.Q1012* expressing metaphase cells display an active spindle assembly checkpoint and reduced microtubule pulling forces. Additionally, Astrin p.Q1012* overexpression impairs the kinetochore localization of endogenous Astrin-SKAP complex suggesting a dominant-negative phenotype. To explore the impact of the Astrin p.L7Qfs*21 variant, I introduced a stop codon at 7 a.a in Astrin-GFP and show that Astrin p.L7* expresses as a shorter protein. Next, I generated N-terminal deletions of Astrin (Δ151 and Δ274), mimicking new transcriptional start sites; these deletion mutants localize normally at spindle microtubules and kinetochores. Moreover, Astrin Δ151 migrates similarly to the short p.L7* on an immunoblot, suggesting that p.M152 and not p.M275 is the new start site in Astrin p.L7*. Lastly, I have shown that the cancer-associated Astrin p.E755K normally localizes at spindle microtubules and kinetochores. In summary, unlike the p.Q1012* variant, the other two variants localize normally during mitosis. My findings explain the occurrence of Astrin p.L7Qfs*21, but not p.Q1012, homozygotes within a healthy general population.

ACKNOWLEDGMENTS

First and foremost, I would like to thank my parents, Muhammad Islam and Razia Kausar, for funding this PhD and supporting me at every step. Second, I am extremely grateful to my supervisor, Prof Viji M. Draviam, for providing this opportunity and for her invaluable advice and support. I also thank my panel members, Dr Ewan Main and Prof Tom Vulliamy, for their continuous support and guidance.

My gratitude goes to all the present and past members of the Draviam Lab – Dr Duccio Conti, Dr Madeleine Hart, David Dang, Parveen Gul, Christoforos Efstathiou, Yeseul Sung, Tami Kashimini, Nadia Osmanu, Xinhong Song, Dr Sophie Danielle Adams and Saanjbati Adhikari - for the constructive feedback and friendship. Special thanks to Duccio and Maddy for training me and to Pari for providing the baits for the pull-down studies. Thanks to Yeseul, with whom I had a fun time standardizing the site-directed point mutagenesis. I would also like to extend my gratitude to Dr Roshan L. Shrestha for sending detailed notes on HeLa FRT/TO cell line generation.

My brother Asad Islam has been a phenomenal support throughout these four years. In addition to his constructive feedback, he wrote the code for part of inter-centromeric distance measurement analysis (not part of this thesis), data extraction, and file conversion (part of chapter 3), thus saving me hours of work.

Many thanks to everyone on FOGG third and fourth-floor for making it an excellent environment to work in. The third-floor coffee hub - where biology meets engineering - will always have a special place in my heart. Special thanks to Dr Ruth Rose for training me in biochemistry and letting me use her equipment. Huge thanks to Dr Petra Ungerer for technical as well as emotional support. The arrival of Thorpe lab at QMUL has been a bonus. It was a fantastic experience discussing science with such extraordinary minds.

I would also like to say thanks to Dr Gary Warnes for his help with FACS sorting. Many thanks to Prof David Van Heel, Karen Hunt and Dr Robin Lerner at Genes and Health for their support with the GH dataset and for trying their best to set up the human studies for this thesis. A special thanks to Dr Jason Lee for training me

in white blood cell extraction from human blood. No one could have predicted the COVID-19 pandemic, but hopefully, the studies will resume soon.

Lastly, my appreciation goes out to my housemate and brother, Dr Saad Islam, for his continuous support and patience and my baby sister, Afifa Islam, for being a constant source of joy even from miles away. My appreciation extends to my friends and extended family for letting me also have a life outside science.

TABLE OF CONTENTS

CHAPTER 1:
INTRODUCTION

CHAPTER 1: INTRODUCTION

1.1 INTRODUCTION

Cancer incidence has been on the rise for decades. It is predicted that 1 in 2 people born in the UK after 1960 will get cancer at some stage of their life; however, the cancer survival rates are only about 50% (*Cancer incidence statistics | Cancer Research UK, 24.02.2021*). With the increasing burden of cancer in the western world, where it may become the leading cause of death due to a) an increase in the aging population and b) better treatment options for other common diseases, ideally, there should be a complementary rise in better treatment options. Causes of cancer include somatic mutations (changes in DNA acquired after conception), and many of these mutations are present in mitotic proteins (Reviewed in: (Levine and Holland 2018)). Germline variations (changes in the DNA acquired at or before conception) in mitotic proteins, on the other hand, can cause developmental disorders such as primary microcephaly and mosaic-variegated aneuploidy (MVA) (Reviewed in: (Degrassi, Damizia, and Lavia 2019)). Children born with microcephaly (reduced head size) can present with a range of symptoms, including intellectual disability and developmental delays. Children born with MVA also have microcephaly, but additionally, they are at an increased risk of early-onset cancers (Reviewed in: (Gilmore and Walsh 2013; Jayaraman, Bae, and Walsh 2018).

This chapter gives an overview of mitosis and then discusses the consequences of known genomic variations in mitotic proteins.

1.2 MITOSIS

Human life starts from a single cell that divides to give rise to trillions of cells, making the adult human body. In addition to growth, cell divisions are required for replenishing damaged cells and reproduction. During mitotic cell division, chromosomes are captured by microtubules (MTs) via a multiprotein complex called the kinetochore (KT) (see **section 1.2.2**). Simultaneously, the spindle assembly checkpoint (SAC) or the "wait signal" is activated (see **section 1.2.4.2**). Initially, the KT-MT attachments are along the lateral walls of the MTs - called lateral attachments

(see **section 1.2.3.1**). Then these lateral attachments are converted into end-on attachments where the KTs are embedded into the MT-ends (see **section 1.2.3.2**). The chromosomes congress and align at the cell's equator (see metaphase cells in **Fig 1.1**). Each sister chromatid is now attached to the MTs coming from the opposite sides, a configuration called biorientation (see metaphase cell in **Fig 1.1**), and the SAC is satisfied. Finally, chromosomes segregate, the cytoplasm divides and two genetically identical daughter cells are produced (**Fig 1.1**; Reviewed in: (Richard Mcintosh 2016)).

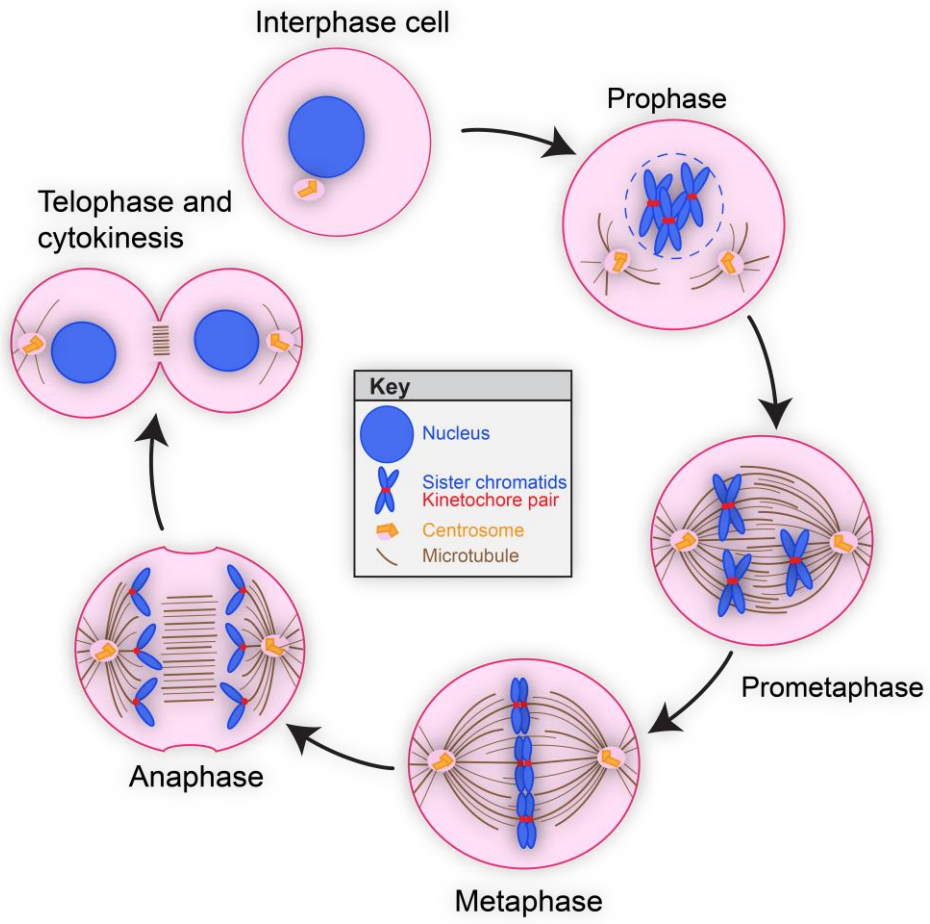

Fig 1.1 Overview of mitosis. Upon mitotic entry, the centrosomes separate and nucleate microtubules (MTs). The chromosomes condense and the nuclear envelope breaks down. In prometaphase, the MTs capture chromosomes via a multiprotein complex called the kinetochore. Then, the chromosomes align at the equator in metaphase. Each sister kinetochore is now attached to MTs emanating from opposite poles- termed biorientation. Biorientation is sensed by the spindle assembly checkpoint, which is then turned off. This marks the onset of anaphase and sister chromatids separate and move towards opposite sides. Finally, chromosomes decondense, the nuclear envelope reforms and the cytoplasm divides, resulting in two daughter cells with an equal amount of genetic material.

1.2.1 MICROTUBULES

For faithful congression and segregation of chromosomes, a large microtubule (MT) based structure assembles to form the mitotic spindle. MTs are tube-like structures made up of dimers of α and β-tubulin capable of dynamically growing (polymerizing) and shrinking (depolymerizing) (**Fig 1.2**; (Mitchison and Kirschner 1984)). In a mitotic cell, MTs nucleate from two centrosomes which progressively move towards the opposite sides to make the two spindle poles. MT nucleation is initiated by ring-shaped γ-tubulin ring complexes (γ-TuRC), which also cap the MT growth at the centrosomes forming the MT minus-end (Moritz et al. 1995; Mitchison and Kirschner 1985). MT plus-ends grow towards the cortex (astral MTs) and the cell's center. The astral MTs anchor the mitotic spindle while the MTs growing towards the center capture the chromosomes and align them at the cell's equator.

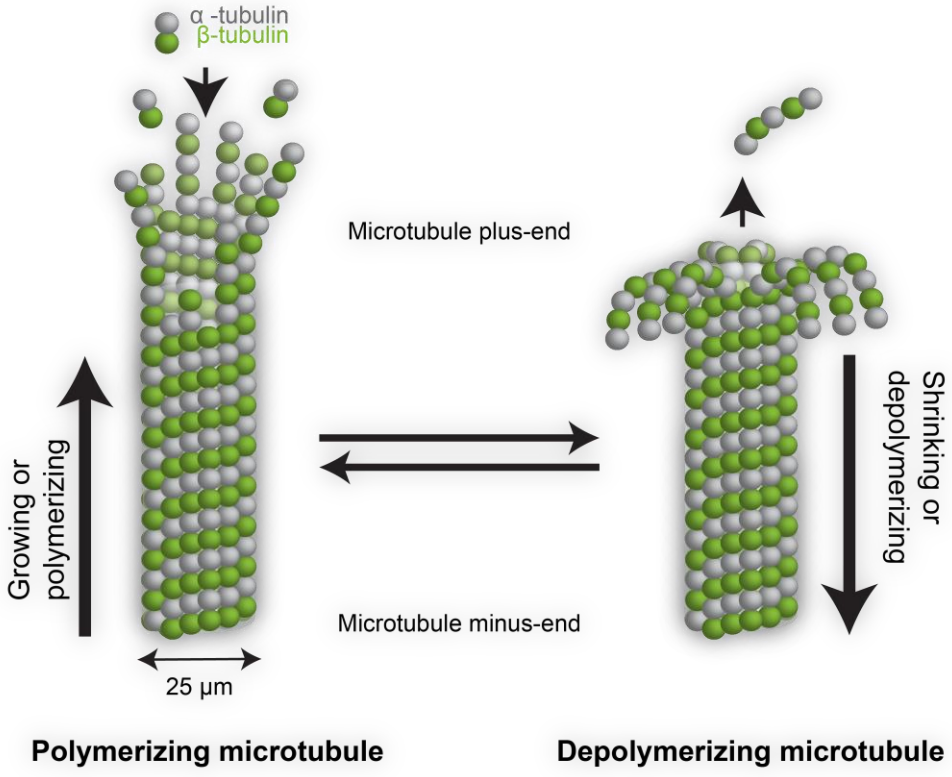

Fig 1.2 Microtubules. Microtubules are tube-like structures made up of dimers of α and β-tubulin. They have a relatively stable minus-end localized at the centrosomes and a dynamic plus-end that grows towards the cortex (astral microtubules) and cell's center. Microtubules rapidly grow (polymerize) by the addition of α/β-tubulin dimers and shrink (depolymerize) by the removal α/β-tubulin.

Using laser microsurgery to destroy centrosomes, Khodjakov et al. (Khodjakov et al. 2000) showed that a functional bipolar spindle could be formed in the absence of centrosomes. MTs can nucleate from chromosomes and MTs themselves (Lüders, Patel, and Stearns 2006; Hayward et al. 2014). Like the centrosome-mediated MT nucleation, chromosome and MT-mediated MT nucleation also require γ-TuRC (Lüders, Patel, and Stearns 2006). However, there are some differences in the pathways, and by manipulating those differences, Hayward et al. (Hayward et al. 2014) showed that inhibiting one pathway leads to an increase in others' activity which can then form the mitotic spindle.

1.2.2 THE KINETOCHORE

The human kinetochore (KT) comprises over 100 proteins (Reviewed in: (Musacchio and Desai 2017; Hara and Fukagawa 2020); a comparison of human and yeast kinetochore is given in **Table 1.1**). In mitosis, KT assembles on the centromeres, regions on the chromosomes specified by centrosomal protein (CENP)-A (Black et al. 2007). CENP-A was first discovered during work on sera of patients diagnosed with the autoimmune syndrome CREST (Calcinosis, Reynaud's syndrome, Esophageal dysmotility, Sclerodactyly, Telangiectasia) (Moroi et al., 1980; Earnshaw and Rothfield, 1985). CREST antisera are widely used as a marker for centromeres and are also used throughout this thesis.

Based on EM studies (Reviewed in: (Cheeseman and Desai 2008)), the KT can be divided into two parts, i.e., the inner and the outer KT.

1.2.2.1 INNER KINETOCHORE OR CCAN

The inner KT is made up of a 16-unit constitutive centromere associated network (CCAN), which is further divided into four groups (CENP-S/T/X/W; CENP-C/N/L; CENP-H/I/K/M; and CENP-O/P/Q/U/R). CCAN assembles on the centromere through CENP-A and provides a platform for assembling the outer kinetochore (Reviewed in: (Nagpal and Fukagawa 2016; Kops and Gassmann 2020)). Interestingly, artificial tethering of CENP-C and T onto the chromosomes at a non-centromeric site is sufficient for assembling a functional kinetochore (Hori et al. 2013; Gascoigne et al. 2011) (**Fig 1.3**).

1.2.2.2 OUTER KINETOCHORE

The core outer KT is made up of a 10-unit KMN (KNL1, Mis12 and NDC80) network. Mis12 complex is a rod-shaped, four-unit complex (Nnf1, Mis12, Dsn1 and Nsl1) that directly interacts with CENP-C at the centromeres (Screpanti et al. 2011; Przewloka et al. 2011) and recruits NDC80 and KNL1 complexes to the outer KT (Petrovic et al. 2010; Cheeseman et al. 2004) (**Fig 1.3**). NDC80 complex is also a rod-shaped, 4-unit complex (Hec1, Nuf2, Spc24 and Spc25). It directly binds to CENP-T at the inner KT (Nishino et al. 2013; Gascoigne et al. 2011) (**Fig 1.3**), thus, providing another point of interaction between the inner and outer KTs. Both NDC80 and KNL1 have MT-binding activity, but KT-MT attachments are mainly formed by the NDC80 complex (Cheeseman et al. 2006; J. G. DeLuca et al. 2006; Umbreit et al. 2012; Wei, Al-Bassam, and Harrison 2007; Bajaj et al. 2018) (**Fig 1.3**). KNL1 complex (KNL1, ZWINT), on the other hand, provides a platform for the assembly of spindle assembly checkpoint (SAC).

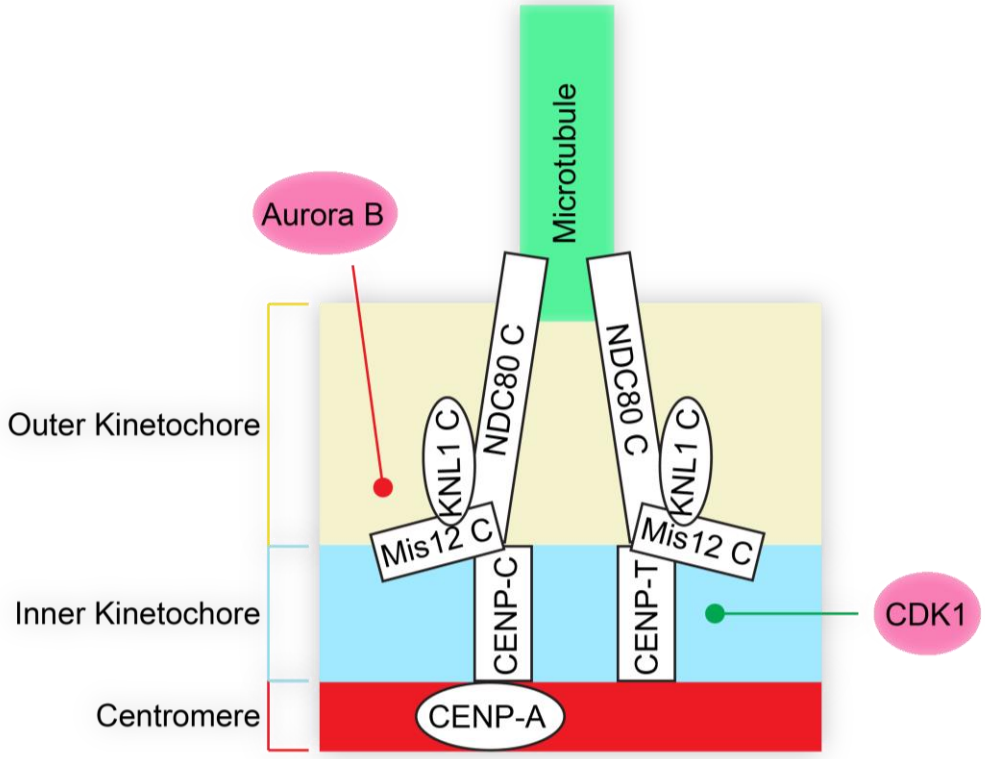

Fig 1.3 A simplistic view of mitotic kinetochore assembly. The deposition of CENP-A specifies the centromeric region of the chromosome (Red box). During mitosis, a 16-unit constitutive centromere associated network (CCAN) assembles on the centromere and forms the inner KT (blue box). CENP-T in the inner KT is phosphorylated by CDK1 kinase (green line). Then, the phosphorylated CENP-T recruits the NDC80 complex (NDC80 C). Alternatively, CENP-C in the inner-KT recruits the Mis12 complex (Mis12 C), and Mis12 C recruits NDC80 C and KNL1 complex (KNL1 C). The Mis12 C mediated NDC80 C recruitment is negatively regulated by Aurora B kinase (red line). The NDC80 C binds to the microtubules, and KNL1 C provides the platform for the assembly of the spindle assembly checkpoint.

The Mis12 and KNL1 complexes start to localize at the KTs during the S phase (Cheeseman et al. 2008; Gascoigne and Cheeseman 2013). However, the NDC80 complex cannot be recruited in S phase as it is extranuclear (Kim et al. 2010b; Gascoigne and Cheeseman 2013), thus, restricting the KT assembly before mitosis. Moreover, NDC80 recruitment at the KT is regulated by two kinases: Aurora B and CDK1. Aurora B kinase phosphorylates the Dsn1 subunit of Mis12 complex and inhibits Mis12-CENP-C binding (Welburn et al. 2010; Petrovic et al. 2016) and, thus, negatively regulates NDC80 recruitment at the KTs (**Fig 1.3**)**.** CDK1 phosphorylates CENP-T, and phospho CENP-T recruits the NDC80 complex at the KTs (Gascoigne et al. 2011) (**Fig 1.3**).

In summary, the inner KT assembles on the chromosomes and recruits the KMN network. The KMN network then forms direct attachments to the MTs and recruits other proteins to assemble the SAC.

Table 1.1. Comparison between human and yeast kinetochore.

	Human		Budding yeast
Inner kinetochore		-	CBF3 complex: Bdc10, Ctf13, Cep3, Skp1.
		CENP-A, CENP-B.	Ybp2, Cse4, Cbf1.
	CCAN	CENP-C	Mif2
		CENP-N, CENP-L.	Chl4, Iml3.
		CENP-O, CENP-P, CENP-Q, CENP-U, CENP-R.	COMA complex: Ctf19, Okp1, Mcm21, Ame1.
		CENP-H, CENP-I, CENP-K, CENP-M.	Ctf3: Mcm16, Ctf3, Mcm22.

		Human	Budding yeast
		CENP-S, CENP-T, CENP-X, CENP-W.	CNN1: Cnn1, Wlp1, Mhf1, Mhf2.
		-	Nkp1, Nkp2.
Outer kinetochore	KMN network	KNL1 complex: KNL1, ZWINT.	SPC105: Spc105, Kre28.
		Mis12 complex: Mis12, Dsn1, Nnf1, Nsl1.	MIND complex: Mtw1, Dsn1, Nnf1, Nsl1.
		NDC80 complex: Hec1, Nuf2, Spc24, Spc25.	NDC80 complex: Ndc80, Nuf2, Spc24, Spc25.
	SKA complex	SKA1, SKA2, SKA3.	DAM/DASH complex: Dam1, Duo1, Spc19, Spc34, Ask1, Dad1, Dad2, Dad3, Dad4, Hsk3.
	Astrin-SKAP complex	Astrin, SKAP, LC8, MYCBP.	-
	RZZ complex and related.	Rod, Zwilch, ZW10, Spindly, Dynein, Dynactin.	-
	Spindle Assembly checkpoint (SAC)	Mps1, Bub1, BubR1, Bub3, Mad1, Mad2, Cdc20, TRIP13, $p31^{comet}$.	Mps1, Bub1, Bub3, Mad1, Mad2, Mad3, Cdc20.
	Chromosome passenger complex (CPC)	Aurora B, INCENP, Survivin, Borealin.	Sli55, Bir1, Nbl1, Ipl1.
	Microtubule-associated proteins (MAPs)	CLASP1, CLASP2, XMAP215, EB1, EB2, CLIP-170, ChTOG.	Stu1, Stu2, Slk19, Blm1, Bik1.
	Motor proteins	Kinesin-8, Kinesin-14, Kinesin-5, BimC.	Kar3, Cin8, Kip2, Kip3, Kar9, Cik1.
	Kinases and phosphatases	CDK1, PLK1, PP1, PP2A, CDC14.	Cdc28, Glc7, Sds22, Pph21, Pph22, Cdc5.

1.2.3 HOW DO CELLS FORM KINETOCHORE-MICROTUBULE ATTACHMENTS?

In early mitosis, the very outer region of the KT (called the fibrous corona) expands over 100 nm and can be seen as a crescent-shaped structure under the microscope (Jokelainen 1967; Zirkle 1970; Bielek 1978; Roos 1973). Expansion of fibrous corona increases the area of possible contact with the MTs and, thus, facilitates the formation of KT-MT attachments. The expansion of fibrous corona requires an outer KT protein complex, the RZZ complex, and is regulated through at least four kinases: CDK1, Aurora B, PLK1 and MPS1 (Sacristan et al. 2018; Pereira et al. 2018; Rodriguez-Rodriguez et al. 2018; Ying et al. 2009; Wynne and Funabiki 2015).

The RZZ complex comprises ROD (Rough deal), Zwilch, and ZW10 (Zest-White 10) proteins. ZW10 binds to ZWINT at the outer KT, but this binding is not essential for the arrival of RZZ at the KTs (Kops et al. 2005; G. Zhang et al. 2015). Instead, the arrival of the RZZ complex at the KTs depends on KNL1 protein and Bub1 kinase (Silió, McAinsh, and Millar 2015; Caldas et al. 2015). Both KNL1 and Bub1 are essential components of the spindle assembly checkpoint (SAC); thus, RZZ establishes crosstalk between attachment and monitoring pathways. Biochemical analysis shows that the RZZ complex is present in a 2:2:2 ratio, and the two molecules of ROD run in an anti-parallel direction with β-propellors in their N-termini (Mosalaganti et al. 2017). ROD and Zwilch directly bind with Spindly protein (Kops et al. 2005; Gama et al. 2017), and together the complex can form a fibrous meshwork *in vitro* (Sacristan et al. 2018; Pereira et al. 2018; Gama et al. 2017).

In addition to forming fibrous corona, Spindly recruits dynein and dynactin proteins (Pereira et al. 2018; Gama et al. 2017). Dynein-dynactin is essential for robust cargo delivery towards the MT minus-ends (McKenney et al. 2014). Uncoupling of fibrous corona using a brief CDK1 inhibition in Nocodazole treated cells revealed that the fibrous corona, in addition to the RZZ-Spindly-Dynein-Dynactin, consists of at least Mad1-Mad2 checkpoint proteins and CENP-E and CENP-F MT plus-end motor proteins (Pereira et al. 2018; Sacristan et al. 2018).

1.2.3.1 LATERAL ATTACHMENTS

KTs are captured by the MTs using the classic "search and capture" pathway (Reviewed in: (Heald and Khodjakov 2015)). The MT plus-ends are continuously polymerizing and depolymerizing and, thus, "searching" for the KTs. For most KTs, the initial MT "capture" is at the lateral walls of the MTs (Itoh et al. 2018; Magidson et al. 2011; Kitajima, Ohsugi, and Ellenberg 2011; Merdes and De Mey 1990; Rieder and Alexander 1990; Kapoor et al. 2006; Tanaka et al. 2005; Barisic et al. 2014). At least two motor proteins drive lateral interactions: CENP-E (MT plus-end motor protein) and dynein (MT minus-end motor protein) (**Fig 1.4**). Usually, a single KT is first captured along the lateral wall of a single MT, and then dynein drives the chromosome pair rapidly (up to 1 µm/s) towards the spindle poles (Rieder and Alexander 1990; Vorozhko et al. 2008; Yang et al. 2007; Li et al. 2007) (**Fig 1.4**). Spindle poles are the area of high MT density, and as the KT moves towards the poles, it attaches to more MTs (~17 in humans) (Rieder 1981; McEwen et al. 2001). This leads to the formation of the prometaphase rosette, a ring-like chromosome arrangement, which is predicted to speed up the formation of spindle assembly in computer simulations (Itoh et al. 2018; Kitajima, Ohsugi, and Ellenberg 2011; Magidson et al. 2011).

Next, CENP-E directs the chromosome movement towards the MT plus-end ((Shrestha and Draviam 2013; Gudimchuk et al. 2013); **Fig 1.4**). CENP-E binds to protein phosphatase 1 (PP1), and this is required for efficient CENP-E-MT interaction (Kim et al. 2010a). Aurora-A kinase at the spindle poles disrupts CENP-E-PP1, thus detaching the chromosome (Kim et al. 2010). During mitosis, MT plus-ends are present at both the cortex and the equator. However, only the MTs at the equator are tyrosinated, a type of post-translational modification. *In vitro* experiments show that CENP-E guided transport is enhanced on tyrosinated MTs (Barisic et al. 2015). Thus, CENP-E preferably binds the chromosomes to MTs that are growing towards the center of the cell. *In vitro* experiments have shown that CENP-F can also track the MT plus-ends and coordinates mitochondrial movements in mitotic cells (Kanfer et al. 2017). However, whether CENP-F assists CENP-E during lateral attachments is not known.

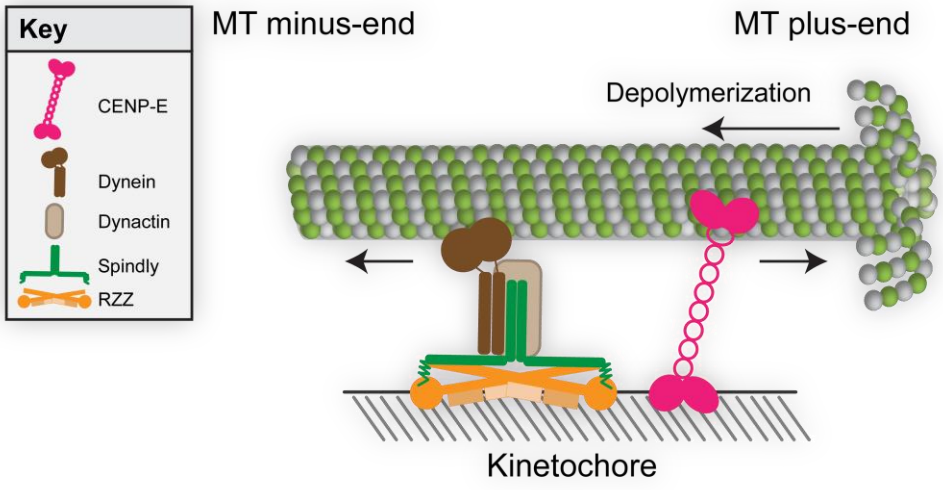

Fig 1.4 Lateral attachments. Upon entry into mitosis, the RZZ complex localizes at the KTs, and the outer KT expands. The RZZ complex recruits spindly protein, which then recruits Dynein-Dynactin proteins. Dynein, a MT minus-end motor protein, moves the chromosomes towards the spindle poles, an area of high MT density. Next, CENP-E, a MT plus-end motor protein, moves the chromosomes toward the MT plus-end. The chromosome movement towards the MT plus-ends is facilitated by MT depolymerization mediated by MCAK protein.

The movement of chromosomes to MT plus-end is also assisted by MT depolymerization (**Fig 1.4**). MT depolymerization shortens the length of the MTs and thus speeds up the delivery of chromosomes to MT plus ends. Moreover, MCAK, a MT depolymerizer, keeps the laterally attached chromosomes in mono-orientation (attached only at one KT; see **Fig 1.6**) (Shrestha and Draviam 2013). Computer simulations predicted that lateral attachments allow the KTs to undergo rapid rotational movements, minimizing merotelic attachments (attachment of both KTs to MTs emanating from the same pole) and speeds up the prometaphase (Magidson et al. 2015; Paul et al. 2009).

1.2.3.2 END-ON ATTACHMENTS

For robust KT-MT attachments, the lateral attachments must be converted into mature or end-on attachments. *In vitro* experiments show that CENP-E and NDC80 complex are sufficient for plus-end tracking and forming end-on attachments; however, NDC80 complex is required for stable attachments (Chakraborty et al. 2019). NDC80-MT binding is under negative regulation by Aurora-B, which reduces its affinity for the

MTs (Cheeseman et al. 2006; J. G. DeLuca et al. 2006). Moreover, the RZZ complex also negatively regulates the NDC80-MT attachments in early mitosis, but the gradual increase in dynein levels in later prometaphase releases this inhibition (Itoh et al. 2018; Cheerambathur et al. 2013).

In addition to the classic "search and capture" pathway, MTs can nucleate from the KTs. A fibrous corona localized complex Nup107-160 recruits the γ-TuRC to the KTs (Mishra et al. 2010). EM studies have shown short, randomly oriented MT stubs in the vicinity of the fibrous corona (Sikirzhytski et al. 2018). These MT stubs can bind to tubulin *in vitro* (Mitchison and Kirschner 1985; Sikirzhytski et al. 2018) and re-orient so that the plus ends are attached to the KTs in an end-on configuration (De Brabander et al. 1981; Witt, Ris, and Borisy 1980; Sikirzhytski et al. 2018). Correlative light electron microscopy shows that the initial KT-MT attachments in this pathway are also lateral but are rapidly converted to end-on attachments in a CENP-E dependent manner (Sikirzhytski et al. 2018).

1.2.3.3 STABILIZATION OF KT-MT ATTACHMENTS

In anaphase, sister chromatids are pulled apart and moved towards the spindle poles via MT depolymerization. *In vitro,* a single NDC80 complex cannot remain attached to the depolymerizing MTs unless the complex is artificially oligomerized (Schmidt et al. 2012; McIntosh et al. 2008; Powers et al. 2009; Volkov et al. 2018). Around 14 NDC80 complexes bind to a single MT, forming a cage-like structure around it (Suzuki, Badger, and Salmon 2015). This clustering of NDC80 requires binding with the SKA complex (Janczyk et al. 2017) (**Fig 1.5**). The SKA complex, made up of three proteins SKA1, 2 and 3, forms a ring-like structure around the MTs. Moreover, *in vitro* studies have shown that the SKA complex can bind both polymerizing and depolymerizing MTs (Monda et al. 2017; Schmidt et al. 2012). However, the SKA-NDC80 binding can happen in the absence of MTs (Veld et al. 2019). SKA binding to the MTs is preferentially near the MT plus-ends, and MT-SKA-NDC80 strengthens KT-MT attachments (Helgeson et al. 2018). The MT-SKA-NDC80 interaction is regulated by CDK1 kinase and PP1 and PP2A phosphatases (Cheerambathur et al. 2017; Janczyk et al. 2017; Sivakumar and Gorbsky 2017; Veld et al. 2019; Zhang et al. 2017).

The SKA complex is not sufficient for stabilizing KT-MT attachments. The Astrin-SKAP complex, which is present at the MTs throughout mitosis, arrives at the KTs only when end-on KT-MT attachments have formed (Shrestha and Draviam 2013; Shrestha et al. 2017; Kuhn and Dumont 2017). The Astrin-SKAP complex is a 4-unit complex comprising of Astrin, SKAP, dynein light chain LC8 and MYC binding protein (MYCBP). Like the NDC80 complex, the Astrin-SKAP complex is also rod-shaped and *in vitro* experiments show that the Astrin-SKAP complex synergistically binds to the MTs with the NDC80 complex (Kern, Wilson-Kubalek, and Cheeseman 2017) (**Fig 1.5**). Moreover, Astrin directly binds to the NDC80 complex ((Kern, Wilson-Kubalek, and Cheeseman 2017; Dunsch et al. 2011; Conti et al. 2019) Tamura PhD, Draviam Lab; unpublished data). Together the data suggest that the Astrin-SKAP complex can generate strong KT-MT attachments. Astrin-SKAP complex-mediated stabilization of KT-MT attachments is regulated by CDK1 and PLK1 kinases (Geraghty et al. 2021; Conti et al. 2020). Phosphatases regulate SKA complex-mediated KT-MT attachments, but whether phosphatases also regulate the Astrin-SKAP complex-mediated stabilization of KT-MT attachments is unknown.

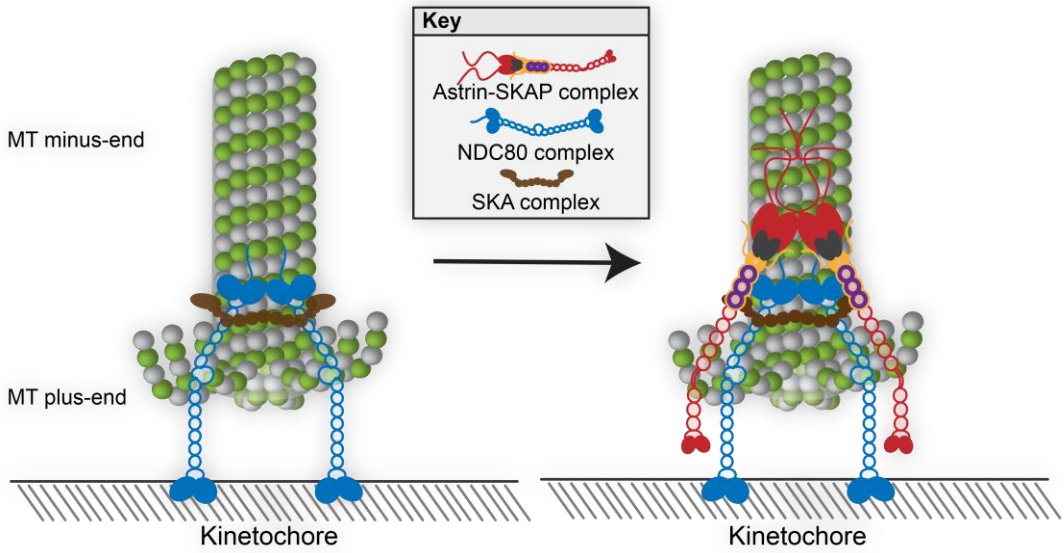

Fig 1.5 Stabilization of end-on attachments. The NDC80 complex converts the lateral KT-MT attachments to end-on attachments. Next, the SKA complex arrives and interacts with both the NDC80 complex and the MTs. The SKA-NDC80 interaction results in the NDC80 complex clustering around the MTs. Finally, the Astrin-SKAP complex arrives and binds to both the NDC80 complex and the MTs, resulting in the stabilization of KT-MT attachments. Once stable end-on attachments are formed, SAC is satisfied and anaphase is initiated.

The arrival of the Astrin-SKAP complex at the KTs positively correlates with the removal of the Mad1-Mad2 checkpoint proteins from the KTs (Kuhn and Dumont, 2017). The removal of the Mad1-Mad2 checkpoint proteins requires the RZZ complex (Barisic et al., 2010), the complex that forms the fibrous corona. The expanded fibrous corona compacts once end-on attachments are formed (Magidson et al., 2015; Sacristan et al., 2018), but whether this happens before or after Astrin arrival is not known.

In summary, the KT assembles at the start of mitosis. The outermost KT expands to form the fibrous corona with the help of the RZZ complex. Initially, the chromosomes are captured at the lateral side of the MTs with the help of CENP-E and dynein. Then, CENP-E and the NDC80 complex convert the lateral attachments to end-on attachments. The SKA complex stabilizes NDC80-MT attachments. Finally, the end-on KT-MT attachments are stabilized by the Astrin-SKAP complex; SAC is satisfied and fibrous corona gets compacted.

1.2.4 HOW DO CELLS ENSURE CORRECT KINETOCHORE-MICROTUBULE ATTACHMENTS ARE FORMED?

During chromosome segregation, sister chromatids are pulled apart by microtubule (MT) pulling forces acting on the kinetochores (KTs). To generate robust load-bearing at the KTs and to ensure only one sister chromatid goes to each daughter cell, each sister KT needs to be attached to the MTs emanating from the opposite spindle poles. This type of attachment is called bi-orientation or amphitelic attachment (**Fig 1.6**). There are three known types of erroneous attachments:

a) merotelic attachment-one KT attaches to MTs arising from both spindle poles

b) syntelic attachment-both sister KTs attach to MTs but on the same side of the spindle

c) monotelic attachment-only one sister KT attaches to the MTs.

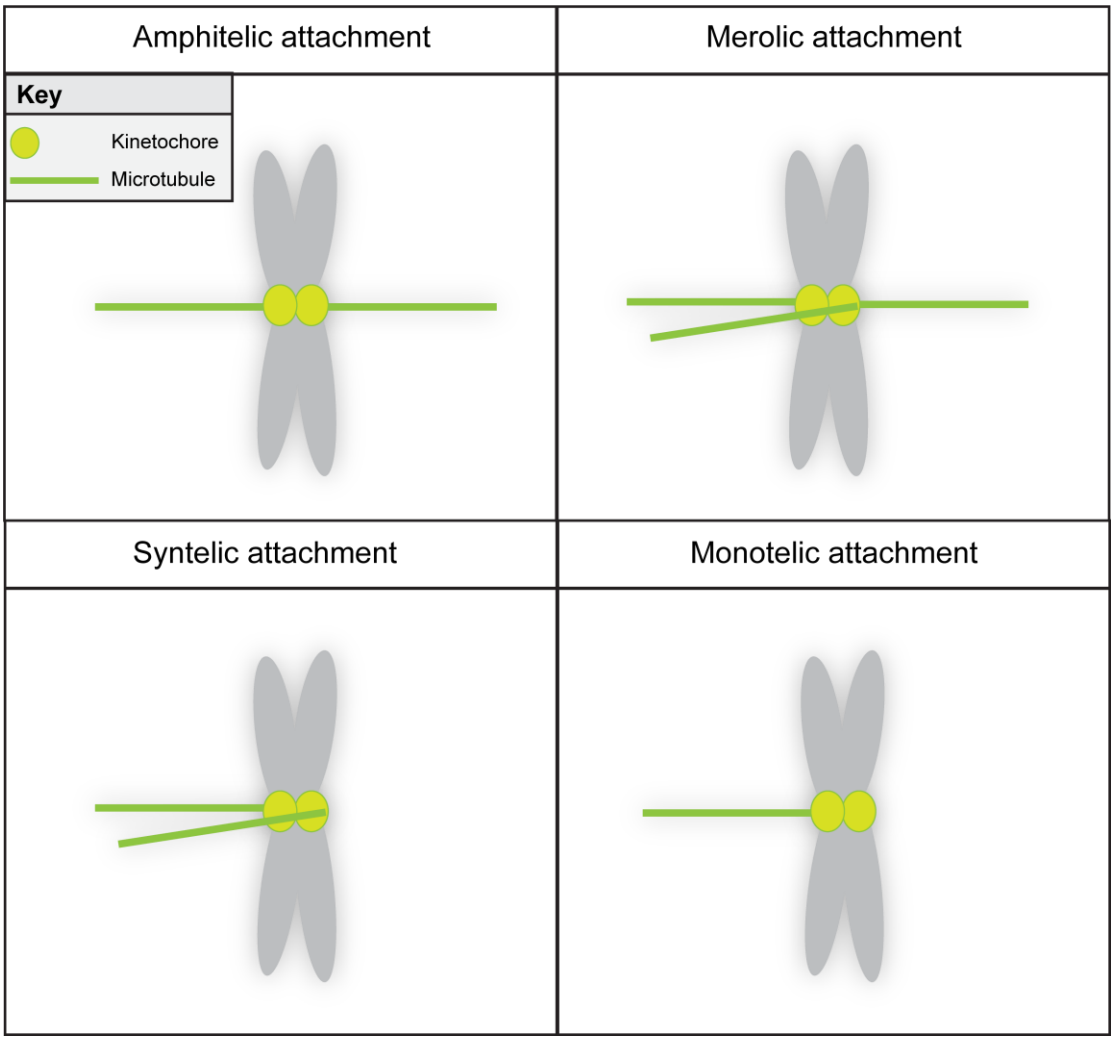

Fig 1.6 Types of kinetochore-microtubule attachments. Amphitelic attachment: each sister kinetochore attaches to microtubules emanating from the opposite spindle pole. Merotelic attachment: one sister kinetochore attaches to microtubules emanating from both spindle poles. Syntelic attachment: both sister kinetochores attach to microtubules emanating from the same spindle pole. Monotelic attachment: only one sister kinetochore is attached to microtubules.

Cells use the error correction pathway to correct erroneous attachments and the spindle assembly checkpoint (SAC) ensures anaphase does not start until all KT-MT attachments are correctly formed.

1.2.4.1 ERROR CORRECTION PATHWAY

MT pulling forces acting on the bioriented KTs increase the distance between sister centromeres (inter-centromeric stretch) and the distance between sister KTs (inter-KT stretch) (Waters et al. 1996; Maresca and Salmon 2009). Moreover, there is an outward stretching of the KT (intra-KT stretch) (Uchida et al. 2009; Maresca and

Salmon 2009) (**Fig 1.7**). Together, the stretching produces "tension," which is sensed by the chromosome passenger complex (CPC). CPC consists of INCENP, Borealin, Survivin, and Aurora B and localizes to the centromeres from prometaphase to metaphase (Honda, Körner, and Nigg 2003; Adams et al. 2001; Klein, Nigg, and Gruneberg 2006). Localization of Aurora B at the centromeres depends on CDK1 kinase (Hümmer and Mayer 2009; Tsukahara, Tanno, and Watanabe 2010). In the absence of "tension," Aurora B phosphorylates several substrates, including the NDC80 and SKA complex to inhibit KT-MT attachments and KNL1 to keep the spindle assembly checkpoint (SAC) active (Welburn et al. 2010; Cheeseman et al. 2006; Pinsky et al. 2006; Wang et al. 2008; DeLuca et al. 2006; Cimini et al. 2006; Guimaraes et al. 2008; Miller, Asbury, and Biggins 2016; Chan et al. 2012). The kinase activity of Aurora B forms a gradient centered at the centromere (Welburn et al. 2010; Liu et al. 2009; Krenn and Musacchio 2015; Samejima et al. 2015; Zaytsev et al. 2016; Wang, Ballister, and Lampson 2011). Once biorientation is achieved, an increase in inter-centromeric, inter-KT, and intra-KT distances physically separate Aurora B from its substrates. Interestingly, intra-KT stretching and not inter-centromeric stretching is essential for anaphase onset (Uchida et al. 2009; Maresca and Salmon 2009). Moreover, expression of an NDC80 mutant with all potential Aurora B sites converted to Alanine to mimic dephosphorylation results in cells entering anaphase even without correct attachments (Etemad, Kuijt, and Kops 2015; Tauchman, Boehm, and DeLuca 2015). Thus, the intra-KT stretching changes the KT structure in a way that directly or indirectly leads to NDC80 dephosphorylation, which satisfies the SAC.

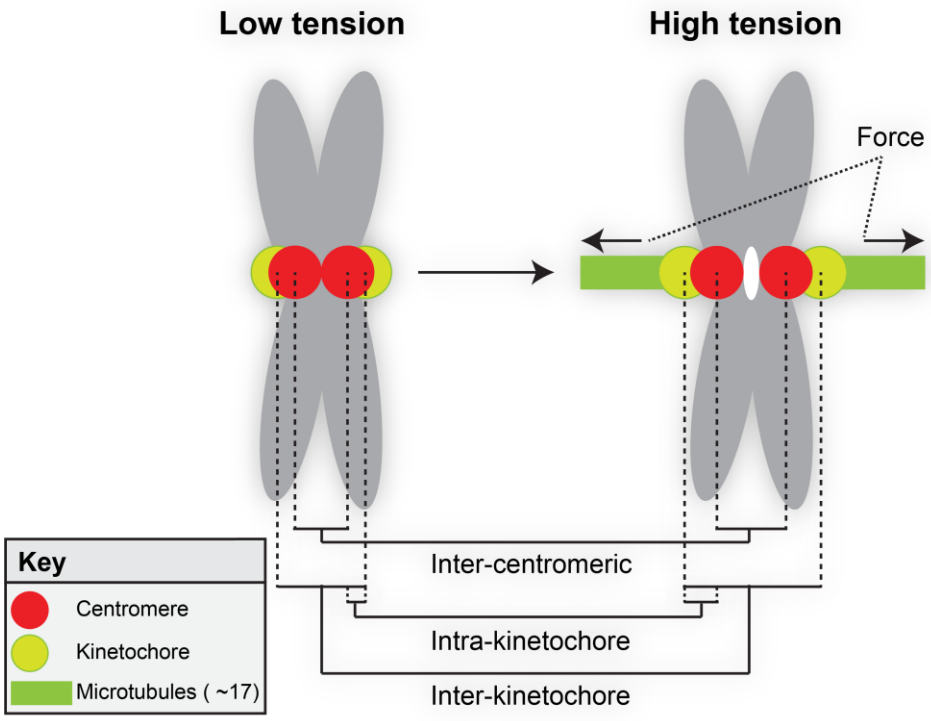

Fig 1.7 Schematic showing low and high tension states. In the absence of MT pulling forces, KTs are under "low tension". When MT pulling forces are applied, the inter-centromeric, inter-KT, and intra-KT distances increase and thus are now in "high tension" states. The intra-KT distances and not inter-KT and inter-centromeric distances satisfy the SAC, suggesting a change in the KT architecture is required for SAC satisfaction.

1.2.4.2 SPINDLE ASSEMBLY CHECKPOINT

Spindle assembly checkpoint (SAC) is a surveillance system of the cell that monitors the KT-MT attachments. When KTs are unattached (early prometaphase), SAC generates a "wait signal," which stays "ON" till the anaphase onset. At the start of mitosis, CDK1-Cyclin-B phosphorylates MPS1 kinase, and the phosphorylated MPS1 is recruited to the KTs (Hayward et al. 2019). At the KTs, MPS1 kinase directly interacts with the NDC80 complex and competes with MTs for its KT localization (Ji, Gao, and Yu 2015; Hiruma et al. 2015; Dou et al. 2015), thus, ensuring that it is recruited only to the unattached KTs. Moreover, MPS1 recruitment is regulated by Aurora B, a kinase that destabilizes NDC80-KT attachments (DeLuca et al. 2006; Welburn et al. 2010; Santaguida et al. 2011; Nijenhuis et al. 2013). However, according to Ji et al. (Ji, Gao, and Yu 2015), phosphorylation of NDC80 can also directly recruit

MPS1. Thus, the SAC crosstalks with both KT-MT attachment and error correction pathways.

MPS1 kinase activates the SAC through KNL1-Bub3-Bub1 (KBB) pathway. First, MPS1 phosphorylates the KNL1 protein at the "MELT" motifs, creating docking sites for Bub3 protein (London et al. 2012; Yamagishi et al. 2014; G. Zhang, Lischetti, and Nilsson 2014) (**Fig 1.8**). Then, KNL1 recruits the Bub proteins. Bub3 is in complex with either BubR1 pseudo kinase or Bub1 kinase, and KNL1 can recruit both complexes (Yamagishi et al. 2014; Shepperd et al. 2012; London et al. 2012; Primorac et al. 2013) (**Fig 1.8**). However, BubR1-Bub3 recruitment is mainly through heterodimerization of BubR1 with Bub1(Zhang et al., 2015; Overlack et al., 2015). Moreover, the BubR1 recruitment at the KTs is regulated by both KT-MT attachment and the error correction pathways. Aurora B kinase phosphorylates KNL1, which positively regulates BubR1 recruitment (Welburn et al. 2010; Nasa et al. 2018) (**Fig 1.8**). Moreover, CENP-E, involved in initial KT-MT attachments, binds to BubR1 in the absence of MT binding (Mao, Desai, and Cleveland 2005). CENP-E-BubR1 binding keeps the SAC active (Mao, Desai, and Cleveland 2005) (**Fig 1.8**).

CDK1 kinase phosphorylates Bub1 to generate a "pseudo-MELT" motif on Bub1 that allows phosphorylation by MPS1 (Zhang et al. 2017; Ji et al. 2017). The MPS1 phosphorylated Bub1 binds to Mad1 and recruits the Mad1-Mad2 complex to the KTs (Faesen et al. 2017; Qian et al. 2017; Zhang et al. 2017; Ji et al. 2017) (**Fig 1.8**). The Mad1-Mad2 complex can also arrive at the KTs through the RZZ complex, the protein complex that forms the expanded fibrous corona (Silió, McAinsh, and Millar 2015; Caldas et al. 2015) (**Fig 1.8**). Mad2 is a core component of the mitotic checkpoint complex (MCC) which, in addition to Mad2, consists of BubR1-Mad3, Bub3, and Cdc20. Once at the unattached KTs, Mad2 undergoes a conformational change from an open to a closed-form in an MPS1 and Mad1 dependent manner, leading to the inhibition of the anaphase-promoting complex/cyclosomes (APC/C) (Faesen et al. 2017; Ji et al. 2017). APC/C remains inhibited till all chromosomes are correctly attached.

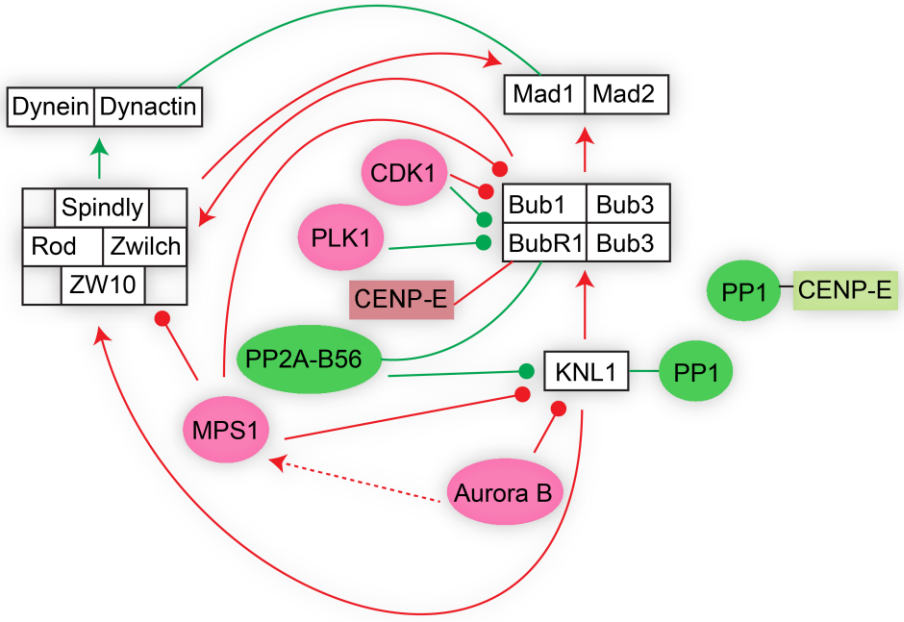

Fig 1.8 Spindle Assembly Checkpoint. The KNL1 protein, a core KT protein, recruits the Bub proteins (Bub1, BubR1 and Bub3). The Bub proteins then recruit the Mad1-Mad2 proteins and the SAC is activated. The Mad1-Mad2 proteins are also recruited by the RZZ complex (ROD, Zwilch and ZW10). Recruitment of checkpoint proteins is positively regulated by CDK1, MPS1 and Aurora B kinase (red knobs) and negatively regulated by CDK1 kinase, PLK1 kinase, PP1 phosphatase and PP2A-B56 phosphatase (green knobs). CENP-E, a KT-MT attachment protein, positively regulates the SAC by binding to BubR1 in the absence of KT-MT attachments (Red box) and negatively regulates by recruiting PP1 phosphatase in the presence of KT-MT attachments (Green box). When correct KT-MT attachments are formed, dynein motor protein removes Mad1-Mad2 proteins. Red lines indicate positive regulation and green lines indicate negative regulation of SAC. Kinases are in pink and phosphatases are in green.

Silencing of SAC requires dephosphorylation by two phosphatases PP1 and PP2A-B56. CDK1 mediated BubR1 phosphorylation generates a PLK1 docking site, and Plk1 mediated phospo BubR1 recruits PP2A-B56 (Suijkerbuijk et al., 2012; Kruse et al., 2013) (**Fig 1.8**). Moreover, CENP-E targets PP1 phosphatase to the KTs (Kim et al., 2010) (**Fig 1.8**). PP2A-B56 dephosphorylates Aurora B mediated phosphorylation at KNL1, allowing the binding of KNL1 to PP1 phosphatase (Suijkerbuijk et al., 2012; Xu et al., 2013; Espert et al., 2014; G. Zhang et al., 2017) (**Fig 1.8**). The tipping of balance towards dephosphorylation at the end of metaphase leads to the inhibition of SAC. Mad1-Mad2 checkpoint proteins leave the KTs in an RZZ complex-dependent manner (Barisic et al. 2010), probably through dynein motor protein (**Fig 1.8**). However, the checkpoint stays sensitive to KT-MT detachments for some time after the

initial silencing and can be reactivated (Clute and Pines 1999; Dick and Gerlich 2013; Vázquez-Novelle et al. 2014). This gives the cells an additional window period for correcting KT-MT attachments to ensure chromosomes segregate accurately.

1.2.4.3 CONSEQUENCES OF CHROMOSOME SEGREGATION ERRORS

In the presence of monotelic and syntelic attachments, SAC does not get silenced, leading to prolonged mitosis. Several studies have shown that prolonged mitosis can lead to the acquisition of DNA damage (Lanni and Jacks 1998; Quignon et al. 2007; Rogakou et al. 1998; Uetake and Sluder 2010; Crasta et al. 2012a; Hayashi et al. 2012; Orth et al. 2012). However, the SAC does not recognize merotelic attachments. In this case, the cell will proceed to anaphase and lead to the generation of lagging chromosomes. Most lagging chromosomes will go to the right daughter cell (Cimini et al. 2001; Cimini, Cameron, and Salmon 2004; Thompson and Compton 2011). However, they may go into the wrong daughter cell leading to an unequal distribution of chromosomes - called numerical aneuploidy (Thompson and Compton 2011). Moreover, chromosomes may get damaged during cytokinesis. In cytokinesis, the cytoplasm is divided by an indentation of the cell membrane called the cytokinetic furrow. The lagging chromosomes can get stuck in the cytokinetic furrow and acquire structural rearrangements - called structural aneuploidy (Janssen et al. 2011; Soto et al. 2017; Santaguida et al. 2017; Hoffelder et al. 2004). Moreover, a nuclear envelope in the daughter cell may form before the lagging chromosome could arrive. These late arrivals form small nuclei called micronuclei, which may or may not join the primary nucleus. Micronuclei have a defective nuclear envelope and dysregulated nuclear envelope repair, leading to dysregulated nucleo-cytoplasmic transport, DNA replication and DNA damage repair (Crasta et al. 2012; Hatch et al. 2013; Zhang et al. 2015; Hart, Adams, and Draviam 2021). Hence, they may accumulate DNA damage or even get fragmented in subsequent cell divisions (Crasta et al. 2012; Hatch et al. 2013). Fragmentation may happen in a single event and the fragments may align randomly (chromothripsis), leading to structural aneuploidy (Ly et al. 2017; Zhang et al. 2015; Stephens et al. 2011).

In summary, SAC is activated at the start of mitosis, which generates a "wait" signal. The error correction pathway destabilizes incorrect KT-MT attachments.

Together, the SAC and error correction pathway ensures that chromosome segregation does not start before all KT-MT are attached correctly. Erroneous KT-MT attachments, if not corrected, can lead to the acquisition of DNA damage and aneuploidy.

1.3 CHROMOSOME SEGREGATION ERRORS AND DISEASE

Mitosis is a tightly regulated process, but mistakes are still made. On average, a human cell produces an estimated 1-10 point mutations (single base changes) in each daughter cell's genome every cycle (Reviewed in: (Lichtenstein 2018)). A newborn can carry over 120, and a 15-year-old can have 100-1000 point mutations in the coding genes alone, which is 1-2% of the genome (Reviewed in: (Fernández, Torres, and Real 2016)). In addition to point mutations, cell division errors can result in structural rearrangements such as deletions, insertions, and whole chromosome gain/loss, but these are less frequent. However, not every change in the genome has a functional consequence (phenotype). A base change can still code the same amino acid (synonymous mutation) or changes the amino acid (missense mutation) but does not impact the protein structure and function. On the other hand, structural rearrangements are more likely to have a phenotype (Collins et al. 2017), possibly because a larger area is changed. Genome-wide association studies (GWAS) of over 100,000 phenotypes suggest that only 10% of the genome changes manifest phenotypically (Leslie, O'Donnell, and Johnson 2014). Genome changes are part of normal evolution and are responsible for variations between individuals. Rarely, these variations can cause miscarriages, developmental disorders, and cancer.

1.3.1 HUMAN GENETIC ANEUPLOIDY DISORDERS

Chromosome segregation errors can result in cells with an abnormal number of chromosomes or aneuploid. Except for monosomy X, monosomies (loss of one chromosome) are embryonically lethal owing to insufficient protein expression. Trisomies (having an extra chromosome) occur in at least 4% of human pregnancies (Hassold and Jacobs 1984). Some trisomies such as trisomy 13 (Patau syndrome), 18 (Edward Syndrome), 21 (Down syndrome), X, and Y result in live birth owing to the small number of genes in these chromosomes. However, most trisomies result in organ

malformation, predispose to cancer, and reduce life expectancy (Reviewed in: (Akutsu et al. 2020)).

1.3.2 PRIMARY MICROCEPHALY

Autosomal recessive primary microcephaly (MCPH) is a rare disorder characterized by a reduction of head circumference (occipitofrontal diameter) >2 standard deviations below the mean for age, birth, and ethnicity (Reviewed in: (Jean, Stuart, and Tarailo-Graovac 2020). Incidence of MCPH is between 1 in 30,000 and 1 in 2,000,000 in non-consanguineous population, but increases to 1 in 10,000 (Northern Pakistan) where consanguineous marriages are common ((Komai, Kishimoto, and Ozaki 1955; Tolmie et al. 1987; Bosch 1958) Reviewed in: (Cox et al. 2006; Woods, Bond, and Enard 2005). There are 27 MCPH genes listed on Online Mendelian Inheritance in Man (OMIM), and 14 of these genes were identified as the cause of microcephaly in families in Northern Pakistan. The first MCPH genes discovered were associated with centrosomes - involved in spindle formation and orientation and, hence, MCPH was considered a "centriolopathy". In early neurogenesis, neural progenitor cells favor symmetric cell divisions, whereas asymmetric cell divisions are favored in late neurogenesis (Reviewed in: (Jean, Stuart, and Tarailo-Graovac 2020; Jayaraman, Bae, and Walsh 2018). This sequence of events is essential for generating a pool of neuronal progenitor cells early on, neuronal cell differentiation and maintaining the ratio of progenitor and differentiated neuronal cells, ultimately affecting the size and function of the brain (Reviewed in: (Jean, Stuart, and Tarailo-Graovac 2020; Jayaraman, Bae, and Walsh 2018). Later research has identified genes involved in DNA transcription and replication, chromosome condensation, kinetochore-microtubule attachment, spindle assembly checkpoint, cytokinesis, cell cycle regulation, DNA damage response and metabolism as causes of MCPH, suggesting other mechanisms may be involved in this disease. Here, I will only discuss kinetochore genes associated with microcephaly and how they may cause MCPH.

MCPH4 (MIM: 604321): CASC5 (encodes KNL1 protein) was the first kinetochore (KT) gene to be implicated in MCPH. KNL1 p.M2041I variant was identified as the cause of microcephaly in three consanguineous Moroccan families and one consanguineous Algerian family with common ancestry (Jamieson et al., 1999;

Genin et al., 2012). All affected individuals presented with reduced head size (-4 to -7 SD) and intellectual disability, and some had developmental delay. Another KNL1 variant p.Met2225Ilefs*7 was identified as the cause of microcephaly in a consanguineous Pakistani family (Szczepanski et al. 2016). The affected individuals were between 22 to 53 years of age with normal height but had reduced head size (-13 and -17 SD) and intellectual disability (Szczepanski et al. 2016). Lastly, a KNL1 compound heterozygous *de novo* frameshift and maternally inherited missense variation was identified in an African American child with microcephaly who had reduced head size (-4.88 SD) at 17 months of age but achieved normal milestones (Zarate et al., 2016).

KNL1 is an essential gene required for assembling spindle assembly checkpoint (SAC), a surveillance system of the cell that monitors KT-microtubule (MT) attachments (see **section 1.2.5.2**). mRNA and protein expression studies in patient-derived primary fibroblast and lymphoblastoid cell lines (LCL) of KNL1 p.Met2225Ilefs*7 variant show that the variation affects an intronic splicing site resulting in skipping of exon 25 (Szczepanski et al. 2016). Moreover, protein expression studies in primary fibroblast and LCL show reduced expression of KNL1 protein (Szczepanski et al. 2016). The reduced expression may be due to the degradation of mRNA by nonsense-mediated decay (NMD), a surveillance pathway in gene expression. Using an engineered human embryonic stem cell (hESC) line and CRISPR technology, Javed et al. (Javed et al., 2018) show that the KNL1 p.M2041I variant also affects splicing. The variation converts an exonic splicing enhancer site to an exonic splicing silencer site and results in skipping of exon 18 (Javed et al. 2018). They further show that brain-specific phenotype is due to high expression of an inhibitory splicing protein heterogeneous nuclear ribonucleoprotein A1 (HNRNPA1) in neural progenitors, which reduces KNL1 protein levels specifically in neural progenitors (Javed et al., 2018).

Immunofluorescence studies on KNL1 p.M2041I variant in hESC cell line show a reduced KT localization, whereas KNL1 p.Met2225Ilefs*7 variant in primary fibroblasts and LCL show an impaired KT localization with off-target signals (Javed et al., 2018; Szczepanski et al., 2016), possibly due to protein misfolding. Further,

expression of the truncated KNL1 p.M2041I variant results in a checkpoint-dependent increase in cell death and reduced neuronal specialization (Szczepanski et al. 2016). Expression of truncated KNL1 p.Met2225Ilefs*7 variant show deformed nuclei, presence of micronuclei, and DNA damage (elevated γ-H2AX and 53bp1) (Javed et al. 2018). Together, the data suggest that the expression of MCPH KNL1 variants results in chromosome segregation defects, DNA damage, and increased apoptosis. Interestingly, CASC5$^{-/-}$ Zebrafish larvae show severe microcephaly phenotype detectable at 3rd-day post fertilization (dpf) before dying at 5-6 dpf (Duerinckx et al. 2020).

MCPH13 (MIM: 616051): A compound heterozygous CENP-E p.D933N and p.K1355E variation (derived from each parent) was identified as the cause of microcephaly in two siblings born of unrelated parents of European descent (Mirzaa et al. 2014). The children (3-5 years of age) had reduced head size (-7 to -9 SD), intellectual disability, and developmental delay (Mirzaa et al. 2014). The phenotype appeared to be more severe in the male child who also had restrictive cardiomyopathy (rigid heart walls) and skeletal deformations and died at the age of 8 (Mirzaa et al. 2014).

Protein expression studies on patient-derived lymphoblastoid cell lines (LCL) show that the CENP-E variant does not affect total protein levels (Mirzaa et al. 2014). However, immunofluorescence studies of HeLa FRT/TO cells expressing CENP-E double mutants show reduced kinetochore (KT) localization and increased incidence of polar chromosomes and abnormal spindles (Mirzaa et al. 2014). CENP-E, a motor protein, is required for moving chromosomes towards the MT plus-ends, which may explain the presence of polar chromosomes (see **section 1.2.4.1**). Moreover, a recent study has shown that large chromosomes are more vulnerable to chromosome congression defects in CENP-E inhibited cells (Tovini and McClelland 2019). Interestingly, the double-mutant phenotype was also observed in cells expressing single mutants (Mirzaa et al. 2014). The parents of affected siblings carry a single variation but appear healthy, suggesting that heterozygous cells only produce normal copies.

Colcemid-treated LCL cells fail to phosphorylate BubR1 kinase, required for spindle assembly checkpoint (SAC) signaling (see **section 1.2.5.2**), consistent with

delayed mitosis in live-cell imaging experiments (Mirzaa et al. 2014). Moreover, the cells display a high incidence of lagging chromosomes and diploid cells, often with different nuclear sizes (Mirzaa et al. 2014). Different nuclear sizes in diploid cells may suggest differences in chromosome numbers, hence, aneuploidy. Studies in the Draviam lab show that CENP-E inhibition produces multinuclear cells with elevated DNA damage in cultured cells (Hart, Adams, and Draviam 2021). Collectively, the data indicate that CENP-E compound heterozygous p.D933N and p.K1355E variation impairs chromosome congression and SAC signaling leading to aneuploidy and DNA damage.

DYNC1I2: Three Dynein Cytoplasmic 1 Intermediate Chain 2 (DYNC1I2) variants were identified as the cause of microcephaly in one family from Northern Pakistan and two families from Europe (Ansar et al. 2019). All patients presented with similar clinical features: reduced head size, developmental delay, and facial dysmorphism. DYNC1I2 is part of the cytoplasmic dynein-1 complex, a multiunit motor complex, that moves towards the microtubule minus-ends (Pfister et al. 2006). One of the DYNC1I2 variants-p.T247C, caused microcephaly in Zebrafish by disrupting the mitotic spindle and increasing apoptosis (Ansar et al. 2019).

SPAG5/Astrin: A compound heterozygous sperm-associated antigen-5 (SPAG5) *de novo* frameshift Lys409Profs*19 and a maternally inherited p.G1063G variant was identified as the cause of microcephaly in a patient from Europe (Boonsawat et al. 2019). The patient presented with reduced head size, intellectual disability, and developmental delay (Boonsawat et al. 2019). mRNA studies from patient-derived fibroblasts show deletion of 11 exonic bp resulting in a predicted p.G1064E*3, but the variants undergo nonsense-mediated decay (NMD) and are not detected in protein expression studies (Boonsawat et al. 2019). SPAG5 encodes Astrin protein which is detected as a doublet in HeLa cells and is required to stabilize kinetochore-microtubule attachments (see **section 1.2.4.3 and 1.4**). Protein expression studies from patient-derived fibroblasts show reduced expression of both Astrin isoforms. However, immunofluorescence studies show normal Astrin localization and normal cell cycle progression. The KNL1 variant also reduced KNL1 expression, but

altered splicing resulting in the deletion of exon 18 in neuronal cells caused the brain-specific phenotype (see above). A similar mechanism may be in play in this patient.

1.3.3 MOSAIC VARIEGATED ANEUPLOIDY

As discussed earlier, segregation errors result in DNA changes; however, every cell will not gain the exact change resulting in more than one genetically distinct cell line in an organism or mosaicism. Mosaic variegated aneuploidy (MVA) is an autosomal recessive syndrome characterized by mosaic aneuploidies, predominantly trisomies and monosomies (Warburton et al. 1991; Hanks et al. 2004). Affected individuals present with severe intrauterine growth retardation, developmental delay, microcephaly, mental retardation, eye anomalies, and other physical abnormalities (Tolmie et al. 1988; Papi et al. 1989; K. Miller et al. 1990; Warburton et al. 1991; Tadashi Kajii et al. 1998; Flejter et al. 1998; Cho et al. 2015; Scheres et al. 1986; Unteregger, Scheres, and J. 1987). Furthermore, these individuals are at an elevated risk of developing cancer, including rhabdomyosarcoma, Wilm's tumor, and leukemia (Limwongse et al. 1999; Kawame et al. 1999; Plaja et al. 2001; T Kajii et al. 2001; Méhes, Kajtár, and Kosztolányi 2002; Jacquemont et al. 2002; Callier et al. 2005; Yost et al. 2017). MVA syndrome has been linked with variations in Bub1B (MVA-1; MIM: 257300) (Rio Frio et al. 2010; Hanks et al. 2004; Matsuura et al. 2006), CEP57 (MVA-2; MIM: 614114) (Snape et al. 2011; García-Castillo et al. 2008; Pinson et al. 2014) and TRIP13 (MVA-3; MIM: 617598) (Yost et al. 2017) genes, all of which are involved in cell division.

MVA-1, the most common form of MVA, is caused by homozygous or compound heterozygous variations in Bub1B gene (encodes BubR1 kinase), essential for robust spindle assembly checkpoint (SAC; see **section 1.2.5.2**). Studies from MVA-1 patient-derived cells show checkpoint deficiency, chromosome alignment defects, and an increased number of cells with micronuclei (Matsuura et al. 2006; Suijkerbuijk et al. 2010). Kops and colleagues showed that MVA-1 variations result in a 2-6 fold decrease in BubR1 protein levels, and the resulting defects can be rescued upon re-expression of BubR1(Suijkerbuijk et al. 2010). Moreover, mice with conditional reduction in BubR1 protein levels in the developing cortex result in checkpoint

insufficiency and massive apoptosis in neural progenitor cells, causing microcephaly (Simmons et al., 2019).

Multisite phosphorylation in a highly conserved domain (665–682 a.a.) very close to the kinase domain of BubR1, called Kinetochore Attachment Regulatory Domain (KARD), leads to recruitment of PP2A-B56 phosphatase to KTs (Suijkerbuijk et al., 2012; Kruse et al., 2013; Xu et al., 2013). PP2A phosphatase is a major phosphatase at the kinetochore-microtubule interface and is involved in the dephosphorylation of various mitotic proteins (See **section 1.2.1 and 1.2.5.2**). In fact, inhibition of Aurora B kinase, part of the error correction pathway (see **section 1.2.5.1**), has been shown to rescue the chromosome segregation defects observed in cells expressing BubR1 with defective PP2A-B56 binding (Suijkerbuijk et al., 2012; Kruse et al., 2013; Xu et al., 2013). Furthermore, Xu et al. (Xu et al. 2013) showed that artificial targeting of B56-PP2A to outer kinetochores in MVA-1 fibroblasts rescues MVA-1 phenotype.

Sieben et al. (Sieben et al. 2020) showed that usually, a reduction of 40–90% in BubR1 protein levels results in tumor predisposition, whereas a reduction of > 90% results in early postnatal lethality. However, not all models in their study fit these criteria (Sieben et al. 2020). Patients with MVA-1 display varying levels of aneuploid cells (10-87%) and levels of BubR1 protein do not correlate with the severity of the disease (Unteregger et al. 1987; Scheres et al. 1986; Warburton et al. 1991; Kajii et al. 2001; Frio et al. 2010), suggesting there are other mechanisms at play,

In $Bub^{-/-}$ mice, more than 50% of cells are aneuploid soon after implantation, results in MVA, and the embryos die between age 7.5 to 13.5 days (Schmid et al., 2014). Moreover, Bub1B variations are found in human recurrent pregnancy loss (RPL) embryos and may cause miscarriages (Schmid et al. 2014).

In summary, genomic variations in checkpoint protein BubR1 can cause pregnancy loss, developmental disorders, and cancer.

1.3.4 CANCER

German zoologist Theodor Boveri first described the effects of aneuploidy in sea urchin embryos undergoing abnormal mitotic divisions (Manchester 1995). He

proposed that an abnormal number of chromosomes may promote cancer (Manchester 1995). BubR1 is perhaps the best example of a kinetochore (KT) gene directly linked to increasing cancer predisposition (see **section 1.3.3**). Approximately 60-70% of cancer cells are aneuploid (Reviewed in: (Weaver and Cleveland 2006)), and most cancers have lagging chromosomes in the rates of 10% and 60% during anaphase (Ganem, Godinho, and Pellman 2009; Silkworth et al. 2009). Increased chromosome missegregation rate or chromosomal instability (CIN) is a hallmark of cancer (Hanahan et al. 2011). Using the lagging chromosome rate and considering $1cm^3$ of tumor tissue has approximately 109 cells, Nicholson and Cimini (Reviewed in: (Nicholson and Cimini 2015)) propose that chromosome missegregation may produce 100,000,000–600,000,000 cells with different karyotypes, structural and numerical changes in the chromosomes. Furthermore, studies have shown that these karyotypes are not entirely random, and specific karyotypic patterns are present in different cancer types and tissues of origin (Ozery-Flato et al. 2011; Gebhart and Liehr 2000). This is fortunate as instead of blindly treating all cancers with the same drug, therapies can be targeted to karyotypic patterns.

Personalized therapy has revolutionized cancer therapy in the last decade. Cancer is uncontrolled cell division, and many of the mitotic genes are dysregulated or dysfunctional in cancers. Moreover, many mitotic proteins are exclusive to cell division, meaning quiescent cells are protected. Among mitotic proteins, drugs targeting microtubules were the first to show pharmacological success (Rowinsky and Donehower 1995) and still are widely used in clinics. However, microtubules have functions outside the cell cycle, do not differentiate between a tumor and a normal cell, and cause severe toxicities (Reviewed in: (Gornstein and Schwarz 2014). CDK inhibitors show some success in hematological cancers but not in solid cancers, possibly due to high proliferation rates in blood cells (Reviewed in: (Dominguez-Brauer et al. 2015; Chan, Koh, and Li 2012)). Aurora kinases and PLK kinases also show some response in hematological malignancies but remain mostly ineffective in solid cancers (Reviewed in: (Dominguez-Brauer et al. 2015; Chan, Koh, and Li 2012)). Anti-mitotic drugs only have a narrow window of opportunity that is the cell division-shortest phase of the cell cycle. The success of drugs targeting microtubules has been attributed to a longer half-life. New drugs with a longer half-life or targeting protein with non-mitotic

functions may increase efficacy. In addition to drugs targeting the microtubules, CDKs, Aurora kinases and Plk1 kinase, other targets currently being exploited include Eg5, kinesin-5, CENP-E, MPS1 kinase, mitotic phosphatases, APC/C-Cdc20, Proteasome. Moreover, work is ongoing to identify biomarkers for cancer and develop therapies against them. One such biomarker is Astrin, whose depletion using miRNA reduces cell proliferation and migration in cancer (Zhang et al. 2016; Yang et al. 2018; Yang et al. 2020; Song et al. 2018).

1.4 ASTRIN

SPAG5 gene (encodes Astrin protein) is upregulated in many cancers, and this upregulation is associated with poor prognosis (Yuan et al. 2014; Abdel-Fatah et al. 2016; Zhang et al. 2016; Zhang et al. 2020; Liu et al. 2018; Liu et al. 2019). Moreover, suppressing SPAG5 gene expression by targeting SPAG5 mRNA using miRNAs causes cell cycle arrest and suppression of cell proliferation and migration in cancer (Zhang et al. 2016; Yang et al. 2018; Yang et al. 2020; Song et al. 2018), suggesting that it may be targeted for cancer treatment. Moreover, a compound heterozygous Astrin variation was identified as the cause of primary microcephaly in a genetic screen of children with microcephaly (Boonsawat et al. 2019). The child presented with reduced head size and intellectual disability (Boonsawat et al. 2019), suggesting the variation reduced the number of brain cells (see **section 1.3.2**). In cultured cells, Astrin depletion results in pre-mature centrosome separation, unstable kinetochore (KT)-microtubule (MT) attachments, loss of sister chromatid cohesion, and a checkpoint-dependent mitotic delay with a significant cell population arrested in mitosis (Thein et al. 2007; Schmidt et al. 2010; Gruber et al. 2002). Together, the data suggest that dysregulated expression or function of Astrin has roles in cancer and developmental disorders.

Astrin and its binding partner SKAP (small kinetochore-associated protein) were first identified from screens performed on human mitotic cells (Mack and Compton 2001). Astrin is an 1193 a.a. long protein with an unstructured N-terminal region and two coiled-coil regions joined by a linker region, and when visualized under electron microscopy, it looks like a ~80 nm lollypop like structure (Gruber et al. 2002). On an SDS-PAGE gel, Astrin migrates as a doublet with an about 20-40 kDa difference,

and mass spectrometry analysis shows that the lower band of Astrin lacks the N-terminal region of Astrin (Thein 2008), raising the possibility that Astrin exists as two isoforms in humans. However, whether the two isoforms are expressed differently in different tissues or have varying roles at various cell cycle stages is not known. On the other hand, SKAP is only 316 a.a. long but has an unstructured N-terminal region and two coil-coiled regions (Friese et al. 2016). Interestingly, SKAP also has two isoforms- a long germline isoform that is not expressed in somatic cells and a short isoform sufficient for its mitotic function (Kern et al. 2016; Vranesic et al. 2016).

Astrin localizes to the centrosomes throughout the cell cycle (Kodani et al. 2015). During S and G2 phase, the C-terminus of Astrin directly interacts with Ninein, a centrosomal protein, and this interaction is required for Astrin's localization at the centrosomes (Cheng et al. 2007). Moreover, Astrin interacts with centrosomal proteins CEP72 and CDK5RAP2 and is required for centrosomal localization of CDK5RAP2 (Kodani et al. 2015). CDK5RAP2 is an MCPH associated protein that recruits many centrosomal proteins, some of which are also associated with MCPH; together, the complex is involved in centrosome duplication (Kodani et al. 2015).

Biochemical studies have shown that Astrin is present as a 4-unit complex containing SKAP, dynein light chain LC8, and MYC binding protein (MYCBP) in a 2:2:2:2 ratio and 465-693 a.a of Astrin are sufficient for forming this complex (Kern, Wilson-Kubalek, and Cheeseman 2017). In prometaphase, SKAP loads the Astrin-SKAP complex onto the MTs in an EB1 and EB3 (MT plus-end tracking proteins) dependent manner (Dunsch et al. 2011; Kern et al. 2016). Moreover, Astrin directly interacts with NuMA, a protein required for normal spindle assembly and orientation. siRNA targeted NuMA depletion studies have shown impaired Astrin localization at the spindle (Chu et al. 2016), suggesting that NuMA may be necessary for the localization of Astrin-SKAP at the spindle. During metaphase, in addition to its presence at the MTs, the Astrin-SKAP complex is selectively targeted to the mature or end-on attached KTs (Shrestha and Draviam 2013; Shrestha et al. 2017; Kuhn and Dumont 2017) through the C-terminus of Astrin (Dunsch et al. 2011; Kern, Wilson-Kubalek, and Cheeseman 2017). However, the binding partner of Astrin at the KTs is not known.

Aurora-A kinase phosphorylates the N-terminus of Astrin, and cells overexpressing Astrin with mutated Aurora-A phospho-site have reduced localization of Astrin-SKAP complex at the KTs, disrupted spindle size, and undergo prolonged mitosis (Chiu et al. 2014). PLK1 kinase phosphorylates the N-terminus of Astrin in a CDK1 dependent manner, and cells overexpressing Astrin with mutated PLK1 binding site have reduced Astrin's localization at the KTs and display unstable KT-MT attachments (Geraghty et al. 2021). Biochemical and yeast two-hybrid studies have shown that Astrin synergistically interacts with the Ndc80 complex through its N-terminus ((Kern, Wilson-Kubalek, and Cheeseman 2017), Tamura PhD, Draviam Lab; unpublished data), placing it near a key KT-MT attachment protein. However, cells with mutated PLK1 binding site or lacking the first 464 a.a. of Astrin can form bipolar spindles and progress through an unperturbed cell cycle (Geraghty et al. 2020), suggesting the loss of N-terminus of Astrin can be compensated.

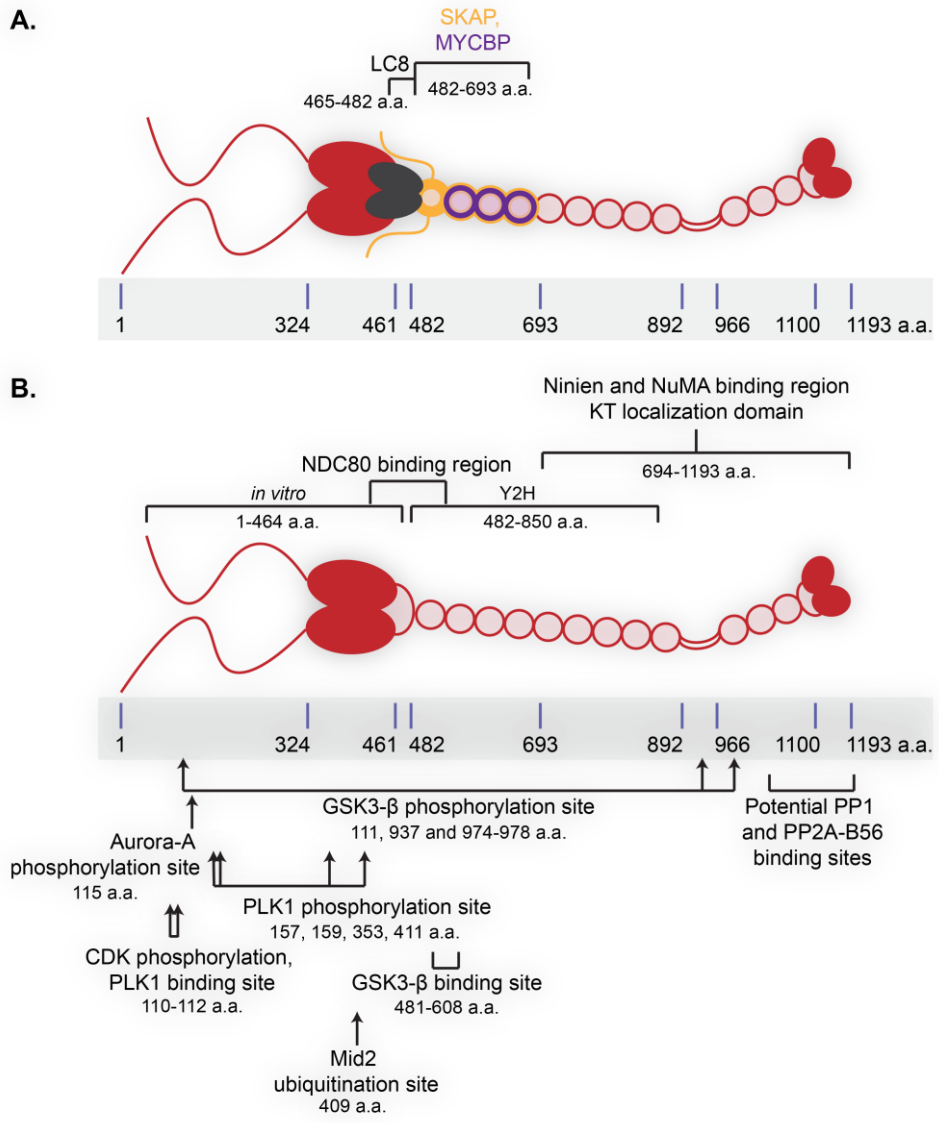

Fig 1.9 Schematic of Astrin protein. A. In mitosis, Astrin (Red) is in a complex with SKAP (yellow), MYCBP (purple) and LC8 (black). The amino acid numbers refer to the position on the Astrin protein. **B.** Astrin interacts with various proteins in a localization-dependent manner (above) and is regulated by post-translational modifications (below).

Astrin replaces Kif2b from the Kif2b-CLASP1 complex (Manning et al. 2010) and SKAP interacts with Kif2b in a GSK3β-dependent manner to inhibit its MT depolymerizing activity (Qin et al. 2016) and thus stabilizing MTs. Moreover, SKAP interacts with CENP-E, a motor protein involved in chromosome congression and checkpoint silencing (Huang et al. 2012). Moreover, Astrin is pulled down by B56 (a subunit of PP2A phosphatase) (Hertz et al. 2016), and a motif search (Dinkel et al.

2016) of Astrin showed potential docking sites for both PP2A-B56 and PP1 phosphatases in the C-terminus of Astrin suggesting that Astrin C-terminus targets phosphatases to the KTs which may be essential for KT-MT attachment stability.

Finally, Astrin undergoes MID2 dependent degradation in telophase, gradually returning to interphase levels, and this is important for normal cytokinesis (Gholkar et al. 2016).

1.5 AIMS OF THE PROJECT

The kinetochore (KT) is made up of over 100 proteins that perform three main functions. KTs attach the chromosomes to the microtubules (MTs), monitor the attachments, and correct them if erroneous attachments are formed. Defects in either of these pathways can cause chromosome missegregation leading to DNA damage and aneuploidy. DNA damage and aneuploidy in somatic cells can cause cancer. However, when these happen in the germ cells, they can lead to pregnancy loss and developmental disorders. Germline genomic variations in several KT proteins have been linked to primary microcephaly (MCPH) and mosaic-variegated aneuploidy (MVA). Moreover, these conditions are more common in highly consanguineous populations such as in Northern Pakistan.

The Astrin-SKAP complex is selectively recruited to the end-on KT-MT attachments and plays a key role in stabilizing the end-on attachment. The recruitment of the Astrin-SKAP complex at the KTs is mediated by Astrin protein. Moreover, a combined heterozygous variation in Astrin has been identified as the cause of primary microcephaly. Hence, the purpose of this study was to combine cell biology, molecular biology and biochemistry to address the following:

1) To identify loss of function (LOF) genomic variations in KT genes in the Genes and Health (GH) database, population genetics study of UK residents of Bangladeshi-Pakistani community
2) To investigate whether the LOF Astrin variants identified in GH can localize normally in mitosis
3) To investigate the functional consequences of the Astrin variant that cannot localize normally in mitosis.

CHAPTER 2: METHODS AND MATERIALS

CHAPTER 2: METHODS AND MATERIALS

2.1 CELL CULTURE

2.1.1 CELL LINES

The following cell lines were used for this thesis:

Table 2.1 List of cell lines used in this thesis.

Cell line	Protein Expressed	Source
HeLa	None	Draviam Lab
HeLa T-Rex YFP-Astrin WT	YFP-Astrin wild type	Duccio Conti (Draviam Lab)
HeLa T-Rex YFP-Astrin 4A	YFP-Astrin 4A	Duccio Conti (Draviam Lab)
HeLa T-Rex YFP-Astrin Q1012*	YFP-Astrin p.Q1012*	Present work

2.1.2 MAINTENANCE CONDITIONS OF CELL LINES

HeLa cells were cultured in Dulbecco's Modified Eagle's Medium supplemented with 10% Fetal Calf Serum (FCS; Fisher, 10270106), 1% Penicillin and Streptomycin (Fisher, 15140122), and 0.1% Amphotericin B (ThermoFisher, 15290-018).

HeLa T-REx were cultured in Dulbecco's Modified Eagle's Medium supplemented with 10% tetracycline-free FCS (LabTech, FB-1001T/500), 1% Penicillin and Streptomycin (Fisher, 15140122), and 0.1% Amphotericin B (ThermoFisher, 15290-018).

All cell lines were maintained as a monolayer at 37°C with a 5% CO2 atmosphere.

2.1.3 PROPAGATION OF CELL LINES

Confluent cells were washed twice with pre-warmed (37°C) Dulbecco's phosphate-buffered saline (1X DPBS) (no Ca_2, no Mg_2; Fisher, 14190250), treated with pre-warmed 1X Trypsin-EDTA (Fisher, 25300054), and incubated for 3-4 minutes at

37°C. Trypsinisation reaction was stopped by adding fresh media (at least the volume of Trypsin-EDTA used), and cells were gently resuspended to break clumps. Cells were counted using a Bright-Line™ hemocytometer (Sigma-Aldrich, Z375357-1EA), and the appropriate number of cells were seeded in new stock plates.

Stock cultures were maintained in sterile 6 cm Nunc cell culture dishes (Fisher, 150288). For larger cultures, cells were maintained in 10 cm Nunc cell culture dishes (Fisher, 150350). For experiments, the respective seeding procedure is indicated in each method.

2.1.4 GENERATION OF STABLE EXPRESSING HELA T-REX CELL LINES

HeLa T-REx cells were seeded into sterile 10 cm Nunc cell culture dishes (Fisher, 150350). When confluence reached 80-90%, cells were transfected (same protocol as in **section 2.1.8**) with plasmids encoding Flippase and the selected pcDNA5 FRT/TO in a 3:7 proportion (6 µg total). The culture was incubated at 37°C for two days to allow plasmid recombination, and then media was supplemented with Hygromycin B (1:200 dilution; Fisher, 10687010). The media was changed every day until single colonies of Hygromycin-resistant cells were visible but not confluent. Single colonies were picked by containing the Trypsinisation reaction around the selected colony using a sterilized 1,000 µl micropipette tip with the extremity cut off. Space between the micropipette tip and the dish was sealed using sterilized silicone grease. Each colony was treated with 50 µl 1X Trypsin-EDTA and incubated for 3 minutes at 37°C. The reaction was stopped by pipetting 100 µl of the fresh media into each micropipette tip. Cells were then gently resuspended and seeded into a 12-well Nunc cell culture dish (Fisher, 150628), one colony per well. Colonies were expanded in tetracycline-free medium (see **section 2.1.2** for details). In alternative to colony picking, the whole plate of Hygromycin-resistant cells was collected as a pooled culture. Finally, expression of YFP-Astrin was induced by changing media to tetracycline-containing medium for 48 hrs. Cells were sorted for YFP using Aria IIIu Cell Sorter, and media was quickly changed back to Tetracycline-free medium.

2.1.5 LONG TERM STORAGE OF CELL LINES

Freezing: For long-term storage, cells were treated with Trypsin-EDTA (see **Section 2.1.3** for details). Once resuspended, cells were centrifuged at 1,500 RPM for 5 minutes, and the pellet was gently resuspended in a pre-chilled freezing medium. Freezing media composed of 45% complete growth media (detailed in **Section 2.1.2** for each cell line), 45% Fetal Calf Serum (FCS) (Fisher, 10270-106), and 10% Dimethylsulfoxide (DMSO) (Sigma-Aldrich, D8418). For cells grown in FCS without Tetracycline, the freezing media used Tetracycline-free FCS (LabTech, FB-1001T/500). The cell suspension was then aliquoted into cryovial tubes (SLS, G122263), 1 ml per tube. The cryovial tubes were stored in a Mr. Frosty^{TM} freezing-container (ThermoFisher, 5100-0001) for at least 24 hours at -80°C. Finally, the tubes were transferred to their respective storage box at -80°C or in liquid nitrogen (-140°C) for more extended storage.

Thawing: Cells were revived by gently thawing the frozen vial in a water bath at 37°C. Once liquid again, 1 ml of appropriate medium was slowly pipetted into each tube, and the content was transferred to a 10 ml tube. Cells were centrifuged at 1,500 RPM for 5 minutes, the supernatant was removed, and the pellets were resuspended with at least 1 ml of appropriate medium. Cells were then seeded into a 6 cm Nunc dish (Fisher, 150288) and incubated at 37°C.

2.1.6 INHIBITORS

The following drugs were used at the indicated concentrations for this thesis:

Table 2.2 List of inhibitors used in this thesis.

Name	Working Concentration	Target	Supplier (cat no.)
MG132	10 μM	Proteasome	Tocris Biosciences (1748)
STLC (S-trityl-L-cysteine)	20 μM	Eg5 kinesin	Fisher (AAL1438403)
Thymidine	2.5 mM	DNA replication	ACROS Organics

Name	Working Concentration	Target	Supplier (cat no.)
Aphidicolin	1 ug/ml	DNA replication	Fisher Bioreagents (BPE615-1)
CENPEi (GSK923295)	10 nM	CENPE motor protein	Seleckchem (S7090)

YFP-Astrin expression in HeLa TRex cell lines was induced by changing the media from tetracycline-free medium to medium containing tetracycline (see **Section 2.1.2** for details).

2.1.7 CELL SYNCHRONIZATION

For mitotic progression studies, cells were synchronized using a double thymidine block. Cells were treated with 2.5 mM thymidine (ACROS organics) for 23 hours to synchronize cells in the S phase. Thymidine was then removed by giving the cells three rounds of two quick washes with media for 30 minutes. After 5 hours, thymidine was added again for another 19-23 hrs. Thymidine was removed as before, and cells were left in a thymidine-free medium for 10 hrs.

2.1.8 PLASMID TRANSFECTION

Plasmid transfection was performed using TurboFect (Fisher, R0531) or DharmaFect (Dharmacon, T2010-03) according to the manufacturer's instructions. In addition to the standard protocol, the transfection medium was removed after 4 hours of incubation and the fresh selected pre-warmed medium was added to each well.

For one well of a 12-well dish (ThermoFisher, 150628) or a 4-well live-cell imaging dish (Fisher, 155383PK), plasmid DNA was incubated in 100 µl of Opti-Mem (Invitrogen, 11058-021) with 1.5 µl of TurboFect or 1.4 µl of DharmaFect reagents. 100 µl of the final mixture was pipetted drop-by-drop onto the coverslip of the selected well. This proportion was scaled up for multiple transfections with the same reagents.

The amount of plasmid DNA used in transfections for this thesis is detailed below:

Table 2.3 Settings for plasmid transfections used in this thesis.

Plasmid DNA	Amount	Transfection reagent	Opti-MEM Volume	Experiment type
YFP-Astrin constructs	750 ng	Turbofect or Dharmafect	100 µl	Fixed-cell
Astrin-GFP constructs	750 ng	Dharmafect	100 µl	Fixed-cell
YFP-Astrin constructs	1µg	Dharmafect	100 µl	Live-cell
YFP-Astrin constructs + CenpB-ds-Red	750 ng YFP + 250 ng ds-Red (1µg)	Dharmafect	100 µl	Live-cell

The complete list of plasmids used for this thesis is presented below:

Table 2.4 List of plasmids used in this thesis.

Name	Backbone	Database Number	Source
Flippase	pOG44	VMD 390	Jayaprakash Arulanandam
His-GST-PP1γ (7-323)	pGAT3	VMD 577	J. Peränen and M. Hyvönen, unpublished
His-Astrin WT	pRSET	VMD 588	Dominique Braun (Draviam Lab)
His-Astrin 4A	pRSET	VMD 589	Dominique Braun (Draviam Lab)
YFP-Astrin WT	pEGFP C1	VMD 633	Duccio Conti (Draviam Lab)
YFP-Astrin 4A	pEGFP C1	VMD 634	Duccio Conti

Name	Backbone	Database Number	Source
			(Draviam Lab)
YFP-Astrin Δ70	pEGFP C1	VMD 635	Duccio Conti (Draviam Lab)
YFP-Astrin p.Q1012*	pEGFP C1	VMD 676	Present work
YFP-Astrin p.E755K	pEGFP C1	VMD 677	Present work
YFP-Astrin Δ151	pEGFP C1	VMD 702	Present work
YFP-Astrin Δ274	pEGFP C1	VMD 701	Present work
Astrin-GFP WT	pEGFP N1	VMD 637	Duccio Conti (Draviam Lab)
Astrin-GFP 7*	pEGFP N1	VMD690	Present work
YFP-Astrin WT	pcDNA5 FRT/TO	VMD 686	Duccio Conti (Draviam Lab)
YFP-Astrin Q1012*	pcDNA5 FRT/TO	VMD 691	Present work
CENPB-ds-Red	pCMV	VMD 691	Draviam Lab

2.1.9 SIRNA TRANSFECTION

siRNA transfection was performed using Oligofectamine (ThermoFisher, 12252011) according to the manufacturer's instructions. All siRNA oligonucleotides dilutions were prepared in Opti-Mem. In addition to the standard protocol, the transfection medium was removed after 4 hours of incubation and the fresh selected pre-warmed medium was added to each well.

Table 2.5 List of siRNA oligonucleotides used in this thesis.

Target	Sequence (5' to 3')	Reference
Astrin (VMD 52)	UCCCGACAACUCACAGAGAAAUU	(Duccio Conti et al. 2019; K. H. Thein et al. 2007)
Stealth Negative siRNA	n.a.	Invitrogen (12935-300)

2.2 BACTERIAL CELL CULTURE

2.2.1 MEDIA AND ANTIBIOTICS

Solid and liquid media for cultivating bacterial cells were prepared as follows:

Table 2.6 Recipes of media for bacterial cell cultures.

Name	Purpose	Composition	Final Volume
LB (Luria-Bertani) liquid medium	Liquid culture	10 g Tryptone 10 g NaCl 5 g Yeast extract	1 L
LA (Luria Agar)	Petri dish culture	10 g Tryptone 10 g NaCl 5 g Yeast extract 15 g Agar	1 L

*Commercial Luria Broth powder (Malford, L24040) was used in later experiments.

For antibiotic selection, solid and liquid media were supplemented with 100 µg/ml Ampicillin (A0166, Sigma) or 50 µg/ml Kanamycin (Melford, MS10-UV10). For expressing His-Astrin plasmids, liquid media was supplemented with 100 µg/ml Ampicillin and 20 µg/ml Chloramphenicol.

2.2.2 TRANSFORMATION OF COMPETENT CELLS

For the transformation procedure, a minimum of 100 ng of plasmid DNA was mixed with at least 50 µl of competent cells and incubated for 20 minutes on ice. A heat-shock was then performed by incubating the cells for 1 minute at 42°C (in a water bath) and immediately placed back on ice. Cells were incubated for at least 2 minutes before the addition of 400 µl of LB medium. Cells were recovered in LB medium at 37°C for at least 30 minutes for Ampicillin selection and 1 hour in case of Kanamycin selection. Finally, cultures were plated onto the LA dish supplemented with the selected antibiotic and incubated at 37°C.

For growing plasmids, plasmids were transformed into plasmid Subcloning Efficiency™ DH5α™ chemically competent E. coli (Fisher, 18265017). For expression of His-Astrin fragments, plasmids were transformed into BL21(DE3)pLysS. For expression of His-GST-PP1γ, plasmids were transformed into BL21(DE3).

2.2.3 PLASMID DNA PURIFICATION

Plasmid purification was performed using three different kits.

Plasmid miniprep: Minipreperations were performed for small-scale plasmid DNA purifications of bacterial cultures, typically a maximum of 5 ml volume per culture. For purifying the plasmid DNA, EZ-10 Spin Column Plasmid DNA Miniprep Kit (NBS biologicals, NBS414) was used as per the manufacturer's instructions. Plasmid DNA was eluted in 30 µl of elution buffer provided by the kit.

Plasmid midiprep: Midipreperations were performed for obtaining high-yield plasmid DNA solutions with good purity to be used for transfection into human cells. For this purpose, 100 ml liquid cultures were used. Plasmid DNA was purified using the Macherey-Nagel NucleoBond Xtra Midi kit (Fisher, 12363348) or Qiagen Plasmid Midi Kit (Qiagen, 12143) as per the manufacturer's instructions. Plasmid DNA was eluted in 50 µl of elution buffer provided by the kit. To check the purification quality, 500 ng of plasmid DNA were inspected via gel electrophoresis (see **section 2.4.2** for details).

Plasmid DNA stocks were stored at -20°C, and working aliquots were prepared to avoid frequent freeze-thawing. For plasmid transfections, 500 ng/µl working aliquots were prepared in sterile dH2O and stored at 4°C.

To measure plasmid DNA concentration, 1.0 µl of plasmid DNA solution was inspected using a NanoDrop™ machine (ThermoFisher).

2.3 PROTEIN METHODS

2.3.1 REAGENTS

The following solutions were used to perform the protein methodologies presented in this thesis work. Reagents were purchased from Sigma-Aldrich and Melford Laboratories Ltd. unless specified.

Table 2.7 Buffers and solutions used in protein methods.

Name	Composition
10X PBS (Phosphate-Buffered Saline)	1.36 mM NaCl 27 mM KCl 188 mM Na_2HPO_4 17 mM KH_2PO_4 pH equilibrated to 7.4
4X SDS (Sodium Dodecyl Sulfate) buffer	160 mM Tris-HCl pH 6.8 20% (w/v) Glycerol 4% (w/v) SDS 0.2% (w/v) Bromophenol blue
Ponceau	0.1% w/w Ponceau S dye 1% v/v Acetic acid
Coomassie stain	0.5 g Coomassie blue 90 ml MeOH 20ml Acetic acid 90 ml H_2O
Coomassie destain	20% MeOH

Name	Composition
	10% acetic acid
	70% dH_2O
GST lysis buffer	50 mM Tris-HCL
	15 mM KCl
	5 mM DTT
	pH equilibrated to 7.7
GST wash buffer	50 mM Tris-HCL
	15 mM KCl
	5 mM DTT
	0.1% 100×Tritone
	pH equilibrated to 7.7
His resuspension buffer	0.4% NP40
	50 mM NaH_2PO_4
	300 mM NaCl
	10 mM Imidazole
	pH equilibrated to 8.0
His elution buffer	0.4% NP40
	50 mM NaH_2PO_4
	300 mM NaCl
	500 mM Imidazole
	pH equilibrated to 8.0
Pull down lysis buffer	1x PBST (1x PBS + 0.1% Tween 20)
	5 mM Sodium Orthovanadate
	0.02% Triton X-100

Name	Composition
	protease inhibitor cocktail (Sigma, 11873580001)
Pull down wash buffer	1x PBS protease inhibitor cocktail
Western Blotting 10X Running buffer	192 mM Glycine 250 mM Tris 34.7 mM SDS
Western Blotting 10X Transfer buffer	192 mM Glycine 250 mM Tris
12% SDS-PAGE Acrylamide resolving gel (total volume 10ml)	2.5 ml 1.5M Tris (pH 8.8) 4 ml 30% Acrylamide 100 µl 10% SDS 100 µl Ammonium Persulfate 4 µl TEMED (Apollo Scientific, BIT7140) 3.3 ml dH_20
8% SDS-PAGE Acrylamide resolving gel (total volume 10ml)	2.5 ml 1.5M Tris (pH 8.8) 2.7 ml 30% Acrylamide (Seven Biotech Ltd) 100 µl 10% SDS 100 µl Ammonium Persulfate 4 µl TEMED 4.6 ml dH_20
4% SDS-PAGE Acrylamide stacking gel (total volume 5ml)	380 µl 1M Tris (pH 6.8) 500 µl 30% Acrylamide 30 µl 10% SDS

Name	Composition
	30 µl Ammonium Persulfate
	3 µl TEMED
	2.1 ml dH_20

2.3.2 PROTEIN EXPRESSION AND PURIFICATION

Colonies from freshly transformed plates (see **section. 2.2.2** for details) were inoculated in 10 ml Luria broth in the presence of appropriate antibodies. For His-GST PP1γ expression, starter culture was added to 100 ml Lauria Broth containing appropriate antibiotic, and the culture was grown to an OD600 of ~0.6. For the expression of His-Astrin fragments, starter culture was added to 1 L Lauria Broth containing appropriate antibiotic, and the culture was grown to an OD600 of ~0.2. Protein expression was induced by the addition of 1 mM IPTG (I6758, Sigma) for 14 hours at 22°C (His-GST-PP1γ), 30 minutes at 37°C (His-Astrin WT), or 3 hours at 25°C (His-Astrin 4A). 100 ml cultures were pelleted at 4,000 RPM, 4°C for 30 minutes and 1 L cultures were pelleted at 14 K RPM, 4°C for 20 minutes. Pellets were stored at −20°C. Protein expression was confirmed by running an SDS-PAGE gel (see **section 2.3.5** for details), staining with Coomassie stain, and destaining with Coomassie destain or water. Gels were scanned using a film scanner and stored immersed in water.

His-GST PP1γ immobilization on beads: Cell pellets were resuspended in 10 ml GST lysis buffer, lysed by sonication (75% Amp, 30 sec on/off, for 2 min; Vibracell VCX130, Sonics), and cleared by centrifugation at 14 K RPM, 4°C for 30 minutes. The cleared supernatant was incubated for an hour with glutathione HiCap Matrix (Qiagen, 3090) at 4°C with continuous rotation and washed twice with GST wash buffer. Immobilized proteins were stored at 4°C. Immobilization on beads was confirmed by Coomassie staining as described above.

Purification of His-Astrin fragments: Cell pellets were thawed on ice for 20 minutes, resuspended in 30 ml His lysis buffer, lysed by sonication (75% Amp, 30 seconds on/off, for 4 minutes), and cleared by centrifugation at 17 K RPM, 4°C for 30 minutes. The cleared supernatant was incubated for an hour with 500 µl HIS-Select® Nickel Affinity Gel (Sigma, P6611) at 4°C with continuous rotation and applied to

empty PD10 columns (GE Healthcare). Next, beads were washed with 100 ml His lysis buffer, and the protein fragments were eluted using His elution buffer in 5-6 Eppendorf's. Elution was confirmed by Bradford assay, eluted fractions were combined and concentrated using Microcep Advance centrifugal device 10K (PALL, Life Sciences) the buffer was exchanged using PD10 buffer exchange columns (GE Healthcare) in 10% glycerol-PBS, and purified proteins were stored at -80°C. Purification was confirmed by Coomassie staining as described above.

2.3.3 PULL DOWN ASSAY

HeLa cells seeded in 10 cm Nunc plates (Fisher, 150350). were grown to 80% confluency and transfected with control and Astrin siRNA (see **section 2.1.9** for details). After 24 hours, cells were arrested with 20 µM STLC (Fisher, AAL1438403) for 24 hours. Cells were scraped on ice, washed with Pull down wash buffer, and lysed in 1 mL Pull down lysis buffer at 75% AMP (Vibracell VCX130, Sonics) for ~15 s. The lysate was cleared of cell debris by centrifugation at 14 K RPM, 4°C for 15 minutes. Half of the cleared lysate was incubated with immobilized His-GST-PP1γ and the other half with His-GST for an hour on a spinning wheel at 14 RPM, 4°C. Beads were washed four times with 500 µL Pull down wash buffer for 5 mins, spun down at 500 RPM at 4°C and resuspended in Pull down wash buffer. The samples were analyzed using SDS-PAGE and immunoblotting (see **section 2.3.5**). The whole procedure was performed on ice.

2.3.4 CO-IMMUNOPRECIPITATION

Purified His-Astrin fragments were incubated with immobilized His-GST-PP1γ or glutathione HiCap Matrix (30900, QIAGEN) for an hour on a spinning wheel at 14 RPM, 4°C. Beads were washed four times with 500 µL 1X PBS for 5 mins, spun down at 4°C, and resuspended in 1X PBS. The samples were analyzed using SDS-PAGE and immunoblotting (see **section 2.3.5**). The whole procedure was performed on ice.

2.3.5 IMMUNOBLOTTING

Cells were lysed with the appropriate volume of boiling 4X SDS buffer and separated on SDS-PAGE gels according to their size using a Mini-protein® Tetra (Bio-Rad) electrophoresis system. Prestained molecular weight markers (either NEB P7706

or NEB P7718) were run in one lane to identify protein sizes. Separated proteins were then transferred onto a PVDF membrane (Immobilolon®-P, 0.45 µm pore size; Millipore, IPVH00010) using a Criterion™ blotter (Bio-Rad). The transfer was performed at 4°C and 15V for 20 hours.

The outcome of the transfer was assessed using Ponceau's stain before proceeding with the immunoblotting. Membranes were washed three times with 1X PSB + 0.1% Tween 20 (Sigma-Aldrich, P9416-50ML), then incubated for one hour in the appropriate blocking buffer. Next, membranes were incubated with primary antibodies overnight at 4°C. Membranes were washed three times with 1X PSB + 0.1% Tween 20, followed by incubation with secondary antibodies for 1 hour. Finally, three washes with 1X PSB + 0.1% Tween 20 were performed and membranes were dried before developing. The fluorescence signal was detected using an Odyssey® machine (Li-Cor Biosciences).

2.3.6 ANTIBODIES USED FOR IMMUNOBLOTTING

Presented below is a complete list of the antibodies used for the immunoblots of this thesis work. All antibodies were diluted in 5% milk in PBS1 + 0.1% Tween 20 blocking buffer.

Table 2.8 List of antibodies used for immunoblotting.

Epitope	Species	Working concentration	Supplier (cat no.)
Primary Antibodies			
Astrin	Rabbit	1:3000	Proteintech (14726-1-AP)
SKAP	Rabbit	1:1000	Atlas Biologicals (HPA042027)
GFP	Rabbit	1:1000	Abcam (ab290)

Epitope	Species	Working concentration	Supplier (cat no.)
γ-Tubulin	Mouse	1:800	Sigma-Aldrich (T6793)
GST	Rabbit	1:1000	Santa Cruz (sc-459)
Secondary Antibodies			
IRDye 680LT anti-Mouse IgG (H+L)	Donkey	1:10,000	Li-Cor (926-68022)
IRDye 800CW anti-Rabit IgG (H+L)	Donkey	1:10,000	Li-Cor (926-32213)

*For secondary antibodies blocking buffer was chosen according to its matching primary antibody.

2.4 MOLECULAR BIOLOGY

2.4.1 PCR REACTIONS

The PCR reactions performed for this thesis work were used for subcloning and direct site mutagenesis. Below are described the settings for preparing the reaction mixtures and the amplification cycles. For each PCR reaction, a master mixture (i.e., all reagents minus the template DNA) was prepared for the total number of the samples plus one spare. Mixtures were kept on ice until placed in the thermal cycler.

Table 2.9 PCR reaction mixtures.

Standard PCR Mixture	
Reagent	Amount
DNA template (25 ng/μl)	1.0 μl
Forward primer (10 μM)	0.6 μl

Reverse primer (10 μM)	0.6 μl
dNTPs (10 mM) (NEB, N0447S)	0.2 μl
5X Phusion buffer	4.0 μl
Phusion polymerase (NEB, M0530S)	0.3 μl
Nuclease free dH2O (Biolabs, B1500L)	13.3 μl
Site-directed mutagenesis PCR Mixture	
Reagent	Amount
DNA template (100 ng/μl)	1.0 μl
Forward primer (10 μM)	0.5 μl
Reverse primer (10 μM)	0.5 μl
dNTPs (10 mM)	0.2 μl
PfuUltra II polymerase buffer	2.5 μl
PfuUltra II polymerase (Agilent, 600670)	0.5 μl
Nuclease free dH2O	19.8 μl

Table 2.10 PCR cycles.

Standard PCR Programme			
Step		Temperature	Time
Initial denaturation		95°C	5 min
Denaturation	30 cycles	95°C	30 secs
Annealing		Primer specific	30 secs
Extension		72°C	5 min
Final Extension		72°C	10 min
Site-directed mutagenesis PCR Programme			
Step		Temperature	Time
Initial denaturation		93°C	2 min

Denaturation	30 cycles	93°C	20 secs
Annealing		Primer specific	30 secs
Extension		72°C	10 min
Final Extension		72°C	12 min

2.4.2 AGAROSE GEL ELECTROPHORESIS AND DNA PURIFICATION FROM GEL.

Agarose gel electrophoresis (Melford Laboratories Ltd, MB1200) was performed to assess the outcome of PCR reactions, DNA purifications, and for size separation of DNA fragments. Gels were prepared in a concentration of 0.5 or 1% in 1X TAE (400 mM Tris, 180 mM Glacial Acetic acid, 10 mM EDTA, pH equilibrated to 8.0). Samples were mixed with 6X loading dye (NEB, B7025) before loading onto the gel. A DNA ladder (NEB, N3200) was added in a separate lane DNA size reference. Electrophoresis was performed using a Geneflow tank system. Voltage and run time were selected accordingly to the sample characteristics.

Fragments of interest were purified using the Zymoclean™Gel DNA Recovery Kit (Zymo Research; D4001T) or EZ-10 Spin Column DNA Gel Extraction Kit (Biobasic, BS353), according to the manufacturer's instructions. DNA was eluted in 10 µl of the elution buffer (EB) provided by the kit.

2.4.3 SUBCLONING AND SITE-DIRECTED MUTAGENESIS

Subcloning was performed following standard procedures. If no restriction site matching the insertion locus on the donor vector was available, a PCR reaction was used to generate the appropriate restriction sites (settings as in **section 2.4.1**). The general settings of reactions used for the methodology are presented below.

Table 2.11 Subcloning reaction methodologies.

1. Restriction		
Reagent	Stock concentration	Working concentration
DNA	n.a.	PCR product or 2-3 µg plasmid DNA

Buffer	10X	1X
Enzyme A (Various)	10,000-20,000 units	10,000 units
Enzyme B (Various)	10,000-20,000 units	10,000 units
dH2O	n.a.	up to 30 µl
Incubate at 37°C for 6 hours + 80°C for 20 minutes for heat-inactivation. All enzymes purchased at NEB or Roche.		
2. Vector de-phosphorylation		
Reagent	Stock concentration	Working concentration
Shrimp Alkaline Phosphatase (GE Healthcare, E70092Y)	n.a.	2.5 µl x 5 µl reaction
Buffer	n.a.	2.5 µl x 5 µl reaction
Reagent	Stock concentration	Working concentration
Incubate at 37°C for 30 minutes + 80°C for 20 minutes heat-inactivation.		
3. Ligation		
Reagent	Stock concentration	Working concentration
Insert DNA	n.a.	According to fragment size
Vector DNA	n.a.	100 ng
Ligase buffer	10X	1X
T4 DNA Ligase (M0202S)	20,000 units/µl	20,000 units
dH2O	n.a	up to 10 µl
Incubate at 24°C for one hour.		

For site-directed mutagenesis, PCR products were digested with DpnI enzyme (NEB, RO176) for 3 hours at 37°C, following the settings as on **Table 2.9** and **2.10**.

Subcloning and site-directed mutagenesis reaction products were transformed into Subcloning Efficiency™ DH5α™ chemically competent E. coli (For details, **see section 2.2.2**). To select positive clones, cells were grown on the appropriate selective media.

2.4.4 DNA SEQUENCING AND ANALYSIS

All plasmids used for the work of this thesis were sequenced by Source BioScience or Eurofins. Sequencing results were analyzed using SnapGene Viewer v5.0.7 and SerialCloner v2.6.1. Plasmid maps were generated using SerialCloner v2.6.1.

2.4.5 PRIMERS

T7 and SP6 primers, used for sequencing of plasmid encoding His-GST PP1γ, were supplied by the sequencing companies. All other primers used for the work of this thesis were purchased from Sigma-Aldrich and are described below:

Table 2.12 List of primers used.

Database number	Sequence (5' to 3')	Use
VMD619	GGACCTGGCTATGAAGGATAAATTACTCTGCCAGCTTACCC	To generate p.E755K mutation in Astrin (Forward primer).
VMD620	GGGTAAGCTGGCAGAGTAATTTATCCTTCATAGCCAGGTCC	To generate p.E755K mutation in Astrin (Reverse primer).
VMD625	GCTAGGCTGCAGGCCTAGGAAGAACAGCATC	To generate p.Q1012* mutation in Astrin (Forward primer).
VMD626	GATGCTGTTCTTCCTAGGCCTGCAGCCTAGC	To generate p.Q1012* mutation in Astrin (Reverse primer).
VMD650	GGCGAGTGAAAAAATAGAGCCTCAGCCTGTCG	To generate p.L7* mutation in Astrin (Forward primer).

Database number	Sequence (5' to 3')	Use
VMD651	CGACAGGCTGAGGCTCTATTTTTTCACTCGCC	To generate p.L7* mutation in Astrin (Reverse primer).
VMD662	GTAGAGCATGGAGCTTCCGGAATGGAGGAAAGAG	To delete 275-1193 a.a. of Astrin + BspeI site (Forward primer).
VMD663	GGTGAAGCAAGGATATCAGCTCTTTAGAGATAAG	To delete 275-1193 or 152-1193 a.a. of Astrin (Reverse primer).
VMD664	CGTTTAGATACCTCCGGAATGGCAGAGAC	To delete 152-1193 a.a. of Astrin + BspeI site (Forward primer).
VMD 370	CACTGGAGATGAGTTGTTGC	To sequence Astrin from 185bp (Reverse).
VMD 371	CTGAGCAGTAGAACTGAGGC	To sequence Astrin from 661bp.
VMD 372	CTCCAGATCTGACTGCCTTG	To sequence Astrin from 1268bp.
VMD 373	GGTTCAGCAGACAGTGAGTC	To sequence Astrin from 1890bp.
VMD 374	CTCAAGGACACTGTAGAGAAC	To sequence Astrin from 2521bp.
VMD 375	ACTCCAACTGCCAGCCTATG	To sequence Astrin from 3293bp.
VMD 585	CCACTGGAGATGAGTTGTTGCTGCC	To sequence Astrin from 181bp (Reverse).
VMD 586	CCACTGGAGATGAGTTGTTGCTGCC	To sequence Astrin from 825bp (Reverse).

Database number	Sequence (5' to 3')	Use
VMD654	CAACGGGACTTTCCAAAATG	To sequence Astrin from 1bp (CMV Forward)
VMD655	CATGGTCCTGCTGGAGTTCG TG	To sequence Astrin from 1bp. (EGFP Forward)

*Yellow = point-mutagenesis; Green = Subcloning; Grey = sequencing

2.5 MICROSCOPY

2.5.1 IMMUNOFLUORESCENCE MICROSCOPY

For immunofluorescence experiments, cells were grown onto ø13 mm round coverslips (WVR, 631-0150). After experimental protocol, cells were fixed either using methanol or formaldehyde.

Methanol fixation: Cells were fixed with ice-cold methanol for one minute, given two quick and two 5-minute washes with 1X PBS + 0.1% Tween 20 and blocked with 1% BSA in 1X PBS + 0.1% Tween 20 for 20 minutes.

Paraformaldehyde fixation: Cells were washed with fresh PHEMM buffer (37°C), pre-fixed for 5 seconds using 4% PFA (Thermo-Fisher, 28908) in PHEMM buffer (37°C), permeabilized for 5 minutes with PHEMM + 1% Triton X-100 + 1:100 Phosphatase Inhibitor Cocktail (100X; Cell Signal, 5872S) (37°C) and fixed again for 20 minutes with 4% PFA in PHEMM buffer (37°C). Coverslips were then washed thrice for 5 minutes each with PHEMM + 0.1% Tween 20 and incubated with 10% BSA in PHEMM buffer for one hour.

After blocking, cells were incubated with primary antibodies overnight at 4°C, followed by two quick and two 5-minute washes with 1X PBS + 0.1% Tween 20. Incubation with secondary antibodies was performed for one hour, followed by two quick washes and two 5-minute washes with 1X PBS + 0.1% Tween 20. For all immunostaining procedures, antibody dilutions were prepared in blocking buffer. Finally, coverslips were mounted onto VWR® Superfrost® Plus Micro slides (WVR, 48311-703) using 6 µl of ProLong® Gold Antifade Mountant (Invitrogen, P-36930) or

4 µl VECTASHIELD® Antifade Mounting Medium (VectorLabs, H-1000). Coverslips were then sealed with clear nail polish and stored at -20°C.

Images of immunostained cells were acquired using 100X NA 1.4 objective on a DeltaVision Core microscope (GE Healthcare) equipped with a CoolSnap HQ Camera (Photometrics). Deconvolution of fixed-cell images and 3D volume rendering were performed using Softworx software.

2.5.2 ANTIBODIES USED IN IMMUNOFLUORESCENCE

A complete list of antibodies, antisera, and stains used for this thesis work is presented below:

Table 2.13 List of antibodies used for immunofluorescence experiments.

Epitope	Species	Working Concentration	Fixation	Supplier (cat no.)
Primary antibodies				
GFP	Mouse	1:1000	Methanol	Roche (11814460001)
GFP	Rabbit	1:1,000	Methanol	Abcam (ab290)
Astrin	Rabbit	1:1,000	Methanol	Proteintech (14726-1-AP)
SKAP	Rabbit	1:800	Methanol	Atlas Biologicals (HPA042027)
ROD	Rabbit	1:500	Methanol	Draviam Lab
Phospho KNL1 p.S24	Rabbit	1:1000	Paraformaldehyde	A gift from Cheeseman Lab (Welburn et al. 2010)

Epitope	Species	Working Concentration	Fixation	Supplier (cat no.)
γH2AX	Rabbit	1:1,000	Methanol	Cell Signaling Technology (9718)
PCNA	Mouse	1:1,000	Methanol	Cell Signaling Technology (2586S)
CREST	Human	1:2,000	Methanol	Antibodies Incorporated (15-234-0001)
Secondary antibodies				
Alexa flour 488 donkey anti- mouse IgG (H+L)	Donkey	1:1000	-	Invitrogen (A21202)
Alexa flour 594 donkey anti- rabbit IgG (H+L)	Donkey	1:1000	-	Invitrogen (A21207)
Alexa flour® 647 goat anti-human IgG (H+L)	Goat	1:1000	-	Invitrogen (A21445)
DAPI	n.a.	1:2,000	-	Sigma-Aldrich (D9542)

2.5.3 LIVE-CELL IMAGING

For live-cell imaging experiments, cells were grown into 4-well cover glass chambered dishes (Lab-tek, 1064716) or 8-well (Fisher, 155411PK). To stain DNA, sir-DNA (Tebu-bio, SC007) was added 10 hours before imaging. Just before imaging, the growth medium was replaced with pre-warmed Leibovitz's L15 medium (Fisher, 11415064). All the imaging sessions were performed at 37°C.

For extended live-cell imaging, the images were acquired every 6 minutes with exposures of 0.1 seconds and at least 3 Z planes, using a 40X NA 0.75 objective on an Applied Precision Deltavision Core microscope (GE Healthcare) using a Cascade2 Camera (Photometrics) under EM mode.

For high-resolution live-cell imaging, the images were acquired with 0.2 seconds exposure and at least 3 Z planes using a 100X NA 1.4 objective on an Applied Precision Deltavision Core microscope using a CoolSnap HQ camera (Photometrics).

2.6 DATA ANALYSIS

For identification of loss of function (LOF) variants in kinetochore genes, the LOF variants list (Excel sheet, 2018) was downloaded from the Genes and health website (Scientific data downloads | East London Genes & Health, 29.01.2020).

For viewing genomic variation spectrum in Astrin-SKAP complex, a) all variations dataset (NEW file format, 2020) was downloaded from Genes and Health website (Scientific data downloads | East London Genes & Health, 29.01.2020), and a list of Astrin-SKAP complex variations were extracted from the dataset, b) data for all four genes were downloaded separately from gnomAD v2.1.1 (CSV format; (gnomAD, 29.01.2020)) and c) data for all four genes were downloaded separately from the COSMIC database (CSV format; (COSMIC | Catalogue of Somatic Mutations in Cancer, 29.01.2020)). All files were converted into a format accepted by cbioportal, and MutationMapper (cBioPortal for Cancer Genomics::MutationMapper, 29.01.2020) was used for generating the lollipop plots.

For PRIDE data analysis, data were downloaded from the PRIDE website (PRIDE - Proteomics Identification Database, 06.03.2018) and analyzed using MATLAB.

For conservation analysis, Astrin sequences were downloaded from Uniprot (Bateman et al. 2021), aligned using Clustal Omega (Rozewicki et al. 2019) and images of aligned sequences were generated using MAFFT (Madeira et al. 2019).

For inter-centromeric distance measurements, Softworx's distance measurement tool was used. The rest of the image and video analysis for this thesis was done manually using Softworx. Representative images for fixed and live-cell imaging studies were generated using Softworx or ImageJ 1.53e.

For measuring band intensities in immunoblots and generating images for figures, Image Studio Lite v5.2 was used. For generating images of Coomassie-stained gels for figures, Image Lab v6.0.1 was used.

Data were collected and stored in Microsoft Excel, graphs were plotted using Graphpad Prism v9.0.1 or Microsoft Excel, and final figures were assembled using Adobe Illustrator CC 2017.

Statistical tests are described in figure legends and were carried out using Graphpad Prism v9.0.1. In statistical tests presented following indications for p values were used; non-significant – ns for $p>0.05$, * for $p < 0.05$, ** for $p<0.01$, *** for $p<0.001$, **** for $p<0.0001$.

CHAPTER 3: RESULTS-I- IDENTIFICATION OF LOF HUMAN ASTRIN VARIANTS

CHAPTER 3: RESULTS-I- IDENTIFICATION OF LOF HUMAN ASTRIN VARIANTS

3.1 INTRODUCTION

Dysfunctional or dysregulated expression of kinetochore (KT) proteins in somatic cells causes chromosomal instability, a hallmark of cancer (Reviewed in: (Levine and Holland 2018)). In addition, genomic variations in KT proteins in early embryonic life can lead to developmental disorders such as primary microcephaly and mosaic-variegated aneuploidy (MVA) (Degrassi, Damizia, and Lavia 2019). Microcephaly, defined as head circumference less than two standard deviations below the mean for age, sex, and ethnicity, causes a range of symptoms including intellectual disability and developmental delays in the affected children (Reviewed in: (Gilmore and Walsh 2013; Jayaraman, Bae, and Walsh 2018). Children with MVA, on the other hand, have an increased risk of childhood cancers in addition to microcephaly and developmental delays (Reviewed in: (Degrassi, Damizia, and Lavia 2019)).

Astrin, part of a four-unit complex: Astrin, SKAP, LC8, and MYCBP, is a MT and KT-associated protein that plays a key role in stabilizing KT-MT attachments to ensure accurate chromosome segregation (Conti et al. 2019; Geraghty et al. 2021; Kern, Wilson-Kubalek, and Cheeseman 2017; Schmidt et al. 2010; Gruber et al. 2002; Manning et al. 2010; Dunsch et al. 2011; Thein et al. 2007; Shrestha and Draviam 2013). Over-expression of Astrin is linked with poor prognosis in several cancers (Yuan et al. 2014; Abdel-Fatah et al. 2016; Liu et al. 2018; Liu et al. 2019; Huang and Li 2020; Zhang et al. 2020). Moreover, a genomic variation in Astrin has been linked with microcephaly in a recent study (Boonsawat et al. 2019).

Primary microcephaly is rare, affecting an estimated 1 in 30,000-250,000 newborns worldwide; however, the prevalence is high in some populations, such as in Northern Pakistan, where it is estimated to be 1 in 10,000 newborns (Komai et al., 1955; Tolmie et al., 1987; Bosch, 1958). In this chapter, I ask whether genomic variations in KT proteins, particularly Astrin, exist in the Genes and Health database, a genetic study on UK residents of Pakistani-Bangladeshi heritage (Finer et al. 2020).

3.2 KINETOCHORE GENE VARIANTS IN GENES AND HEALTH DATABASE

To identify genomic variants in kinetochore (KT) proteins that could compromise chromosomal stability, I screened for loss of function (LOF) variants in the Genes and Health (GH) database (2018 data; (Scientific Data Downloads | East London Genes & Health, 29.01.2020; Finer et al. 2020)). Out of the 142 variants found, 94 variants have never been published, and only six are present as homozygous (**Table 3.1**). Moreover, I found two CENP-E variants and four NCAPD3 variants, both genes are associated with autosomal recessive primary microcephaly (OMIM 616051, OMIM 617984); one BUB1B variant, a gene associated with MVA (OMIM 257300); and two SPAG5 variants, a gene associated with microcephaly (Boonsawat et al. 2019). For the scope of this project, I chose to study LOF variants in the SPAG5 gene (encodes Astrin protein)-p.Q1012* and p.L7Qfs*21.

To ask whether the two variants are specific to the population surveyed in the GH database, I screened two additional databases: COSMIC (38,303 sequences from unique tumor samples; (COSMIC | Catalogue of Somatic Mutations in Cancer, 29.01.2020; Finer et al. 2020)) and gnomAD (141,456 exome and whole-genome sequences from unrelated individuals as part of several international population-specific and disease-specific studies; (GnomAD, 29.01.2020; Karczewski et al. 2020)). I did not find Astrin p.Q1012* variant in either of these databases (**Fig 3.2 and 3.3**). Even in the GH database, there are only two heterozygous individuals for this variation, suggesting it may be specific to the Pakistani-Bangladeshi community surveyed in GH (**Fig 3.1**). In contrast, Astrin p.L7Qfs*21 is present in the gnomAD database as both heterozygous and homozygous (**Fig 3.3**), particularly among individuals with South Asian ancestry, suggesting a wider spread.

I conclude that some of the variants in KT genes in the GH database are predicted to cause loss of function of essential genes. Moreover, Astrin LOF variations in GH appear to be mostly limited to South Asians.

Table 3.1 List of genomic variations in kinetochore proteins in the Genes and Health database.

Chr*	Position	Consequence	Symbol	Feature	Protein position	Amino acids	Existing variation	Allele frequency _ELGH*	Allele frequency _BiB*	Allele frequency _Birm*	Homozygous _ELGH*	Homozygous _BiB*	Homozygous _Birm*
chr1	43360099	Splice donor variant	CDC20	ENST00000372462			rs771036544	0.00013224	0	0	0	0	0
chr1	173811212	Stop gained	CENPL	ENST00000367710	30	R/*	COSM4225956&COSM424626	0.00014397	0	0	0	0	0
chr1	214613917	Splice donor variant	CENPF	ENST00000366955			rs374123290	0.00013231	0	0	0	0	0
chr1	214619167	Stop gained	CENPF	ENST00000366955	174	E/*	rs777632803	0.00020695	0.00020912	0	0	0	0
chr1	214640037	Stop gained	CENPF	ENST00000366955	567	R/*	rs767542466	0.00017088	0	0	0	0	0
chr1	214641127	Stop gained	CENPF	ENST00000366955	930	L/*		0.00013858	0	0	0	0	0
chr1	246843930	Splice acceptor variant	AHCTF1	ENST00000366508			rs148600466	0.00067024	0.00107469	0	0	0	0
chr1	246867243	Splice donor variant	AHCTF1	ENST00000366508			rs141409693	0.00431034	0.00917431	0.0174419	0	0	0
chr1	44750523	Frameshift variant	KIF2C	ENST00000372224	133	L/X		0.00026546	0	0	1	0	0
chr1	163326028	splice_acceptor_variant&5_prime_UTR_variant&intron_variant	NUF2	ENST00000367900				0.00031017	0	0	0	0	0
chr1	229470803	Splice acceptor variant & coding sequence variant & intron variant	NUP133	ENST00000261396	?-618			0.00093985	0	0	0	0	0

Chr*	Position	Consequence	Symbol	Feature	Protein position	Amino acids	Existing variation	Allele frequency _ELGH*	Allele frequency _BiB*	Allele frequency _Birm*	Homozygous _ELGH*	Homozygous _BiB*	Homozygous _Birm*
chr1	63490219	Splice acceptor variant	ITGB3BP	ENST00000371092			rs778483418	0.00031211	0	0	0	0	0
chr1	186343403	Stop gained	TPR	ENST00000367478	1225	R/*		0.00013277	0	0	0	0	0
chr1	211673650	Stop gained	NEK2	ENST00000366999	130	R/*	COSM4491924&COSM4491925&COSM4491926	0.00054795	0	0.00048263	0	0	0
chr1	63453944	Frameshift variant	ITGB3BP	ENST00000371092	191-192	FE/X	rs569350949	0.00279427	0.00058185	0.0005005	0	0	0
chr1	63478774	Frameshift variant	ITGB3BP	ENST00000371092	120	K/X	rs749074680	0.00022017	0.00103263	0.0045977	0	0	1
chr1	186362853	Frameshift variant	TPR	ENST00000613151	226-227	LE/X		0.00023397	0	0	0	0	0
chr1	186362857	Frameshift variant	TPR	ENST00000613151	225-226	-/KX		0.00023159	0	0	0	0	0
chr1	211673576	Frameshift variant	NEK2	ENST00000366999	154	N/X		0.00039894	0	0	1	0	0
chr1	226885638	Frameshift variant	PSEN2	ENST00000422240	153	T/X		0.00013228	0	0	0	0	0
chr2	74370723	Stop gained	DCTN1	ENST00000409567	296	E/*		0.00013305	0	0	0	0	0
chr2	110669451	Splice donor variant	BUB1	ENST00000409311			rs771093692	0.0001351	0	0	0	0	0
chr2	110669499	Stop gained	BUB1	ENST00000409311	174	S/*	COSM1305545	0.00014176	0	0	0	0	0
chr2	200535172	Splice donor variant	SGO2	ENST00000409203				0.00033693	0.00031095	0	0	0	0
chr2	24815504	Frameshift variant	CENPO	ENST00000260662	114-115	-/X		0.00013778	0	0	0	0	0
chr2	24816739	Frameshift variant	CENPO	ENST00000260662	230	S/SX	rs749031613	0.00014249	0.00019223	0	0	0	0

Chr*	Position	Consequence	Symbol	Feature	Protein position	Amino acids	Existing variation	Allele frequency _ELGH*	Allele frequency _BiB*	Allele frequency _Birm*	Homozygous _ELGH*	Homozygous _BiB*	Homozygous _Birm*
chr2	121410944	Frameshift variant	CLASP1	ENST00000397587	754	G/X		0.00013273	0	0	0	0	0
chr2	121410949	Frameshift variant	CLASP1	ENST00000397587	749-752	GLGQ/X		0.0001328	0	0	0	0	0
chr2	168877357	Frameshift variant	SPC25	ENST00000282074	74-76	LIQ/X		0.00044736	0	0	0	0	0
chr2	168877364	Frameshift variant	SPC25	ENST00000282074	73-74	-/KKX		0.00045788	0	0	0	0	0
chr3	32537010	Splice donor variant	DYNC1LI1	ENST00000273130				0.00014201	0	0	0	0	0
chr3	33517176	Splice acceptor variant	CLASP2	ENST00000359576				0.00013477	0	0	0	0	0
chr3	33688283	Stop gained	CLASP2	ENST00000359576	155	L/*		0.00015461	0	0	0	0	0
chr2	24815520	Stop gained	CENPO	ENST00000260662	120	R/*		0.00013448	0	0	0	0	0
chr2	24815623	Stop gained	CENPO	ENST00000260662	154	S/*		0.00013228	0	0	0	0	0
chr2	3477796	Splice donor variant	TRAPPC12	ENST00000382110				0.00013982	0	0	0	0	0
chr2	37094196	Splice donor variant	GPATCH11	ENST00000409774			rs368988833	0.00013252	0	0	0	0	0
chr2	3421985	Stop gained & Inframe insertion	TRAPPC12	ENST00000382110	423-424	-/*LQ		0.00014049	0	0	0	0	0
chr2	3424621	Frameshift variant	TRAPPC12	ENST00000382110	459	L/LX		0.00013242	0	0	0	0	0
chr2	233841874	Frameshift variant	HJURP	ENST00000432087	248	K/X		0.00013326	0.00057186	0	0	0	0
chr4	67519235	Stop gained	CENPC	ENST00000273853	200	S/*		0.00092937	0	0	0	0	0

Chr*	Position	Consequence	Symbol	Feature	Protein position	Amino acids	Existing variation	Allele frequency _ELGH*	Allele frequency _BiB*	Allele frequency _Birm*	Homozygous _ELGH*	Homozygous _BiB*	Homozygous _Birm*
chr4	103140415	Splice acceptor variant	CENPE	ENST00000611174			rs568323371&COSM4425522&COSM4425523	0.00249233	0.00260312	0.00215517	1	0	0
chr4	103141032	Frameshift variant	CENPE	ENST00000611174	1845	K/X		0.00037965	0	0	0	0	0
chr4	184702110	Frameshift variant	CENPU	ENST00000281453	301	N/X	rs765428260	0.0012024	0	0.00139665	0	0	0
chr4	184717142	Frameshift variant	CENPU	ENST00000281453	123-125	ISA/X		0.00175968	0	0	0	0	0
chr4	184717149	Frameshift variant	CENPU	ENST00000281453	123	I/KKNX		0.00171569	0	0	0	0	0
chr4	13579926	Splice donor variant	BOD1L1	ENST00000040738				0.00026589	0	0	0	0	0
chr5	69202505	Splice acceptor variant	CENPH	ENST00000515001			rs753226337	0.00025641	0	0	0	0	0
chr5	69202550	Stop gained	CENPH	ENST00000515001	120	L/*		0.00018322	0.00019771	0	0	0	0
chr5	69202918	Splice acceptor variant	CENPH	ENST00000515001				0.00045732	0	0	0	0	0
chr5	169599012	Stop gained	SPDL1	ENST00000265295	393	R/*	rs371434309	0.00163443	0.00193274	0.00146056	0	0	0
chr5	65551581	Frameshift variant	CENPK	ENST00000514814	74-75	WQ/X		0.00020145	0	0	0	0	0
chr5	65551586	Frameshift variant	CENPK	ENST00000514814	72-73	SQ/X	rs762598205	0.0003827	0.00019849	0.00054825	0	0	0
chr5	69191826	Frameshift variant	CENPH	ENST00000515001	56	E/X		0.00023202	0	0	0	0	0
chr5	163460024	Frameshift variant	NUDCD2	ENST00000302764	9	S/SGX		0.0001327	0	0	0	0	0
chr5	173616332	Frameshift variant	BOD1	ENST00000285908	35	G/GX		0.00018811	0	0	0	0	0

Chr*	Position	Consequence	Symbol	Feature	Protein position	Amino acids	Existing variation	Allele frequency _ELGH*	Allele frequency _BiB*	Allele frequency _Birm*	Homozygous _ELGH*	Homozygous _BiB*	Homozygous _Birm*
chr6	49472184	Splice donor variant	CENPQ	ENST00000335783	NA		rs539329187	0.0003983	0	0	0	0	0
chr6	149746064	Splice acceptor variant	NUP43	ENST00000340413	NA		rs756994816	0.00019478	0	0	0	0	0
chr6	149746482	Frameshift variant	NUP43	ENST00000340413	5	Y/X		0.00026455	0	0	0	0	0
chr7	1936786	Stop gained	MAD1L1	ENST00000406869	570	R/*	rs376905987	0.00013319	0.00019128	0	0	0	0
chr7	2069313	Stop gained	MAD1L1	ENST00000406869	367	Q/*		0.00024237	0	0	0	0	0
chr7	2216278	Stop gained	MAD1L1	ENST00000406869	230	Q/*		0.00013994	0	0	0	0	0
chr7	2216210	Frameshift variant	MAD1L1	ENST00000406869	252	L/LAX		0.00015366	0	0	0	0	0
chr7	102472217	Splice acceptor variant	LRWD1	ENST00000292616			rs746390668	0.0001347	0	0	0	0	0
chr8	10832918	Stop gained	PINX1	ENST00000519088	66	G/*	rs766139889&COSM3884590	0.00013266	0	0	0	0	0
chr8	120502491	Splice acceptor variant	MTBP	ENST00000305949				0.0004686	0	0	0	0	0
chr10	56359474	Splice donor variant	ZWINT	ENST00000373944	NA			0.00030637	0	0	0	0	0
chr10	123157727	Splice acceptor variant	BUB3	ENST00000368865	NA			0.00378788	0	0	0	0	0
chr10	123157728	Splice acceptor variant	BUB3	ENST00000368865	NA			0.0052521	0	0	0	0	0
chr11	47812063	Splice donor variant	NUP160	ENST00000378460	NA			0.00013287	0	0	0	0	0

Chr*	Position	Consequence	Symbol	Feature	Protein position	Amino acids	Existing variation	Allele frequency _ELGH*	Allele frequency _BiB*	Allele frequency _Birm*	Homozygous _ELGH*	Homozygous _BiB*	Homozygous _Birm*
chr11	47821722	Splice donor variant	NUP160	ENST00000378460	NA			0.00026455	0	0	0	0	0
chr11	47848218	Splice donor variant	NUP160	ENST00000526870	NA		rs530402180	0.00013228	0	0	0	0	0
chr11	3778871	Splice donor variant	NUP98	ENST00000324932				0.00013305	0	0	0	0	0
chr11	47818049	Splice donor variant & coding sequence variant & intron variant	NUP160	ENST00000378460	477-?			0.00071463	0	0	0	0	0
chr11	47818056	Frameshift variant & splice region variant	NUP160	ENST00000378460	477	Q/QKKX		0.00069252	0	0	0	0	0
chr11	47848382	Frameshift variant	NUP160	ENST00000526870	13	P/PX		0.00031786	0	0	0	0	0
chr11	113744027	Frameshift variant	ZW10	ENST00000200135	429	S/X		0.00013932	0	0	0	0	0
chr11	134168984	Stop gained	NCAPD3	ENST00000534548	1058	E/*	COSM925153	0.00028209	0	0	0	0	0
chr11	134178937	Splice acceptor variant	NCAPD3	ENST00000534548	NA			0.00014205	0	0	0	0	0
chr11	134203200	Splice acceptor variant	NCAPD3	ENST00000534548	NA			0.00015878	0	0	0	0	0
chr11	134208948	Splice acceptor variant & coding sequence variant	NCAPD3	ENST00000534548	?-266			0.00127065	0	0	0	0	0
chr12	57532283	Stop gained	DCTN2	ENST00000543672	321	W/*		0.00014029	0	0	0	0	0

Chr*	Position	Consequence	Symbol	Feature	Protein position	Amino acids	Existing variation	Allele frequency _ELGH*	Allele frequency _BiB*	Allele frequency _Birm*	Homozygous _ELGH*	Homozygous _BiB*	Homozygous _Birm*
chr12	68719368	Stop gained	NUP107	ENST00000229179	371	Q/*		0.00013224	0	0	0	0	0
chr12	68721916	Stop gained	NUP107	ENST00000229179	463	Q/*		0.00026575	0	0	0	0	0
chr12	122319349	Splice acceptor variant	CLIP1	ENST00000545889			rs113860909&COSM5171831&COSM5171832	0.00013398	0	0	0	0	0
chr12	122539685	Stop gained	KNTC1	ENST00000450485	126	Q/*		0.00031506	0.00058027	0.0004995	0	0	0
chr12	122551524	Splice donor variant	KNTC1	ENST00000450485			rs867677251	0.00029248	0.00038197	0.00094787	0	0	0
chr12	122568373	Splice donor variant	KNTC1	ENST00000450485				0.00013441	0	0	0	0	0
chr12	122570897	Stop gained	KNTC1	ENST00000450485	591	E/*	COSM25648	0.0001957	0	0	0	0	0
chr12	122571049	Stop gained	KNTC1	ENST00000450485	611	Q/*	rs773583890	0.00013333	0	0	0	0	0
chr12	57535066	Frameshift variant	DCTN2	ENST00000543672	119-120	VE/X		0.00050684	0	0	0	0	0
chr12	57535075	Frameshift variant	DCTN2	ENST00000543672	117	T/KKNX		0.00047939	0	0	0	0	0
chr12	102112163	Frameshift variant	NUP37	ENST00000552283	75-76	-/X		0.00013256	0	0	0	0	0
chr12	122542084	Frameshift variant	KNTC1	ENST00000450485	160-161	-/X		0.00016072	0	0	0	0	0
chr12	122568288	Frameshift variant	KNTC1	ENST00000450485	508-509	NE/X		0.0001517	0	0	0	0	0
chr12	122569751	Frameshift variant	KNTC1	ENST00000450485	559-560	SL/SX		0.00013287	0	0	0	0	0

Chr*	Position	Consequence	Symbol	Feature	Protein position	Amino acids	Existing variation	Allele frequency _ELGH*	Allele frequency _BiB*	Allele frequency _Birm*	Homozygous _ELGH*	Homozygous _BiB*	Homozygous _Birm*
chr12	122621878	Splice acceptor variant & coding sequence variant	KNTC1	ENST00000436959	?-15			0.00013326	0	0	0	0	0
chr12	122621882	Frameshift variant splice region variant	KNTC1	ENST00000436959	15	N/NFX		0.00026795	0	0	0	0	0
chr13	21157921	Splice donor variant	SKA3	ENST00000314759			rs151054732	0.0584826	0.0158151	0.0427873	0	0	0
chr13	21159937	Frameshift variant	SKA3	ENST00000314759	293-294	-/TYILYSWX		0.0001414	0	0	0	0	0
chr13	21168145	Frameshift variant	SKA3	ENST00000314759	194-195	KQ/X	rs761949351	0.00013305	0	0	0	0	0
chr13	21172461	Frameshift variant	SKA3	ENST00000314759	70	Q/X	rs151272242&COSM1317935&COSM432211	0.195766	0.133444	0.165934	2	0	0
chr14	102010275	Splice acceptor variant	DYNC1H1	ENST00000360184				0.00057405	0	0	0	0	0
chr14	102026571	Splice acceptor variant & coding sequence variant	DYNC1H1	ENST00000360184	?-2880			0.00146413	0	0	0	0	0
chr14	102026575	Frameshift variant & splice region variant	DYNC1H1	ENST00000360184	2880	D/DFX		0.00170543	0	0	0	0	0
chr14	24179672	Frameshift variant	REC8	ENST00000611366	466	M/X	rs139641571	0.00013323	0	0.00047259	0	0	0

Chr*	Position	Consequence	Symbol	Feature	Protein position	Amino acids	Existing variation	Allele frequency _ELGH*	Allele frequency _BiB*	Allele frequency _Birm*	Homozygous _ELGH*	Homozygous _BiB*	Homozygous _Birm*
chr14	45224030	Frameshift variant	MIS18BP1	ENST00000310806	852-853	-/X		0.00026803	0	0	0	0	0
chr14	45226825	Frameshift variant	MIS18BP1	ENST00000310806	585-586	IG/X		0.00095511	0	0	0	0	0
chr14	45226831	Frameshift variant	MIS18BP1	ENST00000310806	584	L/X		0.00079051	0	0	0	0	0
chr14	45242052	Frameshift variant	MIS18BP1	ENST00000310806	375	N/KKKX		0.00046404	0	0	0	0	0
chr14	45246830	Frameshift variant	MIS18BP1	ENST00000310806	152-153	-/KX		0.00039825	0	0	0	0	0
chr15	40208635	Splice acceptor variant	BUB1B	ENST00000412359			rs528022763	0.00013499	0.00019069	0	0	0	0
chr15	66528941	Stop gained	ZWILCH	ENST00000535141	239	W/*		0.00013312	0	0	0	0	0
chr15	40206405	Frameshift variant	BUB1B	ENST00000412359	667-674	QTACGTIY/X		0.00013721	0	0	0	0	0
chr15	40264813	Frameshift variant	BUB1B-PAK6	ENST00000441369	10	P/X		0.00026462	0	0	0	0	0
chr15	40265912	Frameshift variant	BUB1B-PAK6	ENST00000441369	92	L/LSVISSX		0.00013228	0	0	0	0	0
chr15	40383288	Frameshift variant	KNSTRN	ENST00000608100	13	P/X	rs746725876	0.00013249	0.00019055	0	0	0	0
chr16	81012048	Stop gained	CENPN	ENST00000428963	37	Q/*		0.00013897	0.00038403	0	0	0	0
chr16	15687418	Stop gained	NDE1	ENST00000396355	144	Q/*		0.00013277	0	0.00047259	0	0	0
chr16	88807279	Splice acceptor variant	CDT1	ENST00000301019				0.00013277	0	0	0	0	0

Chr*	Position	Consequence	Symbol	Feature	Protein position	Amino acids	Existing variation	Allele frequency _ELGH*	Allele frequency _BiB*	Allele frequency _Birm*	Homozygous _ELGH*	Homozygous _BiB*	Homozygous _Birm*
chr16	3758045	Splice acceptor variant & coding sequence variant & intron variant	CREBBP	ENST00000262367	?-1124			0.00068431	0	0	0	0	0
chr16	3758046	Splice acceptor variant & coding sequence variant & intron variant	CREBBP	ENST00000262367	?-1124			0.00260552	0	0	0	0	0
chr16	15691299	Frameshift variant	NDE1	ENST00000396355	227	N/X	rs756206942	0.00013235	0.00038124	0.00047214	0	0	0
chr17	58559452	Splice donor variant	TEX14	ENST00000349033			rs752772371	0.0004451	0.00019084	0	1	0	0
chr17	58587667	Splice acceptor variant	TEX14	ENST00000349033			COSM4068209&COSM4068210	0.00013245	0	0	0	0	0
chr17	58611255	Stop gained	TEX14	ENST00000349033	364	Q/*		0.00047423	0	0	0	0	0
chr17	58613423	Stop gained & splice region variant	TEX14	ENST00000349033	335	R/*	rs141801212&COSM3370828&COSM3370829	0.00053952	0.00038595	0.0038059	0	0	0
chr17	8436018	Splice donor variant & 5 prime UTR variant & intron variant	NDEL1	ENST00000334527				0.00014347	0	0	0	0	0
chr17	16353362	Frameshift variant	CENPV	ENST00000299736	25	A/X	rs560390150&rs747644694	0.00507614	0	0	0	0	0

Chr*	Position	Consequence	Symbol	Feature	Protein position	Amino acids	Existing variation	Allele frequency _ELGH*	Allele frequency _BiB*	Allele frequency _Birm*	Homozygous _ELGH*	Homozygous _BiB*	Homozygous _Birm*
chr17	16353364	Frameshift variant	CENPV	ENST00000299736	22-24	AAP/X	rs769584320	0.00452489	0	0	0	0	0
chr17	16353388	Frameshift variant	CENPV	ENST00000299736	15-16	QK/X		0.0133333	0.0319149	0	0	0	0
chr17	16353397	Frameshift variant	CENPV	ENST00000299736	13	R/X		0.00930233	0.0205479	0	0	0	0
chr17	58584572	Frameshift variant	TEX14	ENST00000349033	1033	K/X		0.00013373	0	0	0	0	0
chr17	58601900	Stop gained & frameshift variant	TEX14	ENST00000349033	528	Y/*		0.00024378	0	0	0	0	0
chr17	28579224	Stop gained	SPAG5	ENST00000321765	1012	Q/*		0.00028843	0	0	0	0	0
chr17	28598925	Frameshift variant	SPAG5	ENST00000321765	7	L/X	rs575381663	0.00873016	0.00476372	0.00943396	0	0	0
chr18	2595502	Stop gained	NDC80	ENST00000261597	368	R/*		0.0001347	0	0	0	0	0
chr18	12963158	Splice acceptor variant	SEH1L	ENST00000262124	NA		rs147738564	0.00223464	0	0	0	0	0
chr18	12963159	Splice acceptor variant	SEH1L	ENST00000262124	NA			0.00195799	0	0	0	0	0
chr20	56386380	Frameshift variant	AURKA	ENST00000395915	62-65	QKLV/X	rs755109797	0.0001333	0.00019069	0	0	0	0
chr20	4792537	Splice donor variant	RASSF2	ENST00000379400	NA		rs773175975	0.00039767	0.00057186	0.00047259	0	0	0

MCPH genes

MVA genes

Microcephaly associated genes

ELGH*	BiB*	Birm*
3781	2624	1060
Sample size		

Chr*	Position	Consequence	Symbol	Feature	Protein position	Amino acids	Existing variation	Allele frequency _ELGH*	Allele frequency _BiB*	Allele frequency _Birm*	Homozygous _ELGH*	Homozygous _BiB*	Homozygous _Birm*

***Chr = chromosome, ELGH=East London Genes and Health, BiB = Born in Bradford, Birm = Birmingham.**

Chromosome: Chromosome name.
Position: Mutated base position.
Consequence: Predicted consequence of the mutation based on the transcript indicated.
Symbol: Gene name.
Feature: Transcript name.
Protein position: Position of amino acid affected.
Amino acid: Amino acid name.
Existing variation: Variant identifier if the variant is present in other databases.
Allele frequency: Frequency at which the allele is present in the database subset indicated.
Homozygous: Number of homozygous variants identified in the database subset indicated.

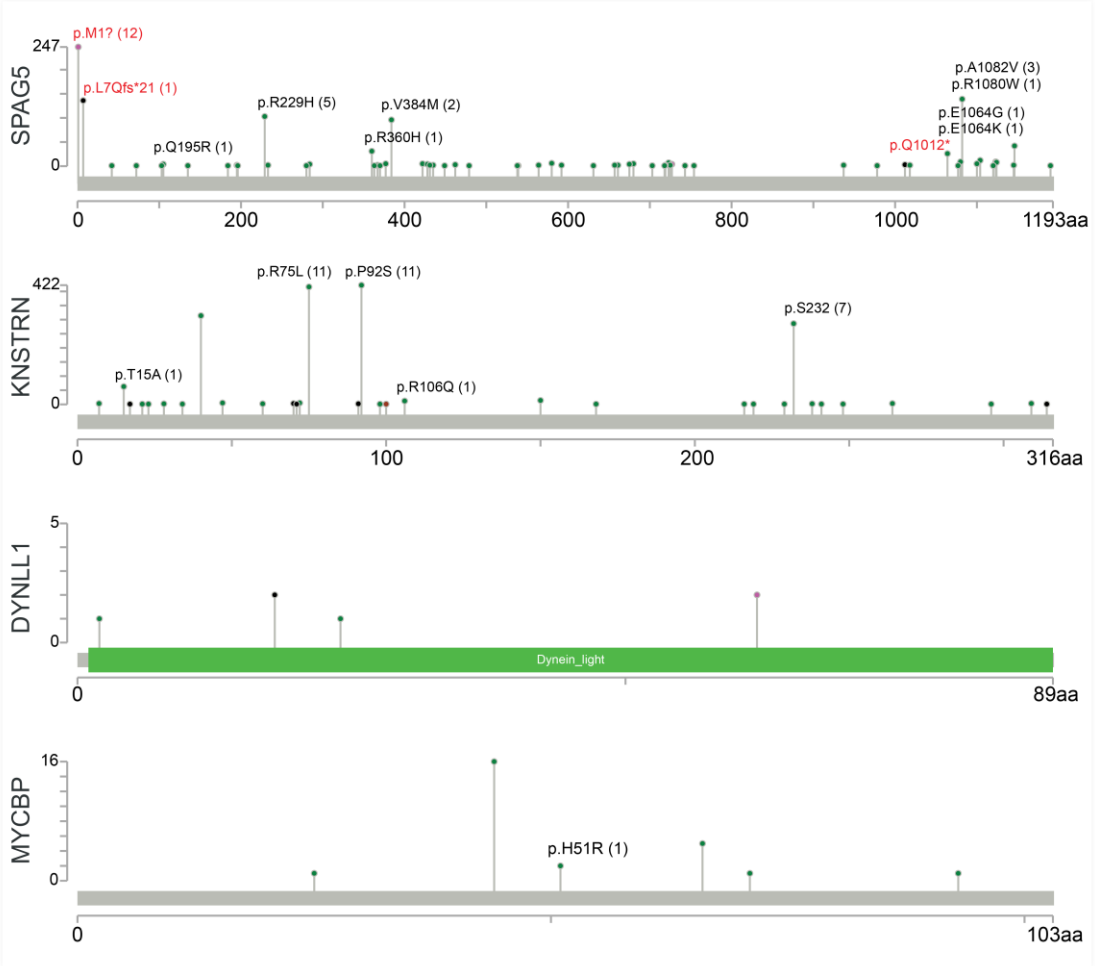

Fig 3.1. Variation spectrum of Astrin-SKAP complex in Genes and Health database. Lollipop plot showing the amino acid position (x-axis) and the number of occurrences (y-axis) of different types of genomic variations in the four Astrin-SKAP complex members A black dot indicates a truncating mutation, a green dot indicates a missense mutation and a purple dot indicates other mutation types. The red font indicates interesting variations. Numbers in brackets indicate the number of homozygous occurrences.

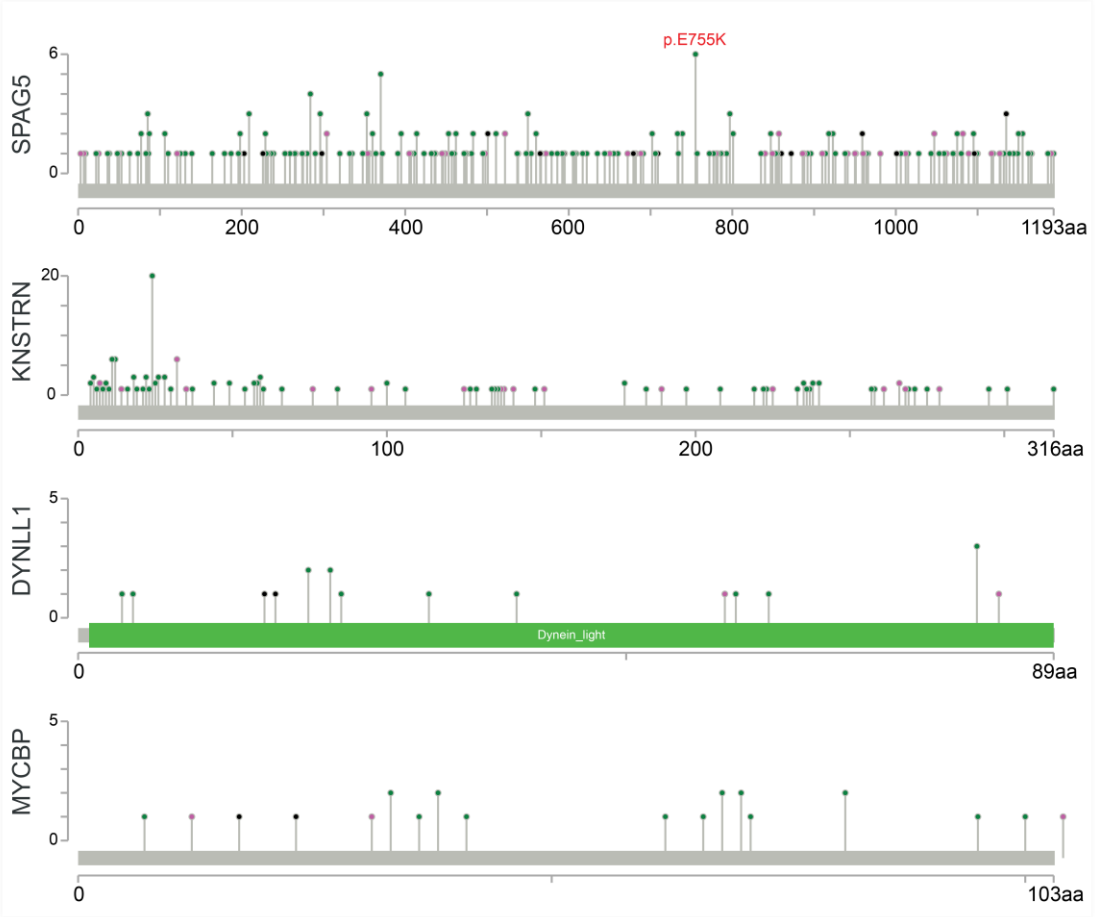

Fig 3.2. Variation spectrum of Astrin-SKAP complex in COSMIC database. Lollipop plot showing the amino acid position (x-axis) and the number of occurrences (y-axis) of different types of genomic variations in the four Astrin-SKAP complex members A black dot indicates a truncating mutation, a green dot indicates a missense mutation and a purple dot indicates other mutation types. The red font indicates interesting variations.

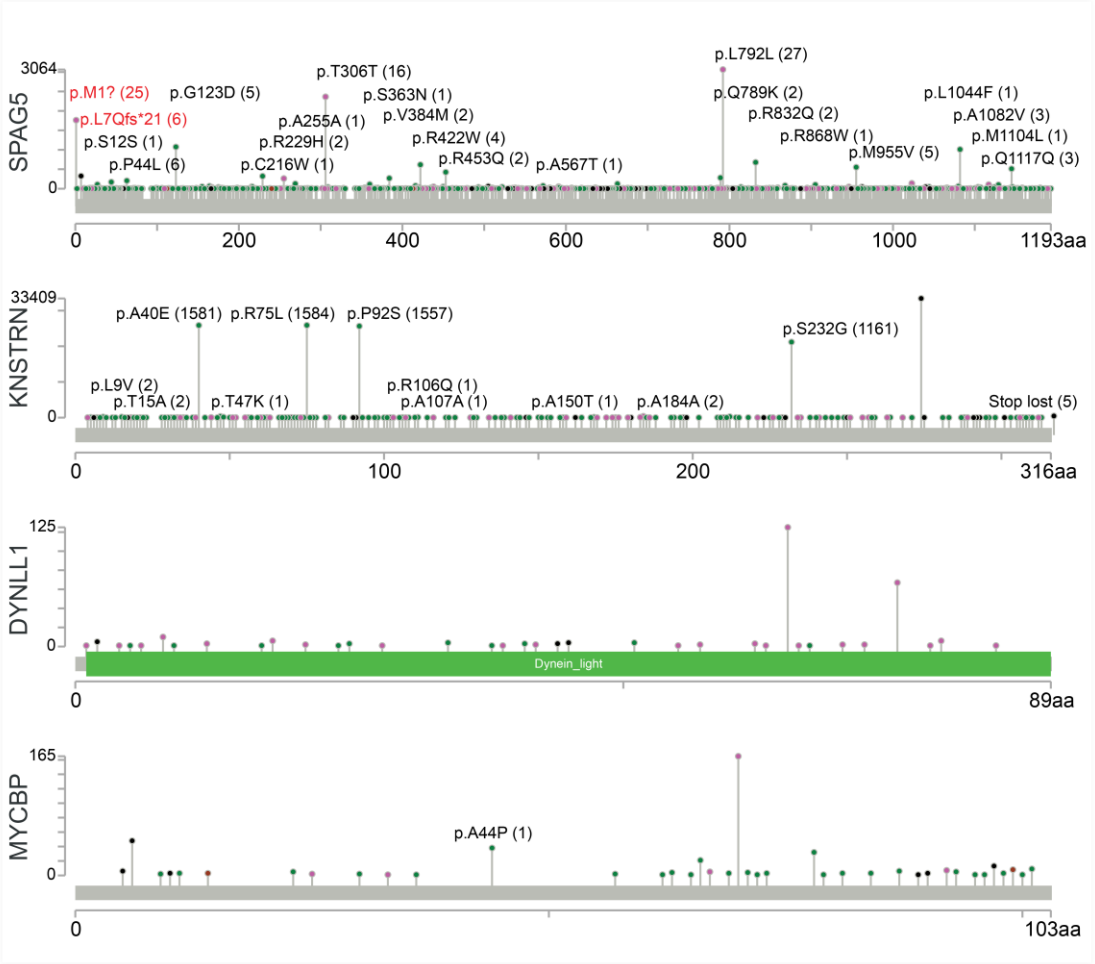

Fig 3.3. Variation spectrum of Astrin-SKAP complex in gnomAD database. Lollipop plot showing the amino acid position (x-axis) and the number of occurrences (y-axis) of different types of genomic variations in the four Astrin-SKAP complex members. A black dot indicates a truncating mutation, a green dot indicates a missense mutation and a purple dot indicates other mutation types. The red font indicates interesting variations. Numbers in brackets indicate the number of homozygous occurrences.

3.3 PERCENTAGE OF TUMOUR SAMPLES WITH SOMATIC MUTATIONS IN ASTRIN-SKAP COMPLEX IS NOT HIGH

The two predicted LOF variants of Astrin were not observed in the COSMIC database (Tate et al. 2019). One possible explanation is that the incidence of somatic mutations in Astrin is low. To test this, I compared the tumor samples bearing somatic mutations in five different categories of genes: a) primary microcephaly (MCPH) genes, b) mosaic-variegated aneuploidy (MVA) genes, c) Astrin-SKAP complex, d) Astrin-SKAP complex interacting partners and e) tumour suppressor genes (only two genes selected in this category as positive controls). In this assessment, I included forty

different tumor tissue types available on the COSMIC database (Tate et al. 2019) and compared the percent mutation burden for each gene in each tumor type. As expected, TP53 gene mutations are found in all tissue types and the percentage of samples with mutation/s is also high (**Fig 3.4**). Mutations in the BRCA1 gene, MCPH genes, and most Astrin-SKAP complex interacting partners are not ubiquitously present in all tissue types suggesting tissue-specificity (**Fig 3.4**). Astrin-SKAP complex, NDC80 complex (one of the interacting partners of Astrin-SKAP complex (Conti et al. 2019; Kern et al. 2017)) and MVA genes, on the other hand, show tissue-specificity, as well as lower incidence, compared to the other three groups suggesting a lower incidence of somatic mutations in Astrin/SKAP genes (**Fig 3.4**, see box). The most mutated position in Astrin was p.E755, converted to a K, which was specifically found in skin cancers (n=3, **Fig 3.4**). I conclude that the percentage of tumor samples with somatic mutations in Astrin-SKAP complex, NDC80 complex and MVA genes is low.

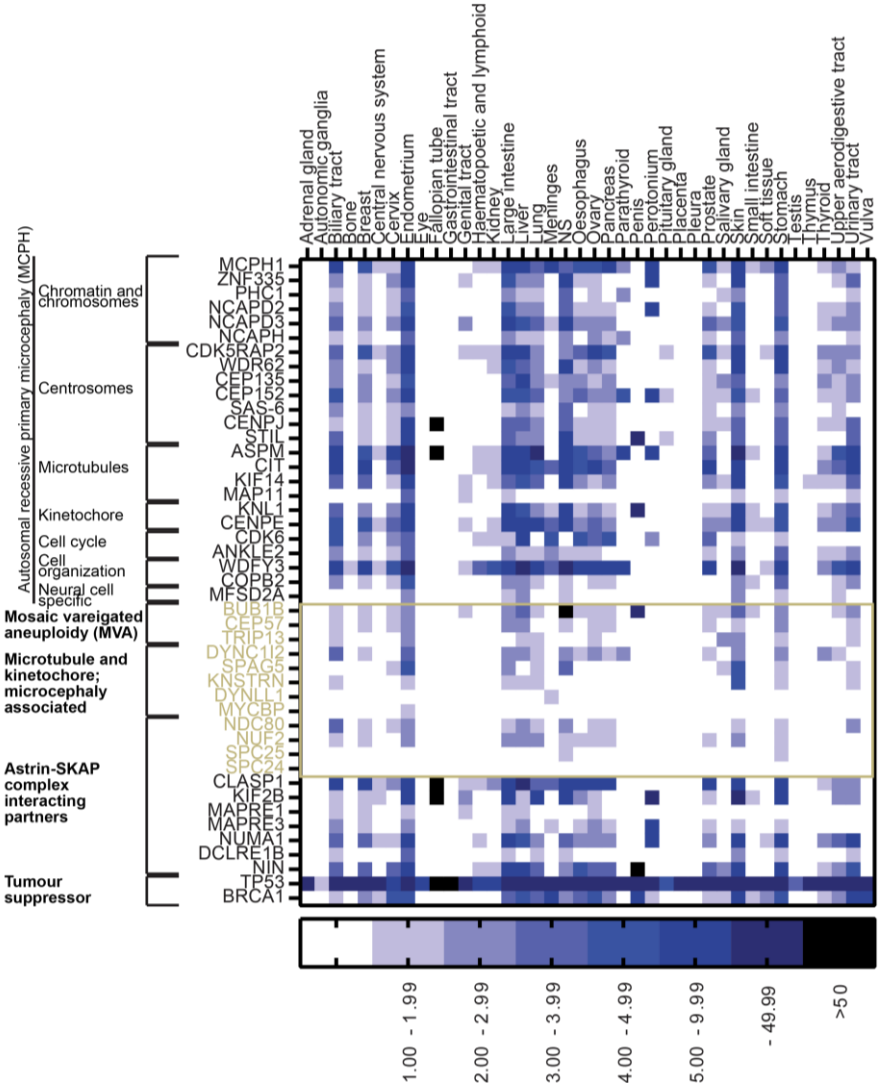

Fig 3.4. The percentage of tumor samples with somatic mutations in the Astrin-SKAP complex is low compared to MCPH and tumor suppressor genes. Heat map showing the percentage of samples with variations in selected genes in different tumor types in the COSMIC database. Box shows genes with a low percentage of tumor samples with somatic mutations.

3.4 PREDICTED CONSEQUENCES OF HUMAN ASTRIN VARIANTS

To investigate the consequences of Astrin p.L7Qfs*21 variant, I first asked whether Astrin$^{1-59}$, part of Astrin protein encoded by the first and second exon of the human SPAG5 gene, is conserved across species. This is important because Astrin is found as two isoforms in epithelial cell lines (HeLa; (Thein 2008)). Conservation analysis using MAFFT (Madeira et al. 2019) suggests that Astrin$^{1-59}$ is conserved in mammals (**Fig 3.5 A**). Next, I asked whether Astrin$^{1-59}$ has been detected in proteomics

studies. For this purpose, I analyzed the proteomics data available on the PRIDE database (Vizcaíno et al. 2016) and found that 1-59 a.a. of Astrin has been detected in the proteomics studies analyzed (**Fig 3.5 B**). Since these proteomic studies could not be qualitatively segregated, it is not clear if the two forms of Astrin are present simultaneously in cells, as shown in HeLa cell mass spectrometry studies (Thein 2008).

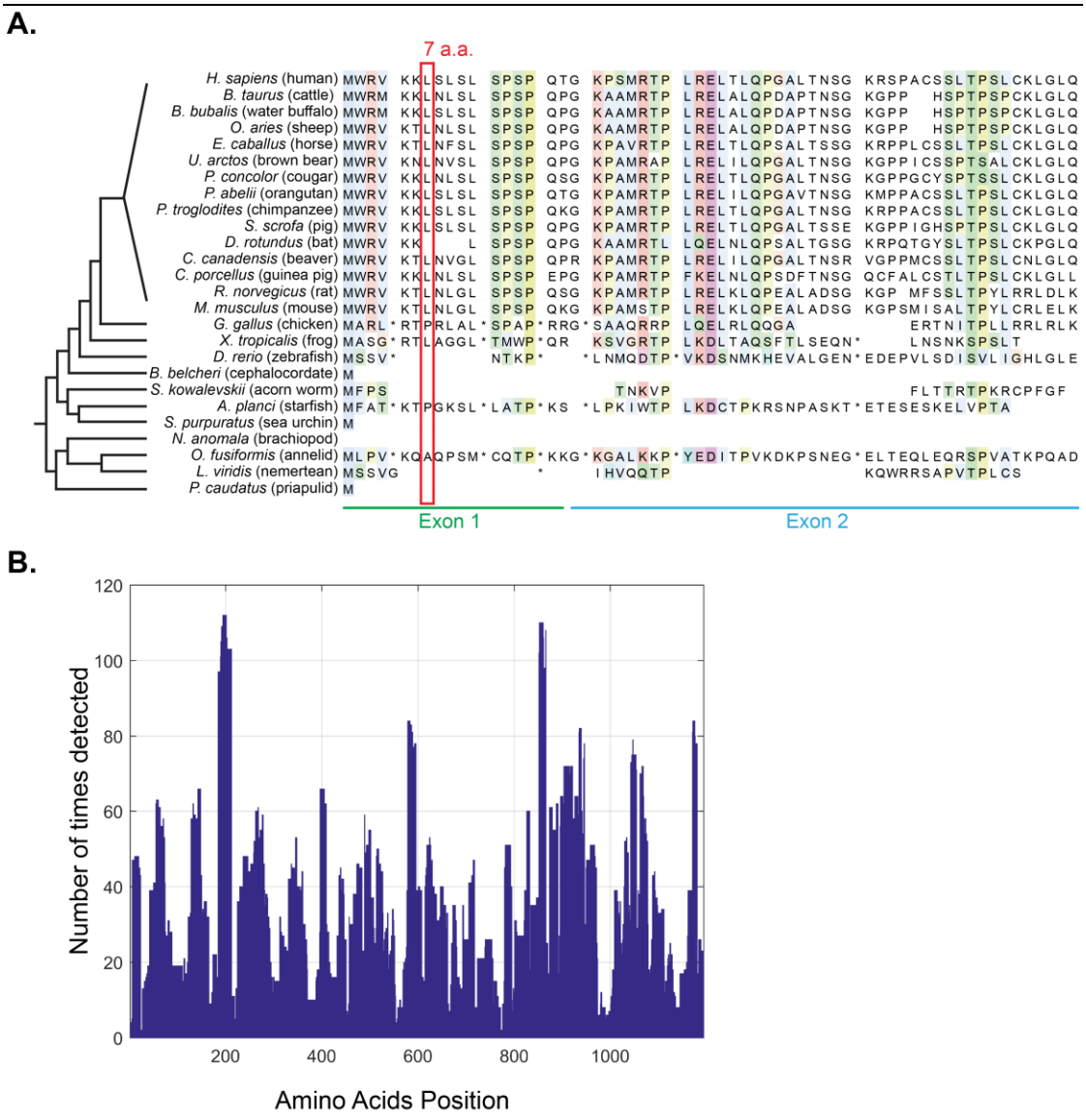

Fig 3.5. N-terminus of Astrin is conserved in mammals and detected in proteomics analysis. A. Conservation analysis of first and second exon of Astrin. Clustal color scheme: Blue represents hydrophobic, Red represents positively charged, Magenta represents negatively charged, Green represents polar, Pink represents Cysteines, Orange represents Glycines, Yellow represents Prolines, Cyan represents aromatic and white represents unconserved residues. **B.** Proteomics data analysis of Astrin from PRIDE database. The x-axis shows the amino acid position in the Astrin sequence, whereas the y-axis shows the number of times the amino acid was detected.

To investigate the consequences of Astrin p.Q1012* variant, I asked whether 1012-1193 a.a. of Astrin is conserved across species. Conservation analysis suggests that this region is conserved in mammals, birds, reptiles, and fish (**Fig 3.6**), suggesting that this region's loss may not be tolerated. Moreover, a motif search resulted in several potential phosphatase docking motifs suggesting it may target phosphatases to the kinetochores (**Fig 3.6**).

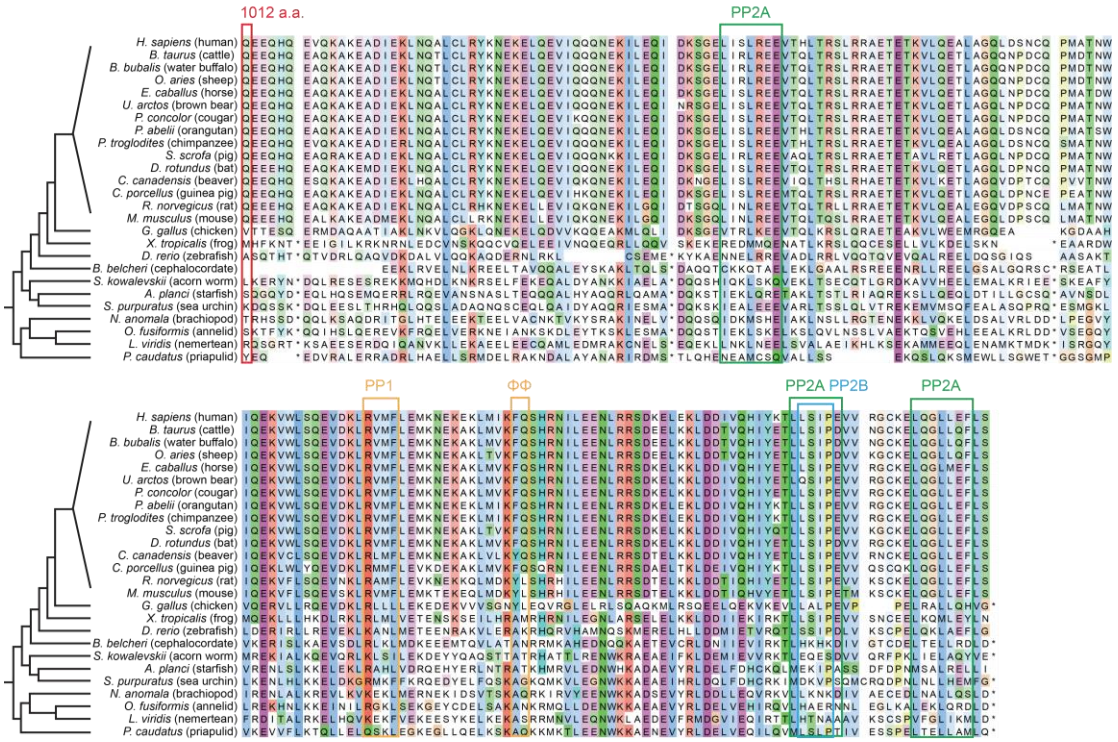

Fig 3.6. C-terminus of Astrin beyond 1011 a.a. is highly conserved across species. Conservation analysis of C-terminus of Astrin beyond 1011 a.a. of Astrin showing potential phosphatase docking motifs. Clustal color scheme: Blue represents hydrophobic, Red represents positively charged, Magenta represents negatively charged, Green represents polar, Pink represents Cysteines, Orange represents Glycines, Yellow represents Prolines, Cyan represents aromatic and white represents unconserved residues.

I conclude that expression of Astrin p.Q1012* variant would result in the loss of highly conserved C-terminus of Astrin, which may explain why the variant is rare and only present as heterozygous. On the other hand, the N-terminus of Astrin is not as conserved but is detected in the proteomic studies giving clues regarding tolerance of Astrin p.L7Qfs*21 variant in healthy individuals.

3.5 DISCUSSION

To ensure faithful segregation of chromosomes, kinetochores (KTs), multiprotein complexes composing of over 100 proteins assemble onto the centromeric regions of the chromosomes and play a key role in attaching chromosomes to the microtubules and stabilizing the said attachments (Reviewed in: (Musacchio and Desai 2017; Yamagishi et al. 2014; Monda and Cheeseman 2018). *In vitro* and *in vivo* studies have shown that many of the KT genes are essential, and their dysregulated expression causes chromosomal instability making them targets for cancer therapy (Reviewed in: (Herman et al. 2015; Jablonski, Liu, and Yen 2003)). Moreover, with the increase in the number of genetic studies being carried out in recent years, it is becoming apparent that genomic variations in KT proteins may also be linked with developmental disorders (Reviewed in: (Degrassi, Damizia, and Lavia 2019). KNL1, a key KT gene, was the first KT gene to be associated with microcephaly (Jamieson et al., 1999), a developmental disorder characterized by reduced head size below three standard deviations. The affected individuals were four siblings born of consanguineous Moroccan parents and had microcephaly, poor growth, and mental retardation (Jamieson et al., 1999). Since then, at least three more KT proteins with genomic variations have been linked to microcephaly or related disorders (OMIM 604321, OMIM 11743, OMIM 602680, (Tahmasebi-Birgani, Ansari, and Carloni 2019; Ansar et al. 2019; Boonsawat et al. 2019). A study on human embryonic cells by introducing microcephaly-specific KNL1 point mutation has shown that the variant's expression leads to neuronal cell-specific phenotype comprising increased cell death, decreased proliferation rate and reduced cell specialization (Javed et al., 2018). Moreover, the cell-specificity is due to the generation of an exonic splicing silencer site that is recognized by an inhibitory splicing protein highly expressed in neural progenitors (Javed et al., 2018). The study explains how humans may survive with genomic variations in essential genes and highlights how the cell-specific expression of these variants may affect health.

Developmental disorders such as microcephaly are more prevalent in populations with increased occurrence of consanguineous marriages. Genes and Health (GH) study in the UK is a genomic study on UK residents of Pakistani-Bangladeshi ancestry, a community known for a higher incidence of consanguineous marriages

(Finer et al. 2020). Here, I have identified 142 LOF variants in KT genes from the GH 2018 LOF variants list (Finer et al. 2020) (**Table 3.1**). Out of these, 94 variants are new, and except for four, all are present only as heterozygous (**Table 3.1**). Moreover, I have identified nine variants of MCPH and MVA genes, including two CENP-E variants, four NCAPD3 variants, one BUB1B variant, and two SPAG5 variants (**Table 3.1**). Out of these, one CENP-E C-terminal frameshift variant-predicted to cause loss of C-terminal microtubule (MT) binding region (Musinipally et al. 2013), three splice acceptor NCAPD3 variants, and one C-terminal stop-gained SPAG5 variant-predicted to cause loss of its KT targeting region (Dunsch et al. 2011; Kern, Wilson-Kubalek, and Cheeseman 2017; Conti et al. 2019), are not listed on *Ensembl* (Yates et al. 2020).

Comparing the somatic mutation burden in the COSMIC database (Tate et al. 2019), I show that the percentage of tumor samples with somatic mutations in MVA genes is lower than those for MCPH and tumor suppressor genes (**Fig 3.4**). Genomic variations in MCPH genes are associated with microcephaly, but variations in MVA genes can cause aneuploidy and early-onset cancer, in addition to microcephaly (Reviewed in: (Degrassi, Damizia, and Lavia 2019)). One possible explanation for the low percentage of tumor samples with somatic mutations in MVA genes is increased protection from the cells to avoid aneuploidy. Genomic variations in SPAG5 and DYN1l2 are associated with microcephaly (Boonsawat et al. 2019; Ansar et al. 2019), and both appear to have a low percentage of tumor samples with somatic mutations (**Fig 3.4**). SPAG5 gene-encodes Astrin protein, part of a 4-unit Astrin-SKAP complex (Kern, Wilson-Kubalek, and Cheeseman 2017). Astrin interacts with NDC80-a key KT-MT attachment protein, and CLASP1-a MT associated protein, and plays a crucial role in stabilizing KT-MT attachments (Kern, Wilson-Kubalek, and Cheeseman 2017; Manning et al. 2010). The COSMIC data analysis shows that all genes in the Astrin-SKAP complex, NDC80 complex, and CLASP1 have a low percentage of tumor samples with somatic mutations (**Fig 3.4**), suggesting like MVA genes, they may also be protected against somatic mutations.

Astrin, a long coiled-coil protein, is required for KT-MT attachment stability (Dunsch et al. 2011; Shrestha et al. 2017; Conti et al. 2019; Kern, Wilson-Kubalek, and Cheeseman 2017). Here, I have identified two human Astrin variants- p.L7Qfs*21 and p.Q1012*, in the GH database. I further show that Astrin p.Q1012* is specific to the

Pakistani-Bangladeshi community in East London, and although Astrin p.L7Qfs*21 variant is present in the gnomAD database, it is mainly found in South Asians (**Table 3.1**, **Fig 3.1**, 3.2 and 3.3). There are only two known individuals with Astrin p.Q1012* variation, and both are heterozygous for it, suggesting it may not be tolerated (**Table 3.1**, **Fig 3.1**). On the other hand, Astrin p.L7Qfs*21 homozygotes are found in gnomAD (n=6) and in GH's all variants 2020 list (n=1), suggesting the variation is tolerated (**Table 3.1**, **Fig 3.1**).

Astrin p.L7Qfs*21 is a frameshift very close to the start site, but it is tolerated in healthy individuals suggesting either a) Astrin is not essential, which contradicts the cell culture studies (Dunsch et al. 2011; Gruber et al. 2002; Schmidt et al. 2010; Thein et al. 2007), or b) a shorter isoform of Astrin is expressed in these individuals and is sufficient for Astrin's function. Western blot and mass spectrometry data of human epithelial cells have shown that Astrin exists as two isoforms (HeLa, (Thein 2008)). However, whether the two Astrin isoforms are tissue-specific and/or have different roles is not known. The PRIDE data analysis suggests that all 1-1193 a.a. of Astrin are detected in mass spec analysis (**Fig 3.4 B**), but whether there is a difference in expression between studies/cell lines is not clear. The N-terminus of Astrin is conserved among mammals but not in birds, reptiles, and fish (**Fig 3.4 A**), suggesting it may have evolved to perform additional roles in higher species. The N-terminal of Astrin is phosphorylated by several kinases such as Aurora-A, CDK1, and GSK3 β and binds Plk1 kinase in a CDK-dependent manner (Cheng et al. 2008; Chiu et al. 2014; Chung et al. 2016; Geraghty et al. 2021). Cells expressing Astrin with mutated Aurora-A phosphorylation site have disrupted spindle size and undergo prolonged mitosis (Chiu et al. 2014). Cells expressing Astrin with mutated Plk1 binding site have unstable KT-MT attachment (Geraghty et al. 2021). However, cells with mutated Plk1 binding site on Astrin or lacking the first 464 amino acids of Astrin can progress through an unperturbed cell cycle (Geraghty et al. 2021). It is possible that cells may be able to tolerate the loss of Astrin N-terminus, which may explain the presence of Astrin p.L7Qfs*21 homozygotes in a healthy population. It is also possible that the lack of Astrin's N-terminus may affect the cell's ability to handle stress. Hence, it would be interesting to study the impact of Astrin p.L7Qfs*21 on Astrin's expression, localization, and function.

The Astrin p.Q1012* variant is predicted to lack the last 182 amino acids in the C-terminal region of Astrin and the whole complex is targeted to the KTs through its C-terminus (Shrestha et al. 2017). Moreover, the C-terminus of Astrin is conserved across mammals, birds, reptiles, and fish, and contains several potential phosphatase docking motifs (**Fig 3.5**, (Conti et al. 2019)). Kinases and phosphatases play a key role in regulating mitosis, including KT-MT attachment stability, spindle assembly checkpoint silencing, and metaphase to anaphase transition (Reviewed in: (Saurin and Kops 2016; Vallardi, Cordeiro, and Saurin 2017)). The data collectively suggests Astrin p.Q1012* variant would not be tolerated by the cells, which may explain the lack of Astrin p.Q1012* homozygotes in a healthy population. However, it would be interesting to see whether the cells will be able to tolerate the variant in the presence of a normal copy of Astrin or would they completely rid themselves of the variant.

CHAPTER 4: RESULTS-II – LOCALIZATION OF HUMAN ASTRIN VARIANTS

CHAPTER 4: RESULTS-II – LOCALIZATION OF HUMAN ASTRIN VARIANTS

4.1 INTRODUCTION

Two Astrin LOF variants (p.L7Qfs*21 and p.Q1012*) were identified from the Genes and Health (GH) database, a genetic study of UK residents of Pakistani-Bangladeshi origin (Finer et al. 2019)) and one Astrin somatic mutant was identified from the COSMIC database ((Tate et al. 2019); see **Chapter 3**).

Presence of human Astrin p.L7Qfs*21 homozygotes suggest a complete loss of Astrin in affected individuals. However, Astrin depletion in cultured mammalian cells leads to the formation of multipolar spindles, chromosome congression and segregation defects, and increased apoptosis (K. H. Thein et al. 2007; Schmidt et al. 2010; Gruber et al. 2002). Unless the Astrin depletion phenotype significantly differs between cultured cells and humans, the presence of this variation in a healthy population makes this scenario unlikely. Alternatively, a shorter isoform of Astrin may be expressed that retains functionality. Astrin migrates as a doublet with a 20-40 kDa difference on an SDS-PAGE gel, and mass spectrometry analysis by Thein (Thein 2008) showed that the lower band of Astrin lacks the N-terminal region raising the possibility that Astrin exists as two isoforms in humans. The N-terminal region of Astrin interacts with NDC80, a key kinetochore (KT) protein involved in KT-microtubule (MT) attachments (Kern, Wilson-Kubalek and Cheeseman, 2017, Tamura PhD, Draviam Lab; unpublished data), and is phosphorylated by CDK1, PLK1, GSK3β, and Aurora-A kinases (Geraghty et al. 2020; Cheng et al. 2008; Chiu et al. 2014). However, a recent study has shown that a lack of the first 464 a.a. has no impact on spindle bipolarity and cell cycle progression but reduces KT-MT attachment stabilization efficiency in metaphase arrested cells (Geraghty et al. 2020), suggesting that the N-terminus may be required only in stress conditions.

Human Astrin p.Q1012* variant is rare and only observed in two individuals. Furthermore, this variant is only present as heterozygous. During interphase, the C-terminus of Astrin (608-1193 a.a.) directly interacts with Ninein, a centrosomal protein with a key role in minus-end MT positioning and anchoring (Cheng et al. 2007). The complex dissociates at the start of mitosis, and Astrin starts to localize at the MTs

through its partner SKAP (Schmidt et al. 2012; Dunsch et al. 2011; Kern et al. 2016; Kern, Wilson-Kubalek, and Cheeseman 2017). During metaphase, in addition to its presence at the MTs, Astrin is selectively recruited to mature or end-on attached KTs (Shrestha and Draviam 2013) through its C-terminus (694-1193 a.a.; (Dunsch et al. 2011; Kern, Wilson-Kubalek, and Cheeseman 2017)). This recruitment occurs in two steps – first as a low-intensity "sleeve," which is connected to the MT signal, and then gradually converting into a brighter "crescent" (Conti et al. 2019). Deletion of the last 70 a.a. of Astrin has no impact on minus-end MT positioning and anchoring but impairs Astrin's localization at the KTs as a "crescent" and de-stabilizes end-on attachments (Conti et al. 2019). Altogether, the data suggest that individuals with Astrin p.Q1012* would have Astrin localization defects during mitosis, impacting Astrin's function.

Astrin p.E755K is a point mutation changing the charge from negative to positive in the NDC80 interacting region (Tamura PhD, Draviam Lab; unpublished data). NDC80 complex is a key KT-MT attachment protein (McCleland et al. 2003), and the change in charge may affect Astrin-NDC80 interaction.

This chapter investigates the localization of the selected Astrin variants at the spindle and KTs. Throughout the chapter, Astrin localization at the KTs is divided into four categories: high (91-100% KTs with Astrin crescents), medium (51-90% KTs with Astrin crescents), low (2-50% KTs with Astrin crescents), and no crescent (0-1% KTs with Astrin crescents), (**Fig 4.1**).

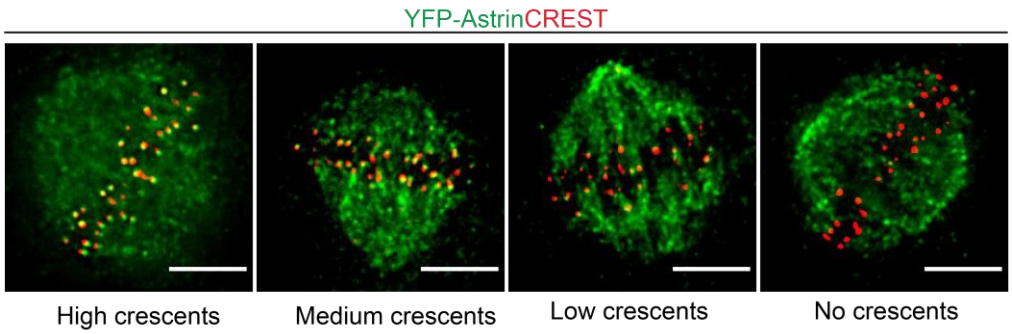

Fig 4.1 Scoring of Astrin localization in metaphase-arrested cells. Representative immunofluorescence images of metaphase arrested Hela cells expressing YFP-Astrin probed for GFP and CREST, centromeric marker, showing high, medium, low and no Astrin crescents. Scale: 5µm.

4.2 LOCALIZATION OF HUMAN ASTRIN P.L7QFS*21 VARIANT

4.2.1 ASTRIN-GFP p.L7* MUTANT EXPRESSES AS A SHORT PROTEIN

To investigate the expression and subcellular localization of human Astrin p.L7Qfs*21 variant, I generated a plasmid encoding a C-terminal GFP tagged Astrin with a stop codon at 7 a.a. (**Fig 4.2 A**). Immunostaining studies in metaphase arrested HeLa cells show an expression of a protein decorating the spindle similar to the Astrin-GFP wild type (WT, n=20, 10 cells from each set; **Fig 4.2 D**). However, both Astrin-GFP WT and p.L7* show a compromised localization at the kinetochores (n=20, 10 cells from each set; **Fig 4.2 D**). The observed compromised localization of Astrin-GFP WT is in agreement with previous studies (Conti et al. 2019). Compared to Astrin-GFP WT, Astrin-GFP p.L7* localization at the KTs is significantly reduced (n=20, 10 cells from each set, $p<0.0001$; **Fig 4.2 D**). Data suggest that Astrin-GFP p.L7* mutant, mimicking Astrin p.L7Qfs*21 is expressed in HeLa cells and may have reduced localization at the KTs.

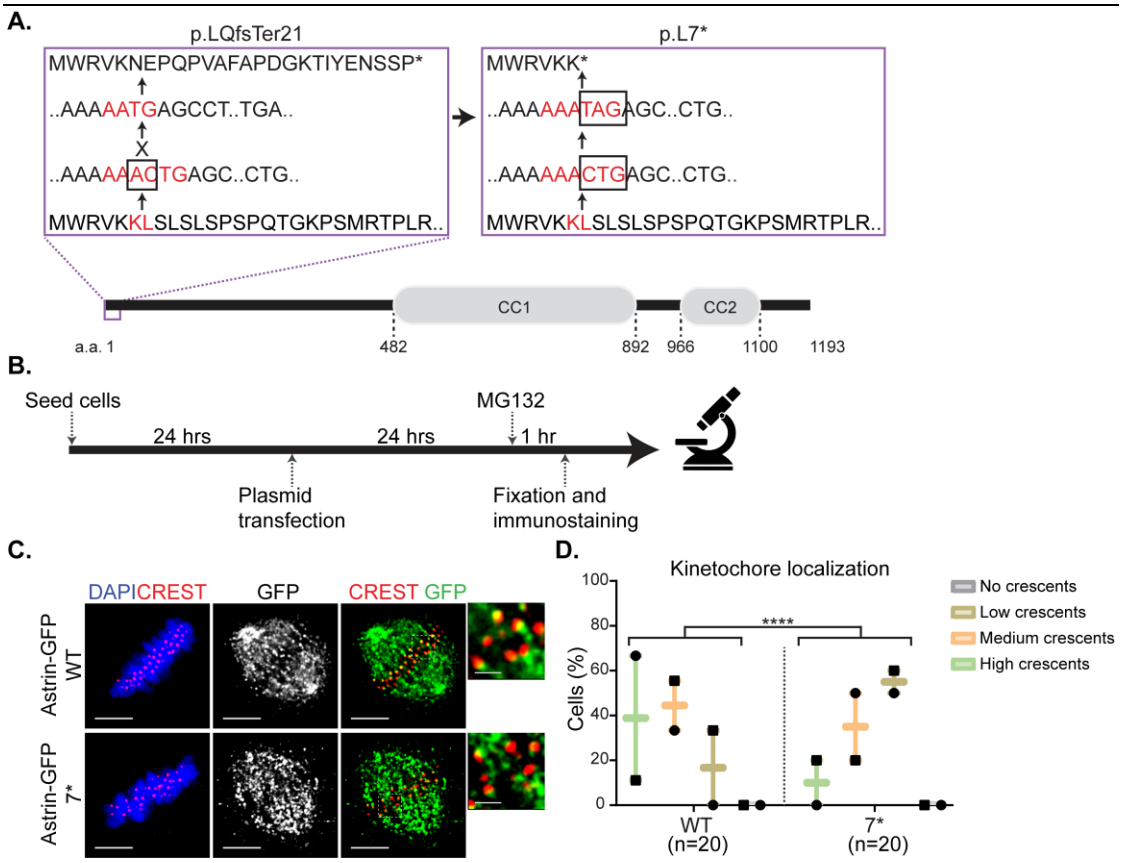

Fig 4.2 Astrin p.L7* is expressed in HeLa cells and localizes to spindle and kinetochores. A. Cartoon showing Astrin p.L7Qfs*21 variant and Astrin-GFP p.L7* mutant. **B.** Experimental regimen**. C.** Representative immunofluorescence images of Astrin-GFP wild type and p.L7* expressing cells treated as in B and probed for GFP and CREST. DNA was stained with DAPI. Scale bars: 5 µm in uncropped images and 1 µm in insets. **D.** Boxplot showing localization of Astrin at the kinetochores (scored as high, medium, low and no crescents as in **Fig 4.1**). Symbols represent independent experiments. n=20 (10 cells from each set). A Chi-square test was performed to find statistical significance. **** represents p<0.0001.

Expression of Astrin-GFP p.L7* despite the stop codon at the 7 a.a. suggests an alternate start site for the expressed protein. To investigate this, I first compared the migration of Astrin-GFP WT and p.L7* proteins on an immunoblot. Data show a strong band at ~190 kDa (expected molecular weight ~163 kDa) for WT and between 135 and 190 kDa for the p.L7* mutant when probed for GFP and Astrin (**Fig 4.3**). The ~190 kDa band of Astrin WT is also detected by Astrin antibody, but Astrin p.L7* band cannot be differentiated from endogenous Astrin bands (**Fig 4.3**). I conclude that a fast-migrating form of Astrin is expressed in Astrin-GFP p.L7*.

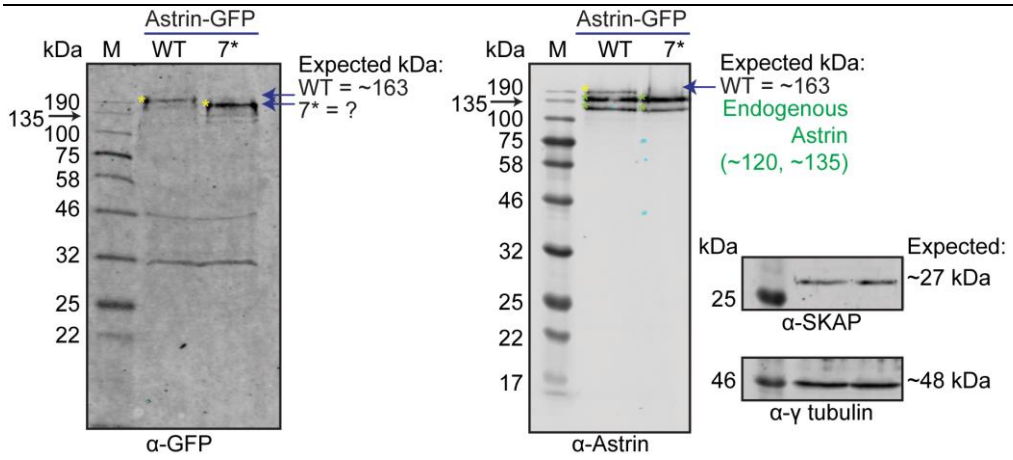

Fig 4.3 Astrin-GFP p.L7* is expressed as a fast-migrating protein. Immunoblot of HeLa cell lysates expressing Astrin-GFP wild type and p.L7* probed for GFP**,** Astrin, SKAP and γ- tubulin (loading control). Data represent at least two independent repeats.

KOZAK sequences, present in the eukaryotic mRNA, play a major role in the initiation of translation (Acevedo et al. 2018). To identify potential start sites for the expression of the short Astrin, I looked for KOZAK sequences in the N-terminus of Astrin and found a potential start site with a strong KOZAK sequence at N-454 and a potential start site with good KOZAK sequence at N-823 with predicted molecular weights similar to Astrin-GFP p.L7*. I then generated N-terminal YFP tagged Astrin

deletion mutants-Δ151 and Δ274, starting from the identified start sites (**Fig 4.4 A**) and expressed them in HeLa cells. Immunoblotting studies show strong bands at a similar height for N and C-terminal tagged Astrin WT (~180 kDa) as expected. A strong band is observed between 180 and 135 kDa for Astrin Δ151, similar to Astrin p.L7* band, whereas Astrin Δ274 band is near 135 kDa (**Fig 4.4 B**). Data suggest that the fast-migrating Astrin protein expressed in Astrin p.L7* starts from 152 a.a. (N-454) of Astrin.

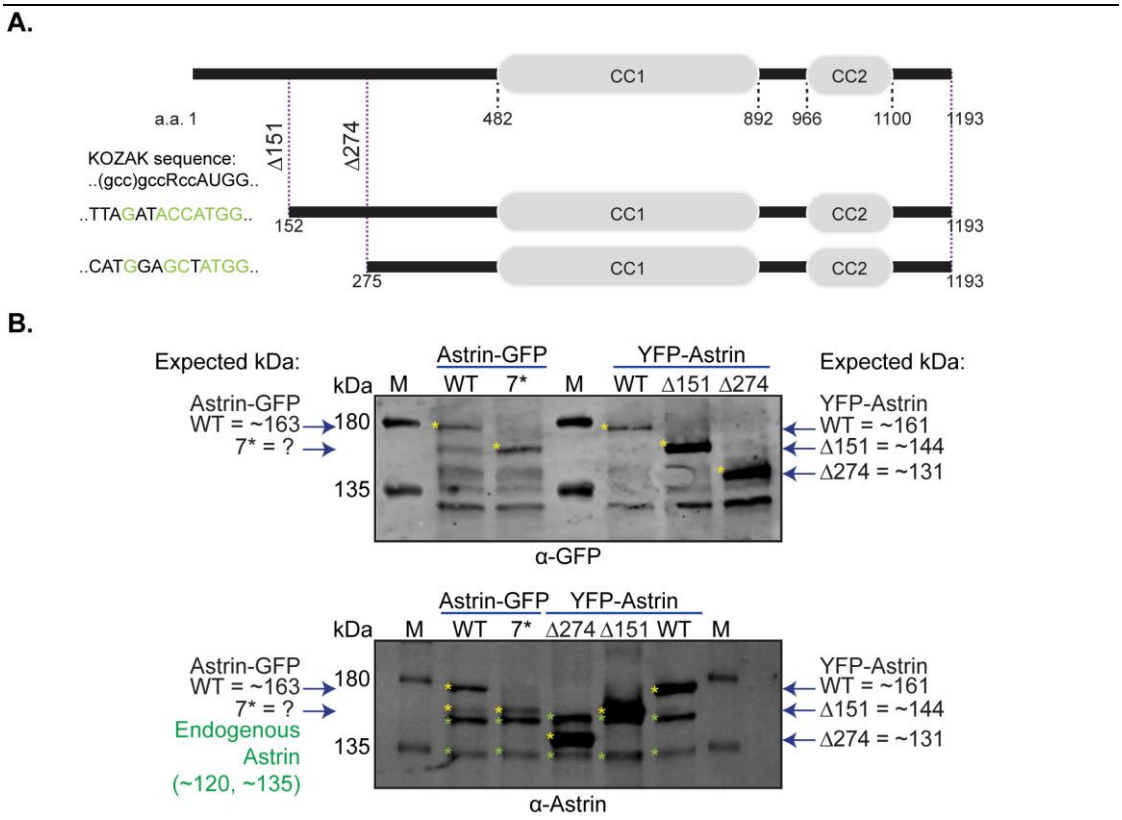

Fig 4.4. Short Astrin protein expressed is similar in size to Astrin Δ151 mutant. A. Cartoon showing N-terminus deletion mutants and KOZAK sequences. **B.** Immunoblots of lysates expressing Astrin-GFP (WT and p.L7*) and YFP-Astrin (WT, Δ151 and Δ274) and probed for GFP and Astrin. Green * indicates endogenous Astrin and yellow * indicates all other Astrin bands.

To conclude, Astrin-GFP p.L7* mutant, mimicking human Astrin p.L7Qfs*21 variant, expresses as a fast migrating Astrin protein similar to Astrin Δ151.

4.2.2 N-TERMINAL ASTRIN MUTANTS LOCALIZE NORMALLY AT THE SPINDLE AND KINETOCHORE

The C-terminal GFP tagged Astrin wild type itself has impaired localization at the kinetochores (KTs). Hence, to precisely determine the subcellular localization of

the fast-migrating Astrin, I investigated the N-terminal Astrin deletion mutants' localization. Immunostaining studies of metaphase arrested cells show that in the presence of endogenous Astrin, both Astrin Δ151 and Δ274 localize normally at the spindle (n=20, 10 cells from each set; **Fig 4.5 B**). Astrin Δ151 localizes normally at the KTs, whereas Astrin Δ274 shows localization defect in two cells from each set (n=20, 10 cells from each set, $p<0.05$; **Fig 4.5 B-C**). Data suggest that Astrin Δ151 localizes normally at the spindle and KTs, whereas Astrin Δ274 has a mild KT localization defect.

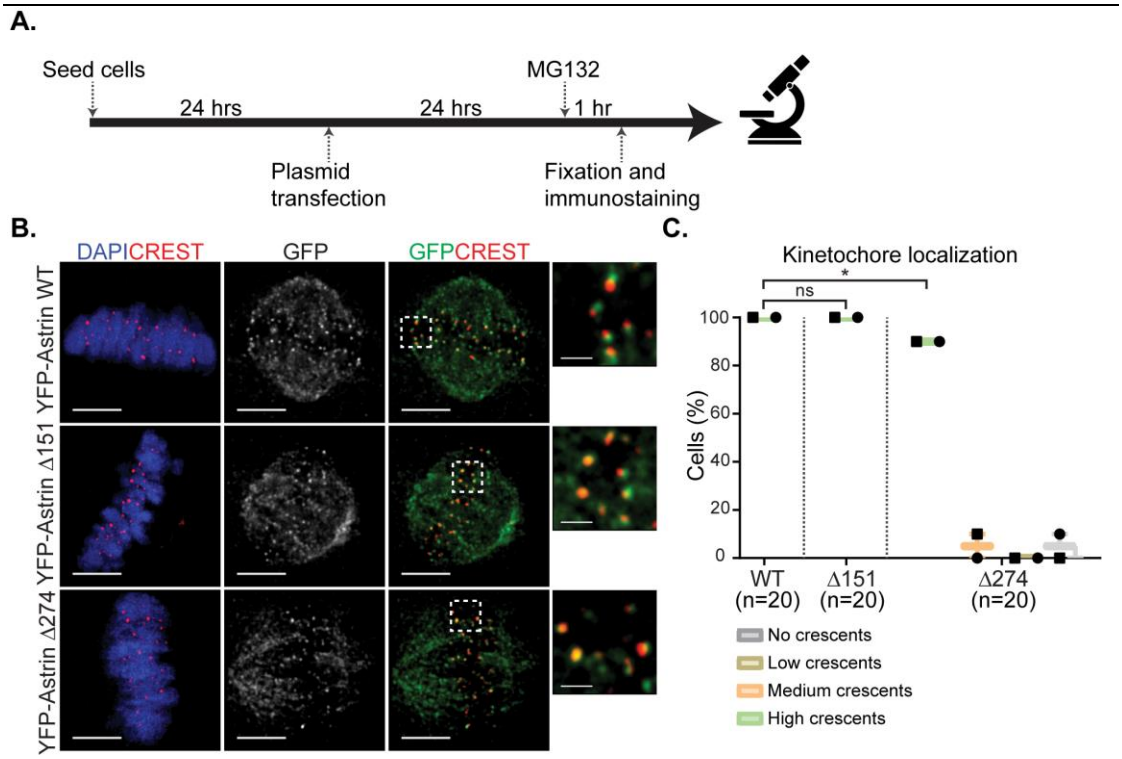

Fig 4.5 Astrin Δ151 localizes normally at the spindle and kinetochores. A. Experimental regimen**. B.** Representative immunofluorescence images of Astrin wild type, Δ151 and Δ274 cells treated as in B and probed for GFP and CREST. DNA was stained with DAPI. Scale bars: 5 µm in uncropped images and 1 µm in insets. **C.** Boxplot showing localization of Astrin at the kinetochores (scored as high, medium, low and no crescents as in **Fig 4.1**). Symbols represent independent experiments. n=20 (10 cells from each set). One-way ANOVA was performed to find statistical significance. * represents $p<0.05$ and ns=not significant.

To investigate whether Astrin Δ274's reduced localization at the KTs is a consequence of competition between the exogenously expressed protein and the endogenous protein, I depleted the cells of endogenous Astrin. Immunostaining studies of metaphase arrested cells show that all Astrin Δ274 localizes normally at the

kinetochores (n=20, 10 cells from each set; **Fig 4.6 B-C**). Further, endogenous SKAP, an interacting partner of Astrin whose localization at the KTs is Astrin-dependent, also localizes normally at the kinetochores. I conclude that the observed localization defect in Astrin Δ274 expressing cells in **Fig 4.5** is likely due to competition with the endogenous Astrin.

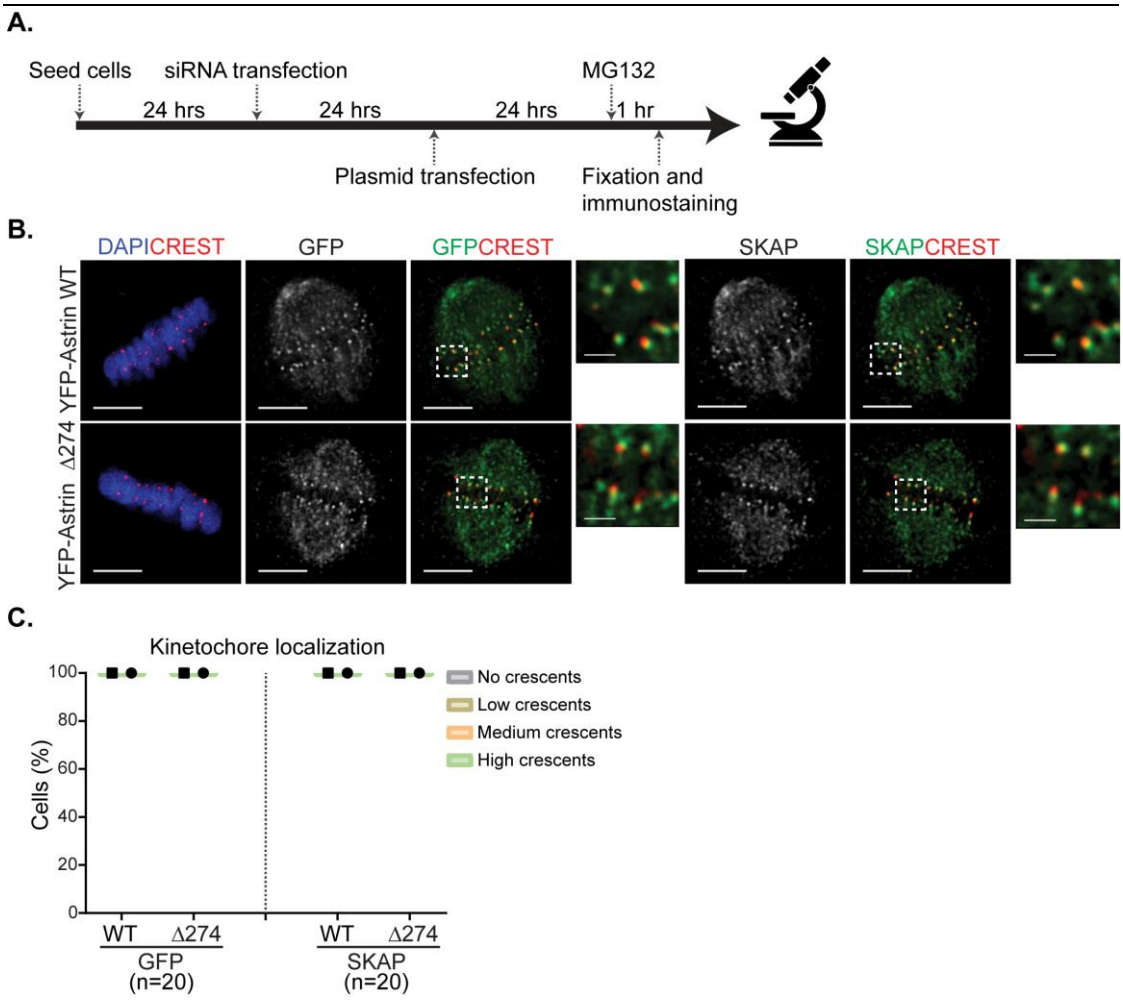

Fig 4.6 Astrin Δ274 localizes normally at the spindle and kinetochores when endogenous Astrin is depleted. A. Experimental regimen **B.** Representative immunofluorescence images of Astrin wild type (WT) and Δ274 expressing cells treated as in A and probed for GFP, SKAP and CREST. DNA was stained with DAPI. Scale bars: 5 µm in uncropped images and 1 µm in insets. **C.** Boxplot showing localization of Astrin at the kinetochores (scored as high, medium, low and no crescents as in **Fig 4.1**). Symbols represent independent experiments. n=20 (10 cells from each set).

Collectively, the data show that Astrin p.L7*, mimicking Astrin p.L7Qfs*21 variant, expresses as a fast migrating form similar to Astrin Δ151 that localizes normally in mitosis. This may explain the presence of Astrin p.L7Qfs*21 variant homozygotes in the population.

4.3 LOCALIZATION OF HUMAN ASTRIN P.Q1012* VARIANT

A stop codon at 1012 a.a. of Astrin will result in a shorter protein lacking a portion of its C-terminus. To precisely determine the Astrin p.Q1012* variant's subcellular localization, I transiently expressed N-terminal YFP tagged Astrin p.Q1012* variant in HeLa cells. Immunostaining studies show that in interphase cells, the YFP signal is exclusively observed in the cytoplasm and on the spindle throughout prophase to telophase (**Fig 4.7 C**). This is in agreement with Astrin localization studies (Mack and Compton 2001; Cheng et al. 2008; Chu et al. 2016).

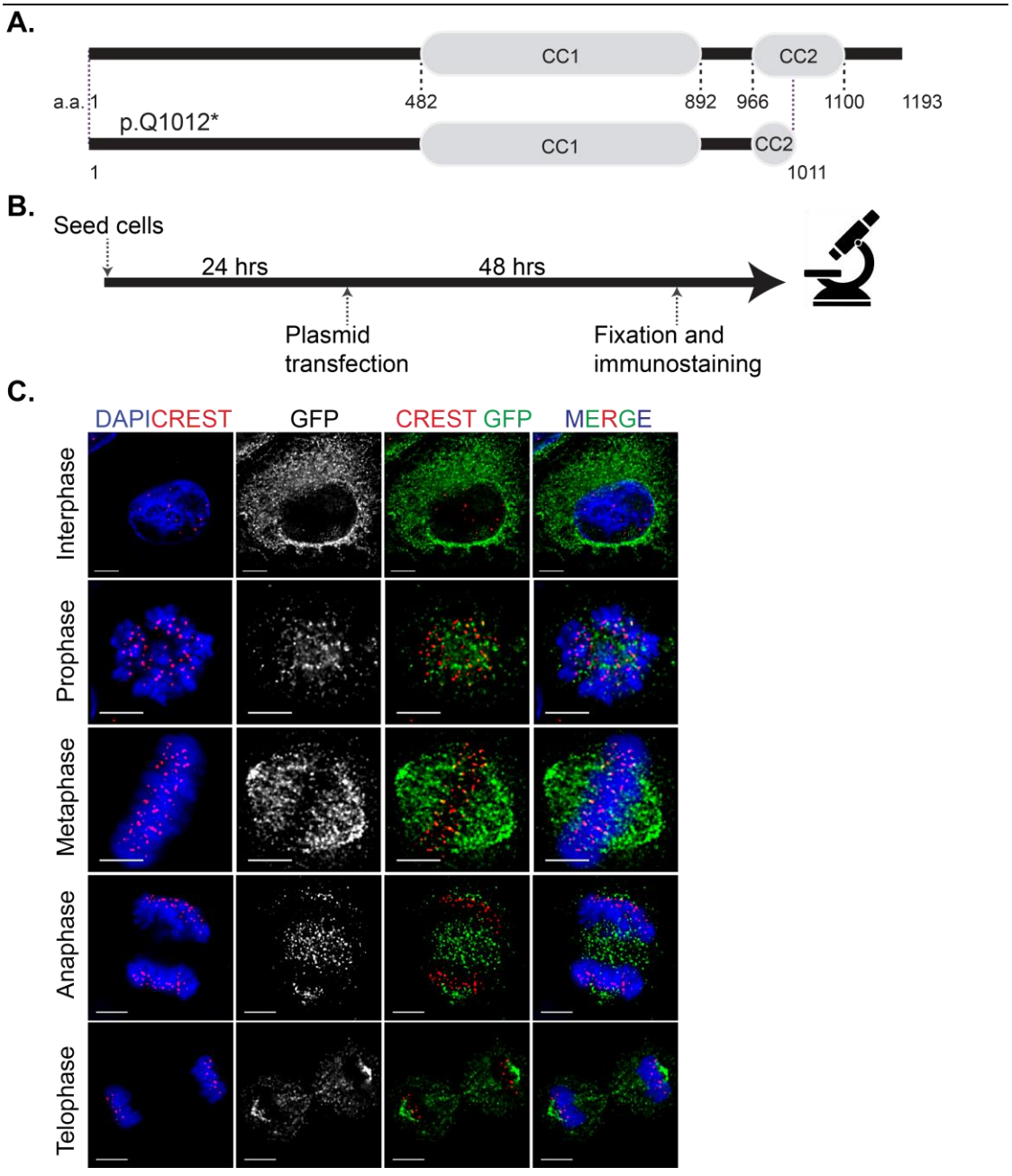

Fig 4.7 Astrin p.Q1012*'s localization through cell cycle. A. Cartoon showing Astrin p.Q1012* variant. **B.** Experimental regimen. **C.** Representative immunofluorescence images of Astrin wild type and p.Q1012* treated as in B and probed for GFP and CREST. DNA was stained with DAPI. Scale bars: 5 µm.

In metaphase arrested cells, YFP-Astrin wild type localize at both spindle and kinetochores (KTs), and its localization at the KTs is as high crescents (**Fig 4.8**). In contrast, Astrin p.Q1012* localizes normally at the spindle, but none of the cells have high crescents ($p<0.0001$), ~15% have medium crescents, ~38% have low crescents, and ~47% have no crescents (**Fig 4.8 C-D**). I conclude that Astrin p.Q1012* cannot be enriched at the outer kinetochore of mitotic cells.

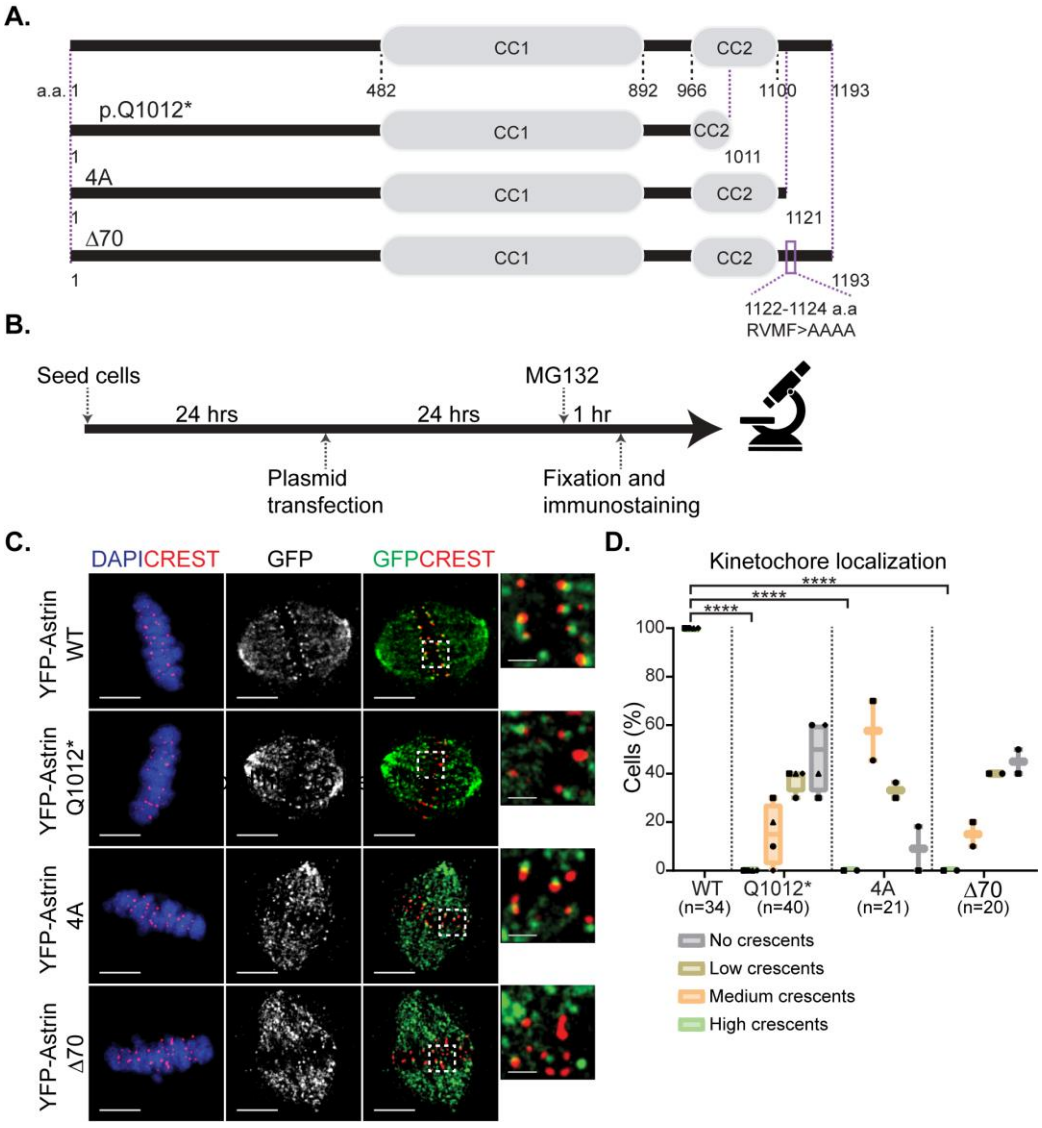

Fig 4.8 Astrin p.Q1012* localizes normally at the spindle but not at the kinetochores. A. Cartoon showing Astrin C-terminus constructs**. B.** Experimental regimen. **C.** Representative immunofluorescence images of Astrin wild type (WT), p.Q1012*, 4A and Δ70 expressing cells treated as in B and probed for GFP and CREST. DNA was stained with DAPI. Scale bars: 5 μm in uncropped images and 1 μm in insets. **D.** Boxplot showing localization of Astrin at the kinetochores (scored as high, medium, low and no crescents). Symbols represent independent experiments. One-way ANOVA was performed to find statistical significance.

Next, I compared Astrin p.Q1012*'s subcellular localization with two Astrin C-terminal mutants reported to present mitotic defects (Conti et al. 2019). Immunostaining studies of metaphase cells show that ~47% of Astrin p.Q1012* cells have no crescents similar to Astrin Δ70 (~45%) but higher than Astrin 4A (~8%, **Fig 4.8 C-D).** I conclude that Astrin p.Q1012*'s KT localization impairment is similar to the C-terminal deletion mutant Astrin Δ70.

To investigate whether Astrin p.Q1012*'s reduced localization at the KTs is a consequence of competition between the exogenously expressed protein and the endogenous protein, I depleted the cells of endogenous Astrin. Immunostaining studies of metaphase arrested cells show that compared to all wild-type cells having high crescents, only ~5% of Astrin p.Q1012* cells have high crescents, ~39% have medium, ~28% have low, and ~28% have no crescents (**Fig 4.9 B-C**). I conclude that Astrin p.Q1012* variant fails to localize at the KTs even in the absence of endogenous Astrin.

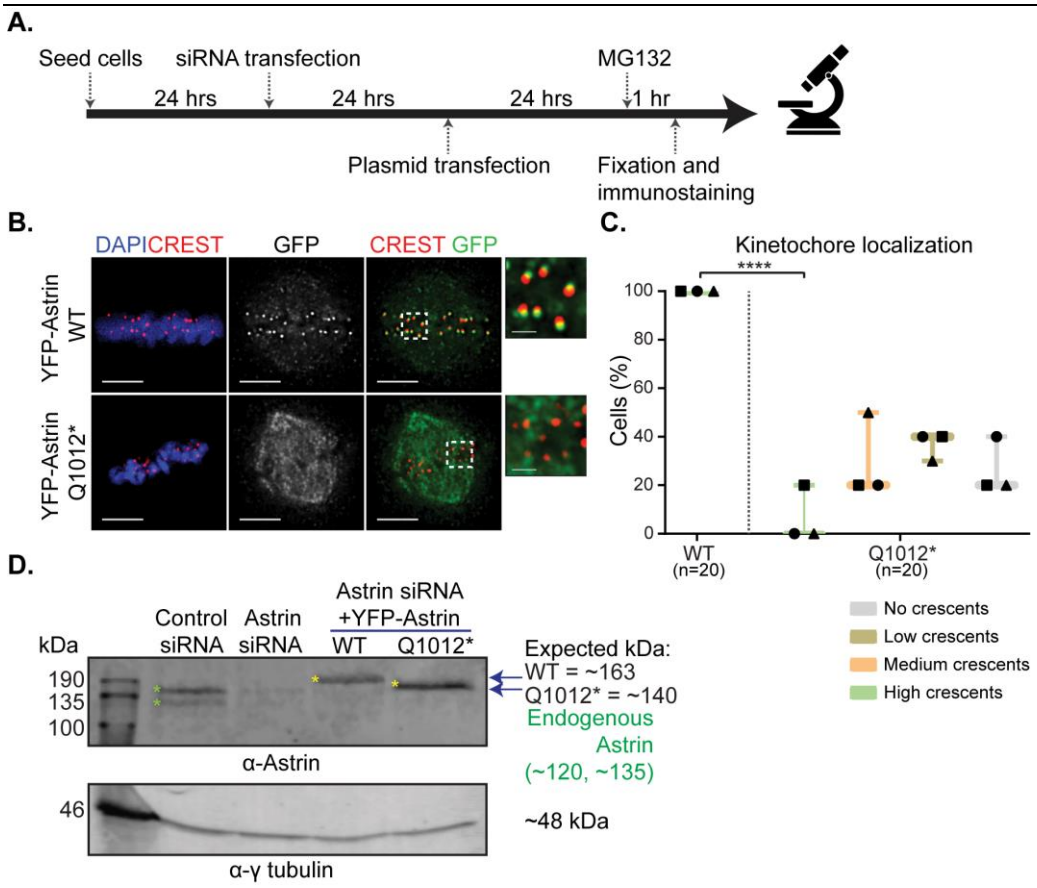

Fig 4.9 Astrin p.Q1012* localizes normally at the spindle but not at the kinetochores in the absence of endogenous Astrin. A. Experimental regimen. **B.** Representative immunofluorescence images of Astrin wild type and p.Q1012* expressing cells treated as in A and probed for GFP and CREST. DNA was stained with DAPI. Scale bars: 5 µm in uncropped images and 1 µm in insets. **C.** Boxplot showing localization of Astrin at the kinetochores (scored as high, medium, low and no crescents). Symbols represent independent experiments. One-way ANOVA was performed to find statistical significance. **D.** Immunoblot showing the extent of Astrin depletion in following Control or Astrin siRNA treatment as indicated.

Collectively, data shows that Astrin p.Q1012* variant fails to localize at the KTs which may explain why it is only found at heterozygous and not homozygous.

4.4 LOCALIZATION OF HUMAN ASTRIN P.E755K MUTANT

Lastly, I investigated the subcellular localization of Astrin p.E755K somatic mutant. Immunostaining studies of metaphase arrested cells show that Astrin p.E755K localizes normally at both the spindle and kinetochores (n=15; **Fig 4.10 C-D**). I conclude that the Astrin p.E755K mutation in unlikely to affect Astrin's localization.

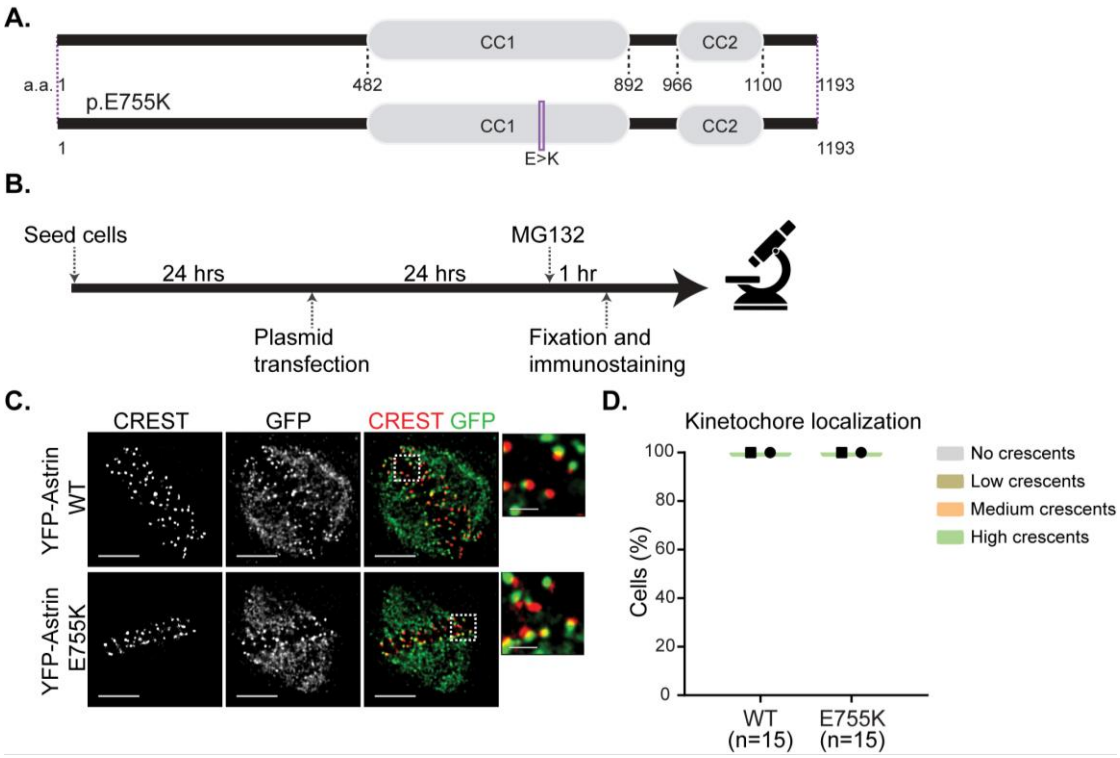

Fig 4.10 Astrin p.E755K localizes normally at the spindle and kinetochores. A. Cartoon showing Astrin constructs. **B.** Experimental regimen. **C.** Representative immunofluorescence images of Astrin wild type and p.E755K expressing cells treated as in B and probed for GFP and CREST. DNA was stained with DAPI. Scale bars: 5 µm in uncropped images and 1 µm in insets. **C.** Boxplot showing localization of Astrin at the kinetochores (scored as high, medium, low and no crescents as in **Fig 4.1**). Symbols represent independent experiments.

I conclude that the human Astrin p.L7QfsTer21 variant expresses as a fast migrating form of Astrin and localizes normally at the metaphase spindle and KTs, explaining why it may be tolerated as homozygous in a healthy population. On the other hand, the human Astrin p.Q1012* variant localizes normally at the spindle but fails to localize at the kinetochores explaining why it is only present as heterozygous. Lastly, the human Astrin p.E755K somatic mutant localizes normally in metaphase cells.

4.5 DISCUSSION

I selected two human genomic variants of Astrin protein from the Genes and Health (GH) database (Finer et al. 2020) and one human somatic mutant from the COSMIC database (Tate et al. 2019) and studied their subcellular localization and function in human epithelial cells. Here, I show that the Astrin p.E755K mutant (COSMIC database) may localize normally at the spindle and kinetochores (KTs) (**Fig**

4.10 B-C). In contrast, Astrin p.Q1012* variant (GH database) localizes at the spindle normally but fails to localize at the KTs similar to C-terminal deletion mutant Δ70 (**Fig 4.7 C**, **4.8 C**, **4.9 B-C**). The Astrin-GFP p.L7*, conforming to Astrin p.L7Qfs*21 variant (GH database), also shows reduced KT localization **(Fig 4.2 C-D**). However, Astrin-GFP WT localization at the KTs is also compromised, albeit less than Astrin-GFP p.L7* **(Fig 4.2 C-D**). The short Astrin protein expressed in Astrin-GFP p.L7* migrates similarly to N-terminal deletion mutant YFP-Astrin Δ151 (**Fig 4.3**, **Fig 4.4 B**), and interestingly, YFP-Astrin Δ151 localizes normally at both the spindle and KTs (**Fig 4.5 B-C**). Moreover, YFP-Astrin Δ274 also localizes normally at both the spindle and KTs in cells depleted of endogenous Astrin (**Fig 4.6 B-C**), suggesting the first 274 a.a. of Astrin may be dispensable for its KT localization. Collectively, the data may explain the high number of heterozygous (n=326) and homozygous (n=6) p.L7Qfs*21 variants in the "normal" population (Karczewski et al. 2020).

Astrin is an 1193 amino acid long protein consisting of an N-terminal globular region and two coiled-coil regions (Gruber et al. 2002; Mack and Compton 2001). Astrin, part of a 4 unit complex consisting of Astrin, small KT-associated protein SKAP, dynein light chain LC8, and MYC binding protein (MYCBP; (Kern, Wilson-Kubalek, and Cheeseman 2017)), localizes at the MTs through its binding partner SKAP (Kern et al. 2016). Astrin-SKAP interaction is through 482-693 a.a. region of Astrin (Friese et al. 2016; Kern, Wilson-Kubalek, and Cheeseman 2017), which is not lost in any of the variants/mutants studied explaining the normal spindle localization. Astrin-SKAP complex starts to localize at the KTs only when mature or end-on KT-MT attachments have formed (Shrestha et al. 2017), and this localization is dependent on the C-terminal region of Astrin (482-1193 a.a; (Dunsch et al. 2011)) explaining the impaired KT localization in the C-terminal deletion variant/mutants. Lack of Astrin p.Q1012* variant at the KTs would compromise Astrin-SKAP complex's function at the KTs, which may explain the absence of Astrin p.Q1012* homozygotes. NDC80 is a key KT-MT attachment protein (McCleland et al. 2003), and Astrin-NDC80 interaction may provide increased stability to KT-MT attachments. Although the Astrin p.E755K mutant normally localizes at the KTs, it still may affect Astrin-NDC80 interaction and, thus, KT-MT attachment stability.

The N-terminal of Astrin is phosphorylated by several kinases such as Aurora-A, CDK1, and GSK3 β and binds Plk1 kinase in a CDK-dependent manner (Cheng et al. 2008; Chiu et al. 2014; Chung et al. 2016; Geraghty et al. 2021). These sites are lost in the N-terminal deletion mutant Astrin Δ151. Cells expressing Astrin with mutated Aurora-A phosphorylation site have disrupted spindle size and undergo prolonged mitosis (Shao-Chih Chiu et al. 2014). Cells expressing Astrin with mutated Plk1 binding site have reduced KT-MT attachment stability (Geraghty et al. 2021). However, cells with mutated Plk1 binding site on Astrin or lacking the first 464 amino acids of Astrin can progress through an unperturbed cell cycle (Geraghty et al. 2021). N-terminus of Astrin is conserved in mammals but not in birds, reptiles, and fish (see **chapter 3**). Proteins may evolve to take more roles in higher species, and sometimes more than one protein is involved in performing one function. It is possible that other proteins compensate for the loss of the N-terminus of Astrin in Astrin p.L7Qfs*21 homozygotes.

Astrin localization studies were conducted by transiently transfecting HeLa cells with plasmids encoding Astrin variants/mutants. Overexpression of proteins can lead to mislocalization and aggregate formation. Moreover, low expressing cells may not have enough protein, which may be inferred as reduced localization during analysis. For this reason, cells with aggregates were excluded from analysis, and cells within an experiment were imaged using the same exposure and care was taken not to include low or high expressing cells. For better accuracy, future studies could make z-projections, measure maximum and minimum intensities, and use these values to select cells for analysis.

All the work done so far assumes that the protein would be expressed in humans as predicted from the genomic variation. However, transcription of the human genome is influenced by several regulatory pathways, including splicing (Reviewed in: (Abramowicz and Gos 2019)). To confirm how the variant expresses in humans, one could generate a CRISPR cell line expressing the variant. If a short Astrin as predicted with this study is expressed in CRISPR Astrin p.L7Qfs*21, the cell line could be used to carry out functional studies, particularly the spindle size and KT-MT attachment stability defects observed in Aurora-A phospho mutant (Chiu et al. 2014) and Plk1 binding mutant (Geraghty et al. 2021) expressing cells. The short Astrin protein

expressed in Astrin p.L7* is approximately 20-30 kDa smaller than the full Astrin. Astrin has two isoforms, and the shorter one is 20-30 kDa smaller than the longer isoform (Thein 2008). Astrin studies so far have been done only using the long isoform of Astrin, and whether there is a difference in functionality is not known. A mass spectrometry analysis could help determine whether the short Astrin expressed in Astrin p.L7Qfs*21 is indeed the short Astrin isoform. The cell line then can help answer whether the isoforms differ in functionality. Expression of the Astrin p.L7Qfs*21 should also be confirmed in human volunteers. Such studies would confirm the size and amount of the protein expressed and confirm Astrin's N-terminus's dispensability.

CHAPTER 5: RESULTS-III- FUNCTIONAL CONSEQUENCES OF HUMAN ASTRIN P.Q1012* VARIANT

CHAPTER 5: RESULTS-III-FUNCTIONAL CONSEQUENCES OF HUMAN ASTRIN P.Q1012* VARIANT

5.1 INTRODUCTION

In chapter 4, I have shown that the human Astrin p.Q1012* variant fails to localize at the metaphase kinetochores (KTs). At the KTs, Astrin interacts with the NDC80 complex, a key player involved in attaching KTs to the microtubules (MTs) ((Kern, Wilson-Kubalek, and Cheeseman 2017), Tamura PhD, Draviam Lab; unpublished data). Moreover, Astrin replaces Kif2b from the Kif2b-CLASP1 complex and stabilizes KT-MT attachments (Manning et al. 2010). KT-MT attachments are monitored by spindle assembly checkpoint (SAC) and Kuhn and Dumont (Kuhn and Dumont 2017) showed that the arrival of Astrin at the KTs coincides with the removal of SAC proteins. The C-terminal region of Astrin lost in the Astrin p.Q1012* variant contains PP1 phosphatase docking site and potential PP2A docking sites (see **Chapter 3**). Mutating the PP1 phosphatase docking site is sufficient to compromise the localization of Astrin at the KTs, albeit less than Astrin p.Q1012* variation (see **Chapter 4**), and prolongs mitosis (Conti et al. 2019). In this chapter, I explore the functional consequences of the Astrin p.Q1012* variant.

5.2 HUMAN ASTRIN P.Q1012* EXPRESSING CELLS DISPLAY CHROMOSOME CONGRESSION AND SEGREGATION DEFECTS

Human Astrin p.Q1012* variant has impaired localization at the kinetochores (KTs), similar to C-terminus Astrin Δ70 mutant localization (see **Chapter 4**). Previous studies have shown that cells stably expressing Astrin Δ70 mutant have prolonged mitosis (Conti et al.2019). To investigate whether this is also true for the Astrin p.Q1012* variant, I generated a conditionally expressing YFP-Astrin p.Q1012* cell line using HeLa FRT/TO Flp-In system. HeLa FRT/TO YFP-Astrin wild type (WT) cell line was already available in the lab. The cells were synchronized using a double thymidine block, YFP-Astrin expression was induced by releasing the cells in a medium containing tetracycline, and low-resolution live-cell imaging was performed for 10 hrs to observe the cells in mitosis (**Fig 5.1 A**). 100 nM sirDNA, a

DNA tracker, was added 10 hrs before imaging for tracking chromosomes. Cells that underwent nuclear envelope breakdown (NEBD) in the last 100 minutes of the movie were excluded from the analysis. Quantitative analysis of cells undergoing mitosis shows that compared to Astrin WT (n=68), a significant number of Astrin p.Q1012* expressing cells (n=32) fail to initiate anaphase within 10 hrs or undergo cell death ($p<0.05$; **Fig 5.1 C**). Moreover, the Astrin p.Q1012* expressing cells that complete mitosis display delayed anaphase onset (AO) (t50 (NEBD to AO): 96 mins for p.Q1012* vs. 60 mins for WT; **Fig 5.1 B, D**). The data suggest that Astrin p.Q1012* expressing cells have prolonged mitosis.

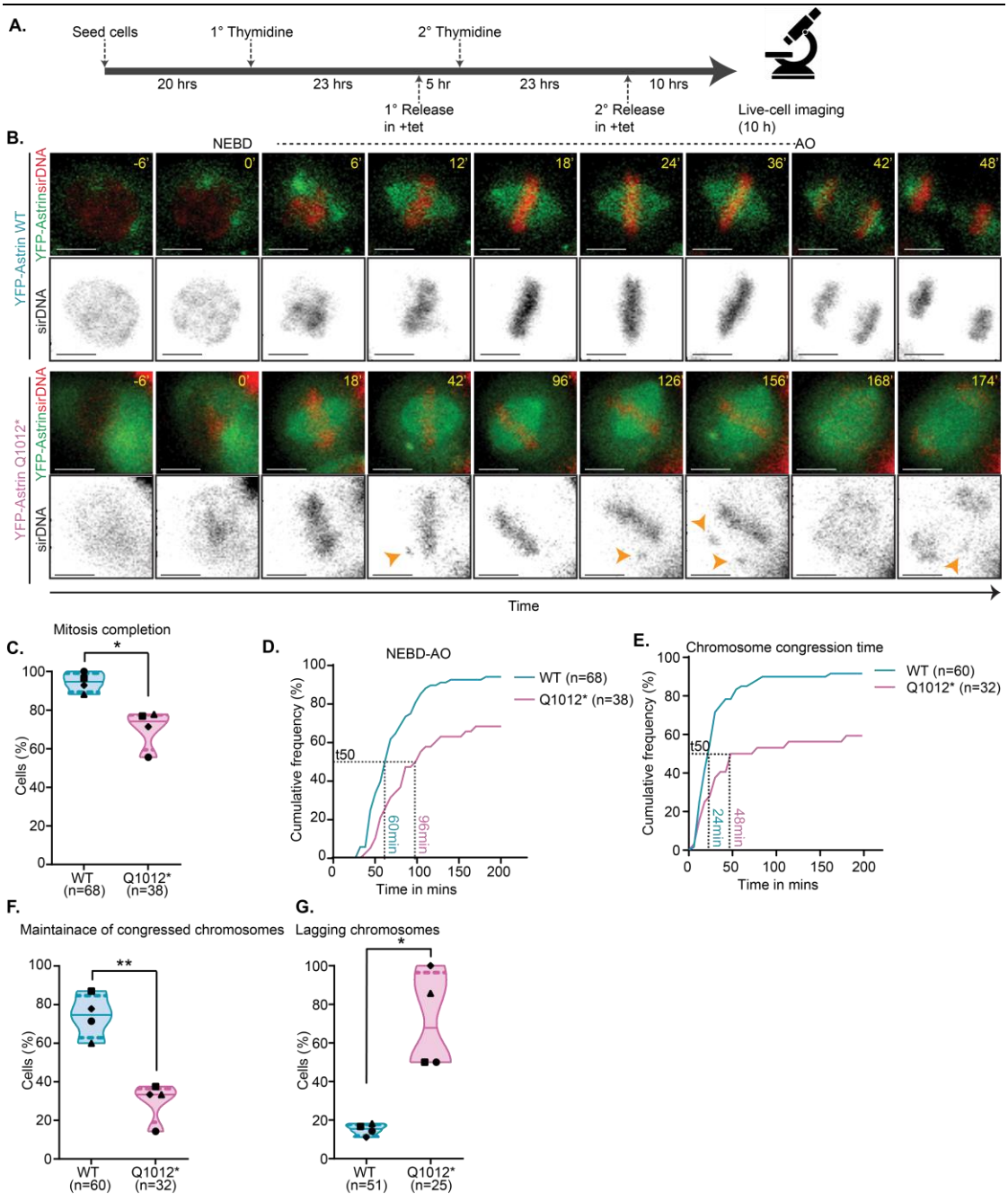
A.
Seed cells
1° Thymidine
2° Thymidine
20 hrs
23 hrs
5 hr
23 hrs
10 hrs
1° Release in +tet
2° Release in +tet
Live-cell imaging (10 h)
B.
NEBD
AO
YFP-Astrin WT
YFP-AstrinsirDNA
sirDNA
YFP-Astrin Q1012*
Time
C.
Mitosis completion
Cells (%)
WT (n=68)
Q1012* (n=38)
D.
NEBD-AO
Cumulative frequency (%)
t50
60min
96min
WT (n=68)
Q1012* (n=38)
Time in mins
E.
Chromosome congression time
Cumulative frequency (%)
t50
24min
48min
WT (n=60)
Q1012* (n=32)
Time in mins
F.
Maintainace of congressed chromosomes
Cells (%)
WT (n=60)
Q1012* (n=32)
G.
Lagging chromosomes
Cells (%)
WT (n=51)
Q1012* (n=25)

Figure 5.1 Human Astrin p.Q1012* expressing cells display chromosome congression and segregation defects. A. Experimental regimen. **B.** Representative time-lapse images of Astrin wild type (WT) and p.Q1012* cells treated as in A. Orange arrowheads represent unaligned chromosomes. NEBD is nuclear envelope breakdown, and AO is anaphase onset. Scale bars: 15 µm. **C.** Violin plot showing the percentage of cells that successfully initiated anaphase. The solid line represents the median, dotted lines represent quartiles, and symbols represent independent sets. **D.** Cumulative frequency graph showing the time taken from NEBD to AO. T50 indicates the time taken by 50% of cells to enter anaphase. **E.** Cumulative frequency graph showing the time taken from NEBD to forming the metaphase plate. T50 indicates the time taken by 50% of cells to form the metaphase plate. **F.** Violin plot showing the percentage of cells that successfully maintained chromosome congression. The solid line represents the median, dotted lines represent quartiles, and symbols represent independent sets. **G.** Violin plot showing the percentage of cells with lagging chromosomes at anaphase. The solid line represents the median, dotted lines represent quartiles, and symbols represent independent sets. (A-G) Data represent four independent sets. Paired t-test was performed to find statistical significance. * represents $p<0.05$ and ** represents $p<0.01$.

To investigate the cause of prolonged mitosis in Astrin p.Q1012* expressing cells, I looked at chromosome congression time in cells that successfully initiated anaphase. Quantitative analysis shows that only 56% of Astrin p.Q1012* expressing cells (n=32) successfully congress their chromosomes compared to 90% of Astrin WT expressing cells (n=60; **Fig 5.1 E**). Furthermore, these cells take a longer time to congress their chromosomes (t50 (NEBD to metaphase): 48 mins for p.Q1012* vs. 24 mins for WT; **Fig 5.1 E**), and once congressed, a significant number of Astrin p.Q1012* expressing cells fail to maintain chromosome congression ($p<0.01$; **Fig 5.1 F**). The data suggest that Astrin p.Q1012* expressing cells have defects in chromosome congression and maintenance. To ask whether the chromosome congression defects observed impact chromosome segregation, I looked at the presence of lagging chromosomes in anaphase cells. Quantitative analysis shows that Astrin p.Q1012* expressing cells (n=25) have a significantly higher incidence of lagging chromosomes in anaphase cells compared to Astrin WT cells (n=51; $p<0.05$; **Fig 5.1 G**).

sirDNA can impact cell cycle progression (Sen, Saurin, and Higgins 2018), and although I used the dye at the recommended concentration, I wanted to confirm that the phenotype observed is not a sirDNA induced artifact. Hence, I repeated the experiment without sirDNA. Quantitative analysis shows that 86% of Astrin p.Q1012* expressing cells (n=144) fail to initiate anaphase within 10 hrs or undergo cell death compared to 99% of Astrin WT (n=57; **Fig 5.2 C**), suggesting that both WT and

p.Q1012* cells do better in non-sirDNA treated cells (**Fig 5.2 C** vs. **Fig 5.1C**). Moreover, both WT and p.Q1012* expressing cells take less time in mitosis when not treated with sirDNA (**Fig 5.2 B, D** vs. **Fig 5.1 B, D**), suggesting that sirDNA contributes to prolonging mitosis. However, compared to the WT, the Astrin p.Q1012* expressing cells still display delayed anaphase onset (AO) (t50 (NEBD to AO): 72 mins for p.Q1012* vs. 48 mins for WT; **Fig 5.2 B, D**). I conclude that the prolonged mitosis phenotype observed in Astrin p.Q1012* expressing cells is not due to the presence of sirDNA.

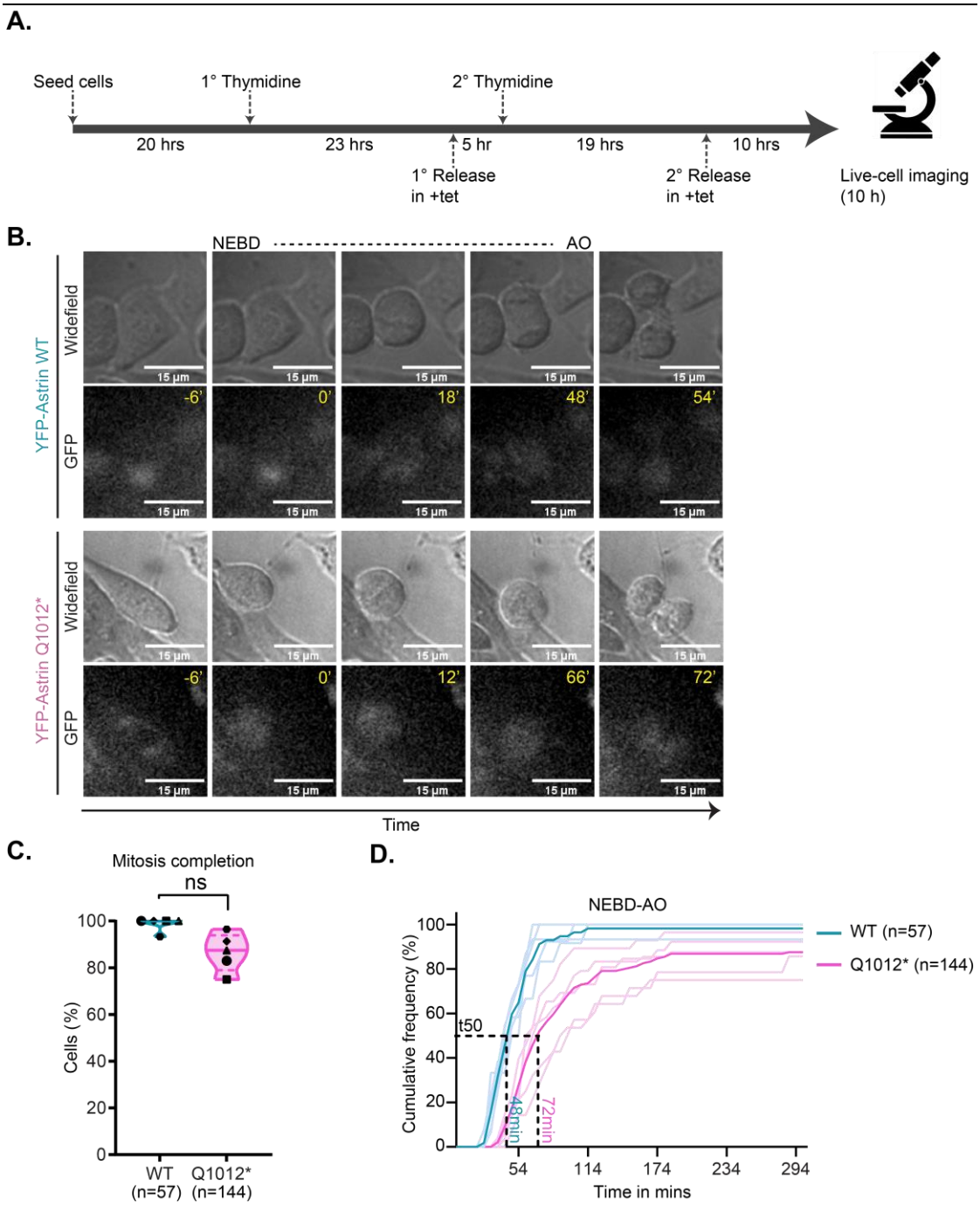

Figure 5.2 Human Astrin p.Q1012* expressing cells display prolonged mitosis in the absence of sirDNA. A. Experimental regimen. **B.** Representative time-lapse images of Astrin wild type (WT) and p.Q1012* cells treated as in A. NEBD is nuclear envelope breakdown, and AO is anaphase onset. Scale bars: 15 µm. **C.** Violin plot showing the percentage of cells that successfully initiated anaphase. The solid line represents the median, dotted lines represent quartiles, and symbols represent independent sets. Paired t-test was performed to find statistical significance. ns=not significant. **D.** Cumulative frequency graph showing the time taken from NEBD to AO. T50 indicates the time taken by 50% of cells to enter anaphase. (A-D) Data represent five independent sets.

Next, I sought to confirm the lagging chromosome phenotype in Astrin p.Q1012* stably expressing cells. For this, I transiently expressed Astrin WT and p.Q1012* variant in HeLa cells for 48 hrs before fixation and counted the number of anaphase cells with lagging chromosomes (**Fig 5.3 A-B**). HeLa cell line is an immortalized cancer cell line that has ~12% anaphase cells with lagging chromosomes (Bakhoum et al., 2014). I find a similar incidence (0-13%) in non-expressing anaphase cells (n=150, 219) and Astrin WT expressing anaphase cells (4-19%; n=69), and the difference between non-expressing and Astrin WT expressing cells is not significant (**Fig 5.4**). In contrast to Astrin WT expressing anaphase cells (n=69), the incidence of lagging chromosomes is significantly increased in Astrin p.Q1012* expressing cells (n=98; $p<0.05$; **Fig 5.3**, **5.4**), confirming the results observed in live-cell imaging studies.

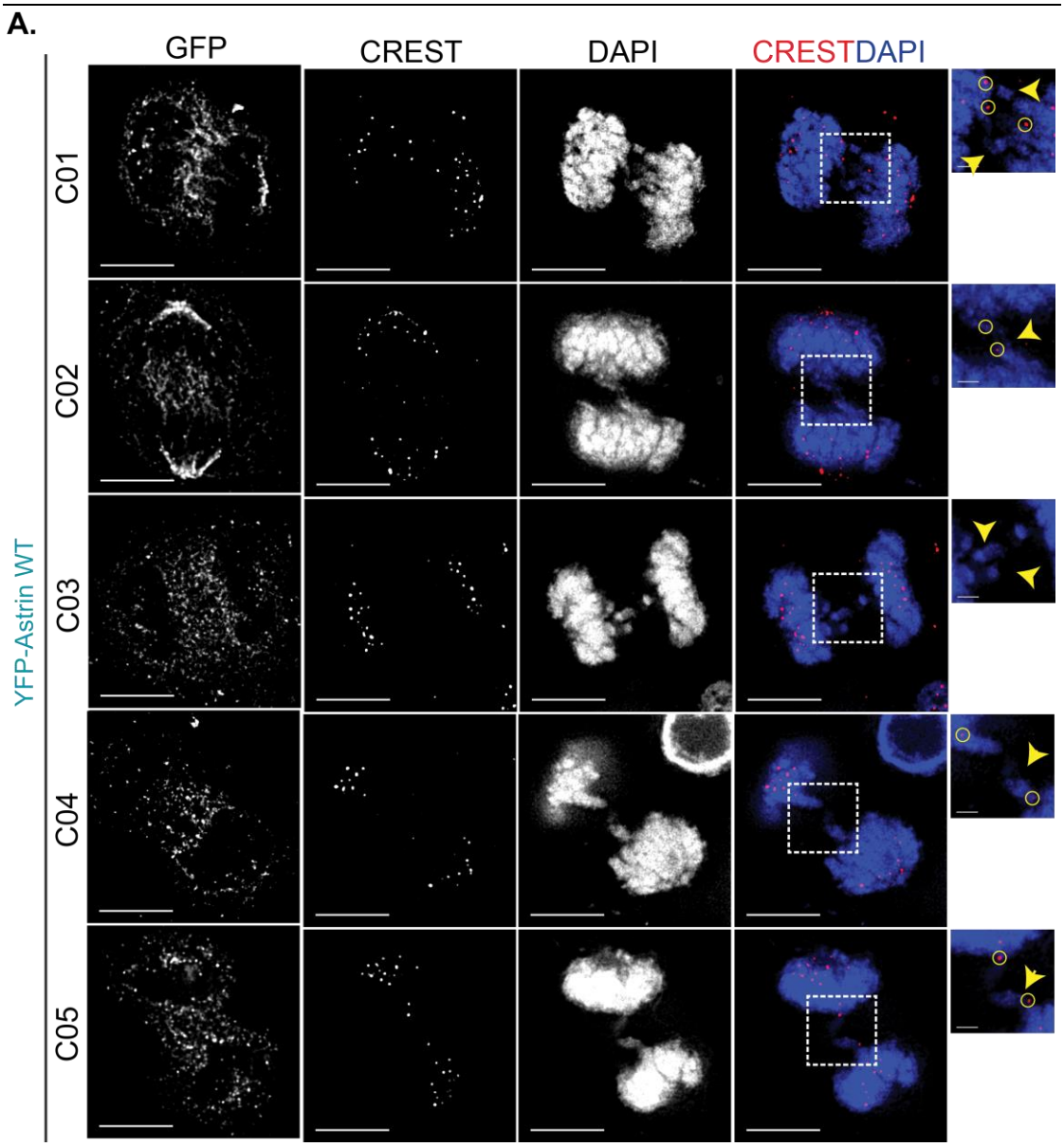
A.
GFP
CREST
DAPI
CRESTDAPI
YFP-Astrin WT
C01
C02
C03
C04
C05

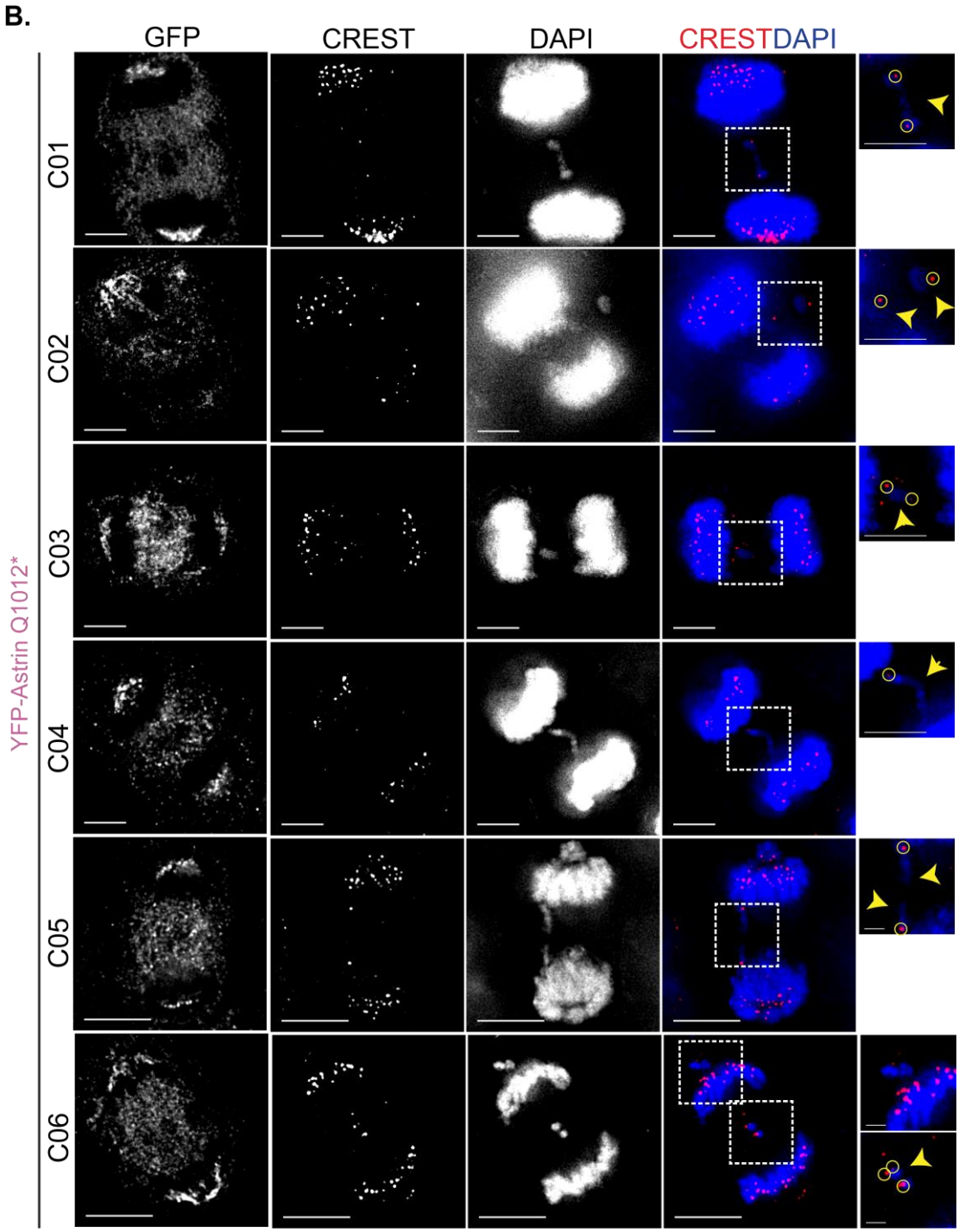

Figure 5.3 Representative images of Astrin wild type (WT) and p.Q1012* anaphase cells with lagging chromosomes. HeLa cells expressing YFP-Astrin WT **(A)** and p.Q1012* **(B)** were fixed 48 hrs post-transfection and probed for GFP and CREST. DNA was stained with DAPI. Scale bar: 15µm. In insets, the scale bar is 1 µm (WT and p.Q1012* C05-06) or 5 µm (p.Q1012*: C01-C04). Yellow arrowheads represent lagging chromosomes, and yellow circles represent centromeric signals on or near lagging chromosomes. Data represent four experiments.

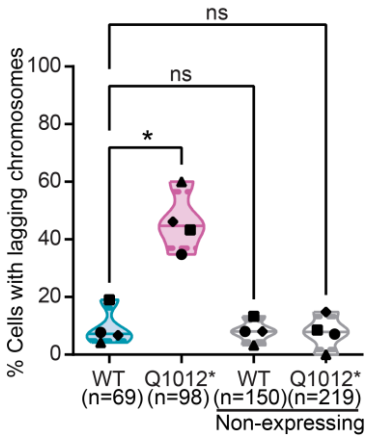

Figure 5.4 Human Astrin p.Q1012* expressing cells have a high incidence of lagging chromosomes in anaphase. The violin plot shows the percentage of anaphase cells with lagging chromosomes in cells transiently expressing Astrin wild type (WT) and p.Q1012* for 48 hrs before fixation. The solid line represents the median, dotted lines represent quartiles, and symbols represent independent sets. One-way ANOVA was performed to find statistical analysis. * represents $p<0.05$, ns=not significant.

The data collectively suggests that human Astrin p.Q1012* variant expressing cells have chromosome congression and maintenance defects resulting in prolonged mitosis. Moreover, these cells display chromosome segregation defects suggesting that the expression of this variant in humans may have health consequences.

5.3 HUMAN ASTRIN P.Q1012* EXPRESSING CELLS HAVE DNA DAMAGE

Both prolonged mitosis and lagging chromosomes at anaphase can result in DNA damage (Reviewed in: (Ganem and Pellman 2012; Tahmasebi-Birgani, Ansari, and Carloni 2019)). Astrin p.Q1012* expressing cells have delayed anaphase onset and display lagging chromosomes in anaphase. To investigate whether Astrin p.Q1012* expressing cells also accumulated DNA damage, I probed HeLa cells transiently expressing the variant with γH2AX, a DNA damage marker (Reviewed in: (Mah, El-Osta, and Karagiannis 2010)). Data indicate that the proportion of γ H2AX positive Astrin p.Q1012* (n=300) expressing cells is significantly higher than the WT (n=300, $p<0.01$; **Fig 5.5 B-C**), suggesting Astrin p.Q1012* expressing cells are prone to DNA damage.

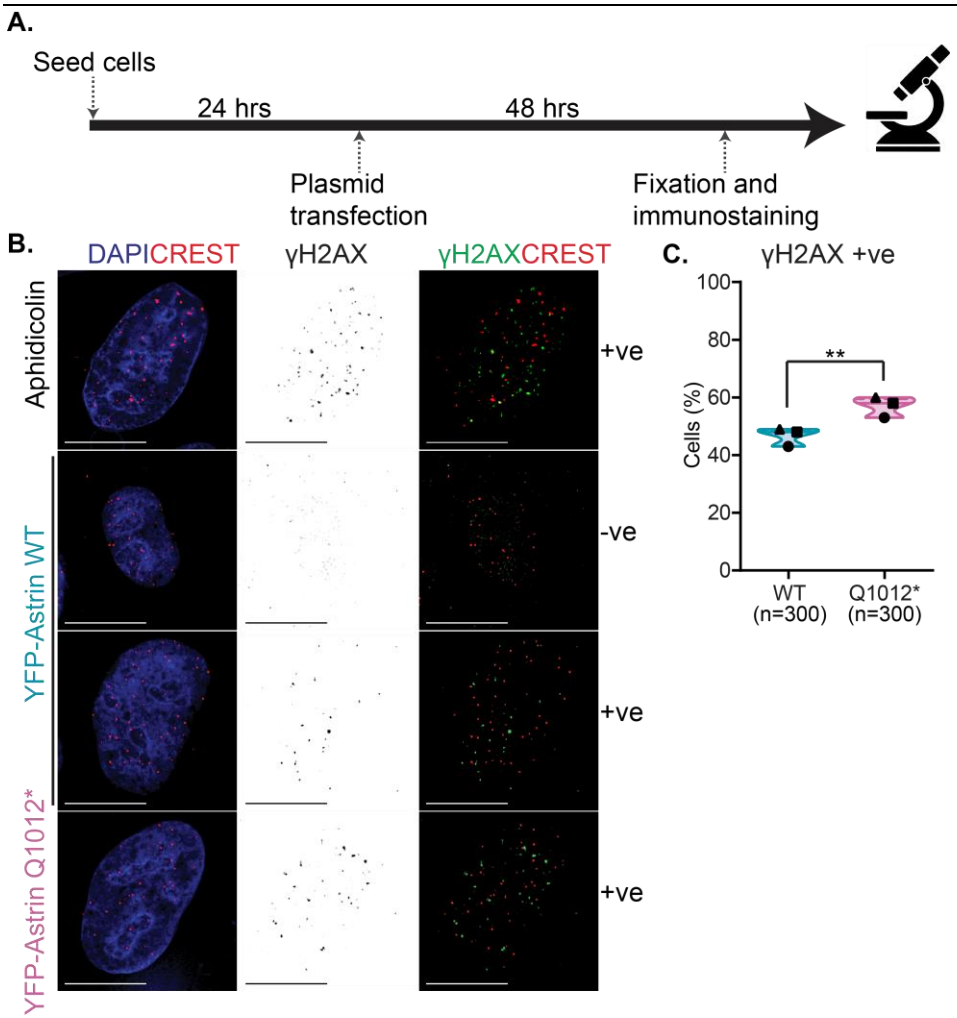

Figure 5.5 Astrin p.Q1012* expression leads to an increased proportion of γH2AX positive cells. **A.** Experimental regimen. **B.** Representative images of Astrin wild type (WT) and p.Q1012* cells treated as in A and probed for GFP, γH2AX, and CREST. 24 hr Aphidicolin treatment was used as a positive control. Scale bars: 15 μm. **C.** Violin plot showing the percentage of gamma H2AX positive cells. The solid line represents the median, dotted lines represent quartiles, and symbols represent independent sets. A paired t-test was performed for statistical analysis. ** represents $p<0.01$.

DNA damage may lead to the accumulation of S-phase cells as the cells try to repair their DNA before going into the next cell cycle (Cliby et al. 2002). To confirm that high γH2AX levels observed with Astrin p.Q1012* expression are due to DNA damage and not due to the enrichment of cells in S-phase, I immunostained cells using antibodies against PCNA, a marker of S-phase (Celis and Celis 1985; Bravo and Macdonald-Bravo 1985), in addition to γH2AX (**Fig 5.6 B**). Moreover, I used stably expressing cells instead of transiently expressing cells and followed the same timeline as the live-cell imaging experiment for YFP-Astrin induction (**Fig 5.6 A**). CENP-E inhibited HeLa cells were used as controls as inhibition of CENP-E, a motor protein

required for chromosome congression, leads to nuclear morphology defects (Hart, Adams, and Draviam 2021). Quantitative analysis shows that 2 hr treatment with CENPE inhibitor significantly increases γH2AX positive and PCNA negative population (n=300, p<0.01; **Fig 5.6 C**); however, the effect is lost when treatment is increased to 16 hrs (**Fig 5.6 C**). Moreover, a significantly higher percentage of Astrin p.Q1012* expressing cells are γH2AX positive and PCNA negative compared to Astrin WT (**Fig 5.6 C**), suggesting high γH2AX positive cells in Astrin p.Q1012* is not due to an accumulation of S- phase cells.

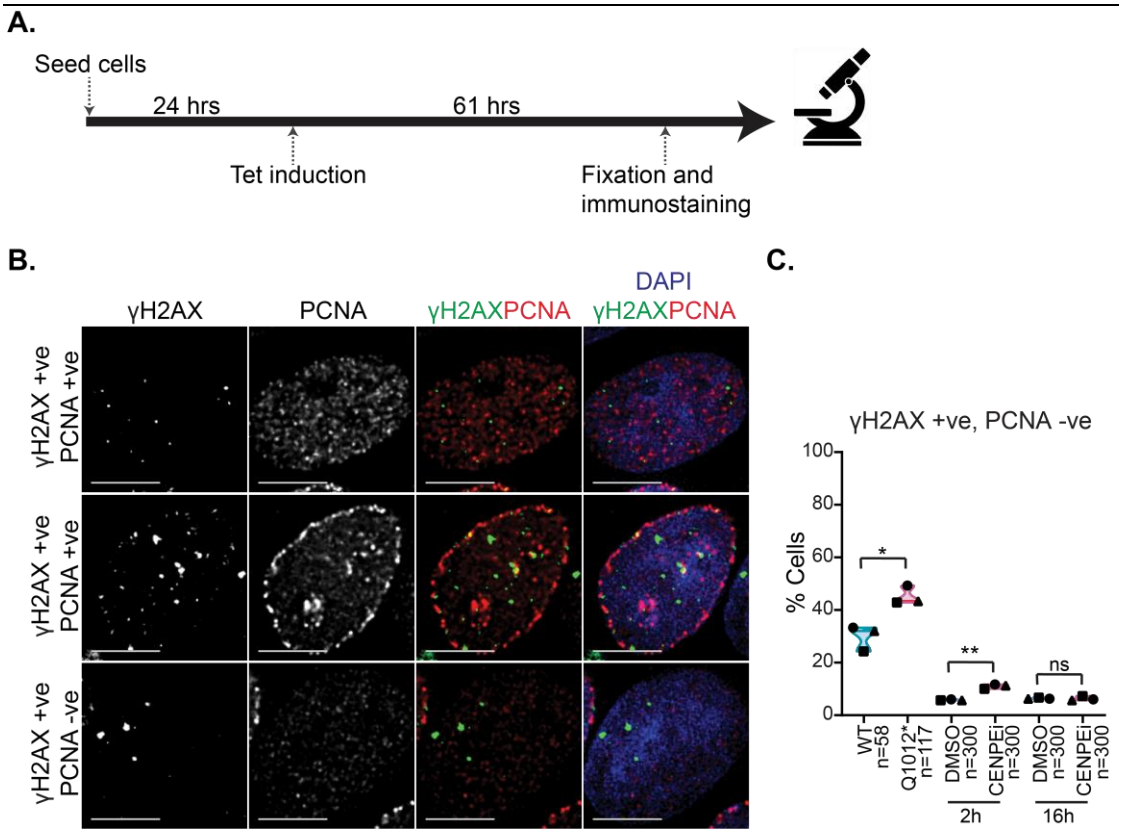

Figure 5.6 Expression of Astrin p.Q1012* variant increases gamma H2AX positive and PCNA negative population. A. Experimental regimen. **B.** Representative images of Astrin p.Q1012* cells treated as in A and probed for γH2AX, PCNA, and CREST. Scale bars: 15 µm. **C.** Violin plot showing the percentage of gamma H2AX positive and PCNA negative cells (subpanel B, bottom row) in the treatments indicated. The solid line represents the median, dotted lines represent quartiles, and symbols represent independent sets. A paired t-test was performed to find statistical significance. * represents p<0.05, ** represents p<0.01.

The data collectively suggests that cells expressing the human Astrin p.Q1012* variant may be prone to DNA damage.

5.4 HUMAN ASTRIN P.Q1012* EXPRESSING CELLS DISRUPT ENDOGENOUS ASTRIN-SKAP COMPLEX'S LOCALIZATION AT THE KINETOCHORES

The functional studies-both live and fixed, were carried out in the presence of endogenous Astrin but show chromosome congression and segregation defects. This led me to question whether the expression of this variant impaired endogenous Astrin-SKAP complex's localization. To answer this, I first probed metaphase arrested, transiently expressing YFP-Astrin WT and p.Q1012* cells with Astrin antibody that detects both exogenous (YFP-Astrin) and endogenous Astrin. The post-transfection time for this study was kept the same as the YFP-Astrin localization studies. I then counted 40 kinetochores per cell (n=10 cells per set) and asked whether the Astrin signal was present or not. Quantitative analysis shows that the Astrin signal at the kinetochores is significantly reduced in Astrin p.Q1012* expressing cells compared to Astrin WT ($p<0.0001$; **Fig 5.7 B-C**), suggesting an impairment of endogenous Astrin localization.

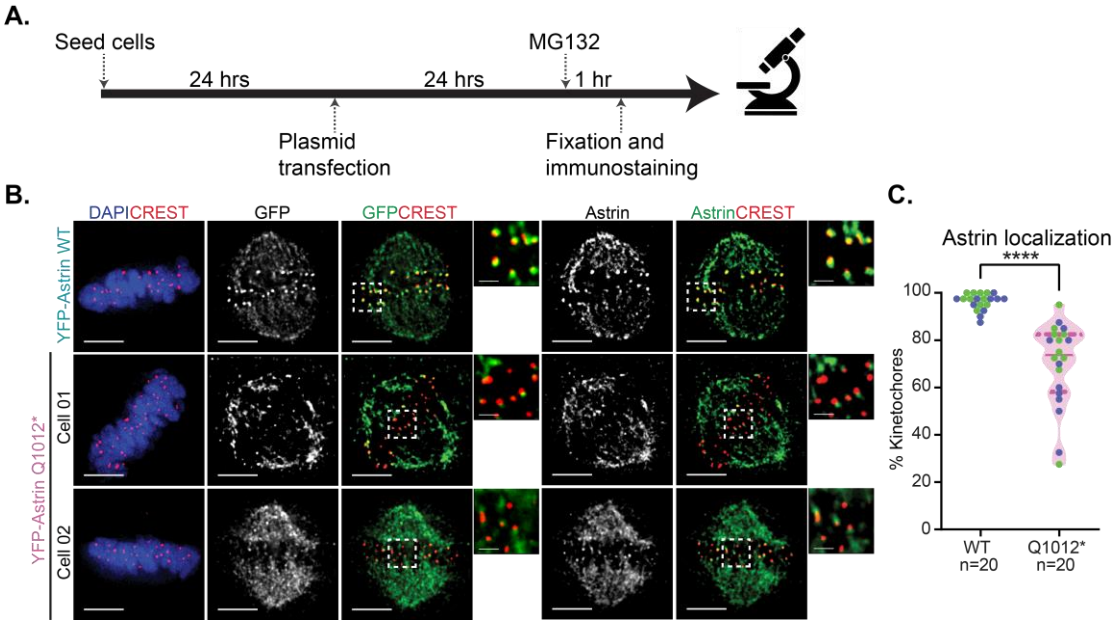

Figure 5.7 Astrin p.Q1012* expressing cells have impaired endogenous Astrin localization. A. Experimental regimen. **B.** Representative images of Astrin wild type (WT) and p.Q1012* cells treated as in A and probed for GFP, Astrin, and CREST. Scale bars: 5 µm in uncropped images and 1 µm in insets. **C.** Violin plot showing the percentage of kinetochores with Astrin (endogenous and exogenous-YFP-Astrin) localized as a crescent. Dots represent independent kinetochores, the solid line represents the median, dotted lines represent quartiles and colors represent independent sets. Mann-Whitney U test was performed to find statistical significance. **** represents $p<0.0001$.

Next, I ran a similar experiment and asked whether localization of endogenous SKAP, whose localization at the kinetochores is dependent on Astrin localization (Dunsch et al. 2011; Kern, Wilson-Kubalek, and Cheeseman 2017), is also impaired. Similar to quantification for Astrin at KTs (**Fig 5.7**), I counted 40 kinetochores per cell (n=10 cells per set) and asked whether the SKAP signal was present or not. Data show that endogenous SKAP localization at the kinetochores is also significantly reduced in Astrin p.Q1012* expressing cells compared to the WT ($p<0.01$; **Fig 5.8 B-C**), suggesting an overall impairment of Astrin-SKAP complex's localization at the KTs of Astrin p.Q1012* expressing cells.

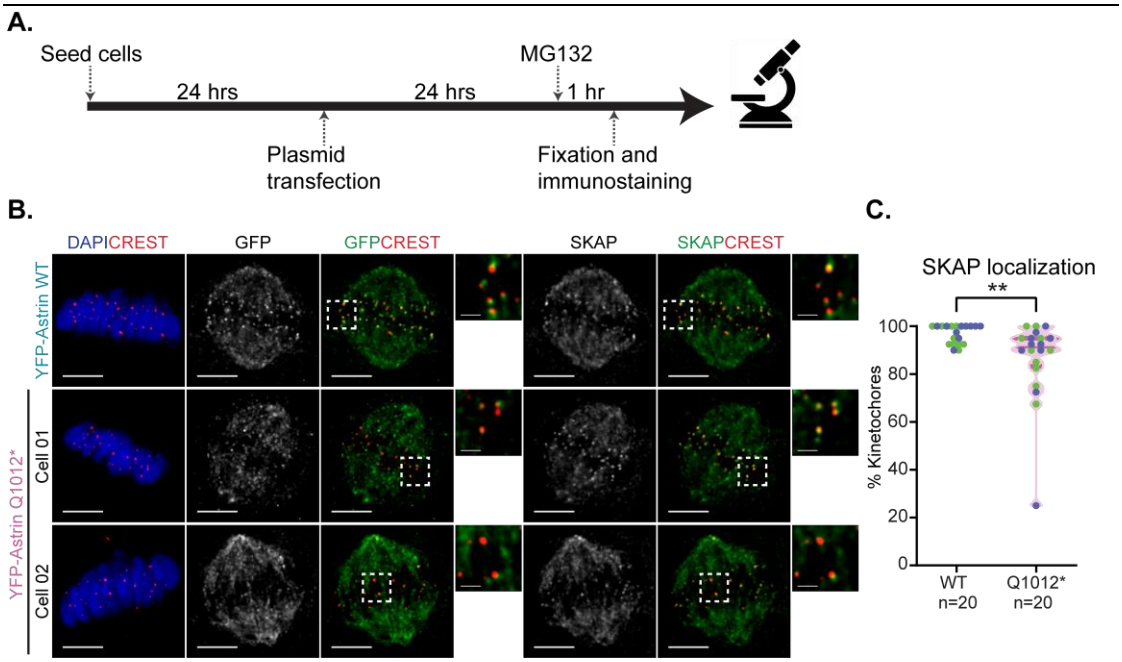

Figure 5.8 Astrin p.Q1012* expressing cells have impaired endogenous SKAP localization. A. Experimental regimen. **B.** Representative images of Astrin wild type and p.Q1012* cells treated as in A and probed for GFP, SKAP, and CREST. Scale bars: 5 µm in uncropped images and 1 µm in insets. **C.** Violin plot showing the percentage of kinetochores with SKAP localized as a crescent. Dots represent independent kinetochores, the solid line represents the median, dotted lines represent quartiles, and colors represent independent sets. Mann-Whitney U test was performed to find statistical significance. ** represents $p<0.01$.

The data collectively indicate that expression of Astrin p.Q1012* variant disrupts endogenous Astrin-SKAP complex's localization, which may explain why Astrin p.Q1012* expressing cells display chromosome congression and segregation defects despite the presence of endogenous Astrin.

5.5 DISCUSSION

Other than Astrin p.L7Qfs*21, no homozygous loss of function (LOF) variants of Astrin are found in the Genes and Health database (a genetic study of UK residents of Pakistani-Bangladeshi ancestry who self-reported as healthy; (Finer et al. 2020)) and gnomAD database (an international coalition of several genetic studies excluding severe pediatric diseases; (Karczewski et al. 2020)). Moreover, a compound heterozygous variation in Astrin has been linked with microcephaly; a child presented with small head size, mild speech delay, and short stature (Boonsawat et al. 2019). Together, the data suggest that genomic variations in Astrin may have health consequences, especially in communities with a high incidence of consanguineous marriages due to high chances of inheriting homozygous variants. The C-terminal human Astrin variant p.Q1012*, found in the Pakistani-Bangladeshi community in East London, normally localizes at the spindle but fails to localize at the metaphase kinetochores (KTs) both in the presence and absence of endogenous Astrin (see **Chapter 4**). Here I show that despite the presence of endogenous Astrin, cells stably expressing the p.Q1012* variant have delayed anaphase onset (**Fig 5.1 B-D**, **5.2 B-D**). Using sirDNA, a DNA tracker, I show that Astrin p.Q1012* expressing cells take longer to form metaphase plate (**Fig 5.1 B, E**). Moreover, once aligned, they fail to maintain chromosome congression (**Fig 5.1 B, F**). At the KTs, Astrin plays an essential role in stabilizing KT-MT attachments by a) interacting with NDC80, a key KT-MT attachment protein ((Kern, Wilson-Kubalek, and Cheeseman 2017); Tamura PhD, Draviam Lab; unpublished data), b) replacing Kif2b from Kif2b-CLASP complex (Manning et al. 2010) and c) possibly through targeting phosphatases to the KTs (Conti et al. 2019; Hertz et al. 2016). Unstable KT-MT attachments may explain delayed chromosome alignment and failure to maintain chromosome congression in Astrin p.Q1012* expressing cells.

Using both fixed and live-cell imaging, I show that Astrin p.Q1012* expressing cells have a higher incidence of lagging chromosomes in anaphase than the WT (**Fig 5.1 B, G**, **Fig 5.3 A-B**, **Fig 5.4**). The Lagging chromosomes can a) go to the wrong daughter cell causing aneuploidy, b) go to the right daughter cell but acquire DNA damage during cytokinesis and/or c) acquire DNA damage in micronuclei which may or may not join the main nucleus (Reviewed in: (Ganem and Pellman 2012; Tahmasebi-

Birgani, Ansari, and Carloni 2019)). In addition to lagging chromosomes, prolonged mitosis can also cause DNA damage (Reviewed in: (Ganem and Pellman 2012)). Using γH2AX as a DNA damage marker, I show a higher incidence of DNA damage in Astrin p.Q1012* expressing cells than the Astrin WT (**Fig 5.5 B-C**, **Fig 5.6 B-C**) that is not due to the accumulation of S-phase cells (**Fig 5.6 B-C**). These experiments were carried out in the HeLa cell line, an immortalized cancer cell line with a high chromosome number (Macville et al. 1999), and should be repeated in other cell lines such as near-diploid RPE1 for confirmation.

Lastly, I show Astrin p.Q1012* variant not only fails to localize at the KTs but also impairs the localization of endogenous Astrin-SKAP complex (**Fig 5.7 B-C**, **Fig 5.8 B-C).** The Astrin-SKAP complex is a four-unit complex with a 2:2:2:2 stoichiometry (Gruber et al. 2002; Kern, Wilson-Kubalek, and Cheeseman 2017). However, which region of Astrin is required for dimerization is not known. It is possible that YFP-Astrin p.Q1012* can form dimers with the endogenous Astrin, and this dimerization impairs endogenous Astrin's localization to KTs. The data suggest that the human Astrin p.Q1012* variant, if expressed, may cause health consequences even if in the presence of a normal copy of Astrin. mRNA and protein expression studies from individuals carrying this variant need to be carried out to see whether this variant is being expressed in the individuals or not. Cells may choose only to transcribe the normal copy of Astrin, or the variant mRNA is degraded through mechanisms such as non-sense mediated mRNA decay (NMD). In the microcephaly child with compound heterozygous variation in Astrin, the faulty copy of Astrin is degraded through NMD, resulting in the expression of only the normal copy of Astrin, albeit in a lower amount, in the patient's fibroblast (Boonsawat et al. 2019). However, the child still develops the developmental disorder. Studies on a microcephaly-linked KNL1 variation, another key KT protein, show that selective expression of the variant in neural cells due to differences in expression of splicing factors leads to increased neural cell apoptosis and reduced neural cell specialization (Javed et al. 2018). The brain-specific phenotype in the microcephaly-linked Astrin variation may also be linked to differences in expression of splicing factors and these differences may also be important for other human Astrin variants.

CHAPTER 6: RESULTS-IV-C-TERMINUS OF ASTRIN IS IMPORTANT FOR SPINDLE CHECKPOINT SIGNALLING

CHAPTER 6: RESULTS-IV-C-TERMINUS OF ASTRIN IS IMPORTANT FOR SPINDLE CHECKPOINT SIGNALLING

6.1 INTRODUCTION

For accurate chromosome segregation, each sister chromatid must attach to the microtubules (MTs) emanating from opposite spindle poles (termed biorientation). Initially, chromosomes are captured along the lateral surface of the MTs through a multiprotein complex called the kinetochore (KT) which assembles at the centromeric region of the chromosomes (Reviewed in: (Yamagishi et al. 2014; Musacchio and Desai 2017; Monda and Cheeseman 2018)). Laterally attached KTs are then brought at the MT-ends forming the end-on attachments (Tanaka and Hirota 2016; Shrestha and Draviam 2013). Once each sister KT is attached to the MT's emanating from the opposite spindle pole, MT's pulling and pushing forces at the KTs increase the distances between the sister centromeres and KTs, generating tension which has been shown to stabilize KT-MT attachments *in vivo* (Dewar et al. 2004; Lampson and Grishchuk 2017; Cane et al. 2013; Harasymiw et al. 2019). Moreover, the forces result in the outward expansion of the KTs as observed by an increase in intra-KT distances, distances between the inner and outer KT proteins, leading to an increase in KT dephosphorylation and inactivation of spindle assembly checkpoint (SAC) (Wan et al. 2009; Maresca and Salmon 2009; Uchida et al. 2009a).

Genetic manipulation studies in budding yeast show that a drop of 1 pN or ~20% of normal-tension per KT increases KT-MT detachment by ~5 fold, and this detachment is Aurora B dependent (Mukherjee, Ali, and Arunachalakasi 2019). Aurora B kinase, a major player in error correction pathway, phosphorylates numerous substrates including residues in the N-terminal region of NDC80, a key attachment protein, to inhibit MT binding and thus destabilizing KT-MT attachments (Guimaraes et al. 2008; Miller, Johnson, and Stukenberg 2008; DeLuca, Lens, and DeLuca 2011). KT-MT attachments are regulated through phosphorylation and dephosphorylation events (Reviewed in: (Saurin and Kops 2016; Vallardi, Cordeiro, and Saurin 2017)); however, whether a phosphatase is involved in KT-MT attachment stability is not known. In addition to destabilizing KT-MT attachments, Aurora-B mediated

phosphorylation of KNL1 inhibits KNL1 binding to PP1 phosphatase, which is required for dephosphorylating "MELT" repeats on KNL1 to inhibit recruitment of BubR1, a spindle assembly checkpoint (SAC) protein (Nijenhuis et al. 2014; Meadows et al. 2011; Rosenberg, Cross, and Funabiki 2011; Liu et al. 2010). SAC proteins such as the BUBs (Bub1, BubR1 and Bub3) and RZZ complex (ROD, ZWILCH and ZW10) arrive at the KTs in early prometaphase and recruit MAD1 and MAD2 checkpoint proteins resulting in inhibition of anaphase-promoting complex/cyclosome (APC/C) (Reviewed in: (Musacchio 2015; Joglekar 2016)). Continued SAC activation gives the cells time to correct erroneous KT-MT attachments and ensures chromosome segregation occurs only once correct attachments are formed.

Aurora B kinase negatively regulates the Astrin-SKAP complex levels at the KTs (Schmidt et al. 2010; Shrestha et al. 2017). Astrin-SKAP complex arrives only at the end-on attached KTs (Shrestha and Draviam 2013), interacts with NDC80 (Kern, Wilson-Kubalek, and Cheeseman 2017), and plays a key role in stabilizing KT-MT attachments (Dunsch et al. 2011; Kern, Wilson-Kubalek, and Cheeseman 2017; Shrestha et al. 2017). Checkpoint proteins such as the BUBs and Mad1/2 are retained at the KTs of Astrin depleted cells (Thein et al. 2007; Schmidt et al. 2010), and live-cell imaging has shown that Astrin's arrival at the KTs coincides with the removal of MAD1 protein (Kuhn and Dumont 2017). Whether the RZZ complex is also retained in Astrin depleted cells is not known. Human Astrin p.Q1012* variant fails to localize at the KTs, leading to chromosome congression defects, delayed anaphase onset, and chromosome segregation defects (see **chapters 4 and 5**). Here, I ask whether Astrin p.Q1012* expressing cells a) can generate tension at the KTs by measuring the inter-centromeric distances and b) retain SAC proteins by immunostaining cells for ROD protein, part of the RZZ complex. I further ask whether the Astrin p.Q1012* cells have high phosphorylation at KNL1 p.S24, an Aurora B target that leads to inhibition of KNL1 PP1 phosphatase interaction (Welburn et al. 2010; Bajaj et al. 2018). Lastly, the C-terminus of Astrin has a potential PP1phosphatase binding site (See **chapter 3**), and here, I ask whether Astrin targets PP1 phosphatase to the KTs by a) pulldown studies in HeLa cells using exogenously expressed PP1 phosphatase and b) co-immunoprecipitation studies by exogenously expressing Astrin fragments and PP1 phosphatase.

6.2 HUMAN ASTRIN P.Q1012* EXPRESSING CELLS HAVE REDUCED INTER-CENTROMERIC DISTANCES

To investigate whether expression of human Astrin p.Q1012* variant affects kinetochore (KT)-microtubule (MT) attachment stability, which could be inferred as inter-centromeric stretching or tension, I co-transfected HeLa cells with plasmids encoding either YFP tagged Astrin WT or p.Q1012* and CENPB-ds-Red (centromeric marker). Time-lapse imaging was performed 24 hrs later, and inter-centromeric distances were measured every minute over a period of ten minutes (**Fig 6.1 A-B**). Inter-centromeric distances in the Astrin WT expressing cells range from 0.3 µm to 1.7 µm (n=9 cells, 5 KT pairs/cell; **Fig 6.1 C-D**). However, they are significantly reduced in the Astrin p.Q1012* expressing cells (0.4-1.3 µm, $p<0.01$; **Fig 6.1 C-D**). Next, I tracked inter-centromeric distance change for five consecutive time-points before and after the time-point at which the KT pair was unstretched, here forth termed t=0. Data indicate that centromeres in Astrin p.Q1012* cells stretch upto approximately 0.2 µm, but this stretching is less compared to the Astrin WT cells (approximately 0.37 µm; **Fig 6.1 E-F**) I conclude that inter-centromeric stretching is reduced in cells expressing Astrin p.Q1012* variant compared to Astrin WT expressing cells.

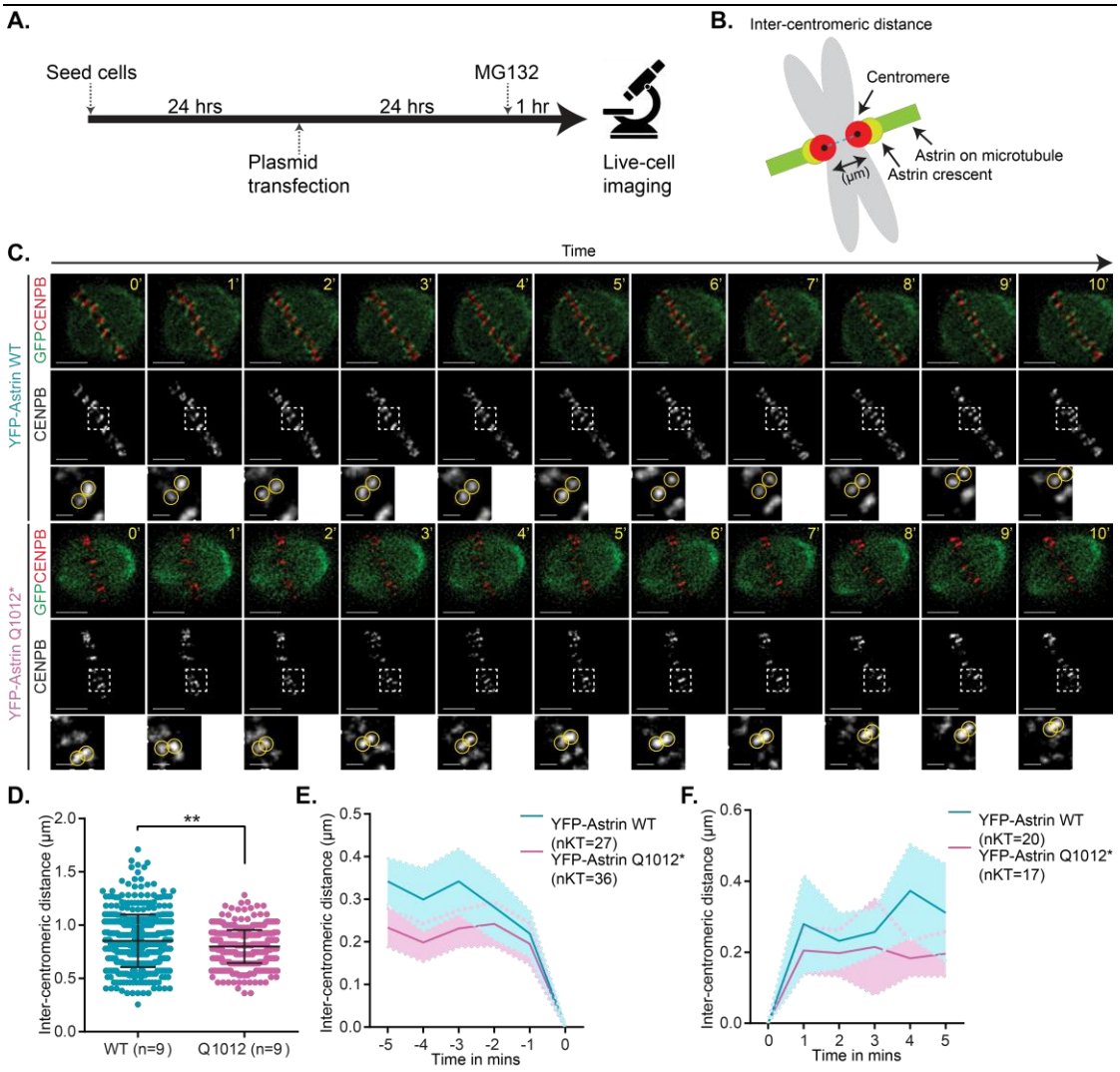

Fig 6.1. Inter-centromeric stretching is reduced in cells expressing Astrin p.Q1012*. A. Experimental regimen. **B.** Cartoon showing inter-centromeric distance as a measurement of inter-centromeric stretching. **C.** Representative time-lapse images of Astrin wild type and p.Q1012* expressing cells treated as in A. Scale bars: 5 μm in uncropped images and 1 μm in insets. Yellow circles indicate individual kinetochores (KTs) of a pair. **D.** Scatterplot showing inter-centromeric distances in cells treated as in A measured for five pairs of KTs per cell over 10 minutes (1 frame/min). "n" is the number of cells. Error bars show mean with SD. Man-Whitney U test was performed for statistical significance. ** represents $p < 0.01$. **E-F.** Change in inter-centromeric distances (normalized to least inter-centromeric distance) over time in cells treated as in A. "0" is the time point of least inter-centromeric distance. The shaded area represents a 95% confidence interval. "nKT" is the number of KTs. **(D-F)** Data represent three independent experiments.

Next, I asked whether inter-centromeric stretching is reduced in Astrin 4A mutant, a PP1 phosphatase docking mutant where a potential PP1 docking domain conforming to RVxF motif in the C-terminus of Astrin is mutated into 4 Alanines to

disrupt Astrin PP1 interaction (Conti et al. 2019). For this, I used a stably expressing YFP-Astrin cell line, transiently expressed CENPB-ds-Red (centromeric marker) and performed time-lapse imaging 24 hrs later. Unlike the Astrin WT, the intensity of the 4A mutant's signal at the KT is not constant. Instead, it appears to be "blinking"-dimming and coming back (Duccio Conti et al. 2019). To ask whether the "blinking" Astrin impacts inter-centromeric distances, time intervals between inter-centromeric distance measurements were reduced to every 4 sec over a period of two minutes. In the absence of endogenous Astrin, inter-centromeric distances in Astrin WT expressing cells range from 0.18 µm to 0.91 µm (**Fig 6.2 B-C**) compared to 0.3 µm to 1.7 µm in the presence of endogenous Astrin (**Fig 6.1 B-C**). Moreover, inter-centromeric distances in Astrin 4A expressing cells are significantly reduced compared to the Astrin WT (0.098-0.67 µm in 4A compared to 0.18-0.91 µm in WT, $p<0.0001$; **Fig 6.2 B-C**). Interestingly, not only the maximum "stretch" but the minimum "stretch" is also reduced in Astrin 4A (**Fig 6.2 C**). Next, I tracked inter-centromeric distance change for one minute before and after the time-point at which the KT pair was unstretched, termed t=0. Data indicate that both Astrin WT and 4A stretch approximately 0.1-0.15 µm (**Fig 6.2 D-E**). I conclude that inter-centromeric distances are reduced in cells expressing the Astrin 4A variant compared to Astrin WT, but the amount of stretching is similar.

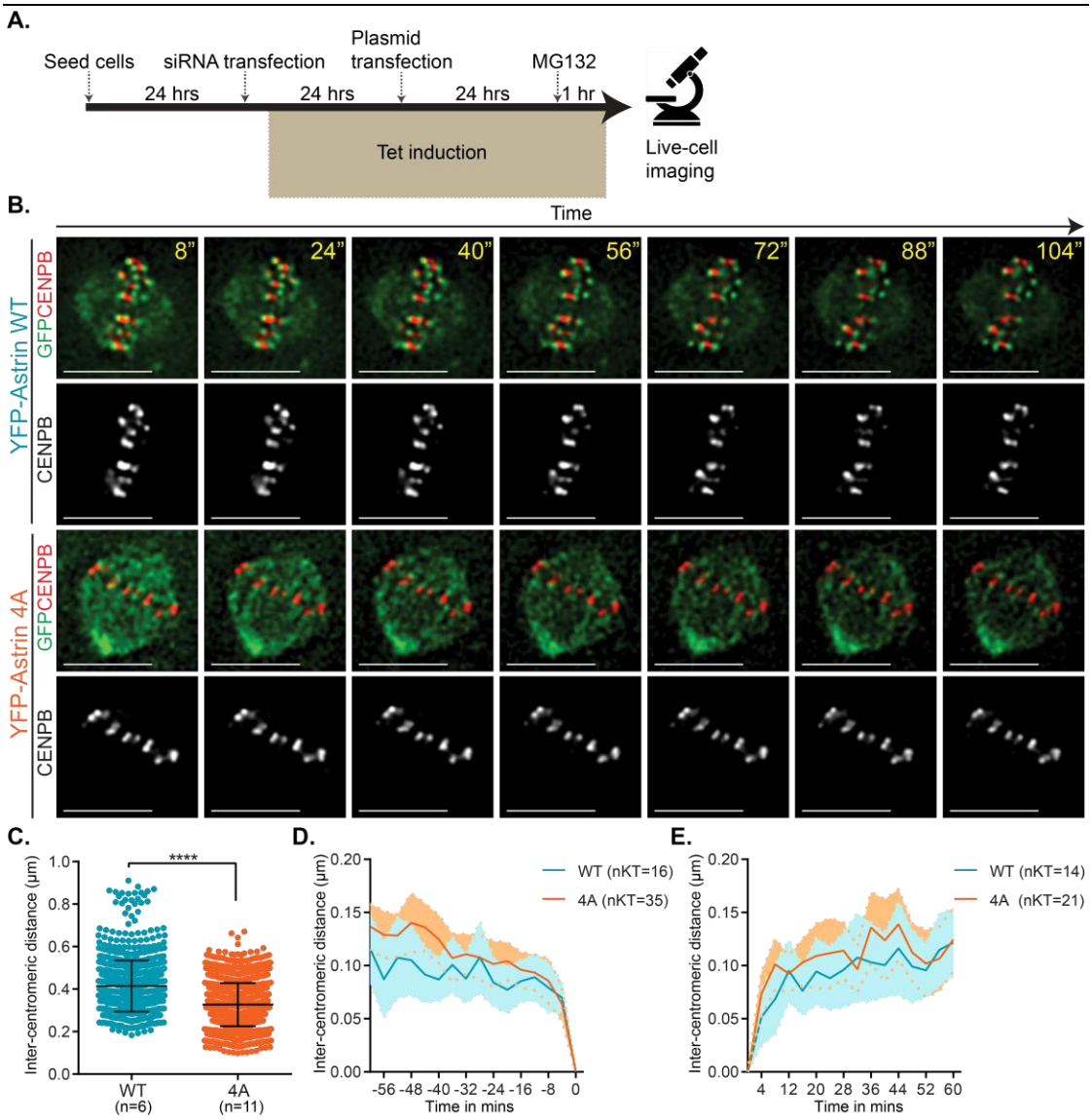

Fig 6.2. Inter-centromeric stretching is reduced in cells expressing Astrin 4A depleted of endogenous Astrin. A. Experimental regimen. **B.** Representative time-lapse images of Astrin wild type and 4A expressing cells treated as in A. Scale bars: 5 µm in uncropped images and 1 µm in insets. **C.** Scatter plot showing inter-centromeric distances in cells treated as in A measured for five pairs of kinetochores (KTs) per cell over 2 minutes (1 frame/4 s). "n" is the number of cells. Error bars show mean with SD. Man-Whitney U test was performed to find statistical significance. **** represents p< 0.0001. **D-E.** Change in inter-centromeric distances (normalized to least inter-centromeric distance) over time in cells treated as in A. "0" is the time point of least inter-centromeric distance. The shaded area represents a 95% confidence interval. "nKT" is the number of KTs. **(D-F)** Data represent four independent experiments.

Collectively, the data suggests that Astrin's C-terminus is required for adequate stretching and unstretching of centromeres.

6.3 HUMAN ASTRIN P.Q1012* EXPRESSING CELLS DISPLAY AN INCREASED INCIDENCE OF CHECKPOINT PROTEIN ROD AT METAPHASE KINETOCHORES

One of the pathways for recruiting checkpoint proteins Mad1/2 at the kinetochores (KTs) involves the RZZ complex (Silió, McAinsh, and Millar 2015; Kops et al. 2005; Buffin et al. 2005). To investigate the spindle assembly checkpoint's status in Astrin p.Q1012* expressing cells, I looked at ROD (part of the RZZ complex) levels at the metaphase KTs. Data indicate that ~77% of the Astrin p.Q1012* cells (n=44) have more than 4 KTs positive for ROD signal compared to only ~13% of Astrin WT cells (n=38, $p<0.01$; **Fig 6.3 B-C**). Next, I compared the ROD levels in Astrin p.Q1012* expressing cells with two Astrin C-terminal mutants: 4A (PP1 docking site mutant) and Δ70 (lacks last 70 a.a. of Astrin including the potential PP1 docking site). Data indicate that only ~23% of cells expressing C-terminal mutants of Astrin have more than 4 KTs positive for ROD (n=21 for both 4A and Δ70), which is higher than the WT but less than the p.Q1012* (**Fig 6.3 B-C**). I conclude that expression of the Astrin p.Q1012* variant increases ROD retention at KTs, and this retention is higher than observed for Astrin 4A and Δ70 mutants. High checkpoint protein levels would delay anaphase onset and lead to an accumulation of metaphase cells. Indeed, in non-MG132 treated cells, there is a higher proportion of Astrin p.Q1012* expressing metaphase cells compared to Astrin WT ($p<0.01$; **Fig 6.3 D**).

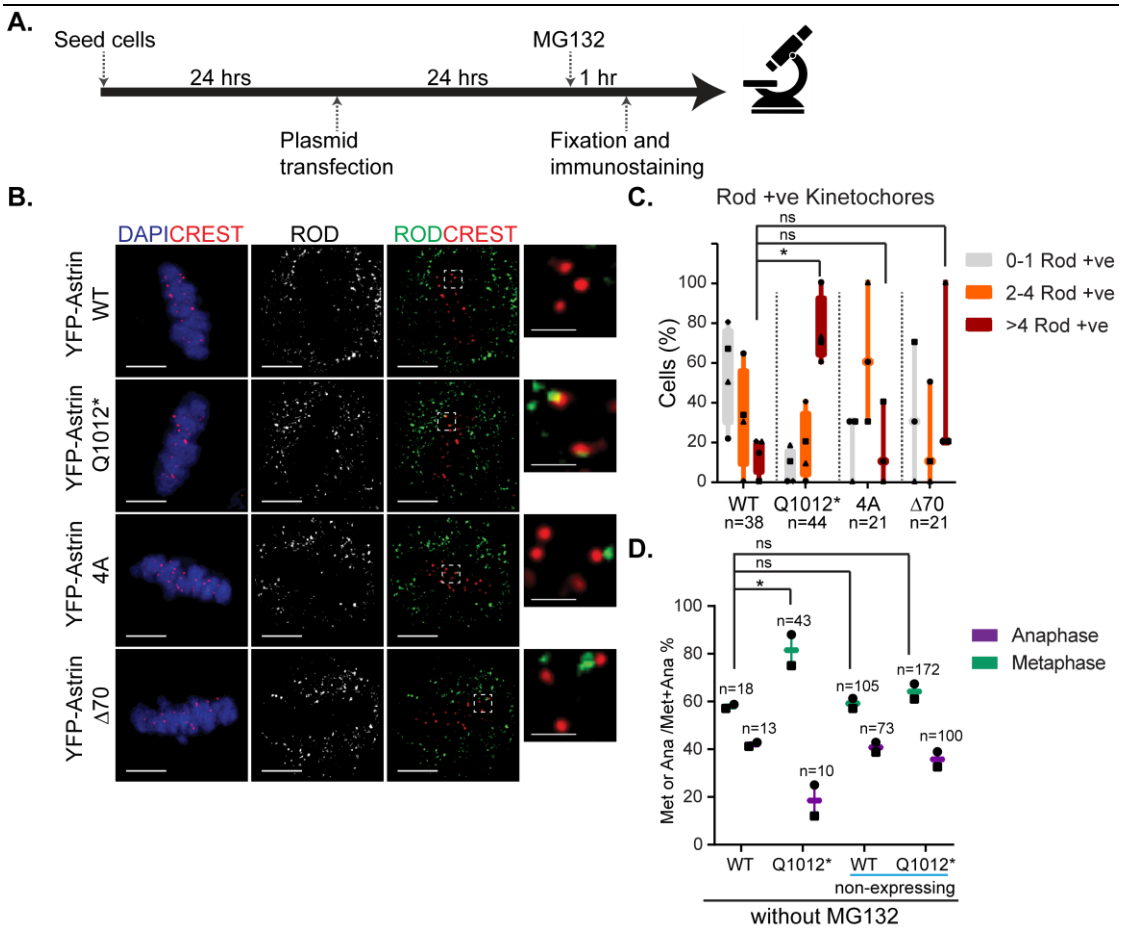

Fig 6.3. Astrin p.Q1012* expressing cells display an increased incidence of ROD positive metaphase kinetochores. A. Experimental regimen. **B**. Representative immunofluorescence images of Astrin wild (WT) type, p.Q1012*, 4A and Δ70 expressing cells treated as in A and probed for GFP, ROD, and CREST. DNA was stained with DAPI. Scale bars: 5 µm in uncropped images and 1 µm in insets. **C.** Box plot showing the number of cells treated as in B with 0-1, 2-4, or >4 kinetochores (KTs) positive for checkpoint protein ROD (ROD +ve KTs). Symbols represent independent experiments. One-way ANOVA was performed to find statistical significance. * represents p<0.01, ns=not significant. **D.** Box plot showing the proportion of metaphase and anaphase cells after 24 hrs of transfection with Astrin WT and p.Q1012* plasmids. Symbols represent independent experiments. One-way ANOVA was performed to find statistical significance. * represents p<0.01, ns=not significant.

6.4 HUMAN ASTRIN P.Q1012* EXPRESSING CELLS HAVE HIGH PHOSPHORYLATION AT KNL1 P.S24

Recruitment of phosphatases at the kinetochores (KTs) and subsequent dephosphorylation of their KT targets is essential for silencing of spindle assembly checkpoint. To investigate whether retention of checkpoint protein ROD in Astrin p.Q1012* expressing variant is due to persistently high phosphorylation status of KT

proteins, I looked at phosphorylation at p.S24 residue of KNL1 whose phosphorylation by Aurora B prevents KNL1-PP1 phosphatase binding (Welburn et al. 2010; Bajaj et al. 2018). For this, I used a phospho antibody targeting p.S24 and data indicate that ~67% metaphase KTs in Astrin p.Q1012* expressing cells are positive for phospho p.S24 compared to ~38% of Astrin wild type (WT; p<0.0001; **Fig 6.4 B-C**). Moreover, Astrin C-terminal mutants also have higher phosphorylation (~64% in Δ70 and ~54% in 4A) than WT (**Fig 6.4 B-C**). I conclude that cells expressing Astrin p.Q1012* have higher phosphorylation at KNL1 p.S24, which is similar to Astrin Δ70.

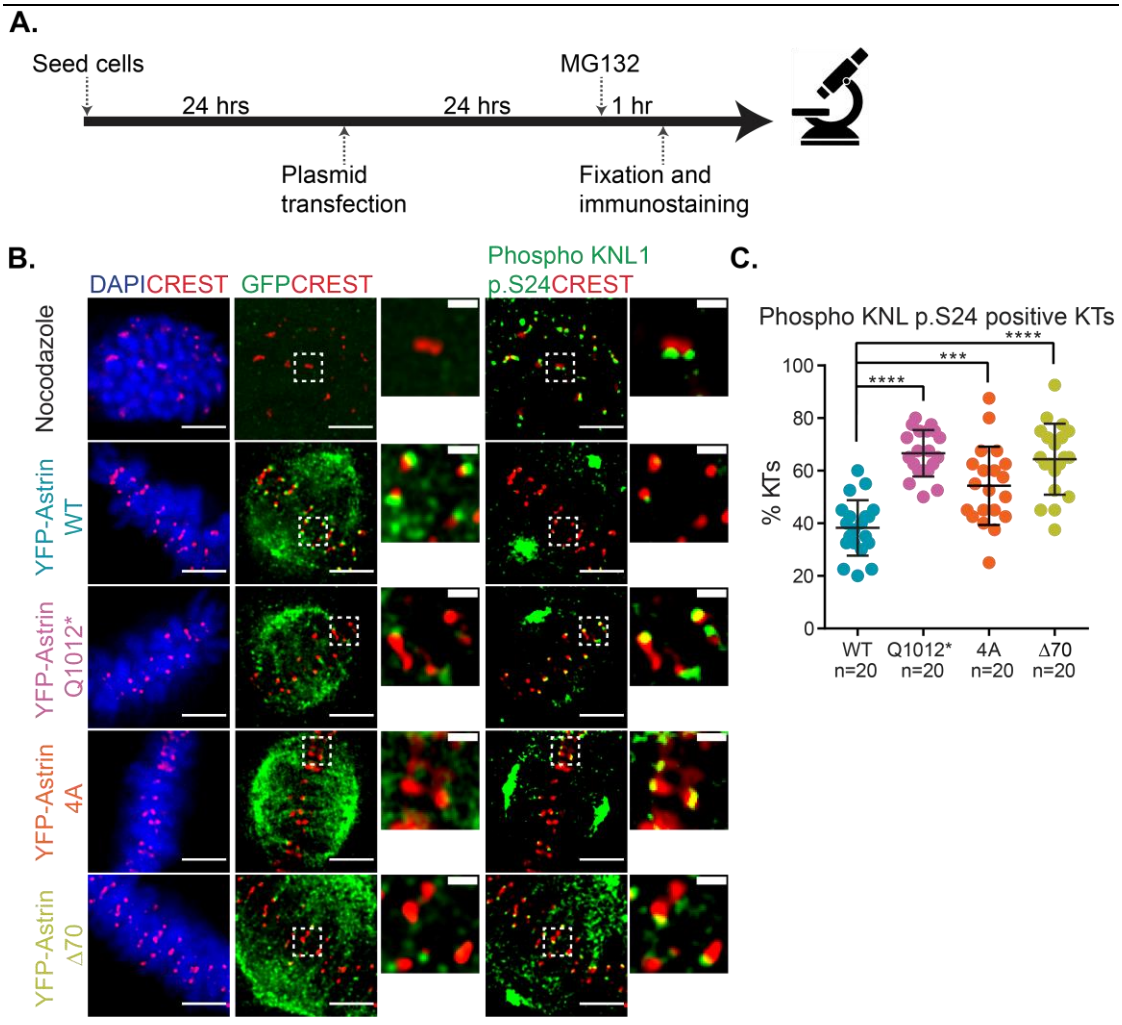

Fig 6.4. Astrin p.Q1012* expressing cells have high phosphorylation at KNL1 p.S24. A. Experimental regimen. **B.** Representative immunofluorescence images of Astrin wild type (WT), p.Q1012*, 4A and Δ70 expressing cells treated as in A and probed for GFP, phospho KNL1 p.S24, and CREST. DNA was stained with DAPI. Scale bars: 5 μm in uncropped images and 1 μm in insets. **C.** Scatter plot showing the percentage of kinetochores positive for phospho KNL1 p.S24 staining. Dots represent individual cells, error bars represent mean with SD and data represents two independent sets. One-way Anova was performed to find statistical significance. *** represents p<0.001, **** represents p<0.0001.

Next, I imaged and analyzed Astrin WT and Δ70 expressing cells depleted of endogenous Astrin for phosphorylation at p.S24 of KNL1. The experiment was set up by a previous postdoc in the lab, Duccio Conti. Data indicate that ~60% of metaphase KTs in Astrin Δ70 expressing cells are positive for phospho KNL1 p.S24 compared to ~33% in Astrin WT (**Fig 6.5 B-C**). I conclude that Astrin Δ70 expressing cells have high phosphorylation at KNL1 p.S24.

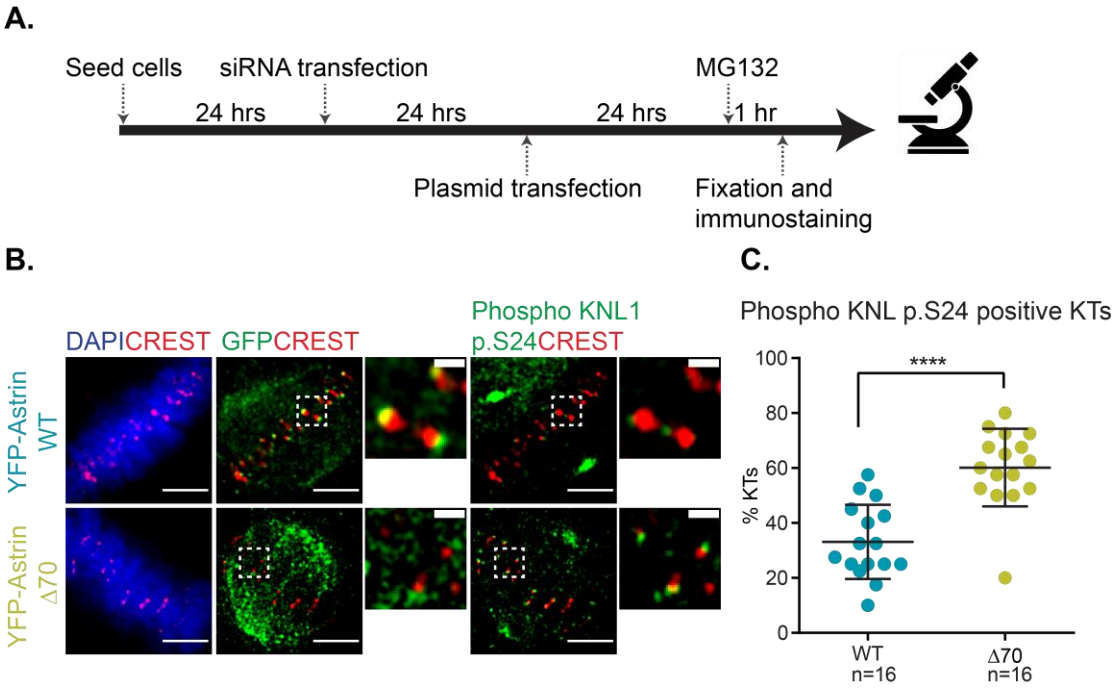

Fig 6.5. Astrin Δ70 expressing cells have high phosphorylation at KNL1 p.S24 in the absence of endogenous Astrin. A. Experimental regimen. **B.** Representative immunofluorescence images of Astrin wild type (WT) and Δ70 expressing cells treated as in A and probed for GFP, phospho KNL1 p.S24, and CREST. DNA was stained with DAPI. Scale bars: 5 μm in uncropped images and 1 μm in insets. **C.** Scatter plot showing the percentage of kinetochores (KTs) positive for phospho KNL1 p.S24 staining. Dots represent individual cells, error bars represent mean with SD and data represents two independent sets. Man-Whitney U test was performed to find statistical significance. **** represents p<0.0001.

Collectively, the data suggest that expression of C-terminal variant and mutants of Astrin prevent successful dephosphorylation of KT proteins.

6.5 ASTRIN IS PULLED DOWN FROM HELA CELLS BY EXOGENOUSLY EXPRESSED PP1 PHOSPHATASE

Bioinformatics analysis shows a potential PP1 docking motif conforming to RVxF in Astrin's C-terminus (Conti et al. 2019). A PhD student in the Lab, Parveen Gul, standardized PP1γ phosphatase pulldown protocol and pulled down endogenous Astrin from HeLa cells (Conti et al. 2019). To investigate sensitivity and reproducibility, I repeated her pulldown experiment using exogenously expressed, purified and bead-bound GST and GST-PP1γ kindly provided by her. Immunoblot analysis shows multiple bands where endogenous Astrin is expected in GST-PP1γ pulldown but not in GST pulldown (**Fig 6.6 A-B**). Next, I ran a coomassie to assess enrichment specific to GST-PP1γ pulldown and the gel shows enrichment of several bands which are not present in the GST pulldown lane (**Fig 6.6 B**).

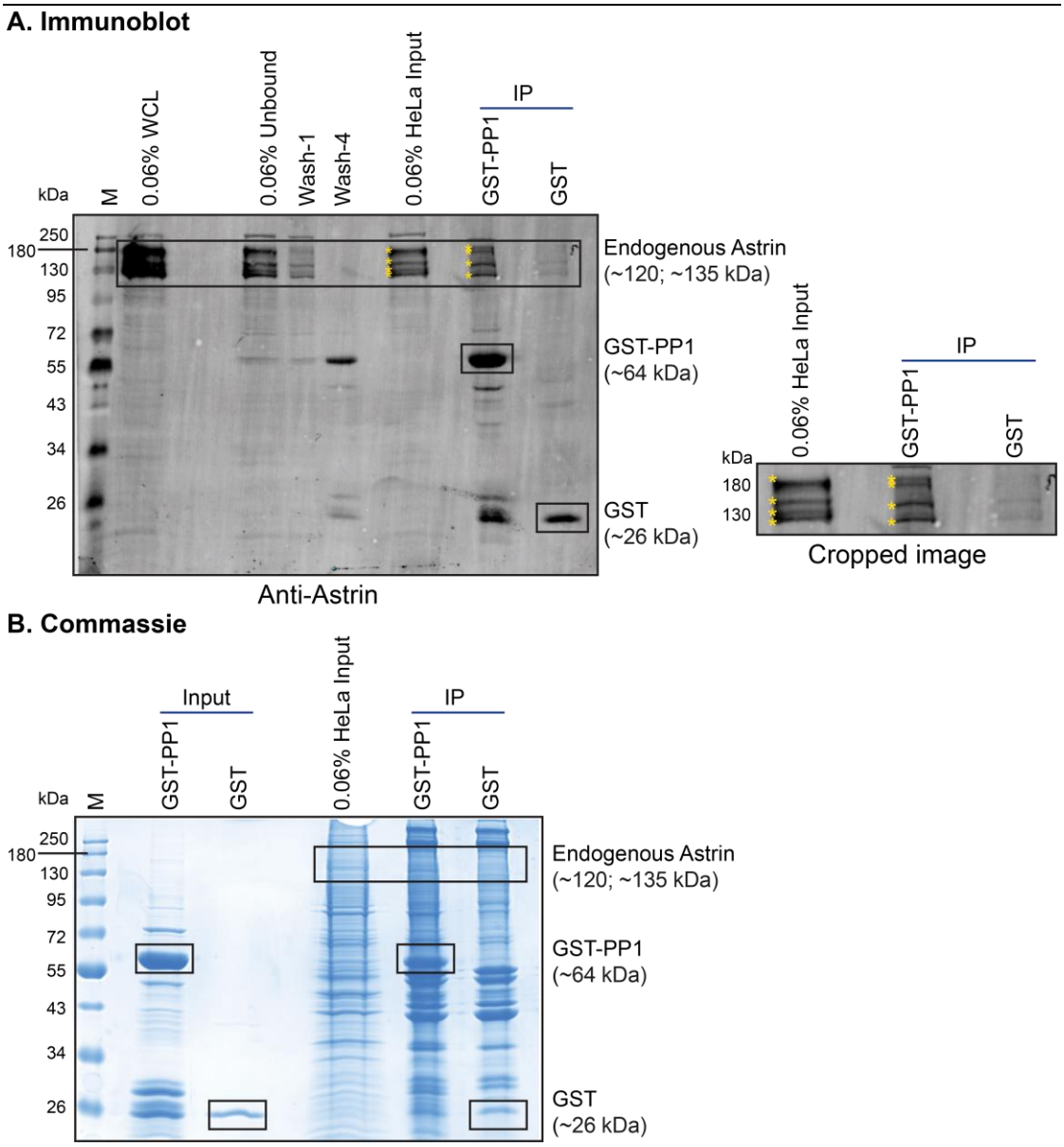

Fig 6.6. Endogenous Astrin is pulled down from HeLa cell lysates by exogenously expressed GST-PP1γ. A. Immunoblot of pulldown assay shows the interaction of GST-PP1γ, but not GST, with Astrin in lysates of mitotically synchronized HeLa cells. Cells were exposed to STLC for 24 hrs prior to lysate generation. Cells were sonicated (WCL=whole cell lysate), soluble fraction was separated by centrifugation (HeLa input) and exposed to exogenously expressed GST and GST-PP1γ bound to glutathione beads. Beads were then centrifuged (unbound) and washed four times (wash-1 and wash-4). Unbound, wash-1 and wash-4 are from GST-PP1 pulldown. Immunoblot was probed with antibody against Astrin. Yellow asterisks show Astrin bands. A cropped image of the immunoblot with Astrin bands is shown on the right. **B.** Coomassie of the same pulldown assay as in A showing the pulldown and inputs. Boxes show indicated proteins. GST and GST-PP1γ were purified by Parveen Gul.

In addition to four bands matching the expected size of Astrin isoforms and Astrin phosphorylated forms, several non-specific bands were detected in the pulldown.

To confirm the detected bands were indeed Astrin, HeLa cells were treated by control siRNA and Astrin siRNA (**Fig 6.7 A**) and exposed to freshly purified GST and GST-PP1γ (**Fig 6.7 B**). Again, immunoblot analysis shows multiple bands of Astrin being pulled down by exogenously expressed GST-PP1γ but not GST, but these bands are absent in cell lysates treated with Astrin siRNA (**Fig 6.7 A-C**). I conclude that Astrin, directly or indirectly, interacts with PP1 phosphatase in HeLa cells.

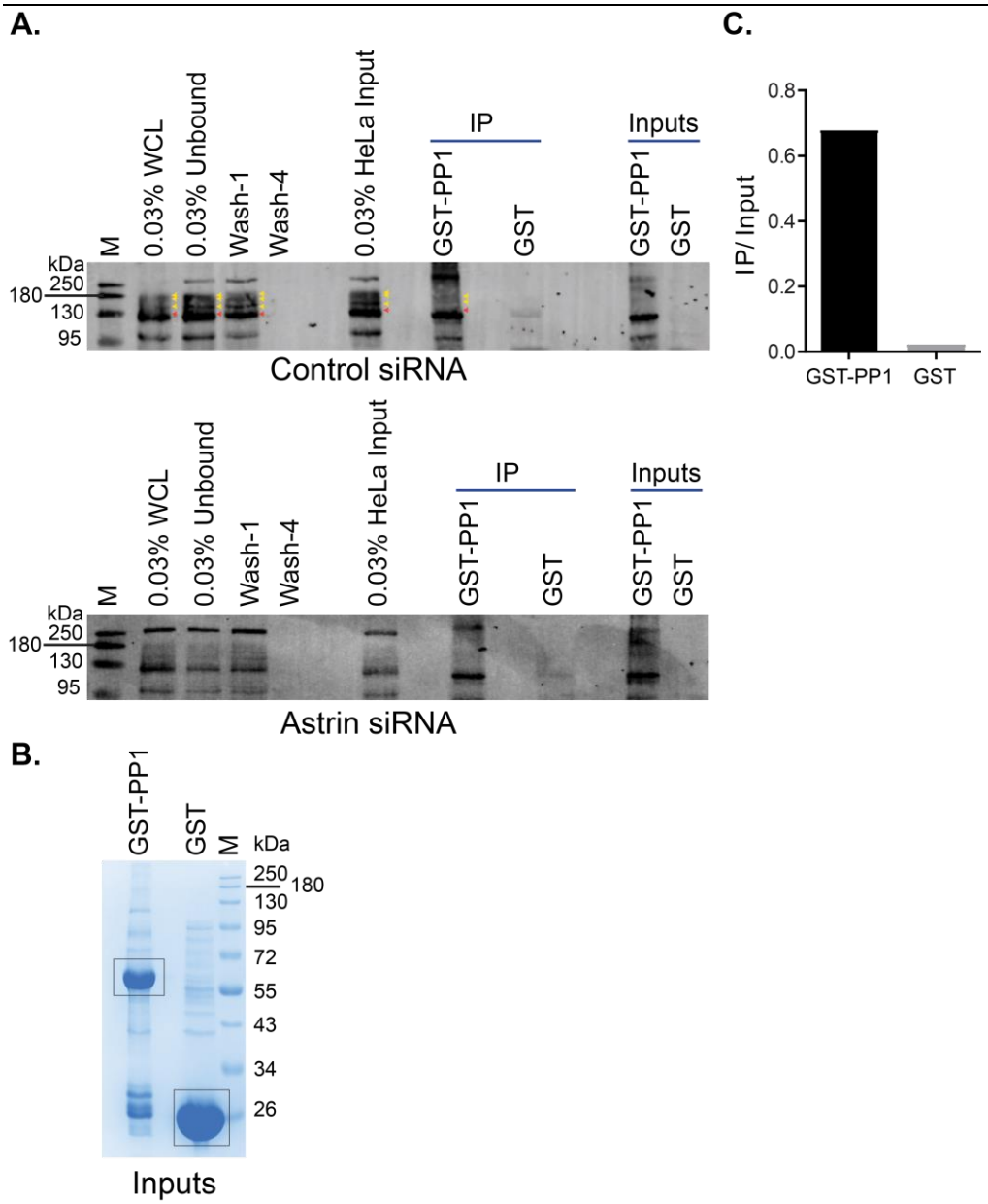

Fig 6.7. Endogenous Astrin is pulled down from HeLa cell lysates by exogenously expressed GST-PP1 gamma in control siRNA treated cells. A. Immunoblot of pulldown assay shows the interaction of GST-PP1γ, but not GST, with Astrin in lysates of mitotically synchronized HeLa cells. Cells were treated with Astrin or Control siRNA, as indicated, and exposed to STLC for 24 hr prior to lysate generation. Immunoblot was probed with an antibody against Astrin. Yellow arrowheads indicate Astrin bands and the red arrow indicates a non-specific band. **B**. Coomassie-stained gel showing purified GST-PP1γ and GST used as bait in A. GST and GST-PP1γ were purified by Parveen Gul. **C.** Graph of the ratio of Astrin intensities in the GST-PP1 or GST pulldown lane relative to input lysate lane.

To investigate whether Astrin and PP1 interaction is direct, I standardized the expression and purification of Astrin C-terminal fragments-WT and 4A, and GST-PP1γ. Using immobilized GST-PP1γ as bait, I coimmunoprecipitated both Astrin WT

and 4A (**Fig 6.8 A-B**). Immunoblot analysis shows PP1γ interacts more with Astrin WT than 4A (**Fig 6.8 B**). However, the experiment does not include a negative control. Moreover, the results could not be reproduced when frozen-thawed purified Astrin fragments were used instead of freshly purified Astrin fragments (**Fig 6.8 C-F**).

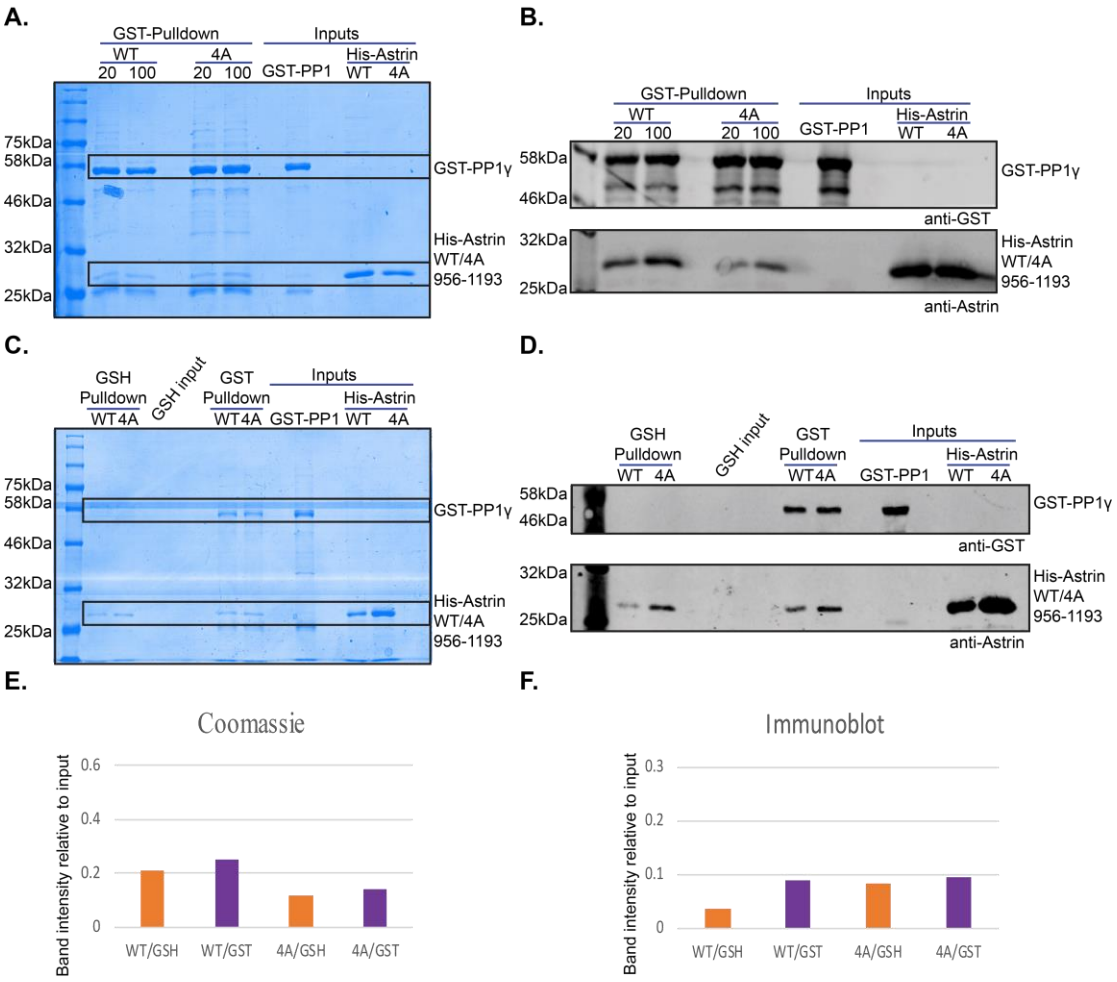

Fig 6.8. Direct interaction study of Astrin fragments and GST-PP1 gamma. A. Coomassie-stained gel of co-immunoprecipitation assay shows Astrin WT and 4A both interacting with GST-PP1γ. Freshly purified Astrin fragments and GST-PP1γ were used. **B**. Immunoblot of the co-immunoprecipitation assay as in A was probed for GST (top) and Astrin (bottom). Astrin-PP1 interaction seems reduced in Astrin 4A. **C.** Coomassie-stained gel of co-immunoprecipitation assay shows Astrin WT and 4A both interacting with GST-PP1γ and GST control. Purified Astrin fragments frozen at -80 C were thawed one day later, and freshly purified GST-PP1γ were used. **D.** Immunoblot of the co-immunoprecipitation assay as in C was probed for GST (top) and Astrin (bottom). Both Astrin fragments interact with GST-PP1γ and GST control. **E-F.** Graphs of the ratio of Astrin intensities in pulldown lanes relative to input lysate lanes in C-D.

Collectively, the data indicate that Astrin is in complex with PP1γ phosphatase in mammalian cells. Preliminary findings suggest that Astrin directly interacts with PP1γ and mutating potential PP1 motif in the C-terminus of Astrin disrupts but does not abolish this interaction.

6.6 DISCUSSION

Microtubule (MT) pulling and pushing forces acting on either side of the sister kinetochores (KTs) results in the generation of tension. *In vivo* studies have shown that tension at the KT-MT interface is important for stabilizing KT-MT attachments (Dewar et al. 2004; Cane et al. 2013; Lampson and Grishchuk 2017; Harasymiw et al. 2019). Moreover, cancer cells have reduced tension (Harasymiw et al. 2019). Tension at the KT-MT interface can increase a) inter-centromeric stretching, b) inter-KT stretching, and c) intra-KT stretching. Using inter-centromeric distances as a readout for KT-MT attachment stability, I show that inter-centromeric distances are reduced in both C-terminal human Astrin variant p.Q1012* and PP1 phosphatase docking mutant Astrin 4A compared to the WT (**Fig 6.1 C-F**, **Fig 6.2 B-C**). Tracking the inter-centromeric distances over time shows that centromeres in Astrin p.Q1012* expressing cells only stretch an average of ~0.2 µm compared to 0.37 µm in the WT (**Fig 6.1 E-F**). In contrast, the Astrin 4A stretches similar to the WT (**Fig 6.2 D-E**) and appear to have reduced minimum inter-centromeric distances (**Fig 6.2 C**). Similar to the inter-centromeric distances, both the maximum and minimum inter-KT distances are reduced in Astrin 4A expressing cells (Duccio Conti et al. 2019). Both of these studies were carried out in the absence of endogenous Astrin. One possible explanation is that the endogenous Astrin in the p.Q1012* study does not let the inter-centromeric distances fall below a specific limit. Compared to cells with endogenous Astrin, depletion of endogenous Astrin reduces inter-centromeric distances in the WT itself (0.18-0.91 compared to 0.3-1.7 µm in the presence of endogenous Astrin; **Fig 6.2 C** vs. **Fig 6.1 D**). However, both cell lines are different (HeLa vs. HeLa FRT/TO), and the method used to express Astrin is also different (transient vs. stable expression). Either of these may be responsible for the differences in the inter-centromeric measurements between the two studies. A future study investigating both Astrin p.Q1012* and 4A together in

the absence of endogenous Astrin could help answer whether the two proteins influence tension at the KTs differently.

The error correction pathway senses reduced tension at the KT-MT interface, leading to Aurora B kinase-dependent KT-MT detachment (Mukherjee, Ali, and Arunachalakasi 2019; Guimaraes et al. 2008; S. A. Miller, Johnson, and Stukenberg 2008; K. F. DeLuca, Lens, and DeLuca 2011). This may explain the presence of unaligned chromosomes in Astrin p.Q1012* expressing cells (See **chapter 5**) and increased incidence of lateral attachments in C-terminal Astrin mutants (4A and ΔC; (Conti et al. 2019)). Lateral attachments have high levels of spindle assembly checkpoint (SAC) proteins (Shrestha and Draviam 2013; Kuhn and Dumont 2017), and indeed all C-terminal Astrin variant/mutants have a high incidence of ROD checkpoint protein (**Fig 6.3 B-C**), and both C-terminal mutants have a high incidence of Mad2 checkpoint protein at the metaphase KTs (Conti et al. 2019). Moreover, ROD positive KTs are higher in Astrin p.Q1012* expressing cells compared to both C-terminal mutants (**Fig 6.3 B-C**). This is surprising as both Astrin p.Q1012* and Δ70 have impaired KT localization to a similar extent (see **chapter 4**). However, Astrin Δ70 has 112 a.a. more than the p.Q1012*, and a motif search in this region found a potential PP2A phosphatase docking site (see **Chapter 3**). Astrin is pulled down by B56_PP2A (Hertz et al. 2016); however, whether this interaction is direct or not is unknown.

Each step of mitosis is tightly regulated through phosphorylation and dephosphorylation events (Reviewed in: (Saurin and Kops 2016; Vallardi, Cordeiro, and Saurin 2017)). Aurora B phosphorylates KNL1 to inhibit KNL1-PP1 phosphatase interaction and SAC silencing (Liu et al. 2010; Meadows et al. 2011; Rosenberg, Cross, and Funabiki 2011; Nijenhuis et al. 2014). Compared to the Astrin WT, all three C-terminal Astrin variant/mutants have high phosphorylation at KNL1 p.S24 (**Fig 6.4 B-C**, **6.5 B-C**). Moreover, the high KNL1 p.S24 phosphorylation in Astrin p.Q1012* expressing cells is higher than the 4A but similar to Δ70 (**Fig 6.4 B-C**). Intra-KT tension and not inter-centromeric and inter-KT tension is required for reduced phosphorylation, SAC silencing, and anaphase onset (Maresca and Salmon 2009; Uchida et al. 2009a; Wan et al. 2009). Both C-terminal Astrin variant/mutant-p.Q1012* and 4A, expressing cells have reduced inter-centromeric distances, and Astrin 4A has reduced inter-KT distances (**Fig 6.1 C-F**; (Conti et al. 2019)); however, whether manipulating C-terminus

of Astrin also influences intra-KT stretching is not known. In the future, live-cell movies of Astrin 4A co-expressing a centromeric marker can be analyzed to determine intra-KT distances changes.

Both C-terminal Astrin deletion variant/mutant-p.Q1012* and Δ70, cells have impaired KT localization and undergo checkpoint dependent prolonged mitosis (See **chapter 4 and 5**, **Fig 6.3 B-C**; (Conti et al. 2019)). Both Astrin p.Q1012* and Δ70 lack a potential PP1-docking motif, and GBP-PP1γ targeting at the C-terminus of Astrin leads to stabilization of KT-MT attachments (Conti et al. 2019). Astrin is pulled down by exogenously expressed GST-PP1γ (**Fig 6.6 A**, **6.7 A, C**), but whether this interaction is direct or indirect is not known. I standardized the expression and purification of His tagged Astrin fragments (956-1193 a.a.), and preliminary co-immunoprecipitation results suggest that Astrin directly interacts with PP1γ phosphatase (**Fig 6.8 A-B**), and this interaction is reduced but not abolished with Astrin 4A mutant. However, the experiment could not be reproduced with frozen-thawed purified Astrin fragments (**Fig 6.8 C-F**) and did not have a negative control (**Fig 6.8 A-B**). To confirm Astrin-PP1 direct interaction, the experiment should be repeated using freshly purified Astrin protein fragments. Lastly, coomassie stained gel of the pulldown assay shows enriched bands in the GST-PP1γ lane (**Fig 6.6 B**). In the future, mass spectrometry studies can be carried out to find PP1γ interacting partners.

CHAPTER 7: DISCUSSION

CHAPTER 7: DISCUSSION

7.1 SUMMARY

Stable end-on kinetochore (KT)-microtubule (MT) attachments are required for accurate chromosome segregation. Genomic variations in KT proteins can cause pregnancy loss, primary microcephaly (MCPH) and cancer-susceptible mosaic variegated aneuploidy (MVA) (Reviewed in: (Degrassi, Damizia, and Lavia 2019)). The incidence of MCPH is higher in populations where consanguineous marriages are common such as in northern Pakistan (Reviewed in: (Cox et al. 2006; Woods, Bond, and Enard 2005)). In this thesis, I first identified genomic variations in KT proteins from the Genes and Health (GH) database (Finer et al. 2020), a population genetic study of UK residents of Pakistani-Bangladeshi origin (**Chapter 3**). Next, I compared the percentage of tumor samples with somatic mutations in seven categories in the COSMIC database (Tate et al. 2019), a database of somatic mutations in cancer (**Chapter 3**). I found that the percentage of tumor samples with somatic mutations in the SPAG5 gene is lower than MCPH and tumor suppressor genes (**Chapter 3**).

SPAG5 gene is a potential biomarker for cancer prognosis and a potential target for cancer therapy (Reviewed in: (He et al. 2020; Z. Ying et al. 2020)). Moreover, a compound heterozygous genomic variation in the SPAG5 gene is associated with microcephaly (Boonsawat et al. 2019). SPAG5 gene encodes Astrin protein, a key KT protein required for stable end-on KT-MT attachments (Thein et al. 2007; Dunsch et al. 2011; Manning et al. 2010; Shrestha et al. 2017; Gruber et al. 2002). I identified two loss of function (LOF) Astrin variants - p.L7Qfs*21 and p.Q1012*- from the GH database and one somatic Astrin mutant p.E755K from the COSMIC database (**Chapter 3**) and investigated their localization in human epithelial cells. My data suggest that Astrin p.L7Qfs*21 may express as a shorter protein (**Chapter 4**). Moreover, both Astrin p.L7Qfs*21 and p.E755K localize normally at the spindle and KTs (**Chapter 4**). However, the Astrin p.Q1012* variant fails to localize at the KTs (**Chapter 4**). Also, Astrin p.Q1012* expressing cells display prolonged mitosis, chromosome misalignment, chromosome missegregation and increased DNA damage (**Chapter 5**).

Next, I investigated three C-terminal Astrin variant/mutants and show that the C-terminus of Astrin is required for imparting MT-mediated pulling forces and silencing of spindle assembly checkpoint (SAC) (**Chapter 6**). Lastly, a PhD student in the lab had successfully pulled down endogenous Astrin with exogenously expressed GST-PP1γ phosphatase. I reproduced the pulldown, and my preliminary data suggest that the C-terminus of Astrin may directly interact with PP1 phosphatase (**Chapter 6**).

In this chapter, I will discuss my work and possible future directions.

7.2 IDENTIFICATION OF LOSS OF FUNCTION GENOMIC VARIATIONS IN KINETOCHORE PROTEINS

GH is a community-based genetic study of people of Pakistani-Bangladeshi origin in East London, Birmingham and Bradford (Finer et al. 2020). This thesis identified 142 LOF genetic variants in KT proteins from the GH database (2018 LOF list; sample size = 7465; (Finer et al. 2020)) (**Chapter 3**). 94 of the 142 variants are not listed on the *Ensembl* (Yates et al. 2020). Only 6 of the 142 KT variants are homozygous variants, and of these 6, only 3 are listed on the *Ensembl* (Yates et al. 2020) (**Chapter 3**). The list includes LOF genomic variations in several essential KT proteins, such as those involved in KT-MT attachment and spindle assembly checkpoint (SAC). Studying these variations can help increase our knowledge of disease and find better treatments.

7.3 SOMATIC MUTATIONS IN KINETOCHORE PROTEINS

This thesis has shown that in the COSMIC database (Tate et al. 2019), the percentage of tumor samples with somatic mutations in the Astrin-SKAP complex (required for stable end-on attachments), NDC80 complex (form the core KT-MT attachments) and MVA genes is lower compared to MCPH and tumor suppressor genes (**Chapter 3**). The low percentage of tumor samples with somatic mutations in these genes could mean that either these genes are located in regions that are less prone to damage or mutations in these genes are not tolerated (Reviewed in: (Nesta, Tafur, and Beck 2021)). This is interesting as the SPAG5 gene that encodes Astrin is upregulated in several cancers (Yuan et al. 2014; Abdel-Fatah et al. 2016; H. Zhang et al. 2016; Zhang et al. 2020; Liu et al. 2018; G. Liu et al. 2019; Song et al. 2018; Yang et al. 2018;

Yang et al. 2020). One possible explanation is that as Astrin is a mitotic protein, its expression is upregulated to drive increased cancer cell proliferation. However, being an essential protein, mutations in Astrin affecting its function may not be tolerated.

This thesis shows that the most frequently observed Astrin mutation in the COSMIC database, Astrin p.E755K (n=3), normally localizes at the metaphase spindle and KTs ((Tate et al. 2019); **Chapter 3, 4**). However, whether the mutant normally localizes throughout the cell cycle was not investigated. Moreover, the mutant may cause functional defects despite normal localization, and this should be investigated in the future.

7.4 HOMOZYGOUS ASTRIN VARIATIONS ARE FOUND IN THE N-TERMINUS OF ASTRIN

This thesis identified two LOF Astrin variants (p.L7Qfs*21 and p.Q1012*) from the GH database and showed that Astrin p.Q1012* (n=2; heterozygous; sample size=8,921) might be exclusive to the Pakistani-Bangladeshi community in East London (Tate et al. 2019; Karczewski et al. 2020; Finer et al. 2020) (**Chapter 3**). The Astrin p.L7Qfs*21 variant, on the other hand, is listed on the GH (hetrozygous=134, homozygous=1; sample size=8,921) and gnomAD (heterozygous=320; homozygous=6; sample size=141,456) but not on the COSMIC database (sample size=38,303) (Tate et al. 2019; Karczewski et al. 2020; Finer et al. 2020) (**Chapter 3**). Interestingly, in the 1000 Genomes project Phase 3, the Astrin p.L7Qfs*21 variant is exclusive to South Asians with an allele frequency of 2% ((Yates et al. 2020); Assessed on: 05-03-2021). There are also five non-South Asians (European, African-American) with this variation on gnomAD (Karczewski et al. 2020). However, the variant is not present on the UK10K database ((Yates et al. 2020); Assessed on: 05-03-2021). A possible explanation for this trend is that the variant originated in South Asia and is now spreading. In the UK, it may still be restricted to the South Asian community.

Interestingly, a homozygous Astrin start loss variant is also listed on the GH (heterozygous=223; homozygous=12; sample size=8,921) and gnomAD (heterozygous=1761; homozygous=25; sample size=141,456) databases (Karczewski et al. 2020; Finer et al. 2020) (**Chapter 3**). Moreover, this variant is also listed on the UK10K database ((Yates et al. 2020); Assessed on: 05-03-2021) and is present in all

ethnicities but more in Europeans (Karczewski et al. 2020), suggesting it may have originated in Europe. Astrin start loss and p.L7Qfs*21 variants are the only homozygous LOF Astrin variants present on the gnomAD database (Karczewski et al. 2020) (**Chapter 3**). Heterozygous Astrin start loss and p.L7Qfs*21 variants are also listed on the GenomaAsia100K and TOPmed databases (Wall et al. 2019; Taliun et al. 2021). Interestingly, no other LOF Astrin variant was listed on the GenomeAsia100K database (Wall et al., 2019). This could be due to the small sample size, but it reinstates that these variations are not rare.

It is intriguing to speculate that two homozygous variations in the N-terminus of Astrin may have originated in two continents and now are spreading to other continents. The presence of homozygous Astrin variations exclusively in the N-terminus suggests that variations are tolerated in the N-terminus but not in the C-terminus.

7.5 HUMAN ASTRIN P.L7QFS*21 VARIANT

7.5.1 HUMAN ASTRIN P.L7QFS*21 MAY EXPRESS AS THE SHORT ASTRIN ISOFORM

Using mass spectrometry, Thein et al. (Thein, 2008) showed that Astrin has two isoforms, and the short isoform lacks the N-terminal amino acid residues. To date, all the Astrin studies have been conducted on the long Astrin isoform, and the function of the short isoform is not known. This thesis suggests that Astrin p.L7Qfs*21 variant may express as a short protein starting from 152 a.a. of Astrin (**Chapter 4**). On an immunoblot, the two Astrin isoforms migrate with a difference of ~15 kDa, which is approximately the same as the Astrin WT and Δ151 (**Chapter 4**), suggesting the short protein expressed is the short Astrin isoform.

Except for one lung cancer cell line HBEC, all immunoblot studies published so far show both Astrin isoforms (**Table 7.1**). However, the transcriptomics data does not show the short isoform expression on the transcript level (Karczewski et al., 2020), suggesting it is formed by a post-translational modification. Both N-terminal and C-terminal Astrin residues were detected in my analysis of proteomics studies in the PRIDE database (**Chapter 3**). However, they were not segregated to compare Astrin isoform expression between cell types or within the same cell type. Future studies

should look into when and how the short Astrin isoform is formed and why the cells need it.

Table 7.1: Astrin isoforms detected in immunoblot studies.

Cell line	Number of bands (untreated/control)	Publication
Cervical cancer cell line (HeLa)	Two	(Mack and Compton 2001; Yang et al. 2006; Cheng et al. 2007; Thein et al. 2007; Duccio Conti et al. 2019; Cheng et al. 2008; Schmidt et al. 2010; Thedieck et al. 2013; Chung et al. 2016; Chu et al. 2016)
Embryonic kidney cell line (Hek293T)	Two	(L. Liu et al. 2009)
Osteosarcoma cell line (U2OS)	Two	(Halim et al. 2013)
Breast cancer cell lines (MDA-MB453, BT474, MCF-7, MDA-MB231, MDA-MB468, MCF10A)	Two	(Thedieck et al. 2013; Canu et al. 2020; Li et al. 2019)
Lung cancer cell lines (A549, HCC827, HCC515, HCC1833, NCI-HI993, NCI-H2347, NCI-H3225, H460, H1299, H1792, H1975, HCC827, Calu-1, PC9)	Two	(Huang and Li 2020; Wang et al. 2019)
Lung cancer cell line (HBEC)	One (low signal despite good	(Wang et al. 2019)

Cell line	Number of bands (untreated/control)	Publication
	loading control signal)	
Hap1 cell line (haploid cells derived from chronic myelogenous leukemia (CML)	Two	Draviam Lab, unpublished
Patient-derived fibroblasts (Microcephaly)	Two	(Boonsawat et al. 2019)
Retinal pigment epithelial cells (RPE-1)	Two	Draviam Lab, unpublished

7.5.2 THE N-TERMINUS OF ASTRIN MAY NOT BE ESSENTIAL

This thesis shows that Astrin Δ151, mimicking the new start site in Astrin p.L7Qfs*21, normally localizes at the spindle and KTs (**Chapter 4**). Moreover, a short Astrin protein starting from 275 a.a. of Astrin can localize normally at the spindle and KTs in the absence of endogenous Astrin (**Chapter 4**). Astrin Δ274 expressing cells have a mild localization defect in the presence of endogenous Astrin (**Chapter 4**), which may be due to the competition with the endogenous Astrin.

Four studies have previously looked at Astrin's N-terminal deletion mutants. Mack and Compton (Mack and Compton 2001) showed that Astrin 161-1193 a.a. normally localizes at the spindle, but the study did not look at the KT localization. Dunsch et al. (Dunsch et al. 2011) showed that Astrin 482-1193 a.a. and Kern et al. (Kern, Wilson-Kubalek, and Cheeseman 2017) showed that Astrin 465-1193 a.a. is sufficient for Astrin's arrival at the spindle and KTs and the formation of a bipolar spindle. However, Astrin 465-1193 a.a. showed compromised localization at KTs in prometaphase arrested cells (Geraghty et al. 2021).

Four kinases phosphorylate the N-terminal of Astrin: Aurora-A, CDK1, PLK1 and GSK3-β (Cheng et al., 2008; Shao-Chih Chiu et al., 2014; Chung et al., 2016; Geraghty et al., 2021). Overexpressing Aurora A phospho mutant disrupts spindle size

while overexpressing PLK1 docking site mutant reduces KT-MT attachment stability (Chiu et al., 2014; Geraghty et al., 2021). Both lead to prolonged mitosis (Chiu et al., 2014; Geraghty et al., 2021). Moreover, the N-terminal region of Astrin interacts with NDC80 and is required for synergistic binding with the MTs (Kern, Wilson-Kubalek and Cheeseman, 2017). The Astrin 465-1193 a.a. expressing cells form unaligned chromosomes earlier than the WT in metaphase arrested cells (Geraghty et al. 2021). Moreover, these cells show reduced MT intensity in prometaphase arrested cells (Geraghty et al. 2021). However, Astrin 465-1193 a.a. was able to rescue Astrin depletion mitotic defects similarly to the WT (Kern, Wilson-Kubalek, and Cheeseman 2017). Also, a live-cell imaging study using a stable expressing cell line showed that Astrin 465-1193 a.a. expressing cells can progress through an unperturbed cell cycle (Geraghty et al. 2021), suggesting that the N-terminus of Astrin is not essential for cell survival.

This thesis shows that amino acids corresponding to the first and second exon of Astrin are conserved in mammals but not in birds, reptiles and fish (**Chapter 3**). A possible explanation is that the Astrin evolved to gain an additional function, but that function is not essential. Unlike human NDC80, the N-terminus of Yeast NDC80 is not essential, but it becomes essential when Dam1 protein is compromised (Demirel et al. 2012). Dam1 protein is part of the Dash/Dam1 complex, a ring-like structure that circles the MTs and interacts with NDC80 to form stable KT-MT attachments (Miranda et al. 2005; Westermann et al. 2005; Jenni and Harrison 2018). In humans, the Dam/Dash1 complex is replaced by the SKA complex (Van Hooff, Snel, and Kops 2017). The SKA complex does not form a complete ring but instead forms W-shaped structures (Jeyaprakash et al. 2012). This structural difference between the Dash/Dam1 complex and the SKA complex may explain why the SKA complex is insufficient for KT-MT stabilization and why the cells need the Astrin-SKAP complex. However, like the N-terminus of yeast NDC80, the N-terminus of human Astrin may only become essential when other KT-MT attachment stability proteins are compromised.

Non-essentiality of the N-terminus of Astrin would explain the homozygous Astrin p.M? and Astrin p.L7Qfs*21 variations. Future studies should look at the function of the short Astrin to confirm whether it is indeed not essential. Moreover, mRNA and protein expression studies should be carried out in humans to confirms the

size and sequence of the Astrin protein expressed in both homozygous N-terminal Astrin variants.

7.6 HUMAN ASTRIN P.Q1012*VARIANT

7.6.1 COMPROMISED KINETOCHORE LOCALIZATION

The Astrin-SKAP complex is present at the MTs throughout mitosis but only localizes at the KTs once the end-on attachments have formed (Shrestha et al. 2017; Shrestha and Draviam 2013; Kuhn and Dumont 2017). The localization of this complex at the KTs requires the C-terminus of Astrin (Dunsch et al. 2011; Kern, Wilson-Kubalek, and Cheeseman 2017). This thesis has shown that a human Astrin p.Q1012* variant fails to localize at the metaphase KTs (**Chapter 4**). The C-terminus of Astrin beyond 1011 a.a. of Astrin is conserved in mammals, birds, reptiles and fish (**Chapter 3**). Work in the lab has shown that the C-terminus of Astrin has a potential PP1 docking motif at 1123-1126 a.a. conforming to RVxF motif and converting it to AAAA (4A) compromises Astrin's localization at the KTs (Conti et al. 2019). Moreover, a C-terminal deletion mutant Δ70 lacking the potential PP1 docking motif fails to localize at the KTs (Conti et al. 2019). In this thesis, I have shown that in addition to the PP1 docking motif, the region lacking in Astrin Δ70 has two potential PP2A and one potential PP2B docking motif (**Chapter 3**). Moreover, a potential PP2A docking motif in the 112 a.a. region is additionally lost in Astrin p.Q1012* (**Chapter 3**). The Astrin p.Q1012* localization at the KTs is reduced compared to Astrin 4A but is comparative to Astrin Δ70 (**Chapter 4**). Work from the lab has shown that artificially tethering PP1γ phosphatase to the C-terminus of Astrin 4A and Δ70 rescues their KT localization defect (Conti et al. 2019). KT localization defect in Astrin p.Q1012* may also rescue similarly. In the future, this could be tested by generating a plasmid with a C-terminal GFP tag and lacking the last 182 a.a. of Astrin and co-expressing it with the mcherry-GBP- PP1γ available in the lab.

7.6.2 MICROTUBULE PULLING FORCES AND CHROMOSOMES MISALIGNMENT

Using inter-centromeric distances as a readout for MT-mediated pulling forces, I have shown that MT-mediated pulling forces are reduced in both Astrin p.Q1012* and 4A expressing cells (**Chapter 6**). The Astrin 4A data is part of the work already

published (Conti et al. 2019). Next, I normalized inter-centromeric distances to minimum inter-centromeric distances for each KT pair and tracked them over time. My data suggest that the amount of stretching is reduced in Astrin p.Q1012* but not in 4A (**Chapter 6**). A possible explanation is that the presence of endogenous Astrin in Astrin p.Q1012*cells was sufficient to maintain minimum inter-centromeric distances but not the maximum inter-centromeric distances. To investigate this, the experiment should be repeated in the absence of endogenous Astrin and Astrin p.Q1012* and 4A should be compared simultaneously. Studies have shown intra-KT and not inter-centromeric stretching is required for SAC silencing (Maresca and Salmon 2009; Uchida et al. 2009b; Wan et al. 2009). Measuring intra-KT distancing is not possible in Astrin p.Q1012* expressing cells with the current experiment settings. However, Astrin 4A's recruitment at the KTs is not as compromised as the p.Q1012* and could be used as a KT marker.

At the KTs, Astrin interacts with both the MTs and the NDC80 complex (Kern, Wilson-Kubalek, and Cheeseman 2017). Moreover, work from the lab shows that Astrin mediated PP1 delivery at the KTs is required for its own enrichment at the KTs (Conti et al. 2019). Together, this leads to the stabilization of end-on attachments. Reduced inter-centromeric distances in Astrin p.Q1012* and 4A cells suggest unstable KT-MT attachments (**Chapter 6**). Unstable KT-MT attachments are prone to break off and may explain prolonged chromosome congression time and failure to maintain chromosome congression in Astrin p.Q1012* cells (**Chapter 5**).

To track the chromosomes, I used sirDNA, a dye that can impair cell cycle progression (Sen, Saurin, and Higgins 2018). My own results indicate impaired mitotic progression observed in Astrin p.Q1012* is more marked in cells with sirDNA (**Chapter 5**). Ideally, a DNA or centromeric marker should be stably expressed to minimize the effect on the cells. I have used a stable expressing HeLa FRT/TO YFP-Astrin cell line for my mitotic expression experiments. However, my attempts to generate a double-expressing HeLa FRT/TO YFP-Astrin CENPB-dsRed (centromeric marker) failed. The cells appeared stressed and underwent massive death. Using a different marker may resolve this issue.

7.6.3 ACTIVE SPINDLE ASSEMBLY CHECKPOINT AND DELAYED ANAPHASE ONSET

KNL1, a core KT protein, directly interacts with PP1 phosphatase (Meadows et al. 2011; Rosenberg, Cross, and Funabiki 2011; Liu et al. 2010). KNL-PP1 interaction is essential for SAC silencing but not for KT-MT attachment stabilization (Shrestha et al. 2017). Aurora B kinase phosphorylates KNL1 at p.S24 and inhibits KNL1-PP1 interaction (Bajaj et al., 2018). This thesis has shown that phosphorylation at KNL1 p.S24 is high at metaphase KTs of Astrin p.Q1012*, 4A and Δ70 expressing cells (**Chapter 6**), suggesting an active SAC. Work from the lab has shown that Astrin 4A and Δ70 expressing cells retain Mad2 checkpoint protein at metaphase KTs and have delayed anaphase onset (Conti et al. 2019). This thesis shows that Astrin p.Q1012*, 4A and Δ70 expressing cells retain ROD checkpoint protein at metaphase KTs and have delayed anaphase onset (**Chapter 5, 6**). Collectively, the studies show that the C-terminus of Astrin is required for SAC silencing.

7.7 ASTRIN RECRUITS PHOSPHATASES TO THE KINETOCHORES

In this thesis, I reproduced previous work in the lab and showed that endogenous Astrin is pulled down by exogenously expressed GST-PP1γ. This is part of the work already published (Conti et al., 2019). Preliminary findings from this thesis suggest that Astrin directly interacts with PP1γ and this interaction is reduced but not abolished in Astrin 4A (**Chapter 6**). The finding could not be reproduced when frozen-thawed Astrin protein fragments were used. In the future, Astrin-PP1γ direct interaction should be confirmed using freshly purified Astrin fragments.

Astrin p.Q1012* and Δ70 have similar phosphorylation levels at KNL1 p.S24 but different ROD checkpoint protein levels (**Chapter 6**). High ROD levels in Astrin p.Q1012* suggest that the 1012-1122 a.a. region of Astrin has an additional role. Work from the lab has shown that tethering PP1γ to short Astrin fragments 694-1122 and 851-1122 a.a. but not 694-850 partially rescues their KT localization defects (Conti et al., 2020). Astrin is pulled down with PP2A-B56 phosphatase (Hertz et al., 2016), suggesting that they both interact in human cells. This thesis identified a potential PP2A phosphatase docking motif in the Astrin 1012-1122 a.a. region (**Chapter 3**). Astrin may

be recruiting PP2A phosphatase through this region. Direct interaction can be investigated in the future using purified Astrin fragments standardized in this thesis.

ROD is part of the RZZ complex, which expands the fibrous corona (outermost KT) in prometaphase (Gama et al., 2017; Pereira et al., 2018; Sacristan et al., 2018). The expanded fibrous corona shrinks once end-on attachments are formed (Magidson et al., 2015; Sacristan et al., 2018). Astrin-PP2A at the KTs may be required for shrinking fibrous corona. This should be investigated in the future by mutating the potential PP2A docking motif identified in this thesis (**Chapter 3**).

7.7.1 CHROMOSOME SEGREGATION DEFECTS AND DNA DAMAGE

This thesis shows that Astrin p.Q1012* expressing cells have a delayed anaphase onset and a high incidence of lagging chromosomes in anaphase (**Chapter 5**). Both prolonged mitosis and lagging chromosomes can lead to DNA damage and aneuploidy (Stephens et al. 2011; Hatch et al. 2013; Lanni and Jacks 1998; Dalton et al. 2007; Quignon et al. 2007; Hoffelder et al. 2004; Janssen et al. 2011; Santaguida et al. 2017; Soto et al. 2017; Crasta et al. 2012b; Zhang et al. 2015; Ly et al. 2017). This thesis shows a high incidence of DNA damage in Astrin p.Q1012* expressing cells (**Chapter 5**). However, these experiments were conducted in HeLa and HeLa FRT/TO cell lines which already have high DNA damage. A near diploid cell line with functional p53 status can be used for better quantification of DNA damage in the future. Moreover, karyotyping should be done to see whether Astrin p.Q1012* expression leads to aneuploidy.

7.7.2 WHAT DOES THIS MEAN FOR THE HUMANS CARRYING THE ASTRIN P.Q1012* VARIATION?

A compound heterozygous Astrin variant has been shown to cause microcephaly (Boonsawat et al. 2019). mRNA studies on patient-derived fibroblasts show a deletion of exon 11, resulting in a predicted p.G1064E*3 (Boonsawat et al. 2019). However, the variant transcript is eliminated through nonsense-mediated decay (NMD) (Boonsawat et al. 2019). Moreover, protein expression studies show the variant is not expressed (Boonsawat et al. 2019). As the Astrin p.Q1012* heterozygotes are reported to be healthy, it is likely that Astrin p.Q1012* transcript also undergoes NMD, and the variant protein is not expressed. However, p.G1064E*3 transcript expression

reduces normal Astrin protein levels (Boonsawat et al. 2019). The patient has microcephaly and reduced stature, suggesting that reduced Astrin levels are insufficient for growth and differentiation (Boonsawat et al. 2019). Hence, mRNA and protein expression studies are needed in individuals with Astrin p.Q1012* variation to assess the size and sequence of transcript/s and the size and level of expressed protein/s. These studies were part of the plan for this thesis, and ethical approval has been obtained. However, due to the COVID-19 pandemic, the studies have been paused.

At the time of the study, the Astrin microcephaly patient was only 2.3 years old and had a mild speech delay and short stature (Boonsawat et al. 2019). The study was published only about two years ago, and whether the child has or eventually will achieve normal milestones is not known. A child carrying a compound heterozygous KNL1 variation initially displayed a developmental delay but achieved normal milestones by 17 months of age (Zarate et al. 2016). The participants in the GH study are all adults who self-report themselves as healthy. An individual with mild speech delay as a child or short stature is unlikely to be picked in the initial screening.

So far, there are only two Astrin p.Q1012* cases in GH, but there are over 100 p.L7Qfs*21cases. My results suggest that humans may tolerate a lack of N-terminus of Astrin. However, inheriting both variations as a compound heterozygous variant may not be tolerated. Moreover, there are several hundred cases of missense Astrin variations in GH. Most are likely to be tolerated, but a few may not, especially in combination with other variants. Hence, humans with Astrin p.Q1012* variation are at risk of frequent pregnancy loss and having children with congenital disabilities and may need genetic counseling.

7.8 GRAPHIC SUMMARY

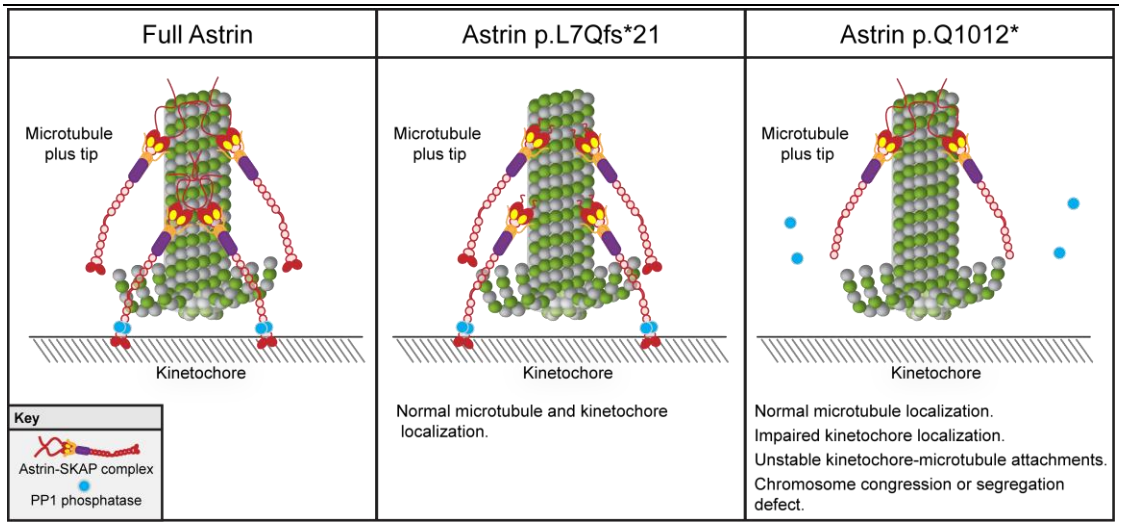

Fig 7.1 Human Astrin is an essential protein that starts to decorate the microtubules (MTs) at the start of mitosis but only arrives at the kinetochores (KTs) once end-on attachments are formed. The arrival of Astrin at the KTs is through its C-terminus. Moreover, the C-terminus of Astrin has a docking site for PP1 phosphatase, and Astrin-mediated PP1 targeting to the KTs is important for KT-MT attachment stability. Lack of the first 151 a.a. in the N-terminus of Astrin does not impair localization of Astrin at both the spindle MTs and KTs despite lacking Aurora A phosphorylation, CDK1 phosphorylation and PLK1 binding sites. Hence, humans carrying homozygous Astrin p.L7Qfs*21 variation may use the transcriptional site at 152 a.a. of Astrin to express a shorter Astrin protein which may localize and function normally. On the other hand, the human Astrin p.Q1012* variant fails to localize at the KTs and leads to unstable KT-MT attachments, chromosome congression and segregation defects even in the presence of endogenous Astrin. In a heterozygous state, cells may not express or destroy the variant copy and the normal copy of Astrin may be sufficient for fulfilling the function of Astrin in the cells. However, homozygous Astrin p.Q1012* variation may not be tolerated and individuals heterozygous for this variant are at risk of fertility issues and having children with developmental disorders.

APPENDIX

APPENDIX

APPENDIX TO CHAPTER 6: RESULTS-IV-C-TERMINUS OF ASTRIN IS IMPORTANT FOR SPINDLE CHECKPOINT SIGNALLING

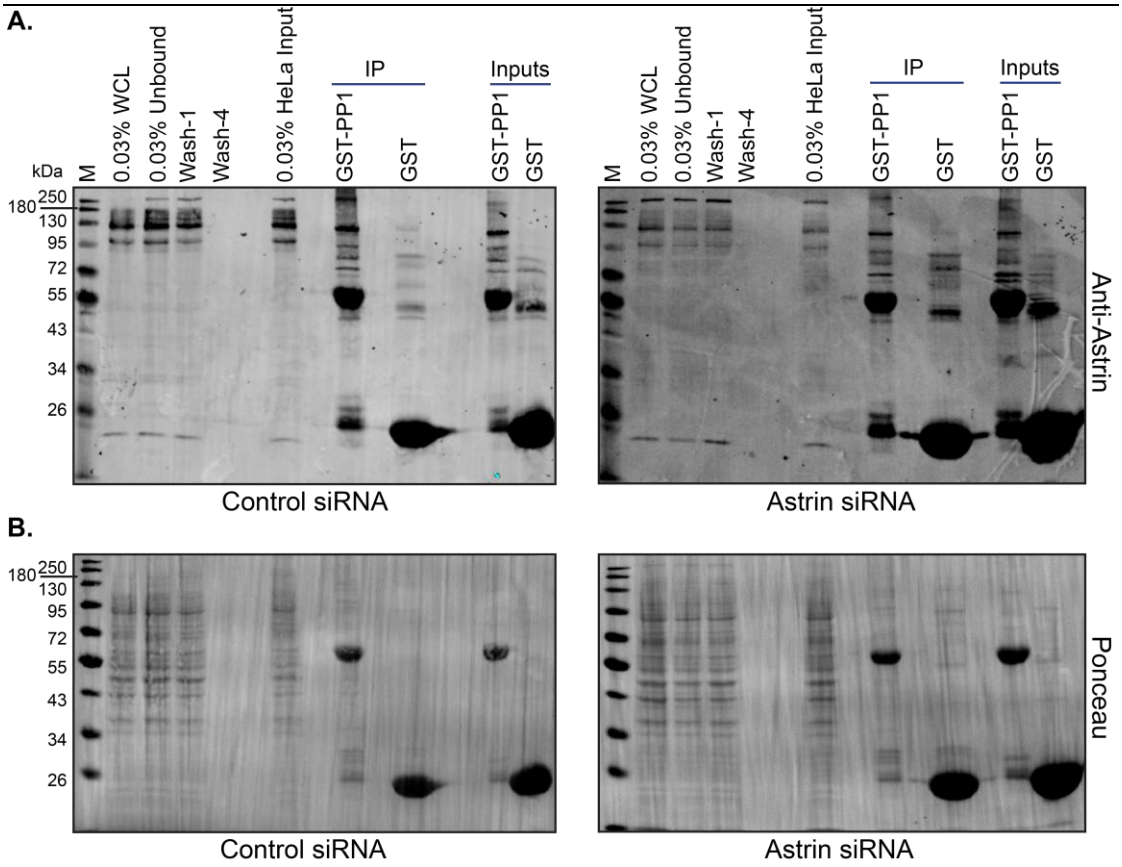

Fig 6.7 - Supplementary Fig 1. A. Immunoblot of pulldown assay shows the interaction of GST-PP1γ, but not GST, with Astrin in lysates of mitotically synchronized HeLa cells. Cells were treated with Astrin or Control siRNA, as indicated, and exposed to STLC for 24 hrs prior to lysate generation. Immunoblot was probed with an antibody against Astrin. WCL = whole cell lysate. **B**. Ponceau stain of the membranes shown in A before blocking in the blocking buffer.

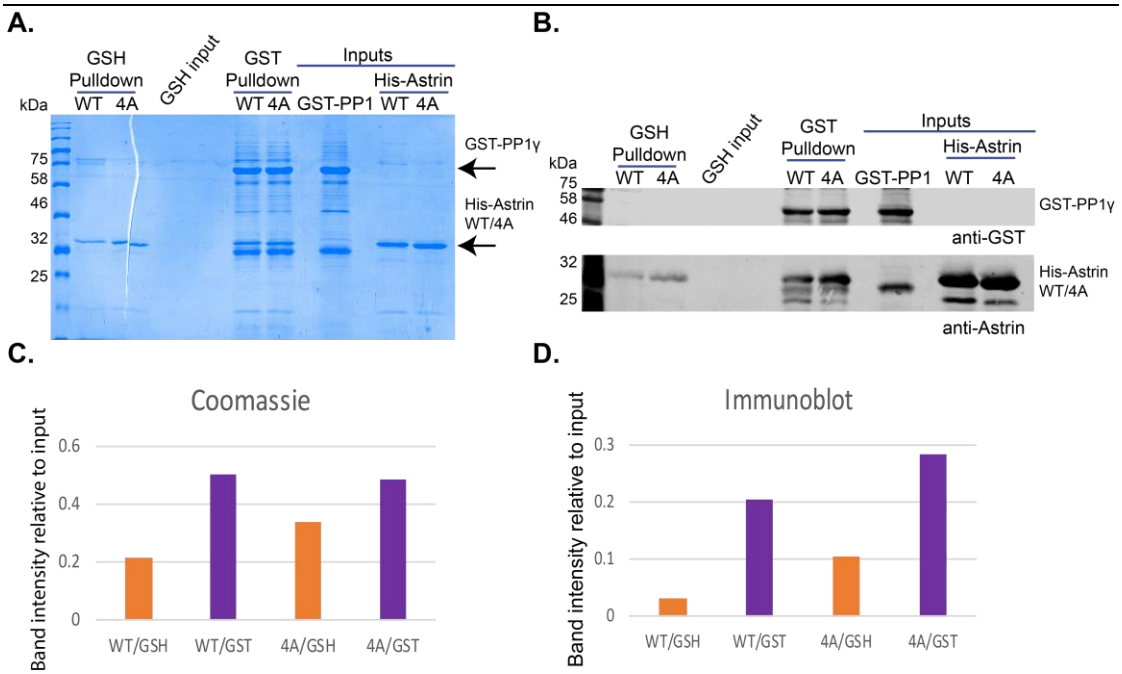

Fig 6.8 – Supplementary Fig 1. Direct interaction study of Astrin fragments and GST-PP1 gamma (third repeat). A. Coomassie-stained gel of co-immunoprecipitation assay shows Astrin WT and 4A both interacting with GST-PP1γ and GST control. Frozen-thawed purified Astrin fragments were used. **B.** Immunoblot of the co-immunoprecipitation assay as in C was probed for GST (top) and Astrin (bottom). Both Astrin fragments interact with GST-PP1γ and GST control. **C-D.** Graphs of the ratio of Astrin intensities in pulldown lanes relative to input lysate lanes in A-B.

BIBLOGRAPHY

Abdel-Fatah, Tarek M A, Devika Agarwal, Dong Xu Liu, Roslin Russell, Oscar M. Rueda, Karen Liu, Bing Xu, et al. 2016. "SPAG5 as a Prognostic Biomarker and Chemotherapy Sensitivity Predictor in Breast Cancer: A Retrospective, Integrated Genomic, Transcriptomic, and Protein Analysis." *The Lancet Oncology* 17 (7): 1004–18. https://doi.org/10.1016/S1470-2045(16)00174-1.

Abramowicz, Anna, and Monika Gos. 2019. "Correction to: Splicing Mutations in Human Genetic Disorders: Examples, Detection, and Confirmation." *Journal of Applied Genetics 2019 60:2* 60 (2): 231–231. https://doi.org/10.1007/S13353-019-00493-Z.

Acevedo, Julieta M, Bernhard Hoermann, Tilo Schlimbach, and Aurelio A Teleman. 2018. "Changes in Global Translation Elongation or Initiation Rates Shape the Proteome via the Kozak Sequence." *Scientific Reports* 8 (1): 4018. https://doi.org/10.1038/s41598-018-22330-9.

Adams, Richard R., Helder Maiato, William C. Earnshaw, and Mar Carmena. 2001. "Essential Roles of Drosophila Inner Centromere Protein (INCENP) and Aurora B in Histone H3 Phosphorylation, Metaphase Chromosome Alignment, Kinetochore Disjunction, and Chromosome Segregation." *Journal of Cell Biology* 153 (4): 865–79. https://doi.org/10.1083/jcb.153.4.865.

Akutsu, Silvia Natsuko, Kazumasa Fujita, Keita Tomioka, Tatsuo Miyamoto, and Shinya Matsuura. 2020. "Applications of Genome Editing Technology in Research on Chromosome Aneuploidy Disorders." *Cells*. NLM (Medline). https://doi.org/10.3390/cells9010239.

Ansar, Muhammad, Farid Ullah, Sohail A. Paracha, Darius J. Adams, Abbe Lai, Lynn Pais, Justyna Iwaszkiewicz, et al. 2019. "Bi-Allelic Variants in DYNC1I2 Cause Syndromic Microcephaly with Intellectual Disability, Cerebral Malformations, and Dysmorphic Facial Features." *American Journal of Human Genetics* 104 (6): 1073–87. https://doi.org/10.1016/j.ajhg.2019.04.002.

Bajaj, Rakhi, Mathieu Bollen, Wolfgang Peti, and Rebecca Page. 2018. "KNL1 Binding to PP1 and Microtubules Is Mutually Exclusive." *Structure* 26 (10): 1327-1336.e4. https://doi.org/10.1016/j.str.2018.06.013.

Barisic, Marin, Paulo Aguiar, Stephan Geley, and Helder Maiato. 2014. "Kinetochore Motors Drive Congression of Peripheral Polar Chromosomes by Overcoming Random Arm-

Ejection Forces." *Nature Cell Biology* 16 (12): 1249–56. https://doi.org/10.1038/ncb3060.

Barisic, Marin, Ricardo Silva E Sousa, Suvranta K. Tripathy, Maria M. Magiera, Anatoly V. Zaytsev, Ana L. Pereira, Carsten Janke, Ekaterina L. Grishchuk, and Helder Maiato. 2015. "Microtubule Detyrosination Guides Chromosomes during Mitosis." *Science* 348 (6236): 799–803. https://doi.org/10.1126/science.aaa5175.

Barisic, Marin, Bénédicte Sohm, Petra Mikolcevic, Cornelia Wandke, Veronika Rauch, Thomas Ringer, Michael Hess, Günther Bonn, and Stephan Geley. 2010. "Spindly/CCDC99 Is Required for Efficient Chromosome Congression and Mitotic Checkpoint Regulation." *Molecular Biology of the Cell* 21 (12): 1968–81. https://doi.org/10.1091/mbc.E09-04-0356.

Bateman, Alex, Maria Jesus Martin, Sandra Orchard, Michele Magrane, Rahat Agivetova, Shadab Ahmad, Emanuele Alpi, et al. 2021. "UniProt: The Universal Protein Knowledgebase in 2021." *Nucleic Acids Research* 49 (D1): D480–89. https://doi.org/10.1093/nar/gkaa1100.

Bielek, E. 1978. "Structure and Ribonucleoprotein Staining of Kinetochores of Colchicine-Treated HeLa Cells." *Cytobiologie* 16 (3): 480–84. https://europepmc.org/article/med/417951.

Black, Ben E., Melissa A. Brock, Sabrina Bédard, Virgil L. Woods, and Don W. Cleveland. 2007. "An Epigenetic Mark Generated by the Incorporation of CENP-A into Centromeric Nucleosomes." *Proceedings of the National Academy of Sciences of the United States of America* 104 (12): 5008–13. https://doi.org/10.1073/pnas.0700390104.

Boonsawat, Paranchai, Pascal Joset, Katharina Steindl, Beatrice Oneda, Laura Gogoll, Silvia Azzarello-Burri, Frenny Sheth, et al. 2019. "Elucidation of the Phenotypic Spectrum and Genetic Landscape in Primary and Secondary Microcephaly." *Genetics in Medicine*, March. https://doi.org/10.1038/s41436-019-0464-7.

BOSCH, J. VAN DEN. 1958. "MICROCEPHALY IN THE NETHERLANDS: A CLINICAL AND GENETICAL STUDY." *Annals of Human Genetics* 23 (2): 91–116. https://doi.org/10.1111/j.1469-1809.1958.tb01455.x.

Brabander, Marc De, Gustaaf Geuens, Jan De Mey, and Marcel Joniau. 1981. "Nucleated Assembly of Mitotic Microtubules in Living PTK2 Cells after Release from Nocodazole Treatment." *Cell Motility* 1 (4): 469–83. https://doi.org/10.1002/cm.970010407.

Bravo, R., and H. Macdonald-Bravo. 1985. "Changes in the Nuclear Distribution of Cyclin

(PCNA) but Not Its Synthesis Depend on DNA Replication." *The EMBO Journal* 4 (3): 655–61. https://doi.org/10.1002/j.1460-2075.1985.tb03679.x.

Buffin, Eulalie, Christophe Lefebvre, Junyong Huang, Mary Elisabeth Gagou, and Roger E. Karess. 2005. "Recruitment of Mad2 to the Kinetochore Requires the Rod/Zw10 Complex." *Current Biology* 15 (9): 856–61. https://doi.org/10.1016/J.CUB.2005.03.052.

Caldas, Gina V, Tina R Lynch, Ryan Anderson, Sana Afreen, Dileep Varma, and Jennifer G DeLuca. 2015. "The RZZ Complex Requires the N-Terminus of KNL1 to Mediate Optimal Mad1 Kinetochore Localization in Human Cells." *Open Biology* 5 (11): 150160. https://doi.org/10.1098/rsob.150160.

Callier, P., L. Faivre, V. Cusin, N. Marle, C. Thauvin-Robinet, D. Sandre, T. Rousseau, et al. 2005. "Microcephaly Is Not Mandatory for the Diagnosis of Mosaic Variegated Aneuploidy Syndrome." *American Journal of Medical Genetics Part A* 137A (2): 204–7. https://doi.org/10.1002/ajmg.a.30783.

"Cancer Incidence Statistics | Cancer Research UK." n.d. Accessed March 9, 2017. http://www.cancerresearchuk.org/health-professional/cancer-statistics/incidence#heading-Four.

Cane, Stuart, Anna A. Ye, Sasha J. Luks-Morgan, and Thomas J. Maresca. 2013. "Elevated Polar Ejection Forces Stabilize Kinetochore-Microtubule Attachments." *Journal of Cell Biology* 200 (2): 203–18. https://doi.org/10.1083/jcb.201211119.

Canu, Valeria, Sara Donzelli, Andrea Sacconi, Federica Lo Sardo, Claudio Pulito, Noa Bossel, Anna Di Benedetto, et al. 2020. "Aberrant Transcriptional and Post-Transcriptional Regulation of SPAG5, a YAP-TAZ-TEAD Downstream Effector, Fuels Breast Cancer Cell Proliferation." *Cell Death and Differentiation*, November, 1–19. https://doi.org/10.1038/s41418-020-00677-9.

"CBioPortal for Cancer Genomics::MutationMapper." n.d. Accessed January 29, 2020. https://www.cbioportal.org/mutation_mapper.

Celis, J. E., and A. Celis. 1985. "Cell Cycle-Dependent Variations in the Distribution of the Nuclear Protein Cyclin Proliferating Cell Nuclear Antigen in Cultured Cells: Subdivision of S Phase." *Proceedings of the National Academy of Sciences of the United States of America* 82 (10): 3262–66. https://doi.org/10.1073/pnas.82.10.3262.

Chakraborty, Manas, Ekaterina V. Tarasovetc, Anatoly V. Zaytsev, Maxim Godzi, Ana C. Figueiredo, Fazly I. Ataullakhanov, and Ekaterina L. Grishchuk. 2019. "Microtubule End Conversion Mediated by Motors and Diffusing Proteins with No Intrinsic

Microtubule End-Binding Activity." *Nature Communications* 10 (1). https://doi.org/10.1038/s41467-019-09411-7.

Chan, K. S., C. G. Koh, and H. Y. Li. 2012. "Mitosis-Targeted Anti-Cancer Therapies: Where They Stand." *Cell Death and Disease*. Nature Publishing Group. https://doi.org/10.1038/cddis.2012.148.

Chan, Ying Wai, A. Arockia Jeyaprakash, Erich A. Nigg, and Anna Santamaria. 2012. "Aurora B Controls Kinetochore–Microtubule Attachments by Inhibiting Ska Complex–KMN Network Interaction." *The Journal of Cell Biology* 196 (5): 563–71. https://doi.org/10.1083/jcb.201109001.

Cheerambathur, Dhanya K., Reto Gassmann, Brian Cook, Karen Oegema, and Arshad Desai. 2013. "Crosstalk between Microtubule Attachment Complexes Ensures Accurate Chromosome Segregation." *Science* 342 (6163): 1239–42. https://doi.org/10.1126/science.1246232.

Cheerambathur, Dhanya K., Bram Prevo, Neil Hattersley, Lindsay Lewellyn, Kevin D. Corbett, Karen Oegema, and Arshad Desai. 2017. "Dephosphorylation of the Ndc80 Tail Stabilizes Kinetochore-Microtubule Attachments via the Ska Complex." *Developmental Cell* 41 (4): 424-437.e4. https://doi.org/10.1016/j.devcel.2017.04.013.

Cheeseman, Iain M., Joshua S. Chappie, Elizabeth M. Wilson-Kubalek, and Arshad Desai. 2006. "The Conserved KMN Network Constitutes the Core Microtubule-Binding Site of the Kinetochore." *Cell* 127 (5): 983–97. https://doi.org/10.1016/j.cell.2006.09.039.

Cheeseman, Iain M., and Arshad Desai. 2008. "Molecular Architecture of the Kinetochore-Microtubule Interface." *Nature Reviews Molecular Cell Biology*. Nature Publishing Group. https://doi.org/10.1038/nrm2310.

Cheeseman, Iain M., Sherry Niessen, Scott Anderson, Francie Hyndman, John R. Yates, Karen Oegema, and Arshad Desai. 2004. "A Conserved Protein Network Controls Assembly of the Outer Kinetochore and Its Ability to Sustain Tension." *Genes and Development* 18 (18): 2255–68. https://doi.org/10.1101/gad.1234104.

Cheeseman, Iain M, Tetsuya Hori, Tatsuo Fukagawa, and Arshad Desai. 2008. "KNL1 and the CENP-H/I/K Complex Coordinately Direct Kinetochore Assembly in Vertebrates." *Molecular Biology of the Cell* 19 (2): 587–94. https://doi.org/10.1091/mbc.E07-10-1051.

Cheng, Tai Shan, Yun Ling Hsiao, Ching Chih Lin, Ching Mei Hsu, Mau Sun Chang, Chu I. Lee, Ricky Chang Tze Yu, Chi Ying F Huang, Shen Long Howng, and Yi Ren Hong.

2007. “HNinein Is Required for Targeting Spindle-Associated Protein Astrin to the Centrosome during the S and G2 Phases.” *Experimental Cell Research* 313 (8): 1710–21. https://doi.org/10.1016/j.yexcr.2007.02.023.

Cheng, Tai Shan, Yun Ling Hsiao, Ching Chih Lin, Chang Tze Ricky Yu, Ching Mei Hsu, Mau Sun Chang, Chu I. Lee, Chi Ying F Huang, Shen Long Howng, and Yi Ren Hong. 2008. “Glycogen Synthase Kinase 3β Interacts with and Phosphorylates the Spindle-Associated Protein Astrin.” *Journal of Biological Chemistry* 283 (4): 2454–64. https://doi.org/10.1074/jbc.M706794200.

Chiu, S-C, J-M M Chen, T-Y W Wei, T-S Cheng, Y-H C Wang, C-F Ku, C-H Lian, C-C J Liu, Y-C Kuo, and C-T R Yu. 2014. “The Mitosis-Regulating and Protein-Protein Interaction Activities of Astrin Are Controlled by Aurora-A-Induced Phosphorylation.” *American Journal of Physiology: Cell Physiology* 307 (5): C466-478. https://doi.org/10.1152/ajpcell.00164.2014.

Chiu, Shao-Chih, Jo-Mei Maureen Chen, Tong-You Wade Wei, Tai-Shan Cheng, Ya-Hui Candice Wang, Chia-Feng Ku, Chiao-Hsuan Lian, Chun-Chih Jared Liu, Yi-Chun Kuo, and Chang-Tze Ricky Yu. 2014. “The Mitosis-Regulating and Protein-Protein Interaction Activities of Astrin Are Controlled by Aurora-A-Induced Phosphorylation.” *American Journal of Physiology-Cell Physiology* 307 (5): C466–78. https://doi.org/10.1152/ajpcell.00164.2014.

Cho, Chi Hyun, Min-Jeong Oh, Chae Seung Lim, Chang Kyu Lee, Yunjung Cho, and Soo-Young Yoon. 2015. “A Case Report of a Fetus with Mosaic Autosomal Variegated Aneuploidies and Literature Review.” *Annals of Clinical and Laboratory Science* 45 (1): 106–9. http://www.ncbi.nlm.nih.gov/pubmed/25696020.

Chu, Xiaogang, Xuanyu Chen, Qingwen Wan, Zhen Zheng, and Quansheng Du. 2016. “Nuclear Mitotic Apparatus (Numa) Interacts with and Regulates Astrin at the Mitotic Spindle.” *Journal of Biological Chemistry* 291 (38): 20055–67. https://doi.org/10.1074/jbc.M116.724831.

Chung, Hee Jin, Ji Eun Park, Nam Soo Lee, Hongtae Kim, and Chang-Young Jang. 2016. “Phosphorylation of Astrin Regulates Its Kinetochore Function.” *The Journal of Biological Chemistry* 291 (34): 17579–92. https://doi.org/10.1074/jbc.M115.712745.

Cimini, Daniela, Lisa A. Cameron, and E. D. Salmon. 2004. “Anaphase Spindle Mechanics Prevent Mis-Segregation of Merotelically Oriented Chromosomes.” *Current Biology* 14 (23): 2149–55. https://doi.org/10.1016/j.cub.2004.11.029.

Cimini, Daniela, Bonnie Howell, Paul Maddox, Alexey Khodjakov, Francesca Degrassi, and E. D. Salmon. 2001. “Merotelic Kinetochore Orientation Is a Major Mechanism of Aneuploidy in Mitotic Mammalian Tissue Cells.” *Journal of Cell Biology* 152 (3): 517–27. https://doi.org/10.1083/jcb.153.3.517.

Cimini, Daniela, Xiaohu Wan, Christophe B. Hirel, and E.D. Salmon. 2006. “Aurora Kinase Promotes Turnover of Kinetochore Microtubules to Reduce Chromosome Segregation Errors.” *Current Biology* 16 (17): 1711–18. https://doi.org/10.1016/j.cub.2006.07.022.

Cindric Vranesic, Anita, Juliane Reiche, Christian Hoischen, Andreas Wohlmann, Jens Bratsch, Karlheinz Friedrich, Berkay Günes, et al. 2016. “Characterization of SKAP/Kinastrin Isoforms: The N-Terminus Defines Tissue Specificity and Pontin Binding.” *Human Molecular Genetics* May 11: ddw140. https://doi.org/10.1093/hmg/ddw140.

Cliby, William A., Kriste A. Lewis, Kia K. Lilly, and Scott H. Kaufmann. 2002. “S Phase and G2 Arrests Induced by Topoisomerase I Poisons Are Dependent on ATR Kinase Function.” *Journal of Biological Chemistry* 277 (2): 1599–1606. https://doi.org/10.1074/jbc.M106287200.

Clute, Paul, and Jonathon Pines. 1999. “Temporal and Spatial Control of Cyclin B1 Destruction in Metaphase.” *Nature Cell Biology* 1 (2): 82–87. https://doi.org/10.1038/10049.

Collins, Ryan L., Harrison Brand, Claire E. Redin, Carrie Hanscom, Caroline Antolik, Matthew R. Stone, Joseph T. Glessner, et al. 2017. “Defining the Diverse Spectrum of Inversions, Complex Structural Variation, and Chromothripsis in the Morbid Human Genome.” *Genome Biology* 18 (1): 1–21. https://doi.org/10.1186/s13059-017-1158-6.

Conti, D., P. Gul, A. Islam, J.M. Martín-Durán, R.W. Pickersgill, and V.M. Draviam. 2019. “Kinetochores Attached to Microtubule-Ends Are Stabilised by Astrin Bound Pp1 to Ensure Proper Chromosome Segregation.” *ELife* 8. https://doi.org/10.7554/eLife.49325.

Conti, Duccio, Xinhong Song, Roshan L. Shrestha, Dominique Braun, and Viji M. Draviam. 2020. “Cells Protect Chromosome-Microtubule Attachments, Independent of Biorientation, Using an Astrin-PP1 and CyclinB-CDK1 Feedback Loop.” *BioRxiv*. bioRxiv. https://doi.org/10.1101/2020.12.24.424312.

“COSMIC | Catalogue of Somatic Mutations in Cancer.” n.d. Accessed January 29, 2020. https://cancer.sanger.ac.uk/cosmic.

Cox, James, Andrew P. Jackson, Jacquelyn Bond, and Christopher G. Woods. 2006. “What

Primary Microcephaly Can Tell Us about Brain Growth." *Trends in Molecular Medicine*. Trends Mol Med. https://doi.org/10.1016/j.molmed.2006.06.006.

Crasta, Karen, Neil J. Ganem, Regina Dagher, Alexandra B. Lantermann, Elena V. Ivanova, Yunfeng Pan, Luigi Nezi, Alexei Protopopov, Dipanjan Chowdhury, and David Pellman. 2012a. "DNA Breaks and Chromosome Pulverization from Errors in Mitosis." *Nature*. Nature Publishing Group. https://doi.org/10.1038/nature10802.

Dalton, W. Brian, Mandayam O. Nandan, Ryan T. Moore, and Vincent W. Yang. 2007. "Human Cancer Cells Commonly Acquire DNA Damage during Mitotic Arrest." *Cancer Research* 67 (24): 11487–92. https://doi.org/10.1158/0008-5472.CAN-07-5162.

Degrassi, Francesca, Michela Damizia, and Patrizia Lavia. 2019. "The Mitotic Apparatus and Kinetochores in Microcephaly and Neurodevelopmental Diseases." *Cells* 9 (1): 49. https://doi.org/10.3390/cells9010049.

DeLuca, Jennifer G., Walter E. Gall, Claudio Ciferri, Daniela Cimini, Andrea Musacchio, and E.D. Salmon. 2006. "Kinetochore Microtubule Dynamics and Attachment Stability Are Regulated by Hec1." *Cell* 127 (5): 969–82. https://doi.org/10.1016/j.cell.2006.09.047.

DeLuca, Keith F., Susanne M.A. Lens, and Jennifer G. DeLuca. 2011. "Temporal Changes in Hec1 Phosphorylation Control Kinetochore - Microtubule Attachment Stability during Mitosis." *Journal of Cell Science* 124 (4): 622–34. https://doi.org/10.1242/jcs.072629.

Demirel, Pinar B., Brice E. Keyes, Mandovi Chaterjee, Courtney E. Remington, and Daniel J. Burke. 2012. "A Redundant Function for the N-Terminal Tail of Ndc80 in Kinetochore-Microtubule Interaction in Saccharomyces Cerevisiae." *Genetics* 192 (2): 753–56. https://doi.org/10.1534/genetics.112.143818.

Dewar, Hiiary Hilary, Kozo Tanaka, Kim Nasmyth, and Tomoyuki U. Tanaka. 2004. "Tension between Two Kinetochores Suffices for Their Bi-Orientation on the Mitotic Spindle." *Nature* 428 (6978): 93–97. https://doi.org/10.1038/nature02328.

Dick, Amalie E., and Daniel W. Gerlich. 2013. "Kinetic Framework of Spindle Assembly Checkpoint Signalling." *Nature Cell Biology* 15 (11): 1370–77. https://doi.org/10.1038/ncb2842.

Dinkel, Holger, Kim Van Roey, Sushama Michael, Manjeet Kumar, Bora Uyar, Brigitte Altenberg, Vladislava Milchevskaya, et al. 2016. "ELM 2016—Data Update and New Functionality of the Eukaryotic Linear Motif Resource." *Nucleic Acids Research* 44 (D1): D294–300. https://doi.org/10.1093/nar/gkv1291.

Dominguez-Brauer, Carmen, Kelsie L. Thu, Jacqueline M. Mason, Heiko Blaser, Mark R.

Bray, and Tak W. Mak. 2015. “Targeting Mitosis in Cancer: Emerging Strategies.” *Molecular Cell*. Cell Press. https://doi.org/10.1016/j.molcel.2015.11.006.

Dou, Zhen, Xing Liu, Wenwen Wang, Tongge Zhu, Xinghui Wang, Leilei Xu, Ariane Abrieu, Chuanhai Fu, Donald L. Hill, and Xuebiao Yao. 2015. “Dynamic Localization of Mps1 Kinase to Kinetochores Is Essential for Accurate Spindle Microtubule Attachment.” *Proceedings of the National Academy of Sciences of the United States of America* 112 (33): E4546–55. https://doi.org/10.1073/pnas.1508791112.

Duerinckx, Sarah, Valérie Jacquemin, Séverine Drunat, Yoann Vial, Sandrine Passemard, Camille Perazzolo, Annick Massart, et al. 2020. “Digenic Inheritance of Human Primary Microcephaly Delineates Centrosomal and Non-Centrosomal Pathways.” *Human Mutation* 41 (2): 512–24. https://doi.org/10.1002/humu.23948.

Dunsch, Anja K., Emily Linnane, Francis A. Barr, and Ulrike Gruneberg. 2011. “The Astrin-Kinastrin/SKAP Complex Localizes to Microtubule plus Ends and Facilitates Chromosome Alignment.” *Journal of Cell Biology* 192 (6): 959–68. https://doi.org/10.1083/jcb.201008023.

Emil Peter Thrane Hertz, Authors, Thomas Kruse, Norman E Davey, Guillermo Montoya, Jesper V Olsen, Jakob Nilsson, Emil Peter Thrane Hertz, Blanca Ló pez-Mé ndez, and Jó Otti Sigurðsson. 2016. “A Conserved Motif Provides Binding Specificity to the PP2A-B56 Phosphatase Molecular Cell A Conserved Motif Provides Binding Specificity to the PP2A-B56 Phosphatase.” *Molecular Cell* 63 (18): 686–95. https://doi.org/10.1016/j.molcel.2016.06.024.

Espert, Antonio, Pelin Uluocak, Ricardo Nunes Bastos, Davinderpreet Mangat, Philipp Graab, and Ulrike Gruneberg. 2014. “PP2A-B56 Opposes Mps1 Phosphorylation of Knl1 and Thereby Promotes Spindle Assembly Checkpoint Silencing.” *Journal of Cell Biology* 206 (7): 833–42. https://doi.org/10.1083/jcb.201406109.

Etemad, Banafsheh, Timo E.F. Kuijt, and Geert J.P.L. Kops. 2015. “Kinetochore-Microtubule Attachment Is Sufficient to Satisfy the Human Spindle Assembly Checkpoint.” *Nature Communications* 6 (December). https://doi.org/10.1038/ncomms9987.

Faesen, Alex C., Maria Thanasoula, Stefano Maffini, Claudia Breit, Franziska Müller, Suzan Van Gerwen, Tanja Bange, and Andrea Musacchio. 2017. “Basis of Catalytic Assembly of the Mitotic Checkpoint Complex.” *Nature* 542 (7642): 498–502. https://doi.org/10.1038/nature21384.

Fernández, Luis C., Miguel Torres, and Francisco X. Real. 2016. “Somatic Mosaicism: On

the Road to Cancer." *Nature Reviews Cancer*. Nature Publishing Group. https://doi.org/10.1038/nrc.2015.1.

Finer, Sarah, Hilary C Martin, Ahsan Khan, Karen A Hunt, Beverley MacLaughlin, Zaheer Ahmed, Richard Ashcroft, et al. 2020. "Cohort Profile: East London Genes & Health (ELGH), a Community-Based Population Genomics and Health Study in British Bangladeshi and British Pakistani People." *International Journal of Epidemiology* 49 (1): 20-21i. https://doi.org/10.1093/ije/dyz174.

Finer, Sarah, Hilary Martin, Karen A Hunt, Beverley MacLaughlin, Richard Ashcroft, Ahsan Khan, Mark I McCarthy, et al. 2019. "Cohort Profile: East London Genes & Health (ELGH), a Community Based Population Genomics and Health Study of British-Bangladeshi and British-Pakistani People." *BioRxiv*, February, 426163. https://doi.org/10.1101/426163.

Flejter, W L, B Issa, B A Sullivan, J C Carey, and A R Brothman. 1998. "Variegated Aneuploidy in Two Siblings: Phenotype, Genotype, CENP-E Analysis, and Literature Review." *American Journal of Medical Genetics* 75 (1): 45–51. http://www.ncbi.nlm.nih.gov/pubmed/9450856.

Friese, Alexandra, Alex C Faesen, Pim J Huis In 't Veld, Josef Fischböck, Daniel Prumbaum, Arsen Petrovic, Stefan Raunser, Franz Herzog, and Andrea Musacchio. 2016. "Molecular Requirements for the Inter-Subunit Interaction and Kinetochore Recruitment of SKAP and Astrin." *Nature Communications* 7: 11407. https://doi.org/10.1038/ncomms11407.

Gama, José B., Cláudia Pereira, Patrícia A. Simões, Ricardo Celestino, Rita M. Reis, Daniel J. Barbosa, Helena R. Pires, et al. 2017. "Molecular Mechanism of Dynein Recruitment to Kinetochores by the Rod-Zw10-Zwilch Complex and Spindly." *Journal of Cell Biology* 216 (4): 943–60. https://doi.org/10.1083/jcb.201610108.

Ganem, Neil J., Susana A. Godinho, and David Pellman. 2009. "A Mechanism Linking Extra Centrosomes to Chromosomal Instability." *Nature* 460 (7252): 278–82. https://doi.org/10.1038/nature08136.

Ganem, Neil J, and David Pellman. 2012. "Linking Abnormal Mitosis to the Acquisition of DNA Damage." *The Journal of Cell Biology* 199 (6): 871–81. https://doi.org/10.1083/jcb.201210040.

García-Castillo, Herbert, Ana Isabel Vásquez-Velásquez, Horacio Rivera, and Patricio Barros-Núñez. 2008. "Clinical and Genetic Heterogeneity in Patients with Mosaic

Variegated Aneuploidy: Delineation of Clinical Subtypes." *American Journal of Medical Genetics Part A* 146A (13): 1687–95. https://doi.org/10.1002/ajmg.a.32315.

Gascoigne, Karen E., and Iain M. Cheeseman. 2013. "CDK-Dependent Phosphorylation and Nuclear Exclusion Coordinately Control Kinetochore Assembly State." *Journal of Cell Biology* 201 (1): 23–32. https://doi.org/10.1083/jcb.201301006.

Gascoigne, Karen E., Kozo Takeuchi, Aussie Suzuki, Tetsuya Hori, Tatsuo Fukagawa, and Iain M. Cheeseman. 2011. "Induced Ectopic Kinetochore Assembly Bypasses the Requirement for CENP-A Nucleosomes." *Cell* 145 (3): 410–22. https://doi.org/10.1016/j.cell.2011.03.031.

Gebhart, E, and T Liehr. 2000. "Patterns of Genomic Imbalances in Human Solid Tumors (Review)." *International Journal of Oncology* 16 (2): 383–99. http://www.ncbi.nlm.nih.gov/pubmed/10639584.

Genin, A., J. Desir, N. Lambert, M. Biervliet, N. Van Der Aa, G. Pierquin, A. Killian, et al. 2012. "Kinetochore KMN Network Gene CASC5 Mutated in Primary Microcephaly." *Human Molecular Genetics* 21 (24): 5306–17. https://doi.org/10.1093/hmg/dds386.

Geraghty, Zoë, Christina Barnard, Pelin Uluocak, and Ulrike Gruneberg. 2020. "The Association of Plk1 with the Astrin-Kinastrin Complex Promotes Formation and Maintenance of a Metaphase Plate." *BioRxiv*, July, 2020.07.01.181933. https://doi.org/10.1101/2020.07.01.181933.

Gholkar, Ankur A, Silvia Senese, Yu-chen Lo, Edmundo Vides, Ely Contreras, Emmanuelle Hodara, Joseph Capri, Julian P Whitelegge, and Jorge Z Torres. 2016. "HHS Public Access" 14 (2): 180–88. https://doi.org/10.1016/j.celrep.2015.12.035.The.

Gilmore, Edward C., and Christopher A. Walsh. 2013. "Genetic Causes of Microcephaly and Lessons for Neuronal Development." *Wiley Interdisciplinary Reviews: Developmental Biology* 2 (4): 461–78. https://doi.org/10.1002/wdev.89.

"GnomAD." n.d. Accessed January 29, 2020. https://gnomad.broadinstitute.org/.

Gornstein, Erica, and Thomas L. Schwarz. 2014. "The Paradox of Paclitaxel Neurotoxicity: Mechanisms and Unanswered Questions." *Neuropharmacology*. https://doi.org/10.1016/j.neuropharm.2013.08.016.

Gruber, Jens, Jens Harborth, Jörg Schnabel, Klaus Weber, and Mechthild Hatzfeld. 2002. "The Mitotic-Spindle-Associated Protein Astrin Is Essential for Progression through Mitosis." *Journal of Cell Science* 115 (Pt 21): 4053–59. https://doi.org/10.1242/jcs.00088.

Gudimchuk, Nikita, Benjamin Vitre, Yumi Kim, Anatoly Kiyatkin, Don W. Cleveland, Fazly I. Ataullakhanov, and Ekaterina L. Grishchuk. 2013. “Kinetochore Kinesin CENP-E Is a Processive Bi-Directional Tracker of Dynamic Microtubule Tips.” *Nature Cell Biology* 15 (9): 1079–88. https://doi.org/10.1038/ncb2831.

Guimaraes, Geoffrey J., Yimin Dong, Bruce F. McEwen, and Jennifer G. DeLuca. 2008. “Kinetochore-Microtubule Attachment Relies on the Disordered N-Terminal Tail Domain of Hec1.” *Current Biology* 18 (22): 1778–84. https://doi.org/10.1016/j.cub.2008.08.012.

Halim, Vincentius a, Monica Alvarez-Fernandez, Yan Juan Xu, Melinda Aprelia, Henk W P van den Toorn, Albert J R Heck, Shabaz Mohammed, and Rene H Medema. 2013. “Comparative Phosphoproteomic Analysis of Checkpoint Recovery Identifies New Regulators of the DNA Damage Response.” *Science Signaling* 6 (272): rs9–rs9. https://doi.org/10.1126/scisignal.2003664.

Hanahan, Douglas, Robert A. Weinberg, K.H. Pan, J.W. Shay, S.N. Cohen, M.B. Taylor, N.W. Clarke, et al. 2011. “Hallmarks of Cancer: The Next Generation.” *Cell* 144 (5): 646–74. https://doi.org/10.1016/j.cell.2011.02.013.

Hanks, Sandra, Kim Coleman, Sarah Reid, Alberto Plaja, Helen Firth, David FitzPatrick, Alexa Kidd, et al. 2004. “Constitutional Aneuploidy and Cancer Predisposition Caused by Biallelic Mutations in BUB1B.” *Nature Genetics* 36 (11): 1159–61. https://doi.org/10.1038/ng1449.

Hara, Masatoshi, and Tatsuo Fukagawa. 2020. “Dynamics of Kinetochore Structure and Its Regulations during Mitotic Progression.” *Cellular and Molecular Life Sciences*. Springer. https://doi.org/10.1007/s00018-020-03472-4.

Harasymiw, Lauren A., Damien Tank, Mark McClellan, Neha Panigrahy, and Melissa K. Gardner. 2019. “Centromere Mechanical Maturation during Mammalian Cell Mitosis.” *Nature Communications* 10 (1): 1–21. https://doi.org/10.1038/s41467-019-09578-z.

Hart, Madeleine, Sophie D. Adams, and Viji M. Draviam. 2021. “Multinucleation Associated DNA Damage Blocks Proliferation in P53-Compromised Cells.” *Communications Biology 2021 4:1* 4 (1): 1–11. https://doi.org/10.1038/s42003-021-01979-5.

Hassold, T. J., and P. A. Jacobs. 1984. “Trisomy in Man.” *Annual Review of Genetics*. Annu Rev Genet. https://doi.org/10.1146/annurev.ge.18.120184.000441.

Hatch, Emily M., Andrew H. Fischer, Thomas J. Deerinck, and Martin W. Hetzer. 2013. “Catastrophic Nuclear Envelope Collapse in Cancer Cell Micronuclei.” *Cell* 154 (1): 47.

https://doi.org/10.1016/j.cell.2013.06.007.

Hayashi, Makoto T., Anthony J. Cesare, James A.J. Fitzpatrick, Eros Lazzerini-Denchi, and Jan Karlseder. 2012. “A Telomere-Dependent DNA Damage Checkpoint Induced by Prolonged Mitotic Arrest.” *Nature Structural and Molecular Biology* 19 (4): 387–94. https://doi.org/10.1038/nsmb.2245.

Hayward, Daniel, Tatiana Alfonso-Pérez, Michael J. Cundell, Michael Hopkins, James Holder, James Bancroft, Lukas H. Hutter, Bela Novak, Francis A. Barr, and Ulrike Gruneberg. 2019. “CDK1-CCNB1 Creates a Spindle Checkpoint-Permissive State by Enabling MPS1 Kinetochore Localization.” *Journal of Cell Biology* 218 (4): 1182–99. https://doi.org/10.1083/jcb.201808014.

Hayward, Daniel, Jeremy Metz, Claudia Pellacani, and James G. Wakefield. 2014. “Synergy between Multiple Microtubule-Generating Pathways Confers Robustness to Centrosome-Driven Mitotic Spindle Formation.” *Developmental Cell* 28 (1): 81–93. https://doi.org/10.1016/j.devcel.2013.12.001.

He, Ji, Andrew R. Green, Yan Li, Stephen Y.T. Chan, and Dong Xu Liu. 2020. “SPAG5: An Emerging Oncogene.” *Trends in Cancer*. Cell Press. https://doi.org/10.1016/j.trecan.2020.03.006.

Heald, Rebecca, and Alexey Khodjakov. 2015. “Thirty Years of Search and Capture: The Complex Simplicity of Mitotic Spindle Assembly.” *Journal of Cell Biology* 211 (6): 1103–11. https://doi.org/10.1083/jcb.201510015.

Helgeson, Luke A., Alex Zelter, Michael Riffle, Michael J. MacCoss, Charles L. Asbury, and Trisha N. Davis. 2018. “Human Ska Complex and Ndc80 Complex Interact to Form a Load-Bearing Assembly That Strengthens Kinetochore–Microtubule Attachments.” *Proceedings of the National Academy of Sciences of the United States of America* 115 (11): 2740–45. https://doi.org/10.1073/pnas.1718553115.

Herman, Jacob A., Chad M. Toledo, James M. Olson, Jennifer G. DeLuca, and Patrick J. Paddison. 2015. “Molecular Pathways: Regulation and Targeting of Kinetochore-Microtubule Attachment in Cancer.” *Clinical Cancer Research* 21 (2): 233–39. https://doi.org/10.1158/1078-0432.CCR-13-0645.

Hiruma, Yoshitaka, Carlos Sacristan, Spyridon T. Pachis, Athanassios Adamopoulos, Timo Kuijt, Marcellus Ubbink, Eleonore Von Castelmur, Anastassis Perrakis, and Geert J.P.L. Kops. 2015. “Competition between MPS1 and Microtubules at Kinetochores Regulates Spindle Checkpoint Signaling.” *Science* 348 (6240): 1264–67.

https://doi.org/10.1126/science.aaa4055.

Hoffelder, Diane R., Li Luo, Nancy A. Burke, Simon C. Watkins, Susanne M. Gollin, and William S. Saunders. 2004. “Resolution of Anaphase Bridges in Cancer Cells.” *Chromosoma* 112 (8): 389–97. https://doi.org/10.1007/s00412-004-0284-6.

Honda, Reiko, Roman Körner, and Erich A. Nigg. 2003. “Exploring the Functional Interactions between Aurora B, INCENP, and Survivin in Mitosis.” *Molecular Biology of the Cell* 14 (8): 3325–41. https://doi.org/10.1091/mbc.E02-11-0769.

Hooff, Jolien J.E. Van, Berend Snel, and Geert J.P.L. Kops. 2017. “Unique Phylogenetic Distributions of the Ska and Dam1 Complexes Support Functional Analogy and Suggest Multiple Parallel Displacements of Ska by Dam1.” *Genome Biology and Evolution* 9 (5): 1295–1303. https://doi.org/10.1093/gbe/evx088.

Hori, Tetsuya, Wei Hao Shang, Kozo Takeuchi, and Tatsuo Fukagawa. 2013. “The CCAN Recruits CENP-A to the Centromere and Forms the Structural Core for Kinetochore Assembly.” *Journal of Cell Biology* 200 (1): 45–60. https://doi.org/10.1083/jcb.201210106.

Huang, Ruijia, and Aili Li. 2020. “SPAG5 Is Associated with Unfavorable Prognosis in Patients with Lung Adenocarcinoma and Promotes Proliferation, Motility and Autophagy in A549 Cells.” *Experimental and Therapeutic Medicine* 20 (5): 1–1. https://doi.org/10.3892/etm.2020.9205.

Huang, Yuejia, Wenwen Wang, Phil Yao, Xiwei Wang, Xing Liu, Xiaoxuan Zhuang, Feng Yan, et al. 2012. “CENP-E Kinesin Interacts with SKAP Protein to Orchestrate Accurate Chromosome Segregation in Mitosis.” *Journal of Biological Chemistry* 287 (2): 1500–1509. https://doi.org/10.1074/jbc.M111.277194.

Huis In ’T Veld, Pim J., Vladimir A. Volkov, Isabelle D. Stender, Andrea Musacchio, and Marileen Dogterom. 2019. “Molecular Determinants of the Ska-Ndc80 Interaction and Their Influence on Microtubule Tracking and Force-Coupling.” *ELife* 8 (December). https://doi.org/10.7554/eLife.49539.

Hümmer, Stefan, and Thomas U. Mayer. 2009. “Cdk1 Negatively Regulates Midzone Localization of the Mitotic Kinesin Mklp2 and the Chromosomal Passenger Complex.” *Current Biology* 19 (7): 607–12. https://doi.org/10.1016/j.cub.2009.02.046.

Itoh, Go, Masanori Ikeda, Kenji Iemura, Mohammed Abdhullahel Amin, Sei Kuriyama, Masamitsu Tanaka, Natsuki Mizuno, Hiroko Osakada, Tokuko Haraguchi, and Kozo Tanaka. 2018. “Lateral Attachment of Kinetochores to Microtubules Is Enriched in

Prometaphase Rosette and Facilitates Chromosome Alignment and Bi-Orientation Establishment." *Scientific Reports* 8 (1): 1–18. https://doi.org/10.1038/s41598-018-22164-5.

Jablonski, S. A., S. T. Liu, and Tim J. Yen. 2003. "Targeting the Kinetochore for Mitosis-Specific Inhibitors." *Cancer Biology and Therapy*. Taylor & Francis. https://doi.org/10.4161/cbt.2.3.384.

Jacquemont, Sébastien, Michelle Bocéno, Jean Marie Rival, Françoise Méchinaud, and Albert David. 2002. "High Risk of Malignancy in Mosaic Variegated Aneuploidy Syndrome." *American Journal of Medical Genetics* 109 (1): 17–21; discussion 16. http://www.ncbi.nlm.nih.gov/pubmed/11932988.

Jamieson, C. R., C. Govaerts, and M. J. Abramowicz. 1999. "Primary Autosomal Recessive Microcephaly: Homozygosity Mapping of MCPH4 to Chromosome 15 [4]." *American Journal of Human Genetics*. University of Chicago Press. https://doi.org/10.1086/302640.

Jamieson, C. Ruth, Cédric Govaerts, and Marc J. Abramowicz. 1999. "Primary Autosomal Recessive Microcephaly: Homozygosity Mapping of MCPH4 to Chromosome 15." *The American Journal of Human Genetics* 65 (5): 1465–69. https://doi.org/10.1086/302640.

Janczyk, Paweł, Katarzyna A. Skorupka, John G. Tooley, Daniel R. Matson, Cortney A. Kestner, Thomas West, Owen Pornillos, and P. Todd Stukenberg. 2017. "Mechanism of Ska Recruitment by Ndc80 Complexes to Kinetochores." *Developmental Cell* 41 (4): 438-449.e4. https://doi.org/10.1016/j.devcel.2017.04.020.

Janssen, Aniek, Marja Van Der Burg, Karoly Szuhai, Geert J.P.L. Kops, and René H. Medema. 2011. "Chromosome Segregation Errors as a Cause of DNA Damage and Structural Chromosome Aberrations." *Science* 333 (6051): 1895–98. https://doi.org/10.1126/science.1210214.

Jayaraman, Divya, Byoung Il Bae, and Christopher A. Walsh. 2018. "The Genetics of Primary Microcephaly." *Annual Review of Genomics and Human Genetics*. Annual Reviews Inc. https://doi.org/10.1146/annurev-genom-083117-021441.

Jean, Francesca, Amanda Stuart, and Maja Tarailo-Graovac. 2020. "Dissecting the Genetic and Etiological Causes of Primary Microcephaly." *Frontiers in Neurology*. Frontiers Media S.A. https://doi.org/10.3389/fneur.2020.570830.

Jenni, Simon, and Stephen C. Harrison. 2018. "Structure of the DASH/Dam1 Complex Shows Its Role at the Yeast Kinetochore-Microtubule Interface." *Science* 360 (6388): 552–58.

https://doi.org/10.1126/science.aar6436.

Jeyaprakash, Arockia A., Anna Santamaria, Uma Jayachandran, Ying Wai Chan, Christian Benda, Erich A. Nigg, and Elena Conti. 2012. “Structural and Functional Organization of the Ska Complex, a Key Component of the Kinetochore-Microtubule Interface.” *Molecular Cell* 46 (3): 274–86. https://doi.org/10.1016/j.molcel.2012.03.005.

Ji, Zhejian, Haishan Gao, Luying Jia, Bing Li, and Hongtao Yu. 2017. “A Sequential Multi-Target Mps1 Phosphorylation Cascade Promotes Spindle Checkpoint Signaling.” *ELife* 6 (January). https://doi.org/10.7554/eLife.22513.

Ji, Zhejian, Haishan Gao, and Hongtao Yu. 2015. “Kinetochore Attachment Sensed by Competitive Mps1 and Microtubule Binding to Ndc80C.” *Science* 348 (6240): 1260–64. https://doi.org/10.1126/science.aaa4029.

Joglekar, Ajit. 2016. “A Cell Biological Perspective on Past, Present and Future Investigations of the Spindle Assembly Checkpoint.” *Biology* 5 (4): 44. https://doi.org/10.3390/biology5040044.

Jokelainen, Pentti T. 1967. “The Ultrastructure and Spatial Organization of the Metaphase Kinetochore in Mitotic Rat Cells.” *Journal of Ultrasructure Research* 19 (1–2): 19–44. https://doi.org/10.1016/S0022-5320(67)80058-3.

Kajii, T, T Ikeuchi, Z Q Yang, Y Nakamura, Y Tsuji, K Yokomori, M Kawamura, S Fukuda, S Horita, and A Asamoto. 2001. “Cancer-Prone Syndrome of Mosaic Variegated Aneuploidy and Total Premature Chromatid Separation: Report of Five Infants.” *American Journal of Medical Genetics* 104 (1): 57–64. http://www.ncbi.nlm.nih.gov/pubmed/11746029.

Kajii, Tadashi, Tohru Kawai, Tohru Takumi, Hideo Misu, Osamu Mabuchi, Yasuhiko Takahashi, Mariko Tachino, Fumio Nihei, and Tatsuro Ikeuchi. 1998. “Mosaic Variegated Aneuploidy with Multiple Congenital Abnormalities: Homozygosity for Total Premature Chromatid Separation Trait.” *American Journal of Medical Genetics* 78 (3): 245–49. https://doi.org/10.1002/(SICI)1096-8628(19980707)78:3<245::AID-AJMG7>3.0.CO;2-O.

Kanfer, Gil, Martin Peterka, Vladimir K. Arzhanik, Alexei L. Drobyshev, Fazly I. Ataullakhanov, Vladimir A. Volkov, and Benoît Kornmann. 2017. “CENP-F Couples Cargo to Growing and Shortening Microtubule Ends.” Edited by Manuel Théry. *Molecular Biology of the Cell* 28 (18): 2400–2409. https://doi.org/10.1091/mbc.e16-11-0756.

Kapoor, Tarun M, Michael A Lampson, Polla Hergert, Lisa Cameron, Daniela Cimini, E D Salmon, Bruce F McEwen, and Alexey Khodjakov. 2006. “Chromosomes Can Congress to the Metaphase Plate before Biorientation.” *Science (New York, N.Y.)* 311 (5759): 388–91. https://doi.org/10.1126/science.1122142.

Karczewski, Konrad J., Laurent C. Francioli, Grace Tiao, Beryl B. Cummings, Jessica Alföldi, Qingbo Wang, Ryan L. Collins, et al. 2020. “The Mutational Constraint Spectrum Quantified from Variation in 141,456 Humans.” *Nature* 581 (7809): 434–43. https://doi.org/10.1038/s41586-020-2308-7.

Kawame, H., Yoko Sugio, Yuichi Fuyama, Yoshihiro Hayashi, Hideaki Suzuki, Kenji Kurosawa, and Kihei Maekawa. 1999. “Syndrome of Microcephaly, Dandy-Walker Malformation, and Wilms Tumor Caused by Mosaic Variegated Aneuploidy with Premature Centromere Division (PCD): Report of a New Case and Review of the Literature.” *Journal of Human Genetics* 44 (4): 219–24. https://doi.org/10.1007/s100380050147.

Kern, David. M., Elizabeth. M. Wilson-Kubalek, and Iain. M. Cheeseman. 2017. “Astrin-SKAP Complex Reconstitution Reveals Its Kinetochore Interaction with Microtubule-Bound Ndc80.” *BioRxiv*. https://doi.org/10.1101/151399.

Kern, David M., Peter K. Nicholls, David C. Page, and Iain M. Cheeseman. 2016. “A Mitotic SKAP Isoform Regulates Spindle Positioning at Astral Microtubule plus Ends.” *Journal of Cell Biology* 213 (3): 315–28. https://doi.org/10.1083/jcb.201510117.

Khodjakov, Alexey, Richard W. Cole, Berl R. Oakley, and Conly L. Rieder. 2000. “Centrosome-Independent Mitotic Spindle Formation in Vertebrates.” *Current Biology* 10 (2): 59–67. https://doi.org/10.1016/S0960-9822(99)00276-6.

Kim, Yumi, Andrew J. Holland, Weijie Lan, and Don W. Cleveland. 2010a. “Aurora Kinases and Protein Phosphatase 1 Mediate Chromosome Congression through Regulation of CENP-E.” *Cell* 142 (3): 444–55. https://doi.org/10.1016/j.cell.2010.06.039.

Kitajima, Tomoya S., Miho Ohsugi, and Jan Ellenberg. 2011. “Complete Kinetochore Tracking Reveals Error-Prone Homologous Chromosome Biorientation in Mammalian Oocytes.” *Cell* 146 (4): 568–81. https://doi.org/10.1016/j.cell.2011.07.031.

Klein, Ulf R., Erich A. Nigg, and Ulrike Gruneberg. 2006. “Centromere Targeting of the Chromosomal Passenger Complex Requires a Ternary Subcomplex of Borealin, Survivin, and the N-Terminal Domain of INCENP.” *Molecular Biology of the Cell* 17 (6): 2547–58. https://doi.org/10.1091/mbc.E05-12-1133.

Kodani, Andrew, Timothy W. Yu, Jeffrey R. Johnson, Divya Jayaraman, Tasha L. Johnson, Lihadh Al-Gazali, Laszló Sztriha, et al. 2015. “Centriolar Satellites Assemble Centrosomal Microcephaly Proteins to Recruit CDK2 and Promote Centriole Duplication.” *ELife* 4 (AUGUST2015). https://doi.org/10.7554/eLife.07519.

KOMAI, T., K. KISHIMOTO, and Y. OZAKI. 1955. “Genetic Study of Microcephaly Based on Japanese Material.” *American Journal of Human Genetics* 7 (1): 51–65. https://www.ncbi.nlm.nih.gov/pmc/articles/PMC1716566/.

Kops, Geert J.P.L., and Reto Gassmann. 2020. “Crowning the Kinetochore: The Fibrous Corona in Chromosome Segregation.” *Trends in Cell Biology*. Elsevier Ltd. https://doi.org/10.1016/j.tcb.2020.04.006.

Kops, Geert J P L, Yumi Kim, Beth A A Weaver, Yinghui Mao, Ian McLeod, John R Yates, Mitsuo Tagaya, and Don W Cleveland. 2005. “ZW10 Links Mitotic Checkpoint Signaling to the Structural Kinetochore.” *The Journal of Cell Biology* 169 (1): 49–60. https://doi.org/10.1083/jcb.200411118.

Krenn, Veronica, and Andrea Musacchio. 2015. “The Aurora B Kinase in Chromosome Bi-Orientation and Spindle Checkpoint Signaling.” *Frontiers in Oncology*. Frontiers Media S.A. https://doi.org/10.3389/fonc.2015.00225.

Kruse, T., G. Zhang, M. S. Y. Larsen, T. Lischetti, W. Streicher, T. Kragh Nielsen, S. P. Bjorn, and J. Nilsson. 2013. “Direct Binding between BubR1 and B56-PP2A Phosphatase Complexes Regulate Mitotic Progression.” *Journal of Cell Science* 126 (5): 1086–92. https://doi.org/10.1242/jcs.122481.

Kuhn, Jonathan, and Sophie Dumont. 2017. “Spindle Assembly Checkpoint Satisfaction Occurs via End-on but Not Lateral Attachments under Tension.” *The Journal of Cell Biology* 216 (6): 1533–42. https://doi.org/10.1083/jcb.201611104.

Lampson, Michael, and Ekaterina Grishchuk. 2017. “Mechanisms to Avoid and Correct Erroneous Kinetochore-Microtubule Attachments.” *Biology* 6 (1): 1. https://doi.org/10.3390/biology6010001.

Lanni, Jennifer S., and Tyler Jacks. 1998. “Characterization of the P53-Dependent Postmitotic Checkpoint Following Spindle Disruption.” *Molecular and Cellular Biology* 18 (2): 1055–64. https://doi.org/10.1128/mcb.18.2.1055.

Leslie, Richard, Christopher J. O’Donnell, and Andrew D. Johnson. 2014. “GRASP: Analysis of Genotype-Phenotype Results from 1390 Genome-Wide Association Studies and Corresponding Open Access Database.” *Bioinformatics* 30 (12).

https://doi.org/10.1093/bioinformatics/btu273.

Levine, Michelle S., and Andrew J. Holland. 2018. “The Impact of Mitotic Errors on Cell Proliferation and Tumorigenesis.” *Genes and Development*. Cold Spring Harbor Laboratory Press. https://doi.org/10.1101/gad.314351.118.

Li, Ming, Anqi Li, Shuling Zhou, Hong Lv, and Wentao Yang. 2019. “SPAG5 Upregulation Contributes to Enhanced C-MYC Transcriptional Activity via Interaction with c-MYC Binding Protein in Triple-Negative Breast Cancer.” *Journal of Hematology & Oncology* 12 (1): 14. https://doi.org/10.1186/s13045-019-0700-2.

Li, Yan, Wei Yu, Yun Liang, and Xueliang Zhu. 2007. “Kinetochore Dynein Generates a Poleward Pulling Force to Facilitate Congression and Full Chromosome Alignment.” *Cell Research* 17 (8): 701–12. https://doi.org/10.1038/cr.2007.65.

Lichtenstein, Anatoly V. 2018. “Genetic Mosaicism and Cancer: Cause and Effect.” *Cancer Research*. American Association for Cancer Research Inc. https://doi.org/10.1158/0008-5472.CAN-17-2769.

Limwongse, C, S Schwartz, M Bocian, and N H Robin. 1999. “Child with Mosaic Variegated Aneuploidy and Embryonal Rhabdomyosarcoma.” *American Journal of Medical Genetics* 82 (1): 20–24. http://www.ncbi.nlm.nih.gov/pubmed/9916837.

Liu, Dan, Gerben Vader, Martijn J.M. Vromans, Michael A. Lampson, and Susanne M.A. Lens. 2009. “Sensing Chromosome Bi-Orientation by Spatial Separation of Aurora B Kinase from Kinetochore Substrates.” *Science* 323 (5919): 1350–53. https://doi.org/10.1126/science.1167000.

Liu, Dan, Mathijs Vleugel, Chelsea B. Backer, Tetsuya Hori, Tatsuo Fukagawa, Iain M. Cheeseman, and Michael A. Lampson. 2010. “Regulated Targeting of Protein Phosphatase 1 to the Outer Kinetochore by KNL1 Opposes Aurora B Kinase.” *Journal of Cell Biology* 188 (6): 809–20. https://doi.org/10.1083/jcb.201001006.

Liu, Guodong, Shan Liu, Guanyi Cao, Weihuan Luo, Peng Li, Shiping Wang, and Yu Chen. 2019. “SPAG5 Contributes to the Progression of Gastric Cancer by Upregulation of Survivin Depend on Activating the Wnt/β-Catenin Pathway.” *Experimental Cell Research* 379 (1): 83–91. https://doi.org/10.1016/j.yexcr.2019.03.024.

Liu, J. Y., Q. H. Zeng, P. G. Cao, D. Xie, F. Yang, L. Y. He, Y. B. Dai, et al. 2018. “SPAG5 Promotes Proliferation and Suppresses Apoptosis in Bladder Urothelial Carcinoma by Upregulating Wnt3 via Activating the AKT/MTOR Pathway and Predicts Poorer Survival.” *Oncogene* 37 (29): 3937–52. https://doi.org/10.1038/s41388-018-0223-2.

Liu, Lingling, Shamima Akhter, Jae Bum Bae, Sudit S. Mukhopadhyay, Christopher T. Richie, Xiaojun Liu, and Randy Legerski. 2009. “SNMIB/Apollo Interacts with Astrin and Is Required for the Prophase Cell Cycle Checkpoint.” *Cell Cycle* 8 (4): 628–38. https://doi.org/10.4161/cc.8.4.7791.

London, Nitobe, Steven Ceto, Jeffrey A. Ranish, and Sue Biggins. 2012. “Phosphoregulation of Spc105 by Mps1 and PP1 Regulates Bub1 Localization to Kinetochores.” *Current Biology* 22 (10): 900–906. https://doi.org/10.1016/j.cub.2012.03.052.

Lüders, Jens, Urvashi K. Patel, and Tim Stearns. 2006. “GCP-WD Is a γ-Tubulin Targeting Factor Required for Centrosomal and Chromatin-Mediated Microtubule Nucleation.” *Nature Cell Biology* 8 (2): 137–47. https://doi.org/10.1038/ncb1349.

Ly, Peter, Levi S. Teitz, Dong H. Kim, Ofer Shoshani, Helen Skaletsky, Daniele Fachinetti, David C. Page, and Don W. Cleveland. 2017. “Selective y Centromere Inactivation Triggers Chromosome Shattering in Micronuclei and Repair by Non-Homologous End Joining.” *Nature Cell Biology* 19 (1): 68–75. https://doi.org/10.1038/ncb3450.

Mack, G J, and D a Compton. 2001. “Analysis of Mitotic Microtubule-Associated Proteins Using Mass Spectrometry Identifies Astrin, a Spindle-Associated Protein.” *Proceedings of the National Academy of Sciences of the United States of America* 98 (25): 14434–39. https://doi.org/10.1073/pnas.261371298.

Macville, Merryn, Evelin Schröck, Hesed Padilla-Nash, Catherine Keck, B. Michael Ghadimi, Drazen Zimonjic, Nicholas Popescu, and Thomas Ried. 1999. “Comprehensive and Definitive Molecular Cytogenetic Characterization of HeLa Cells by Spectral Karyotyping.” *Cancer Research* 59 (1).

Madeira, Fábio, Young Mi Park, Joon Lee, Nicola Buso, Tamer Gur, Nandana Madhusoodanan, Prasad Basutkar, et al. 2019. “The EMBL-EBI Search and Sequence Analysis Tools APIs in 2019.” *Nucleic Acids Research* 47 (W1): W636–41. https://doi.org/10.1093/nar/gkz268.

Magidson, Valentin, Christopher B. O’Connell, Jadranka Lončarek, Raja Paul, Alex Mogilner, and Alexey Khodjakov. 2011. “The Spatial Arrangement of Chromosomes during Prometaphase Facilitates Spindle Assembly.” *Cell* 146 (4): 555–67. https://doi.org/10.1016/j.cell.2011.07.012.

Magidson, Valentin, Raja Paul, Nachen Yang, Jeffrey G. Ault, Christopher B. O’Connell, Irina Tikhonenko, Bruce F. Mcewen, Alex Mogilner, and Alexey Khodjakov. 2015. “Adaptive Changes in the Kinetochore Architecture Facilitate Proper Spindle

Assembly." *Nature Cell Biology* 17 (9): 1134–44. https://doi.org/10.1038/ncb3223.

Mah, L. J., A. El-Osta, and T. C. Karagiannis. 2010. "Th2AX: A Sensitive Molecular Marker of DNA Damage and Repair." *Leukemia*. Nature Publishing Group. https://doi.org/10.1038/leu.2010.6.

Manchester, Keith L. 1995. "Theodor Boveri and the Origin of Malignant Tumours." *Trends in Cell Biology* 5 (10): 384–87. https://doi.org/10.1016/S0962-8924(00)89080-7.

Manning, Amity L, Samuel F Bakhoum, Stefano Maffini, Clara Correia-Melo, Helder Maiato, and Duane A Compton. 2010. "CLASP1, Astrin and Kif2b Form a Molecular Switch That Regulates Kinetochore-Microtubule Dynamics to Promote Mitotic Progression and Fidelity." *The EMBO Journal* 29 (20): 3531–43. https://doi.org/10.1038/emboj.2010.230.

Mao, Yinghui, Arshad Desai, and Don W. Cleveland. 2005. "Microtubule Capture by CENP-E Silences BubR1-Dependent Mitotic Checkpoint Signaling." *Journal of Cell Biology* 170 (6): 873–80. https://doi.org/10.1083/jcb.200505040.

Maresca, Thomas J., and Edward D. Salmon. 2009. "Intrakinetochore Stretch Is Associated with Changes in Kinetochore Phosphorylation and Spindle Assembly Checkpoint Activity." *Journal of Cell Biology* 184 (3): 373–81. https://doi.org/10.1083/jcb.200808130.

Matsuura, Shinya, Yoshiyuki Matsumoto, Ken-ichi Morishima, Hideki Izumi, Hiroshi Matsumoto, Emi Ito, Keisuke Tsutsui, et al. 2006. "MonoallelicBUB1B Mutations and Defective Mitotic-Spindle Checkpoint in Seven Families with Premature Chromatid Separation (PCS) Syndrome." *American Journal of Medical Genetics Part A* 140A (4): 358–67. https://doi.org/10.1002/ajmg.a.31069.

McCleland, Mark L., Richard D. Gardner, Marko J. Kallio, John R. Daum, Gary J. Gorbsky, Daniel J. Burke, and P. Todd Stukenberg. 2003. "The Highly Conserved Ndc80 Complex Is Required for Kinetochore Assembly, Chromosome Congression, and Spindle Checkpoint Activity." *Genes and Development* 17 (1): 101–14. https://doi.org/10.1101/gad.1040903.

McEwen, B. F., G. K.T. Chan, B. Zubrowski, M. S. Savoian, M. T. Sauer, and T. J. Yen. 2001. "CENP-E Is Essential for Reliable Bioriented Spindle Attachment, but Chromosome Alignment Can Be Achieved via Redundant Mechanisms in Mammalian Cells." *Molecular Biology of the Cell* 12 (9): 2776–89. https://doi.org/10.1091/mbc.12.9.2776.

McIntosh, J. Richard, Ekaterina L. Grishchuk, Mary K. Morphew, Artem K. Efremov, Kirill Zhudenkov, Vladimir A. Volkov, Iain M. Cheeseman, Arshad Desai, David N. Mastronarde, and Fazly I. Ataullakhanov. 2008. "Fibrils Connect Microtubule Tips with Kinetochores: A Mechanism to Couple Tubulin Dynamics to Chromosome Motion." *Cell* 135 (2): 322–33. https://doi.org/10.1016/j.cell.2008.08.038.

McKenney, Richard J., Walter Huynh, Marvin E. Tanenbaum, Gira Bhabha, and Ronald D. Vale. 2014. "Activation of Cytoplasmic Dynein Motility by Dynactin-Cargo Adapter Complexes." *Science* 345 (6194): 337–41. https://doi.org/10.1126/science.1254198.

Meadows, John C., Lindsey A. Shepperd, Vincent Vanoosthuyse, Theresa C. Lancaster, Alicja M. Sochaj, Graham J. Buttrick, Kevin G. Hardwick, and Jonathan B.A. Millar. 2011. "Spindle Checkpoint Silencing Requires Association of PP1 to Both Spc7 and Kinesin-8 Motors." *Developmental Cell* 20 (6): 739–50. https://doi.org/10.1016/j.devcel.2011.05.008.

Méhes, K., P. Kajtár, and G. Kosztolányi. 2002. "Association of Nonsyndromic Wilms Tumor with Premature Centromere Division (PCD)." *American Journal of Medical Genetics* 112 (2): 215–16. https://doi.org/10.1002/ajmg.10661.

Merdes, A., and J. De Mey. 1990. "The Mechanism of Kinetochore-Spindle Attachment and Polewards Movement Analyzed in PtK2 Cells at the Prophase-Prometaphase Transition." *European Journal of Cell Biology* 53 (2): 313–25.

Miller, K, W Müller, L Winkler, M R Hadam, J H Ehrich, and S D Flatz. 1990. "Mitotic Disturbance Associated with Mosaic Aneuploidies." *Human Genetics* 84 (4): 361–64. http://www.ncbi.nlm.nih.gov/pubmed/2307459.

Miller, Matthew P., Charles L. Asbury, and Sue Biggins. 2016. "A TOG Protein Confers Tension Sensitivity to Kinetochore-Microtubule Attachments." *Cell* 165 (6): 1428–39. https://doi.org/10.1016/j.cell.2016.04.030.

Miller, Stephanie A., Michael L. Johnson, and P. Todd Stukenberg. 2008. "Kinetochore Attachments Require an Interaction between Unstructured Tails on Microtubules and Ndc80Hec1." *Current Biology* 18 (22): 1785–91. https://doi.org/10.1016/j.cub.2008.11.007.

Miranda, J. J.L., Peter De Wulf, Peter K. Sorger, and Stephen C. Harrison. 2005. "The Yeast DASH Complex Forms Closed Rings on Microtubules." *Nature Structural and Molecular Biology* 12 (2): 138–43. https://doi.org/10.1038/nsmb896.

Mirzaa, Ghayda M., Benjamin Vitre, Gillian Carpenter, Iga Abramowicz, Joseph G. Gleeson,

Alex R. Paciorkowski, Don W. Cleveland, William B. Dobyns, and Mark O'Driscoll. 2014. "Mutations in CENPE Define a Novel Kinetochore-Centromeric Mechanism for Microcephalic Primordial Dwarfism." *Human Genetics* 133 (8): 1023–39. https://doi.org/10.1007/s00439-014-1443-3.

Mishra, Ram Kumar, Papia Chakraborty, Alexei Arnaoutov, Beatriz M.A. Fontoura, and Mary Dasso. 2010. "The Nup107-160 Complex and γ-TuRC Regulate Microtubule Polymerization at Kinetochores." *Nature Cell Biology* 12 (2): 164–69. https://doi.org/10.1038/ncb2016.

Mitchison, T. J., and M. W. Kirschner. 1985. "Properties of the Kinetochore in Vitro. I. Microtubule Nucleation and Tubulin Binding." *Journal of Cell Biology* 101 (3): 755–65. https://doi.org/10.1083/jcb.101.3.755.

Mitchison, Tim, and Marc Kirschner. 1984. "Dynamic Instability of Microtubule Growth." *Nature* 312 (5991): 237–42. https://doi.org/10.1038/312237a0.

Monda, Julie K., and Iain M. Cheeseman. 2018. "The Kinetochore-Microtubule Interface at a Glance." *Journal of Cell Science* 131 (16). https://doi.org/10.1242/jcs.214577.

Monda, Julie K., Ian P. Whitney, Ekaterina V. Tarasovetc, Elizabeth Wilson-Kubalek, Ronald A. Milligan, Ekaterina L. Grishchuk, and Iain M. Cheeseman. 2017. "Microtubule Tip Tracking by the Spindle and Kinetochore Protein Ska1 Requires Diverse Tubulin-Interacting Surfaces." *Current Biology* 27 (23): 3666-3675.e6. https://doi.org/10.1016/j.cub.2017.10.018.

Moritz, Michelle, Michael B. Braunfeld, John W. Sedat, Bruce Alberts, and David A. Agard. 1995. "Microtubule Nucleation by γ-Tubulin-Containing Rings in the Centrosome." *Nature* 378 (6557): 638–40. https://doi.org/10.1038/378638a0.

Mosalaganti, Shyamal, Jenny Keller, Anika Altenfeld, Michael Winzker, Pascaline Rombaut, Michael Saur, Arsen Petrovic, et al. 2017. "Structure of the RZZ Complex and Molecular Basis of Its Interaction with Spindly." *Journal of Cell Biology* 216 (4): 961–81. https://doi.org/10.1083/jcb.201611060.

Mukherjee, Aghna, Shaikh Faruque Ali, and Arockiarajan Arunachalakasi. 2019. "Shape Prediction of a Composite Wing Panel under the Action of an SMA Wire and an MFC Bimorph." In *Active and Passive Smart Structures and Integrated Systems XIII*, edited by Alper Erturk, 10967:63. SPIE. https://doi.org/10.1117/12.2514294.

Musacchio, Andrea. 2015. "The Molecular Biology of Spindle Assembly Checkpoint Signaling Dynamics." *Current Biology* 25 (20): R1002–18.

https://doi.org/10.1016/j.cub.2015.08.051.

Musacchio, Andrea, and Arshad Desai. 2017. “A Molecular View of Kinetochore Assembly and Function.” *Biology* 6 (1): 5. https://doi.org/10.3390/biology6010005.

Musinipally, Vivek, Stuart Howes, Gregory M. Alushin, and Eva Nogales. 2013. “The Microtubule Binding Properties of CENP-E’s C-Terminus and CENP-F.” *Journal of Molecular Biology* 425 (22): 4427–41. https://doi.org/10.1016/j.jmb.2013.07.027.

Nagpal, Harsh, and Tatsuo Fukagawa. 2016. “Kinetochore Assembly and Function through the Cell Cycle.” *Chromosoma*. Springer Science and Business Media Deutschland GmbH. https://doi.org/10.1007/s00412-016-0608-3.

Nasa, Isha, Scott F. Rusin, Arminja N. Kettenbach, and Greg B. Moorhead. 2018. “Aurora B Opposes PP1 Function in Mitosis by Phosphorylating the Conserved PP1-Binding RVxF Motif in PP1 Regulatory Proteins.” *Science Signaling* 11 (530): 8669. https://doi.org/10.1126/scisignal.aai8669.

Nesta, Alex V., Denisse Tafur, and Christine R. Beck. 2021. “Hotspots of Human Mutation.” *Trends in Genetics* 37 (8): 717–29. https://doi.org/10.1016/J.TIG.2020.10.003.

Nicholson, Joshua M., and Daniela Cimini. 2015. “Link between Aneuploidy and Chromosome Instability.” In *International Review of Cell and Molecular Biology*, 315:299–317. https://doi.org/10.1016/bs.ircmb.2014.11.002.

Nijenhuis, Wilco, Eleonore Von Castelmur, Dene Littler, Valeria De Marco, Eelco Tromer, Mathijs Vleugel, Maria H.J. Van Osch, Berend Snel, Anastassis Perrakis, and Geert J.P.L. Kops. 2013. “A TPR Domain-Containing N-Terminal Module of MPS1 Is Required for Its Kinetochore Localization by Aurora B.” *Journal of Cell Biology* 201 (2): 217–31. https://doi.org/10.1083/jcb.201210033.

Nijenhuis, Wilco, Giulia Vallardi, Antoinette Teixeira, Geert J.P.L. Kops, and Adrian T. Saurin. 2014. “Negative Feedback at Kinetochores Underlies a Responsive Spindle Checkpoint Signal.” *Nature Cell Biology* 16 (12): 1257–64. https://doi.org/10.1038/ncb3065.

Nishino, Tatsuya, Florencia Rago, Tetsuya Hori, Kentaro Tomii, Iain M. Cheeseman, and Tatsuo Fukagawa. 2013. “CENP-T Provides a Structural Platform for Outer Kinetochore Assembly.” *EMBO Journal* 32 (3): 424–36. https://doi.org/10.1038/emboj.2012.348.

Omer Javed, Attya, Yun Li, Julien Muffat, Kuan-Chung Su, Malkiel A. Cohen, Tenzin Lungjangwa, Patrick Aubourg, Iain M. Cheeseman, and Rudolf Jaenisch. 2018. “Microcephaly Modeling of Kinetochore Mutation Reveals a Brain-Specific

Phenotype." *Cell Reports* 25 (2): 368-382.e5. https://doi.org/10.1016/j.celrep.2018.09.032.

Orth, James D., Alexander Loewer, Galit Lahav, and Timothy J. Mitchison. 2012. "Prolonged Mitotic Arrest Triggers Partial Activation of Apoptosis, Resulting in DNA Damage and P53 Induction." *Molecular Biology of the Cell* 23 (4): 567–76. https://doi.org/10.1091/mbc.E11-09-0781.

Overlack, Katharina, Ivana Primorac, Mathijs Vleugel, Veronica Krenn, Stefano Maffini, Ingrid Hoffmann, Geert J P L Kops, and Andrea Musacchio. 2015. "A Molecular Basis for the Differential Roles of Bub1 and BubR1 in the Spindle Assembly Checkpoint." *ELife* 4 (January): e05269. https://doi.org/10.7554/eLife.05269.

Ozery-Flato, Michal, Chaim Linhart, Luba Trakhtenbrot, Shai Izraeli, and Ron Shamir. 2011. "Large-Scale Analysis of Chromosomal Aberrations in Cancer Karyotypes Reveals Two Distinct Paths to Aneuploidy." *Genome Biology* 12 (6): R61. https://doi.org/10.1186/gb-2011-12-6-r61.

Papi, L, E Montali, G Marconi, R Guazzelli, U Bigozzi, P Maraschio, and O Zuffardi. 1989. "Evidence for a Human Mitotic Mutant with Pleiotropic Effect." *Annals of Human Genetics* 53 (Pt 3): 243–48. http://www.ncbi.nlm.nih.gov/pubmed/2596830.

Paul, Raja, Roy Wollman, William T. Silkworth, Isaac K. Nardi, Daniela Cimini, and Alex Mogilner. 2009. "Computer Simulations Predict That Chromosome Movements and Rotations Accelerate Mitotic Spindle Assembly without Compromising Accuracy." *Proceedings of the National Academy of Sciences of the United States of America* 106 (37): 15708–13. https://doi.org/10.1073/pnas.0908261106.

Pereira, Cláudia, Rita M. Reis, José B. Gama, Ricardo Celestino, Dhanya K. Cheerambathur, Ana X. Carvalho, and Reto Gassmann. 2018. "Self-Assembly of the RZZ Complex into Filaments Drives Kinetochore Expansion in the Absence of Microtubule Attachment." *Current Biology* 28 (21): 3408-3421.e8. https://doi.org/10.1016/j.cub.2018.08.056.

Petrovic, Arsen, Jenny Keller, Yahui Liu, Katharina Overlack, Juliane John, Yoana N. Dimitrova, Simon Jenni, et al. 2016. "Structure of the MIS12 Complex and Molecular Basis of Its Interaction with CENP-C at Human Kinetochores." *Cell* 167 (4): 1028-1040.e15. https://doi.org/10.1016/j.cell.2016.10.005.

Petrovic, Arsen, Sebastiano Pasqualato, Prakash Dube, Veronica Krenn, Stefano Santaguida, Davide Cittaro, Silvia Monzani, et al. 2010. "The MIS12 Complex Is a Protein Interaction Hub for Outer Kinetochore Assembly" 190 (5): 835–52.

https://doi.org/10.1083/jcb.201002070.

Pfister, K. Kevin, Paresh R. Shah, Holger Hummerich, Andreas Russ, James Cotton, Azlina Ahmad Annuar, Stephen M. King, and Elizabeth M.C. Fisher. 2006. “Genetic Analysis of the Cytoplasmic Dynein Subunit Families.” *PLoS Genetics*. PLoS Genet. https://doi.org/10.1371/journal.pgen.0020001.

Pinsky, B. A., C. V. Kotwaliwale, S. Y. Tatsutani, C. A. Breed, and S. Biggins. 2006. “Glc7/Protein Phosphatase 1 Regulatory Subunits Can Oppose the Ipl1/Aurora Protein Kinase by Redistributing Glc7.” *Molecular and Cellular Biology* 26 (7): 2648–60. https://doi.org/10.1128/MCB.26.7.2648-2660.2006.

Pinson, Lucile, Linda Mannini, Marjolaine Willems, Francesco Cucco, Nicolas Sirvent, Thierry Frebourg, Valentina Quarantotti, et al. 2014. “CEP57 Mutation in a Girl with Mosaic Variegated Aneuploidy Syndrome.” *American Journal of Medical Genetics Part A* 164 (1): 177–81. https://doi.org/10.1002/ajmg.a.36166.

Plaja, A, T Vendrell, D Smeets, E Sarret, T Gili, V Català, C Mediano, and J M Scheres. 2001. “Variegated Aneuploidy Related to Premature Centromere Division (PCD) Is Expressed in Vivo and Is a Cancer-Prone Disease.” *American Journal of Medical Genetics* 98 (3): 216–23. http://www.ncbi.nlm.nih.gov/pubmed/11169558.

Powers, Andrew F., Andrew D. Franck, Daniel R. Gestaut, Jeremy Cooper, Beth Gracyzk, Ronnie R. Wei, Linda Wordeman, Trisha N. Davis, and Charles L. Asbury. 2009. “The Ndc80 Kinetochore Complex Forms Load-Bearing Attachments to Dynamic Microtubule Tips via Biased Diffusion.” *Cell* 136 (5): 865–75. https://doi.org/10.1016/j.cell.2008.12.045.

“PRIDE - Proteomics Identification Database.” n.d. Accessed January 29, 2020. https://www.ebi.ac.uk/pride/.

Primorac, Ivana, John R. Weir, Elena Chiroli, Fridolin Gross, Ingrid Hoffmann, Suzan van Gerwen, Andrea Ciliberto, and Andrea Musacchio. 2013. “Bub3 Reads Phosphorylated MELT Repeats to Promote Spindle Assembly Checkpoint Signaling.” *ELife* 2013 (2). https://doi.org/10.7554/eLife.01030.

Przewloka, Marcin R., Zsolt Venkei, Victor M. Bolanos-Garcia, Janusz Debski, Michal Dadlez, and David M. Glover. 2011. “CENP-C Is a Structural Platform for Kinetochore Assembly.” *Current Biology* 21 (5): 399–405. https://doi.org/10.1016/j.cub.2011.02.005.

Qian, Junbin, Maria Adelaida García-Gimeno, Monique Beullens, Maria Giulia Manzione,

Gerd Van der Hoeven, Juan Carlos Igual, Miguel Heredia, Pascual Sanz, Lendert Gelens, and Mathieu Bollen. 2017. “An Attachment-Independent Biochemical Timer of the Spindle Assembly Checkpoint.” *Molecular Cell* 68 (4): 715-730.e5. https://doi.org/10.1016/j.molcel.2017.10.011.

Qin, Bo, Dan Cao, Huihui Wu, Fei Mo, Hengyi Shao, Jane Chu, Michael Powell, et al. 2016. “Phosphorylation of SKAP by GSK3β Ensures Chromosome Segregation by a Temporal Inhibition of Kif2b Activity.” *Scientific Reports* 6 (August): 38791. https://doi.org/10.1038/srep38791.

Quignon, F., L. Rozier, A. M. Lachages, A. Bieth, M. Simili, and M. Debatisse. 2007. “Sustained Mitotic Block Elicits DNA Breaks: One-Step Alteration of Ploidy and Chromosome Integrity in Mammalian Cells.” *Oncogene* 26 (2): 165–72. https://doi.org/10.1038/sj.onc.1209787.

Richard Mcintosh, J. 2016. “Mitosis.” *Cold Spring Harbor Perspectives in Biology* 8 (9). https://doi.org/10.1101/cshperspect.a023218.

Rieder, C. L., and S. P. Alexander. 1990. “Kinetochores Are Transported Poleward along a Single Astral Microtubule during Chromosome Attachment to the Spindle in Newt Lung Cells.” *Journal of Cell Biology* 110 (1): 81–95. https://doi.org/10.1083/jcb.110.1.81.

Rieder, Conly L. 1981. “The Structure of the Cold-Stable Kinetochore Fiber in Metaphase PtK1 Cells.” *Chromosoma* 84 (1): 145–58. https://doi.org/10.1007/BF00293368.

Rio Frio, Thomas, Josée Lavoie, Nancy Hamel, Felipe C. Geyer, Yaël B. Kushner, David J. Novak, Landon Wark, et al. 2010. “Homozygous *BUB1B* Mutation and Susceptibility to Gastrointestinal Neoplasia.” *New England Journal of Medicine* 363 (27): 2628–37. https://doi.org/10.1056/NEJMoa1006565.

Rodriguez-Rodriguez, Jose Antonio, Clare Lewis, Kara L. McKinley, Vitali Sikirzhytski, Jennifer Corona, John Maciejowski, Alexey Khodjakov, Iain M. Cheeseman, and Prasad V. Jallepalli. 2018. “Distinct Roles of RZZ and Bub1-KNL1 in Mitotic Checkpoint Signaling and Kinetochore Expansion.” *Current Biology* 28 (21): 3422-3429.e5. https://doi.org/10.1016/j.cub.2018.10.006.

Rogakou, Emmy P., Duane R. Pilch, Ann H. Orr, Vessela S. Ivanova, and William M. Bonner. 1998. “DNA Double-Stranded Breaks Induce Histone H2AX Phosphorylation on Serine 139.” *Journal of Biological Chemistry* 273 (10): 5858–68. https://doi.org/10.1074/jbc.273.10.5858.

Roos, U. P. 1973. “LIGHT AND ELECTRON MICROSCOPY OF RAT KANGAROO

CELLS IN MITOSIS. II. KINETOCHORE STRUCTURE AND FUNCTION." *LIGHT AND ELECTRON MICROSCOPY OF RAT KANGAROO CELLS IN MITOSIS. II. KINETOCHORE STRUCTURE AND FUNCTION*.

Rosenberg, Jessica S., Frederick R. Cross, and Hironori Funabiki. 2011. "KNL1/Spc105 Recruits PP1 to Silence the Spindle Assembly Checkpoint." *Current Biology* 21 (11): 942–47. https://doi.org/10.1016/j.cub.2011.04.011.

Rowinsky, Eric K., and Ross C. Donehower. 1995. "Paclitaxel (Taxol)." Edited by Alastair J.J. Wood. *New England Journal of Medicine* 332 (15): 1004–14. https://doi.org/10.1056/NEJM199504133321507.

Rozewicki, John, Songling Li, Karlou Mar Amada, Daron M. Standley, and Kazutaka Katoh. 2019. "MAFFT-DASH: Integrated Protein Sequence and Structural Alignment." *Nucleic Acids Research* 47 (W1): W5–10. https://doi.org/10.1093/nar/gkz342.

Sacristan, Carlos, Misbha Ud Din Ahmad, Jenny Keller, Job Fermie, Vincent Groenewold, Eelco Tromer, Alexander Fish, et al. 2018. "Dynamic Kinetochore Size Regulation Promotes Microtubule Capture and Chromosome Biorientation in Mitosis." *Nature Cell Biology* 20 (7): 800–810. https://doi.org/10.1038/s41556-018-0130-3.

Samejima, Kumiko, Melpomeni Platani, Marcin Wolny, Hiromi Ogawa, Giulia Vargiu, Peter J. Knight, Michelle Peckham, and William C. Earnshaw. 2015. "The Inner Centromere Protein (INCENP) Coil Is a Single α-Helix (SAH) Domain That Binds Directly to Microtubules and Is Important for Chromosome Passenger Complex (CPC) Localization and Function in Mitosis." *Journal of Biological Chemistry* 290 (35): 21460–72. https://doi.org/10.1074/jbc.M115.645317.

Santaguida, Stefano, Amelia Richardson, Divya Ramalingam Iyer, Ons M'Saad, Lauren Zasadil, Kristin A. Knouse, Yao Liang Wong, Nicholas Rhind, Arshad Desai, and Angelika Amon. 2017. "Chromosome Mis-Segregation Generates Cell-Cycle-Arrested Cells with Complex Karyotypes That Are Eliminated by the Immune System." *Developmental Cell* 41 (6): 638-651.e5. https://doi.org/10.1016/j.devcel.2017.05.022.

Santaguida, Stefano, Claudio Vernieri, Fabrizio Villa, Andrea Ciliberto, and Andrea Musacchio. 2011. "Evidence That Aurora B Is Implicated in Spindle Checkpoint Signalling Independently of Error Correction." *The EMBO Journal* 30 (8): 1508–19. https://doi.org/10.1038/emboj.2011.70.

Saurin, Adrian T., and Geert J.P.L. Kops. 2016. "Studying Kinetochore Kinases." In *Methods in Molecular Biology*, 1413:333–47. Humana Press Inc. https://doi.org/10.1007/978-1-

4939-3542-0_21.

Scheres, J. M. J. C., T. W. J. Hustinx, J. D. Madan, K., Beltman, and D. Lindhout. 1986. “A Mitotic Mutant Causing Non-Disjunction in Man. (Abstract).” *7th International Congress of Human Genetics, Berlin*.

Schmid, Michael, Claus Steinlein, Qi Tian, Amy E. Hanlon Newell, Manfred Gessler, Susan B. Olson, Andreas Rosenwald, Burkhard Kneitz, and Lev M. Fedorov. 2014. “Mosaic Variegated Aneuploidy in Mouse BubR1 Deficient Embryos and Pregnancy Loss in Human.” *Chromosome Research* 22 (3): 375–92. https://doi.org/10.1007/s10577-014-9432-x.

Schmidt, Jens C., Haribabu Arthanari, Andras Boeszoermenyi, Natalia M. Dashkevich, Elizabeth M. Wilson-Kubalek, Nilah Monnier, Michelle Markus, et al. 2012. “The Kinetochore-Bound Ska1 Complex Tracks Depolymerizing Microtubules and Binds to Curved Protofilaments.” *Developmental Cell* 23 (5): 968–80. https://doi.org/10.1016/j.devcel.2012.09.012.

Schmidt, Jens C., Tomomi Kiyomitsu, Tetsuya Hori, Chelsea B. Backer, Tatsuo Fukagawa, and Iain M. Cheeseman. 2010. “Aurora B Kinase Controls the Targeting of the Astrin-SKAP Complex to Bioriented Kinetochores.” *Journal of Cell Biology* 191 (2): 269–80. https://doi.org/10.1083/jcb.201006129.

“Scientific Data Downloads | East London Genes & Health.” n.d. Accessed January 29, 2020. http://www.genesandhealth.org/research/scientific-data-downloads.

Screpanti, Emanuela, Anna De Antoni, Gregory M. Alushin, Arsen Petrovic, Tiziana Melis, Eva Nogales, and Andrea Musacchio. 2011. “Direct Binding of Cenp-C to the Mis12 Complex Joins the Inner and Outer Kinetochore.” *Current Biology* 21 (5): 391–98. https://doi.org/10.1016/j.cub.2010.12.039.

Sen, Onur, Adrian T. Saurin, and Jonathan M.G. Higgins. 2018. “The Live Cell DNA Stain SiR-Hoechst Induces DNA Damage Responses and Impairs Cell Cycle Progression.” *Scientific Reports* 8 (1). https://doi.org/10.1038/s41598-018-26307-6.

Shepperd, Lindsey A., John C. Meadows, Alicja M. Sochaj, Theresa C. Lancaster, Juan Zou, Graham J. Buttrick, Juri Rappsilber, Kevin G. Hardwick, and Jonathan B.A. Millar. 2012. “Phosphodependent Recruitment of Bub1 and Bub3 to Spc7/KNL1 by Mph1 Kinase Maintains the Spindle Checkpoint.” *Current Biology* 22 (10): 891–99. https://doi.org/10.1016/j.cub.2012.03.051.

Shrestha, Roshan L., Duccio Conti, Naoka Tamura, Dominique Braun, Revathy A.

Ramalingam, Konstanty Cieslinski, Jonas Ries, and Viji M. Draviam. 2017. “Aurora-B Kinase Pathway Controls the Lateral to End-on Conversion of Kinetochore-Microtubule Attachments in Human Cells.” *Nature Communications* 8 (1): 150. https://doi.org/10.1038/s41467-017-00209-z.

Shrestha, Roshan L., and Viji M. Draviam. 2013. “Lateral to End-on Conversion of Chromosome-Microtubule Attachment Requires Kinesins Cenp-e and MCAK.” *Current Biology* 23 (16): 1514–26. https://doi.org/10.1016/j.cub.2013.06.040.

Sieben, Cynthia J., Karthik B. Jeganathan, Grace G. Nelson, Ines Sturmlechner, Cheng Zhang, Willemijn H. Van Deursen, Bjorn Bakker, et al. 2020. “BubR1 Allelic Effects Drive Phenotypic Heterogeneity in Mosaic-Variegated Aneuploidy Progeria Syndrome.” *Journal of Clinical Investigation* 130 (1): 171–88. https://doi.org/10.1172/JCI126863.

Sikirzhytski, Vitali, Fioranna Renda, Irina Tikhonenko, Valentin Magidson, Bruce F. McEwen, and Alexey Khodjakov. 2018. “Microtubules Assemble near Most Kinetochores during Early Prometaphase in Human Cells.” *Journal of Cell Biology* 217 (8): 2647–59. https://doi.org/10.1083/jcb.201710094.

Silió, Virginia, Andrew D. McAinsh, and Jonathan B. Millar. 2015. “KNL1-Bubs and RZZ Provide Two Separable Pathways for Checkpoint Activation at Human Kinetochores.” *Developmental Cell* 35 (5): 600–613. https://doi.org/10.1016/j.devcel.2015.11.012.

Silkworth, William T., Isaac K. Nardi, Lindsey M. Scholl, and Daniela Cimini. 2009. “Multipolar Spindle Pole Coalescence Is a Major Source of Kinetochore Mis-Attachment and Chromosome Mis-Segregation in Cancer Cells.” Edited by Kevin G. Hardwick. *PLoS ONE* 4 (8): e6564. https://doi.org/10.1371/journal.pone.0006564.

Sivakumar, Sushama, and Gary J. Gorbsky. 2017. “Phosphatase-Regulated Recruitment of the Spindle- and Kinetochore-Associated (Ska) Complex to Kinetochores.” *Biology Open* 6 (11): 1672–79. https://doi.org/10.1242/bio.026930.

Snape, Katie, Sandra Hanks, Elise Ruark, Patricio Barros-Núñez, Anna Elliott, Anne Murray, Andrew H Lane, et al. 2011. “Mutations in CEP57 Cause Mosaic Variegated Aneuploidy Syndrome.” *Nature Genetics* 43 (6): 527–29. https://doi.org/10.1038/ng.822.

Song, Lingqin, Zhijun Dai, Shuqun Zhang, Haifeng Zhang, Chengcheng Liu, Xiaobin Ma, Di Liu, Ying Zan, and Xiaoran Yin. 2018. “MicroRNA-1179 Suppresses Cell Growth and Invasion by Targeting Sperm-Associated Antigen 5-Mediated Akt Signaling in Human Non-Small Cell Lung Cancer.” *Biochemical and Biophysical Research Communications*

504 (1): 164–70. https://doi.org/10.1016/j.bbrc.2018.08.149.

Soto, Mar, Jonne A. Raaijmakers, Bjorn Bakker, Diana C.J. Spierings, Peter M. Lansdorp, Floris Foijer, and René H. Medema. 2017. “P53 Prohibits Propagation of Chromosome Segregation Errors That Produce Structural Aneuploidies.” *Cell Reports* 19 (12): 2423–31. https://doi.org/10.1016/j.celrep.2017.05.055.

Stephens, Philip J., Chris D. Greenman, Beiyuan Fu, Fengtang Yang, Graham R. Bignell, Laura J. Mudie, Erin D. Pleasance, et al. 2011. “Massive Genomic Rearrangement Acquired in a Single Catastrophic Event during Cancer Development.” *Cell* 144 (1): 27–40. https://doi.org/10.1016/j.cell.2010.11.055.

Suijkerbuijk, S.J.E, M. Vleugel, A. Teixeira, and G.J.P.L. Kops. 2012. “Integration of Kinase and Phosphatase Activities by BUBR1 Ensures Formation of Stable Kinetochore-Microtubule Attachments.” *Developmental Cell* 23 (4): 745–55. https://doi.org/10.1016/j.devcel.2012.09.005.

Suijkerbuijk, Saskia J E, Maria H J van Osch, Frank L Bos, Sandra Hanks, Nazneen Rahman, and Geert J P L Kops. 2010. “Molecular Causes for BUBR1 Dysfunction in the Human Cancer Predisposition Syndrome Mosaic Variegated Aneuploidy.” *Cancer Research* 70 (12): 4891–4900. https://doi.org/10.1158/0008-5472.CAN-09-4319.

Suijkerbuijk, Saskia J E, Mathijs Vleugel, Antoinette Teixeira, and Geert J P L Kops. 2012. “Integration of Kinase and Phosphatase Activities by BUBR1 Ensures Formation of Stable Kinetochore-Microtubule Attachments.” *Developmental Cell* 23 (4): 745–55. https://doi.org/10.1016/j.devcel.2012.09.005.

Suzuki, Aussie, Benjamin L. Badger, and Edward D. Salmon. 2015. “A Quantitative Description of Ndc80 Complex Linkage to Human Kinetochores.” *Nature Communications* 6 (September). https://doi.org/10.1038/ncomms9161.

Szczepanski, Sandra, Muhammad Sajid Hussain, Ilknur Sur, Janine Altmüller, Holger Thiele, Uzma Abdullah, Syeda Seema Waseem, et al. 2016. “A Novel Homozygous Splicing Mutation of CASC5 Causes Primary Microcephaly in a Large Pakistani Family.” *Human Genetics* 135 (2): 157–70. https://doi.org/10.1007/s00439-015-1619-5.

Tahmasebi-Birgani, Maryam, Hossein Ansari, and Vinicio Carloni. 2019. “Defective Mitosis-Linked DNA Damage Response and Chromosomal Instability in Liver Cancer.” *Biochimica et Biophysica Acta - Reviews on Cancer*. Elsevier B.V. https://doi.org/10.1016/j.bbcan.2019.05.008.

Taliun, Daniel, Daniel N. Harris, Michael D. Kessler, Jedidiah Carlson, Zachary A. Szpiech,

Raul Torres, Sarah A. Gagliano Taliun, et al. 2021. “Sequencing of 53,831 Diverse Genomes from the NHLBI TOPMed Program.” *Nature* 590 (7845): 290–99. https://doi.org/10.1038/s41586-021-03205-y.

Tanaka, Kozo, and Toru Hirota. 2016. “Chromosomal Instability: A Common Feature and a Therapeutic Target of Cancer.” *Biochimica et Biophysica Acta (BBA) - Reviews on Cancer* 1866 (1): 64–75. https://doi.org/10.1016/j.bbcan.2016.06.002.

Tanaka, Kozo, Naomi Mukae, Hilary Dewar, Mark Van Breugel, Euan K. James, Alan R. Prescott, Claude Antony, and Tomoyuki U. Tanaka. 2005. “Molecular Mechanisms of Kinetochore Capture by Spindle Microtubules.” *Nature* 434 (7036): 987–94. https://doi.org/10.1038/nature03483.

Tate, John G., Sally Bamford, Harry C. Jubb, Zbyslaw Sondka, David M. Beare, Nidhi Bindal, Harry Boutselakis, et al. 2019. “COSMIC: The Catalogue Of Somatic Mutations In Cancer.” *Nucleic Acids Research* 47 (D1): D941–47. https://doi.org/10.1093/nar/gky1015.

Tauchman, Eric C., Frederick J. Boehm, and Jennifer G. DeLuca. 2015. “Stable Kinetochore-Microtubule Attachment Is Sufficient to Silence the Spindle Assembly Checkpoint in Human Cells.” *Nature Communications* 6 (December). https://doi.org/10.1038/ncomms10036.

Thedieck, Kathrin, Birgit Holzwarth, Mirja Tamara Prentzell, Christopher Boehlke, Kathrin Kläsener, Stefanie Ruf, Annika Gwendolin Sonntag, et al. 2013. “Inhibition of MTORC1 by Astrin and Stress Granules Prevents Apoptosis in Cancer Cells.” *Cell* 154 (4): 859–74. https://doi.org/10.1016/j.cell.2013.07.031.

Thein, K. 2008. “Functional Characterization of the Mitotic-Spindle and Kinetochore Associated Protein Astrin.” *Dissertation*. file:///storage/www/librarian/library/04638.pdf.

Thein, Kerstin H., Julia Kleylein-Sohn, Erich A. Nigg, and Ulrike Gruneberg. 2007. “Astrin Is Required for the Maintenance of Sister Chromatid Cohesion and Centrosome Integrity.” *Journal of Cell Biology* 178 (3): 345–54. https://doi.org/10.1083/jcb.200701163.

Thompson, Sarah L., and Duane A. Compton. 2011. “Chromosome Missegregation in Human Cells Arises through Specific Types of Kinetochore-Microtubule Attachment Errors.” *Proceedings of the National Academy of Sciences of the United States of America* 108 (44): 17974–78. https://doi.org/10.1073/pnas.1109720108.

Tolmie, J. L., M. McNay, J. B.P. Stephenson, D. Doyle, and J. M. Connor. 1987. "Microcephaly: Genetic Counselling and Antenatal Diagnosis after the Birth of an Affected Child." *American Journal of Medical Genetics* 27 (3): 583–94. https://doi.org/10.1002/ajmg.1320270311.

Tolmie, J L, E Boyd, P Batstone, M E Ferguson-Smith, L al Roomi, and J M Connor. 1988. "Siblings with Chromosome Mosaicism, Microcephaly, and Growth Retardation: The Phenotypic Expression of a Human Mitotic Mutant?" *Human Genetics* 80 (2): 197–200. http://www.ncbi.nlm.nih.gov/pubmed/3169747.

Tovini, Laura, and Sarah E. McClelland. 2019. "Impaired CENP-E Function Renders Large Chromosomes More Vulnerable to Congression Failure." *Biomolecules* 9 (2). https://doi.org/10.3390/biom9020044.

Tsukahara, Tatsuya, Yuji Tanno, and Yoshinori Watanabe. 2010. "Phosphorylation of the CPC by Cdk1 Promotes Chromosome Bi-Orientation." *Nature* 467 (7316): 719–23. https://doi.org/10.1038/nature09390.

Uchida, Kazuhiko S.K., Kentaro Takagaki, Kazuki Kumada, Youko Hirayama, Tetsuo Noda, and Toru Hirota. 2009a. "Kinetochore Stretching Inactivates the Spindle Assembly Checkpoint." *Journal of Cell Biology* 184 (3): 383–90. https://doi.org/10.1083/jcb.200811028.

Uetake, Yumi, and Greenfield Sluder. 2010. "Prolonged Prometaphase Blocks Daughter Cell Proliferation Despite Normal Completion of Mitosis." *Current Biology* 20 (18): 1666–71. https://doi.org/10.1016/j.cub.2010.08.018.

Umbreit, Neil T., Daniel R. Gestaut, Jerry F. Tien, Breanna S. Vollmar, Tamir Gonen, Charles L. Asbury, and Trisha N. Davis. 2012. "The Ndc80 Kinetochore Complex Directly Modulates Microtubule Dynamics." *Proceedings of the National Academy of Sciences of the United States of America* 109 (40): 16113–18. https://doi.org/10.1073/pnas.1209615109.

Unteregger, G., J. M. J. C. Scheres, and Hustinx T. W. J. 1987. "Changes in the Nuclear Protein Pattern in Fibroblasts from a Patient with Premature Centromere Division (PCD)." *In: Klassische Und Molekulare Zytogenetik: Tagungsbericht. Saarbrucken/Homburg: Universitat Des Saarlandes, Medizinische Fakultat Homburg/Saar 1987. Pp. 331-334.*

Vallardi, Giulia, Marilia Henriques Cordeiro, and Adrian Thomas Saurin. 2017. "A Kinase-Phosphatase Network That Regulates Kinetochore-Microtubule Attachments and the

SAC.” *Progress in Molecular and Subcellular Biology*. NLM (Medline). https://doi.org/10.1007/978-3-319-58592-5_19.

Vázquez-Novelle, María Dolores, Laurent Sansregret, Amalie E. Dick, Christopher A. Smith, Andrew D. Mcainsh, Daniel W. Gerlich, and Mark Petronczki. 2014. “Cdk1 Inactivation Terminates Mitotic Checkpoint Surveillance and Stabilizes Kinetochore Attachments in Anaphase.” *Current Biology* 24 (6): 638–45. https://doi.org/10.1016/j.cub.2014.01.034.

Vizcaíno, Juan Antonio, Attila Csordas, Noemi del-Toro, José A. Dianes, Johannes Griss, Ilias Lavidas, Gerhard Mayer, et al. 2016. “2016 Update of the PRIDE Database and Its Related Tools.” *Nucleic Acids Research* 44 (D1): D447–56. https://doi.org/10.1093/nar/gkv1145.

Volkov, Vladimir A., Pim J. Huis In ’T Veld, Marileen Dogterom, and Andrea Musacchio. 2018. “Multivalency of NDC80 in the Outer Kinetochore Is Essential to Track Shortening Microtubules and Generate Forces.” *ELife* 7 (April). https://doi.org/10.7554/eLife.36764.

Vorozhko, Valeriya V., Michael J. Emanuele, Marko J. Kallio, P. Todd Stukenberg, and Gary J. Gorbsky. 2008. “Multiple Mechanisms of Chromosome Movement in Vertebrate Cells Mediated through the Ndc80 Complex and Dynein/Dynactin.” *Chromosoma* 117 (2): 169–79. https://doi.org/10.1007/s00412-007-0135-3.

Wall, Jeffrey D., Eric W. Stawiski, Aakrosh Ratan, Hie Lim Kim, Changhoon Kim, Ravi Gupta, Kushal Suryamohan, et al. 2019. “The GenomeAsia 100K Project Enables Genetic Discoveries across Asia.” *Nature* 576 (7785): 106–11. https://doi.org/10.1038/s41586-019-1793-z.

Wan, Xiaohu, Ryan P. O’Quinn, Heather L. Pierce, Ajit P. Joglekar, Walt E. Gall, Jennifer G. DeLuca, Christopher W. Carroll, et al. 2009. “Protein Architecture of the Human Kinetochore Microtubule Attachment Site.” *Cell* 137 (4): 672–84. https://doi.org/10.1016/j.cell.2009.03.035.

Wang, Enxiu, Edward R. Ballister, and Michael A. Lampson. 2011. “Aurora B Dynamics at Centromeres Create a Diffusion-Based Phosphorylation Gradient.” *Journal of Cell Biology* 194 (4): 539–49. https://doi.org/10.1083/jcb.201103044.

Wang, Hong-Wei, Sydney Long, Claudio Ciferri, Stefan Westermann, David Drubin, Georjana Barnes, and Eva Nogales. 2008. “Architecture and Flexibility of the Yeast Ndc80 Kinetochore Complex.” *Journal of Molecular Biology* 383 (4): 894–903. https://doi.org/10.1016/j.jmb.2008.08.077.

Wang, Tong, Kaimi Li, Hongyong Song, Dongliang Xu, Yueling Liao, Bo Jing, Wenzheng Guo, et al. 2019. “P53 Suppression Is Essential for Oncogenic SPAG5 Upregulation in Lung Adenocarcinoma.” *Biochemical and Biophysical Research Communications* 513 (2): 319–25. https://doi.org/10.1016/j.bbrc.2019.03.198.

Warburton, D, K Anyane-Yeboa, P Taterka, C Y Yu, and D Olsen. 1991. “Mosaic Variegated Aneuploidy with Microcephaly: A New Human Mitotic Mutant?” *Annales de Genetique* 34 (3–4): 287–92. http://www.ncbi.nlm.nih.gov/pubmed/1809239.

Waters, Jennifer C., Timothy J. Mitchison, Conly L. Rieder, and Edward D. Salmon. 1996. “The Kinetochore Microtubule Minus-End Disassembly Associated with Poleward Flux Produces a Force That Can Do Work.” *Molecular Biology of the Cell* 7 (10): 1547–58. https://doi.org/10.1091/mbc.7.10.1547.

Weaver, Beth AA, and Don W Cleveland. 2006. “Does Aneuploidy Cause Cancer?” *Current Opinion in Cell Biology* 18 (6): 658–67. https://doi.org/10.1016/j.ceb.2006.10.002.

Wei, Ronnie R, Jawdat Al-Bassam, and Stephen C Harrison. 2007. “The Ndc80/HEC1 Complex Is a Contact Point for Kinetochore-Microtubule Attachment.” *Nature Structural & Molecular Biology* 14 (1): 54–59. https://doi.org/10.1038/nsmb1186.

Welburn, Julie P.I., Mathijs Vleugel, Dan Liu, John R. Yates, Michael A. Lampson, Tatsuo Fukagawa, and Iain M. Cheeseman. 2010. “Aurora B Phosphorylates Spatially Distinct Targets to Differentially Regulate the Kinetochore-Microtubule Interface.” *Molecular Cell* 38 (3): 383–92. https://doi.org/10.1016/j.molcel.2010.02.034.

Westermann, Stefan, Agustin Avila-Sakar, Hong Wei Wang, Hanspeter Niederstrasser, Jonathan Wong, David G. Drubin, Eva Nogales, and Georjana Barnes. 2005. “Formation of a Dynamic Kinetochore-Microtubule Interface through Assembly of the Dam1 Ring Complex.” *Molecular Cell* 17 (2): 277–90. https://doi.org/10.1016/j.molcel.2004.12.019.

Witt, Patricia L., Hans Ris, and Gary G. Borisy. 1980. “Origin of Kinetochore Microtubules in Chinese Hamster Ovary Cells.” *Chromosoma* 81 (3): 483–505. https://doi.org/10.1007/BF00368158.

Woods, C. Geoffrey, Jacquelyn Bond, and Wolfgang Enard. 2005. “Autosomal Recessive Primary Microcephaly (MCPH): A Review of Clinical, Molecular, and Evolutionary Findings.” *American Journal of Human Genetics*. University of Chicago Press. https://doi.org/10.1086/429930.

Wynne, David J., and Hironori Funabiki. 2015. “Kinetochore Function Is Controlled by a

Phosphodependent Coexpansion of Inner and Outer Components." *Journal of Cell Biology* 210 (6): 899–916. https://doi.org/10.1083/jcb.201506020.

Xu, P., E. A. Raetz, M. Kitagawa, D. M. Virshup, and S. H. Lee. 2013. "BUBR1 Recruits PP2A via the B56 Family of Targeting Subunits to Promote Chromosome Congression." *Biology Open* 2 (5): 479–86. https://doi.org/10.1242/bio.20134051.

Yamagishi, Yuya, Takeshi Sakuno, Yuhei Goto, and Yoshinori Watanabe. 2014. "Kinetochore Composition and Its Function: Lessons from Yeasts." *FEMS Microbiology Reviews*. Oxford Academic. https://doi.org/10.1111/1574-6976.12049.

Yang, Ting, Sijuan Tian, Linlin Wang, Yaohui Wang, and Juan Zhao. 2020. "MicroRNA-367-3p Overexpression Represses the Proliferation and Invasion of Cervical Cancer Cells through Downregulation of SPAG5-Mediated Wnt/β-Catenin Signalling." *Clinical and Experimental Pharmacology and Physiology* 47 (4): 687–95. https://doi.org/10.1111/1440-1681.13222.

Yang, Yu-Feng, Mei-Fang Zhang, Qiu-Hong Tian, Jia Fu, Xia Yang, Chris Zhiyi Zhang, and Hong Yang. 2018. "SPAG5 Interacts with CEP55 and Exerts Oncogenic Activities via PI3K/AKT Pathway in Hepatocellular Carcinoma." *Molecular Cancer* 17 (1): 117. https://doi.org/10.1186/s12943-018-0872-3.

Yang, Yuh-Cheng Cheng, Yun-Ting Ting Hsu, Chao-Chih Chih Wu, Hsiang-Ting Ting Chen, and Mau-Sun S. Chang. 2006. "Silencing of Astrin Induces the P53-Dependent Apoptosis by Suppression of HPV18 E6 Expression and Sensitizes Cells to Paclitaxel Treatment in HeLa Cells." *Biochemical and Biophysical Research Communications* 343 (2): 428–34. https://doi.org/10.1016/j.bbrc.2006.02.166.

Yang, Zhenye, U. Serdar Tulu, Patricia Wadsworth, and Conly L. Rieder. 2007. "Kinetochore Dynein Is Required for Chromosome Motion and Congression Independent of the Spindle Checkpoint." *Current Biology* 17 (11): 973–80. https://doi.org/10.1016/j.cub.2007.04.056.

Yates, Andrew D., Premanand Achuthan, Wasiu Akanni, James Allen, Jamie Allen, Jorge Alvarez-Jarreta, M. Ridwan Amode, et al. 2020. "Ensembl 2020." *Nucleic Acids Research* 48 (D1): D682–88. https://doi.org/10.1093/nar/gkz966.

Ying, Wai Chan, Luca L. Fava, Andreas Uldschmid, Michael H.A. Schmitz, Daniel W. Gerlich, Erich A. Nigg, and Anna Santamaria. 2009. "Mitotic Control of Kinetochore-Associated Dynein and Spindle Orientation by Human Spindly." *Journal of Cell Biology* 185 (5): 859–74. https://doi.org/10.1083/jcb.200812167.

Ying, Zhenguang, Jing Yang, Wei Li, Xia Wang, Zeyao Zhu, Weipeng Jiang, Chunman Li, and Ou Sha. 2020. “Astrin: A Key Player in Mitosis and Cancer.” *Frontiers in Cell and Developmental Biology*. Frontiers Media S.A. https://doi.org/10.3389/fcell.2020.00866.

Yost, Shawn, Bas de Wolf, Sandra Hanks, Anna Zachariou, Chiara Marcozzi, Matthew Clarke, Richarda M de Voer, et al. 2017. “Biallelic TRIP13 Mutations Predispose to Wilms Tumor and Chromosome Missegregation.” *Nature Genetics* 49 (7): 1148–51. https://doi.org/10.1038/ng.3883.

Yuan, L-J, J-D Li, L Zhang, J-H Wang, T Wan, Y Zhou, H Tu, et al. 2014. “SPAG5 Upregulation Predicts Poor Prognosis in Cervical Cancer Patients and Alters Sensitivity to Taxol Treatment via the MTOR Signaling Pathway.” *Cell Death & Disease* 5 (May 2014): e1247. https://doi.org/10.1038/cddis.2014.222.

Zarate, Yuri A., Julie A. Kaylor, Katherine Bosanko, Sarah Lau, Jose Vargas, and Hanlin Gao. 2016a. “First Clinical Report of an Infant with Microcephaly and *CASC5* Mutations.” *American Journal of Medical Genetics Part A* 170 (8): 2215–18. https://doi.org/10.1002/ajmg.a.37726.

Zaytsev, Anatoly V., Dario Segura-Pena, Maxim Godzi, Abram Calderon, Edward R. Ballister, Rumen Stamatov, Alyssa M. Mayo, et al. 2016. “Bistability of a Coupled Aurora B Kinase-Phosphatase System in Cell Division.” *ELife* 5 (JANUARY2016). https://doi.org/10.7554/eLife.10644.

Zhang, Cheng Zhong, Alexander Spektor, Hauke Cornils, Joshua M. Francis, Emily K. Jackson, Shiwei Liu, Matthew Meyerson, and David Pellman. 2015. “Chromothripsis from DNA Damage in Micronuclei.” *Nature* 522 (7555): 179–84. https://doi.org/10.1038/nature14493.

Zhang, Gang, Thomas Kruse, Blanca López-Méndez, Kathrine Beck Sylvestersen, Dimitriya H. Garvanska, Simone Schopper, Michael Lund Nielsen, and Jakob Nilsson. 2017. “Bub1 Positions Mad1 Close to KNL1 MELT Repeats to Promote Checkpoint Signalling.” *Nature Communications* 8 (June). https://doi.org/10.1038/ncomms15822.

Zhang, Gang, Tiziana Lischetti, Daniel G. Hayward, and Jakob Nilsson. 2015. “Distinct Domains in Bub1 Localize RZZ and BubR1 to Kinetochores to Regulate the Checkpoint.” *Nature Communications* 6 (June): 7162. https://doi.org/10.1038/ncomms8162.

Zhang, Gang, Tiziana Lischetti, and Jakob Nilsson. 2014. “A Minimal Number of MELT Repeats Supports All the Functions of KNL1 in Chromosome Segregation.” *Journal of*

Cell Science 127 (4): 871–84. https://doi.org/10.1242/jcs.139725.

Zhang, Hongtuan, Shadan Li, Xiong Yang, Baomin Qiao, Zhihong Zhang, and Yong Xu. 2016. "MiR-539 Inhibits Prostate Cancer Progression by Directly Targeting SPAG5." *Journal of Experimental & Clinical Cancer Research : CR* 35 (1): 60. https://doi.org/10.1186/s13046-016-0337-8.

Zhang, Mei, Ling Sha, Ning Hou, Chuanbing Shi, and Lin Tan. 2020. "High Expression of Sperm-Associated Antigen 5 Correlates with Poor Survival in Ovarian Cancer." *Bioscience Reports* 40 (2). https://doi.org/10.1042/BSR20193087.

Zhang, Qian, Sushama Sivakumar, Yujue Chen, Haishan Gao, Lu Yang, Zhu Yuan, Hongtao Yu, and Hong Liu. 2017. "Ska3 Phosphorylated by Cdk1 Binds Ndc80 and Recruits Ska to Kinetochores to Promote Mitotic Progression." *Current Biology* 27 (10): 1477-1484.e4. https://doi.org/10.1016/j.cub.2017.03.060.

Zirkle, Raymond E. 1970. "Ultraviolet-Microbeam Irradiation of Newt-Cell Cytoplasm: Spindle Destruction, False Anaphase, and Delay of True Anaphase." *Radiation Research* 41 (3): 516. https://doi.org/10.2307/3572841.